

ABSTRACT

Title of dissertation: NONLINEAR OBSERVER/CONTROLLER
 DESIGNS FOR SPACECRAFT
 ATTITUDE CONTROL SYSTEMS
 WITH UNCALIBRATED GYROS

Julie K. Thienel, Doctor of Philosophy, 2004

Dissertation directed by: Professor Robert M. Sanner
 Department of Aerospace Engineering

Gyroscopes, or gyros, are vital sensors in spacecraft onboard attitude control systems. Gyro measurements are corrupted, though, due to errors in alignment and scale factor, biases, and noise. This work proposes a class of adaptive nonlinear observers for calibration of spacecraft gyros. Observers for each of the calibration parameters are separately developed, then combined. Lyapunov stability analysis is used to demonstrate the stability and convergence properties of each design. First, an observer to estimate gyro bias is developed, both with and without added noise effects. The observer is shown to be exponentially stable without any additional conditions. Next a scale factor observer is developed, followed by an alignment

observer. The scale factor and alignment observers are both shown to be Lyapunov stable. Additionally, if the angular velocity meets a persistency of excitation (PE) condition, the scale factor and alignment observers are exponentially stable. Finally, the three observers are combined, and the combination is shown to be stable, with exponential stability if the angular velocity is persistently exciting. The specific PE condition for each observer is given in detail.

Next, the adaptive observers are combined with a class of nonlinear control algorithms designed to asymptotically track a general time-varying reference attitude. This algorithm requires feedback from rate sensors, such as gyros. The miscalibration discussed above will seriously degrade the performance of these controllers. While the adaptive observers can eliminate this miscalibration, it is not immediately clear that the observers can be safely combined with the controller in this case. There is, in general, no "separation principle" for nonlinear systems, as there is for linear systems. However, Lyapunov analysis of the coupled controller-observer dynamics shows that the closed-loop system will be stable for the class of observers proposed. With only gyro bias miscalibration, the closed-loop system is in fact asymptotically stable. For more general combinations of miscalibration, closed-loop stability is ensured with modest constraints on the observer/controller design parameters. These constraints are identified in detail. It is also shown that the constraints are not required if the angular velocity can be a priori guaranteed to be persistently exciting.

NONLINEAR OBSERVER/CONTROLLER DESIGNS
FOR SPACECRAFT ATTITUDE CONTROL SYSTEMS
WITH UNCALIBRATED GYROS

by

Julie K. Thienel

Dissertation to be submitted to the Faculty of the Graduate School of the
University of Maryland, College Park in partial fulfillment
of the requirements for the degree of
Doctor of Philosophy
2004

Advisory Committee:

Professor Robert M. Sanner, Chair/Advisor
Professor Benjamin Kadem
Dr. F. Landis Markley
Professor Darryll Pines
Professor Norman M. Wereley

© Copyright by
Julie K. Thienel
2004

Dedication

This work is dedicated to my family; to my two sons for the incredible joy they bring to my life, to my mother and late father for their endless support, and to my husband for all his love.

Acknowledgements

I am very grateful to the many people that have helped and supported me throughout the development of this work, and throughout my years in graduate school. I would like to thank those that took the time and effort to serve on my examining committee, Dr. Benjamin Kedem, Dr. Norman Wereley, and Dr. Darryll Pines, all of the University of Maryland, and Dr. Landis Markley of the NASA Goddard Space Flight Center. I have been fortunate to work with and learn from Dr. Markley for many years. I would especially like to thank my advisor, Dr. Robert Sanner. He provided me with challenges, taught great classes, and guided me through an interesting research project.

I also have many colleagues to thank. I am very grateful to Mr. Rich Luquette of the NASA Goddard Space Flight Center. Rich patiently listened as I worked through tough derivations, provided valuable feedback and review, and made me laugh. I want to thank Dr. Itzhack Bar-Itzhack of the Technion-Israel Institute of Technology. I am very fortunate to have Dr. Bar-Itzhack as a close and dear friend, as well as a mentor and colleague. Dr. Bar-Itzhack provides encouragement when I need it, and is a very patient teacher. I would also like to thank Mr. Rick Harman and Mr. Tom Stengle of the NASA Goddard Space Flight Center. Rick is the MATLAB[®] guru and provider of coffee. Mr. Tom Stengle is my supervisor, he has always supported my seemingly never ending pursuit of higher education.

I have many friends to thank as well. I am blessed with so many wonderful,

supportive friends. I got a lot of help and encouragement from so many people. Thanks especially to Cheryl, Robin, Julie, and Margie.

Finally, I want to thank my family. My parents have helped me and guided me all of my life. They supported me in all the decisions I have made, good and bad. I wish my dad had lived long enough to finally see me finish my graduate work. I want to especially thank my mom for the two years she stayed with me and took care of my two boys and me. Thanks to my brothers for making me tough and encouraging me to work hard. My brother Kurt is an inspiration to me. I am very grateful to my sons, Joshua and Kyle. They are the joy of my life. They have been so patient with me through my years of graduate school. Finally, I want to thank my wonderful husband, Steve. He makes me laugh when I need it the most, and he has brought adventure, fun, and happiness to my life. He gives me support and encouragement, and most importantly, he gives me his love.

TABLE OF CONTENTS

List of Tables	ix
List of Figures	xi
1 Introduction	1
1.1 Background	1
1.1.1 Overview of Gyro Calibration Scenario	3
1.1.2 Linear Gyro Calibration Methods	6
1.1.3 Nonlinear Gyro Calibration Methods	12
1.2 Dissertation Outline	14
2 Mathematical Overview	17
2.1 Terminology	17
2.2 Lyapunov Stability	22

2.3	A Nonlinear Attitude Controller	25
3	Gyro Bias Calibration	32
3.1	Nonlinear Estimator for Constant Gyro Bias	32
3.2	Estimator Simulation Results	37
3.3	Closed Loop Stability	39
3.4	Closed Loop Simulation Results	44
3.5	Gyro Noise	46
3.6	Estimator and Closed Loop Simulation Results with Noise	49
4	Scale Factor Calibration	55
4.1	Nonlinear Estimator for Constant Scale Factor	55
4.2	Estimator Simulation Results	63
4.3	Closed Loop Stability	66
4.4	Closed Loop Simulation Results	72
5	Gyro Alignment Calibration	75
5.1	Nonlinear Estimator for Gyro Alignment	75
5.2	Estimation Simulation Results	88
5.3	Closed Loop Stability	90
5.4	Closed Loop Simulation Results	95

6	Combined Parameter Estimation	98
6.1	Scale Factor and Gyro Bias Estimator	98
6.2	Estimator Simulation Results	106
6.3	Closed Loop Stability	108
6.4	Closed Loop Simulation Results	113
6.5	Alignment and Gyro Bias Estimator	116
6.6	Estimator Simulation Results	126
6.7	Closed Loop Stability	128
6.8	Closed Loop Simulation Results	133
6.9	Alignment, Scale Factor, and Gyro Bias Estimator	136
6.10	Estimator Simulation Results	149
6.11	Closed Loop Stability	151
6.12	Closed Loop Simulation Results	157
7	Comparison to a Pseudo-Linear Kalman Filter	160
7.1	Comparison of Gyro Bias Estimation	166
7.2	Comparison of Scale Factor Estimation	167
7.3	Comparison of Misalignment Estimation	169
7.4	Comparison of Misalignment, Scale Factor, and Bias Estimation . . .	170

8	Concluding Remarks	174
8.1	Future Direction	178
8.2	Final Summary	179
	Bibliography	181

LIST OF TABLES

3.1	Bias Estimator Simulation Initial Conditions	37
3.2	Bias Estimator Simulation Initial Conditions	44
4.1	Scale Factor Estimator Simulation Initial Conditions	63
4.2	Scale Factor Estimator/Controller Simulation Initial Conditions . . .	73
5.1	Alignment Estimation Simulation Initial Conditions	88
5.2	Alignment Estimator and Controller Simulation Initial Conditions . .	95
6.1	Scale Factor and Bias Estimator Simulation Initial Conditions	106
6.2	Scale Factor and Bias Estimator/Controller Simulation Initial Condi- tions	114
6.3	Alignment and Gyro Bias Estimator Simulation Initial Conditions . .	127
6.4	Alignment and Bias Estimator/ Controller Simulation Initial Conditions	134
6.5	Alignment, Scale Factor, and Gyro Bias Estimator Simulation Initial Conditions	151

6.6	Alignment, Scale Factor and Bias Estimator/ Controller Simulation	
	Initial Conditions	157
7.1	Bias Estimation Comparison	167
7.2	Scale Factor Estimation Comparison	169
7.3	Alignment Estimation Comparison	171
7.4	Bias Estimation Comparison	172
7.5	Scale Factor Estimation Comparison	172
7.6	Alignment Estimation Comparison	173
8.1	Summary of PE Conditions	176

LIST OF FIGURES

1.1	Coordinate Frames	4
2.1	Estimation Approach	18
2.2	Closed Loop Control	29
2.3	Coupled Estimator/Controller Errors With Gyro Bias	31
3.1	Gyro Bias Estimator Errors, $\omega(t) = [3, -4, 5]$ deg/sec	38
3.2	Gyro Bias Estimator Errors with α Reduced, $\omega(t) = [3, -4, 5]$ deg/sec	38
3.3	Gyro Bias Estimation Errors, $\omega(t) = [0, 0, 0]$	39
3.4	Gyro Bias Estimation Errors, $\omega(t) = [30, -40, 50]$ deg/sec	40
3.5	Coupled Estimator/Controller Errors With Gyro Bias	45
3.6	Gyro Bias Estimation Errors with Added Noise	50
3.7	Gyro Bias Estimation Errors with Added Noise, Standard Deviations Increased	51
3.8	Closed Loop Control with Gyro Bias Error and Added Noise	52

3.9	Closed Loop Control Attitude Tracking Errors with Gyro Bias and Added Noise	53
3.10	Closed Loop Control Rate Tracking Errors with Gyro Bias and Added Noise	53
3.11	Closed Loop Attitude Tracking Errors with (a) K_D Doubled (b) $\frac{1}{2}\sigma$ and $\frac{1}{2}\sigma_b$	54
4.1	Scale Factor Estimation Errors with Constant Angular Velocity . . .	64
4.2	Scale Factor Estimation Errors with $\omega_z = 0$	65
4.3	Scale Factor Estimation Errors with Exponential Angular Velocity . .	65
4.4	Scale Factor Estimation Errors with Large Inverse Scale Factor	66
4.5	Coupled Estimator/Controller Errors with Scale Factor Errors	74
5.1	Alignment Estimation with Constant Angular Velocity	89
5.2	Alignment Estimation with PE Angular Velocity	89
5.3	Closed Loop Alignment Estimator/Controller with Constant $\omega_d(t)$. .	96
5.4	Closed Loop Alignment Estimator/Controller with PE $\omega_d(t)$	97
6.1	Bias and Scale Factor Estimation Errors with Constant Angular Velocity	107
6.2	Bias and Scale Factor Estimation Errors with Sinusoidal Angular Velocity	107
6.3	Bias and Scale Factor Estimator Errors with Large Inverse Scale Factor	108
6.4	Coupled Estimator/Controller Errors with Scale Factor and Bias Errors	115

6.5	Alignment and Gyro Bias Estimation with Constant Angular Velocity	127
6.6	Alignment and Gyro Bias Estimator with PE Angular Velocity	128
6.7	Coupled Estimator/Controller Errors with Alignment and Bias Errors	135
6.8	Combined Estimators with PE Angular Velocity	150
6.9	Coupled Estimator/Controller Errors with Alignment, Scale Factor, and Bias Errors	159

Chapter 1

Introduction

High precision estimation and control algorithms, to achieve unprecedented levels of pointing accuracy, will be required to support future aerospace missions. New missions will require increased performance, at a lower cost. The vehicle estimation and control algorithms must support large and fast angular maneuvers autonomously, utilizing low cost sensors with looser tolerances than traditional sensors. In order to provide the required tolerances throughout the expanded flight envelope, precise knowledge of the spacecraft rotation rate is required. This work focuses on methods to autonomously improve the rate estimate for aerospace control systems, given potentially low cost rate sensors such as micro-mechanical system (MEMS) rate sensors containing large miscalibrations. The emphasis is on spacecraft attitude control systems, but the algorithms are applicable to other aerospace scenarios.

1.1 Background

Gyroscopes, also known as Inertial Reference Units (IRU) or gyros, are part of the attitude control system of most three-axis stabilized spacecraft. They measure the

spacecraft angular rate. There are several types of gyros for spacecraft use. Mechanical gyros are supported by gimbals, which attempt to precess when the spacecraft rotates. The current applied to null the gimbal is proportional to the spacecraft rate. Mechanical gyros either provide single axis or two axis rate information. Hemispherical resonator gyros contain a quartz crystal shell which oscillates at a specific amplitude and frequency. Changes in the spacecraft angular orientation are determined by measuring the force needed to rebalance the standing wave pattern. Another type of spacecraft gyro is a ring laser gyro. Two light waves, travelling in opposite directions, combine to produce a standing wave pattern. The angular rate is determined by detecting changes in the intensity of the light as the spacecraft rotates. Fiber-optic gyros also contain two beams, travelling in opposite directions within a fiber. A detector measures the signal power of the combined signals. The angular rate is related to the change in the signal power. [1] A final example of a spacecraft gyro is a MEMS gyro. MEMS gyros are silicon structures that are electrostatically forced to oscillate within a plane. The angular rate is determined by measuring out of plane oscillations. [2]

Unfortunately, the gyro measurements are corrupted by errors in alignment, scale factor, and bias, as well as random noise [3]. Most of the gyros flown on missions supported by the NASA Goddard Space Flight Center are very low noise/low bias gyros [4], [5]. MEMS gyros, however, can have noise and bias levels many orders of magnitudes higher than the typical NASA mission gyros [2, 6].

1.1.1 Overview of Gyro Calibration Scenario

The attitude of a vehicle is typically defined as the orientation of a body fixed coordinate system with respect to an inertial coordinate system. Figure 1.1 depicts the body coordinate system of a vehicle, rotating at the true angular velocity $\boldsymbol{\omega}(t)$ with respect to an inertial coordinate system. The gyro measures the vehicle angular velocity. However, due to the corruptions, the measured angular velocity is not the same as the true angular velocity. The relationship between the measured and true angular velocity is often given as [3]

$$\boldsymbol{\omega}_g(t) = \Gamma R_g^T \boldsymbol{\omega}(t) + \mathbf{b}_g(t) + \boldsymbol{\nu}_g(t) \quad (1.1)$$

where $\boldsymbol{\omega}_g(t)$ is the measured angular velocity, Γ is a matrix of scale factors, R_g is the gyro alignment which is a transformation from the gyro coordinate frame to the spacecraft body frame, $\mathbf{b}_g(t)$ is a bias, and $\boldsymbol{\nu}_g(t)$ is a zero mean noise. Gyro calibration methods are designed to give the best estimates of the scale factors, alignment, and bias. Several algorithms for estimating the calibration components, as well as the noise characteristics, are available. Most algorithms rely on linear techniques, assuming the calibration parameters are small, and the algorithms are not coupled directly with the spacecraft control. An overview of many of the linear estimation techniques is presented next, followed by an overview of the limited number of existing nonlinear methods. A few definitions are necessary, however, before introducing the existing methods.

The attitude of a spacecraft can be represented by a quaternion, consisting of

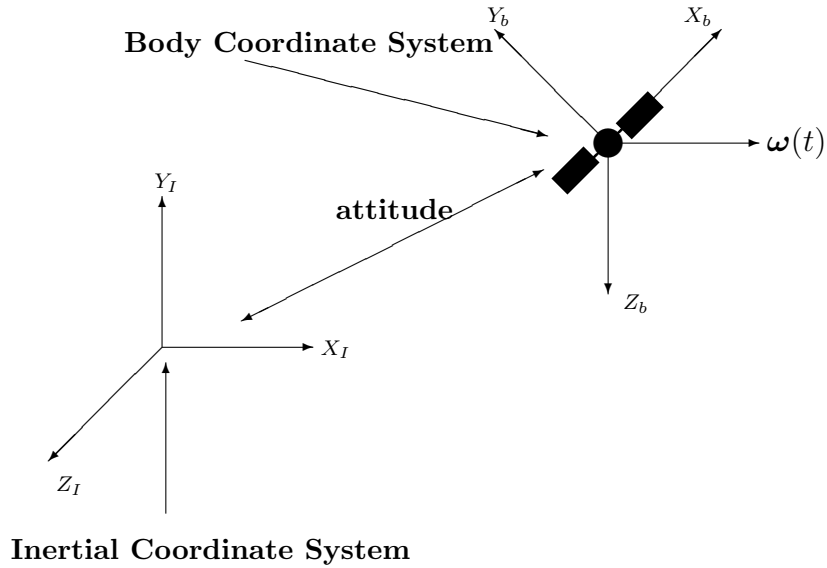


Figure 1.1: Coordinate Frames

a rotation angle and unit rotation vector \mathbf{e} , known as the Euler axis, and a rotation ϕ about this axis so that [7]

$$\mathbf{q} = \begin{bmatrix} \mathbf{e} \sin(\frac{\phi}{2}) \\ \cos(\frac{\phi}{2}) \end{bmatrix} = \begin{bmatrix} \boldsymbol{\varepsilon} \\ \eta \end{bmatrix} \quad (1.2)$$

where \mathbf{q} is the quaternion, partitioned into a vector part, $\boldsymbol{\varepsilon}$, and a scalar part, η . Typically, in spacecraft attitude applications, the quaternion represents the rotation from an inertial coordinate system to the spacecraft body coordinate system, as depicted in figure 1.1. Note that $\|\mathbf{q}\| = \mathbf{1}$ by definition. The rotation matrix for a specific attitude can be computed from the quaternion components as [7]

$$R(\mathbf{q}) = (\eta^2 - \boldsymbol{\varepsilon}^T \boldsymbol{\varepsilon})\mathbf{I} + 2\boldsymbol{\varepsilon}\boldsymbol{\varepsilon}^T - 2\eta S(\boldsymbol{\varepsilon}) \quad (1.3)$$

where \mathbf{I} is a 3x3 identity matrix and $S(\boldsymbol{\varepsilon})$ is a matrix representation of the vector

cross product operation.

$$S(\boldsymbol{\varepsilon}) = \begin{bmatrix} 0 & -\varepsilon_z & \varepsilon_y \\ \varepsilon_z & 0 & -\varepsilon_x \\ -\varepsilon_y & \varepsilon_x & 0 \end{bmatrix}$$

The rotation matrix is orthogonal such that $R^T R = I$. Note also that $R(\mathbf{q})\boldsymbol{\varepsilon} = \boldsymbol{\varepsilon}$.

A relative rotation between coordinate frames is computed as [8]

$$\tilde{\mathbf{q}} = \begin{bmatrix} \tilde{\boldsymbol{\varepsilon}} \\ \tilde{\eta} \end{bmatrix} = \mathbf{q}_1 \otimes \mathbf{q}_2^{-1} = \begin{bmatrix} \eta_2 I - S(\boldsymbol{\varepsilon}_2) & -\boldsymbol{\varepsilon}_2 \\ \boldsymbol{\varepsilon}_2^T & \eta_2 \end{bmatrix} \begin{bmatrix} \boldsymbol{\varepsilon}_1 \\ \eta_1 \end{bmatrix} \quad (1.4)$$

Where $\tilde{\mathbf{q}}$ represents the rotation from the frame defined by \mathbf{q}_2 to the frame defined by \mathbf{q}_1 . Note that $\|\tilde{\boldsymbol{\varepsilon}}\| = 0$, $\tilde{\eta} = \pm 1$ indicates that the frame 2 is aligned with frame

1. Note that the vector part of $\tilde{\mathbf{q}}$ is

$$\tilde{\boldsymbol{\varepsilon}} = \tilde{\mathbf{e}} \sin\left(\frac{\tilde{\phi}}{2}\right)$$

$\tilde{\boldsymbol{\varepsilon}}$ points along the eigenaxis of the relative rotation, and the length of $\tilde{\boldsymbol{\varepsilon}}$ varies directly with the size of the eigenaxis rotation, $\tilde{\phi}$.

With known calibrations, the angular velocity can be recovered from the measured angular velocity given in equation 1.1 as

$$\boldsymbol{\omega}(t) = C\boldsymbol{\omega}_g(t) - \mathbf{b}(t) - \boldsymbol{\nu}(t) \quad (1.5)$$

where $C = (\Gamma R_g^T)^{-1} = R_g \Gamma_I$ and $\Gamma_I = \Gamma^{-1}$. The bias, $\mathbf{b}(t)$, is the effective bias in the body frame, and similarly, $\boldsymbol{\nu}(t)$ is a zero mean noise in the body frame.

1.1.2 Linear Gyro Calibration Methods

The most commonly used algorithm for spacecraft gyro calibration at the NASA Goddard Space Flight Center is the Davenport gyroscope calibration algorithm, presented by Davenport and Welter in [9]. From equation 1.5, the angular velocity is written without the noise as

$$\boldsymbol{\omega}(t) = C\boldsymbol{\omega}_g(t) - \mathbf{b} \quad (1.6)$$

where C and a constant bias, \mathbf{b} , are unknown. Estimates of C and \mathbf{b} , given as \hat{C} and $\hat{\mathbf{b}}$, respectively, are made based on pre-launch calibration and mounting of the gyros on the spacecraft. \hat{C} and $\hat{\mathbf{b}}$ are assumed to be close to the true C and \mathbf{b} . An estimate of the angular velocity is given as

$$\hat{\boldsymbol{\omega}}(t) = \hat{C}\boldsymbol{\omega}_g(t) - \hat{\mathbf{b}} \quad (1.7)$$

Subtracting equation 1.7 from 1.6 results in the following

$$\tilde{\boldsymbol{\omega}}(t) = \boldsymbol{\omega}(t) - \hat{\boldsymbol{\omega}}(t) = -M\hat{\boldsymbol{\omega}}(t) + \mathbf{d}$$

where $M = \mathbf{I} - C\hat{C}$ and $\mathbf{d} = (\mathbf{I} - M)\hat{\mathbf{b}} - \mathbf{b}$. Given the above assumptions, M and \mathbf{d} are small.

The calibration procedure consists of several controlled angular maneuvers of the spacecraft about each of the body axes. For a given controlled maneuver from an initial attitude represented as $\mathbf{q}(t_0)$ to a final attitude represented as $\mathbf{q}(t_f)$, an error, based on equation 2.6 in Section 2.1, is computed as

$$\mathbf{e} = v(\mathbf{q}(t_f) \otimes \hat{\mathbf{q}}(t_f, \hat{\boldsymbol{\omega}})) - \frac{1}{2} \int_{t_0}^{t_f} \tilde{\boldsymbol{\omega}}(\tau) d\tau$$

where $v(\mathbf{q}_f \otimes \hat{\mathbf{q}}(t_f, \hat{\boldsymbol{\omega}}))$ represents the vector part of the quaternion product, as computed using equation 1.4. The estimated final attitude, represented as $\hat{\mathbf{q}}(t_f, \hat{\boldsymbol{\omega}})$, is computed by propagating the initial quaternion, $\mathbf{q}(t_0)$, to t_f using the estimated angular velocity, $\hat{\boldsymbol{\omega}}$. The initial and final quaternions, $\mathbf{q}(t_0)$ and $\mathbf{q}(t_f)$, are computed by an accurate sensor, such as a star sensor. A least squares estimation approach is used to find M and \mathbf{d} which minimizes $\|\mathbf{e}\|^2$ over all the controlled maneuvers. The estimation is performed in batch mode by ground support personnel. A variation on this algorithm is presented in [10]. Adjustments are made to reduce the required volume of data, and to extend the algorithm to study individual gyro scale factor adjustments.

Another approach used in estimating the gyro calibration parameters is an extended Kalman filter (EKF). In contrast to a linear Kalman filter, an EKF estimates error terms in the desired states due to a nonlinear relationship, either in the state equation or in the measurement equation, or both. Typically the error terms are derived by expanding the nonlinear equation in a Taylor series [11]. Alternatively a perturbation method can be applied, as in [12]. The EKF algorithm is designed to estimate small corrections to nominal state estimates. In the case of gyro calibration, the calibration parameters are assumed to contain small errors. The transformation matrix, R_g , is considered to represent small rotations of each of the gyro axes away

from the corresponding body axes. The matrix is usually written as [13]

$$R_g = \mathbf{I} + \begin{bmatrix} 0 & m_{xy} & m_{xz} \\ m_{yx} & 0 & m_{yz} \\ m_{zx} & m_{zy} & 0 \end{bmatrix} = \mathbf{I} + M$$

where m_{ij} is the projection of the i-gyro axis on the j-body axis. The three gyro axes are described by unit vectors, closely aligned to the three corresponding spacecraft body axes. Therefore, m_{ij} is assumed to be a small misalignment angle. Similarly, the scale factor matrix Γ is written as

$$\Gamma = \mathbf{I} + \begin{bmatrix} k_x & 0 & 0 \\ 0 & k_y & 0 \\ 0 & 0 & k_z \end{bmatrix} = \mathbf{I} + K$$

where k_i are assumed to be small scale factor errors. The measured angular velocity is then given as

$$\boldsymbol{\omega}_g(t) = (\mathbf{I} + K)(\mathbf{I} + M)^T \boldsymbol{\omega}(t) + \mathbf{b} = \boldsymbol{\omega}(t) + \Delta\boldsymbol{\omega}(t) \quad (1.8)$$

where $\Delta\boldsymbol{\omega}(t)$ contains the calibration errors terms, including the bias. The product of KM^T is assumed to be small and is not included. $\Delta\boldsymbol{\omega}(t)$ is then written as

$$\Delta\boldsymbol{\omega}(t) = \Omega \mathbf{x} \quad (1.9)$$

Ω is a 3x12 matrix containing the angular velocity and \mathbf{x} is a 12x1 vector containing the terms m_{ij} , k_i , and \mathbf{b} . Equation 1.9 is typically augmented with the attitude into an EKF algorithm.

An early work by Farrenkopf and Iwens [14] documents the initial development of an onboard EKF algorithm to estimate the spacecraft attitude and only the gyro biases from equation 1.9. Murrell [15] documents the development of a similar onboard filtering algorithm to estimate the attitude and gyro biases. Additional works by Farrenkopf [16] and Markley and Reynolds [5] look at the accuracy of a single axis Kalman filter, estimating a single axis attitude angle and gyro bias. In later works, such as in [17], the state is expanded to include the gyro misalignment and scale factor errors from equation 1.9, along with other sensor calibration states. In estimating the misalignment and scale factor errors, observability is achieved by maneuvering the spacecraft about the spacecraft body axes.

Bar-Itzhack in [13] presents a pseudolinear Kalman filter that estimates the spacecraft attitude and gyro calibration parameters. In this approach, nonlinear equations are written as linear equations, dependent on state estimates. Equation 1.9 is included as the gyro error model in this approach. The typical gyro configuration consists of three gyros (or more to provide redundancy) mounted along the spacecraft body axes. In [18], a gyro quadruplet is calibrated. The gyro configuration considered contains more than three (prime) gyros, not aligned along the spacecraft body axes.

In [19], several gyro calibration algorithms are presented and compared, including the Davenport algorithm above. The 'Delta-Bias' algorithm, like the Davenport algorithm, estimates corrections to C and \mathbf{b} given in equation 1.6. An adjusted rate is computed for a given time interval using estimates of C and \mathbf{b} as in equation 1.7.

The difference between the measured rate and adjusted, or estimated, rate is assumed to be equal to a bias calculated independently during the given time interval. The angular velocity difference is cast as a linear function of the small differences between \hat{C} and C and between $\hat{\mathbf{b}}$ and \mathbf{b} . A least squares approach is used to estimate the corrections by minimizing the error between the calculated bias and the linearized angular velocity difference. Since the algorithm does not directly utilize an attitude comparison, it is not considered to be as accurate as the other linear calibration methods. It also requires at least four periods during which the rates are different, linearly independent, and constant.

The next algorithm presented in [19] is a ‘Filter-Smoother’ algorithm, based on the EKF discussed above, but with an additional smoother step run backwards. The gyro errors are determined by a weighted average of the forward and backward estimates. The final algorithm is the ‘BiCal’ algorithm, an extension of a batch-least squares attitude determination algorithm. The basic batch-least squares algorithm minimizes a loss function, composed of sensor residuals, in order to estimate the attitude. The residuals are computed as the difference between a measured vector observation and an estimate of the same vector. Typically the measured vectors are line of sight vectors to the sun, stars, or the earth, or a measurement of the earth’s magnetic field vector, all in body coordinates. The estimated observation vector is computed with an attitude estimate and the corresponding computed vector direction in inertial coordinates from an almanac or model. Since the observations

occur at different times, the attitude in the loss function must be the attitude at the time of the observation. In order to estimate a single attitude, an epoch attitude is propagated to each observation time using an approach such as that of equation 2.6 in Section 2.1. The angular velocity is expressed as a linear function of small errors in C and \mathbf{b} . The small errors are included in the states to be estimated through the minimization of the loss function.

Finally, several authors address the statistical characteristics of gyros and the noise sources. In [20], the noise characteristics of the rate-integrating gyros onboard the Cosmic Background Explorer (COBE) are evaluated. The noise sources are estimated using the single-axis Farrenkopf model above and also presented in [21]. In [4], Sedlak, et al. study the performance of rate sensing gyros onboard the Upper Atmosphere Research Satellite, the Extreme Ultraviolet Explorer, and the Rossi X-Ray Timing Explorer. The gyro noise characteristics are estimated by studying the Kalman filter covariance matrix evolution over time. The gyro bias trends are evaluated using a batch least-squares, differential correction attitude determination algorithm. The application of the Allan variance method in characterizing gyro error sources is presented in [22]. In [23], an alternative, online algorithm for estimating gyro noise parameters is presented. Finally, Reynolds [24] presents an optimal and sub-optimal method for estimating gyro noise parameters. The approach is based on maximum likelihood estimation and produces both noise estimates and uncertainties in the estimates.

1.1.3 Nonlinear Gyro Calibration Methods

The linear gyro calibration methods are designed to estimate small corrections to nominal, pre-launch estimates of the alignment, scale factor, and bias. A nonlinear approach could potentially estimate gyro alignment, scale factor, and biases of arbitrary size. A few approaches exist which utilize nonlinear estimation techniques, however there are shortcomings in all of the approaches. All the published methods tend to follow a similar Lyapunov development to determine stability in the estimation, most are driven by a measurable attitude error. Alonso, et al. in [25] develop a nonlinear estimator for relative attitude and rate estimation with an application to formation flying. Salcudean in [26] develops a nonlinear estimator for angular rate estimation. Both estimators are driven by a computed attitude error. However, in order to estimate the rate, both estimators require knowledge or estimation of spacecraft torques. The stability of the estimator developed by Salcudean requires an assumption that the system eventually behaves as a linear time invariant system.

In [27], Vik, et al. develop an angular velocity estimator, in addition to a position and velocity estimator, for use in a Global Positioning System (GPS)/Inertial Navigation System (INS). The angular velocity estimator is actually a nonlinear estimator for gyro calibration, similar to that designed in this thesis. The estimator is designed to estimate corrections to the gyro measurements, particularly misalignment and scale factor corrections, along with gyro biases. The misalignment and scale factor errors are assumed to be small, as given in equation 1.9. All the error

terms are modelled as exponentially decaying, first-order equations. The Lyapunov analysis proves that the estimator, given the above assumptions, is exponentially stable. A closed-loop analysis of the estimator, coupled with a feedback control law, is not presented.

Nonlinear estimators for gyro bias estimation are also examined by Boskovic, et al. in [28] and [29]. In [28], the bias is assumed to be constant, which differs from the exponentially decaying model of [27]. However, the bias is assumed to lie in a small, bounded set. Second order terms are neglected in the estimator development and in the Lyapunov proof of stability. The estimator is coupled with a controller, designed to drive the spacecraft rates to zero, and the spacecraft body coordinates to the inertial coordinates. With the second order terms neglected, the closed loop system is stable for the single scenario presented. In [29], the gyro bias estimator is designed for use in attitude tracking. Here the bias estimator is driven by a computed attitude error, as in [25], [26], and [27]. However, the attitude error is computed as a vector difference, rather than a rotational error, without consideration to the normality constraint of the attitude. The Lyapunov proof of stability is limited. An adaptive tracking controller is coupled to the estimator. Closed-loop stability is based on an assumption of the faster speed of the estimator as compared to the controller. A brief observation of the angular velocity tracking is provided, without proof.

1.2 Dissertation Outline

As the previous discussion indicates, combined estimator-controller designs for the attitude control of rigid flight vehicles are a subject of active research [27, 28, 29]. Successful design of such architectures is complicated by the fact that there is, in general, no separation principle for nonlinear systems. In contrast to linear systems, ‘certainty equivalence’ substitution of the states from an exponentially converging estimator into a nominally stabilizing, state feedback control law does not necessarily guarantee stable closed-loop operation for the coupled systems [30, 31]. In this work, one version of this problem is considered, in particular, the task of forcing the attitude of a rigid vehicle to asymptotically track a (time-varying) reference attitude using feedback from rate sensors with persistent nonzero errors. The analysis is presented in the following order.

The second chapter introduces the terminology used throughout the document. A high level overview of Lyapunov stability concepts is included. Finally, an introduction of the nonlinear control law is presented. This control law is used in combination with each of the gyro estimators in the closed loop stability analysis.

The third chapter presents the development of a nonlinear estimator for the case of constant gyro bias, combined with the nonlinear control scheme for attitude control of a spacecraft discussed in Chapter 2. In order to estimate the bias, an angular velocity estimator is utilized, similar in development to [26, 27], using the estimated bias state in a certainty equivalence fashion with the nonlinear control

law proposed by Egeland and Godhavn in [32]. The analysis demonstrates that the resulting system provides stable closed-loop operation with asymptotic tracking. The analysis is extended to consider the effects of uniformly bounded gyro noise on the stability analysis.

The fourth chapter presents a nonlinear estimator for estimating constant scale factors. The gyro bias estimator is extended to estimate the scale factors. The estimator is stable, and if the angular velocity is bounded, the attitude error is asymptotically stable. Additionally, if each axis of the angular velocity meets a persistency of excitation condition, the scale factor estimator is exponentially stable. Combining the scale factor estimator with the nonlinear control scheme results in stable tracking if an a priori bound is known for the scale factors. If the angular velocity meets the persistency of excitation condition, the closed loop system is asymptotically stable.

The fifth chapter presents a nonlinear estimator for the case of alignment errors. The estimator for the constant gyro bias is extended to estimate, instead, a constant alignment error. The algorithm does not require an assumption that the alignment errors are small. The analysis demonstrates that the estimator is stable, and the alignment estimates converge exponentially to the true alignment, under the necessary persistency of excitation conditions. Here the persistency of excitation condition confirms that the angular velocity must change directions in order to estimate the alignment. Finally, the estimator is combined with the controller of

[32]. The closed-loop system is nominally stable if an a priori bound is known on the alignment error. Asymptotic stability is achieved if the angular velocity meets the persistency of excitation condition.

The sixth chapter presents combinations of the three estimators. In each case, the estimator stability is addressed. The estimator is coupled to the nonlinear control algorithm and the stability is examined.

The seventh chapter presents a comparison between the nonlinear gyro calibration estimators and a linearized calibration algorithm. The three nonlinear gyro calibration estimators (and a combination of all three) are compared to the 'implicit' pseudo-linear algorithm developed by Bar-Itzhack and Harman [13].

The eighth chapter contains a summary of the research and concluding remarks. Areas of future research are outlined.

Chapter 2

Mathematical Overview

2.1 Terminology

This work presents nonlinear estimation algorithms designed to estimate gyro alignment, scale factor, and bias. Figure 2.1 shows a high level block diagram of the estimation scheme. The true satellite attitude and rate are again represented by the quaternion, \mathbf{q} and $\boldsymbol{\omega}(t)$, respectively. Sensors provide measurements of the attitude and rate. The attitude measurement is assumed to be perfect. The rate measurement, $\boldsymbol{\omega}_g(t)$, however is corrupted by the calibration errors. The rate measurement is used to propagate an estimate of the attitude, $\hat{\mathbf{q}}$, along with estimates of the calibration parameters, denoted generically as $\hat{\mathbf{a}}$ in figure 2.1. The true attitude is compared to the estimated attitude, and the rotational error between the two, $\tilde{\mathbf{q}}$, is used to correct the calibration estimates. The attitude and estimated angular velocity, $\hat{\boldsymbol{\omega}}$, computed with the estimated calibration components, are then available as input to a feedback control scheme.

Definitions of the attitude and rate are given in Chapter 1. Several additional

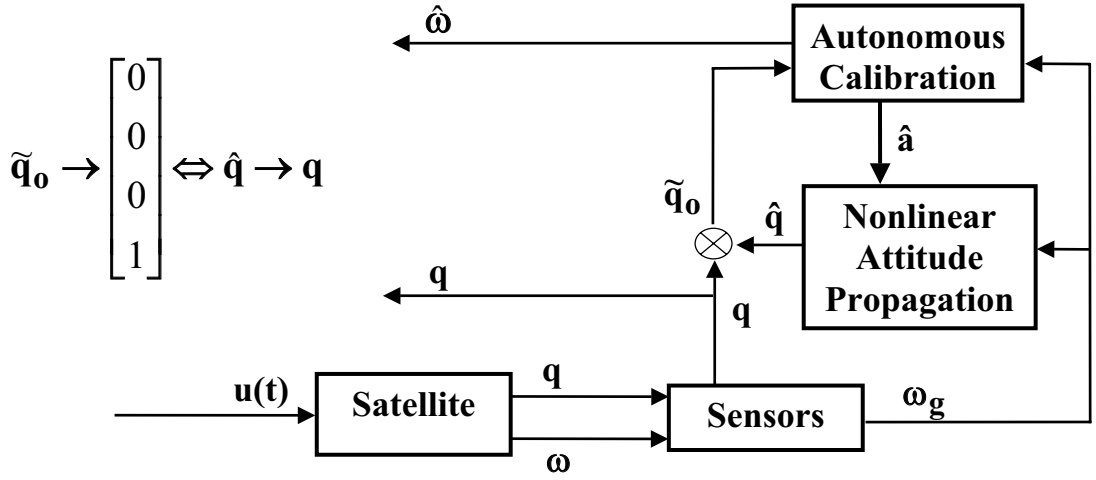


Figure 2.1: Estimation Approach

definitions are necessary in the development of the estimation and control algorithms. First, several definitions of vector and matrix norms are given, followed by additional equations pertaining to the attitude, rate, and calibration parameter definitions.

In this work all matrix norms are assumed to be the matrix induced two norm unless otherwise explicitly stated. For a general matrix X , the induced two-norm is computed as [33]

$$\|X\| = \|X\|_2 = (\lambda_{max}(X^T X))^{\frac{1}{2}}$$

All vector norms are assumed to be the Euclidean norm. For a general vector, $\mathbf{x} = [x_1, x_2 \dots x_n]^T$, the two-norm is [33]

$$\|\mathbf{x}\| = \|\mathbf{x}\|_2 = \left(\sum_{i=1}^n |x_i|^2 \right)^{\frac{1}{2}}$$

The sign function is defined as

$$\text{sign}(a) = \begin{cases} 1 & a > 0 \\ 0 & a = 0 \\ -1 & a < 0 \end{cases} \quad (2.1)$$

The norm of the rotation matrix is

$$\|R\| = 1$$

The determinant of the rotation matrix is [7]

$$|R| = 1$$

The rotation matrix is non-singular. The norm of the outer product of ε is

$$\|\varepsilon\varepsilon^T\| = [\lambda_{\max}((\varepsilon\varepsilon^T)^T\varepsilon\varepsilon^T)]^{\frac{1}{2}} = \|\varepsilon\|^2$$

The matrix $R(\mathbf{q}) - \mathbf{I}$ is used frequently in the development of the alignment estimator, and is given as

$$R(\mathbf{q}) - \mathbf{I} = -2\varepsilon^T\varepsilon\mathbf{I} + 2\varepsilon\varepsilon^T - 2\eta S(\varepsilon) \quad (2.2)$$

and the norm of $R(\mathbf{q}) - \mathbf{I}$ is

$$\|R(\mathbf{q}) - \mathbf{I}\| = \lambda_{\max}[4((\varepsilon^T\varepsilon)\mathbf{I} - \varepsilon\varepsilon^T)]^{\frac{1}{2}} = 2\|\varepsilon\|$$

The kinematic equation for the quaternion is given as

$$\dot{\mathbf{q}}(t) = \begin{bmatrix} \dot{\varepsilon}(t) \\ \dot{\eta}(t) \end{bmatrix} = \frac{1}{2}Q(\mathbf{q}(t))\boldsymbol{\omega}(t) \quad (2.3)$$

where $\boldsymbol{\omega}(t)$ is the spacecraft angular velocity in body coordinates and

$$Q(\mathbf{q}(t)) = \begin{bmatrix} \eta(t)\mathbf{I} + S(\boldsymbol{\varepsilon}(t)) \\ -\boldsymbol{\varepsilon}(t)^T \end{bmatrix} = \begin{bmatrix} Q_1(\mathbf{q}(t)) \\ -\boldsymbol{\varepsilon}(t)^T \end{bmatrix} \quad (2.4)$$

where, by inspection, $Q_1(\mathbf{q}(t)) = \eta(t)\mathbf{I} + S(\boldsymbol{\varepsilon}(t))$. The kinematic equation for an attitude matrix is [34]

$$\dot{R}(\mathbf{q}(t)) = -S(\boldsymbol{\omega}(t))R(\mathbf{q}(t)) \quad (2.5)$$

Note that for small $\boldsymbol{\varepsilon}$ and small $\boldsymbol{\omega}(t)$, the kinematic equation becomes

$$\begin{bmatrix} \dot{\boldsymbol{\varepsilon}}(t) \\ \dot{\eta}(t) \end{bmatrix} = \begin{bmatrix} \frac{1}{2}\boldsymbol{\omega}(t) \\ 0 \end{bmatrix} \quad (2.6)$$

The Davenport calibration algorithm presented in chapter 1 is based on equation 2.6.

The angular velocity, $\boldsymbol{\omega}(t)$, is again

$$\boldsymbol{\omega}(t) = R_g \Gamma_I \boldsymbol{\omega}_g(t) - \mathbf{b}(t) - \boldsymbol{\nu}(t)$$

This work considers only the case of three, orthogonal gyros. Therefore, $R_g = R(\mathbf{q}_g)$ is an orthogonal gyro alignment matrix, written as a function of the quaternion, \mathbf{q}_g .

If Γ , \mathbf{q}_g , and $\mathbf{b}(t)$ are known, an unbiased estimate of $\boldsymbol{\omega}(t)$ is

$$\hat{\boldsymbol{\omega}}(t) = C\boldsymbol{\omega}_g(t) - \mathbf{b}(t)$$

This work considers the case where Γ , \mathbf{q}_g , and $\mathbf{b}(t)$ are *unknown* and of *arbitrary* size.

In this work, the gyro alignment and scale factors are assumed to be constant.

In other words,

$$\dot{\mathbf{q}}_g(t) = \mathbf{0} \quad (2.7)$$

$$\dot{\gamma}_i(t) = 0 \quad (2.8)$$

The bias is initially assumed to be constant, then a 'random walk' is considered.

$$\dot{\mathbf{b}}(t) = 0 \quad (2.9)$$

and

$$\dot{\mathbf{b}}(t) = \boldsymbol{\nu}_b(t) \quad (2.10)$$

If $\hat{\mathbf{b}}(t)$, $\hat{\mathbf{q}}_g(t)$, and $\hat{\Gamma}_I(t)$ are estimates of the bias, alignment quaternion, and inverted scale factor matrix, respectively, an estimate of the angular velocity is given as

$$\hat{\boldsymbol{\omega}}(t) = R(\hat{\mathbf{q}}_g(t))\hat{\Gamma}_I(t)\boldsymbol{\omega}_g(t) - \hat{\mathbf{b}}(t) \quad (2.11)$$

For the case of bias error only (assuming the alignment and scale factor matrices are known), 2.11 becomes

$$\hat{\boldsymbol{\omega}}(t) = R(\mathbf{q}_g)\Gamma_I\boldsymbol{\omega}_g(t) - \hat{\mathbf{b}}(t) \quad (2.12)$$

The equation is rewritten accordingly for an alignment estimate with the bias and scale factor known, as

$$\hat{\boldsymbol{\omega}}(t) = R(\hat{\mathbf{q}}_g(t))\Gamma_I\boldsymbol{\omega}_g(t) - \mathbf{b}(t) \quad (2.13)$$

where $R(\hat{\mathbf{q}}_g(t))$ represents the rotation from gyro coordinates to an estimated body frame. Finally, for an estimate of the inverted scale factor matrix 2.11, with the

alignment and bias known, becomes

$$\hat{\boldsymbol{\omega}}(t) = R(\mathbf{q}_g)\hat{\Gamma}_I(t)\boldsymbol{\omega}_g(t) - \mathbf{b}(t) \quad (2.14)$$

or similarly for any other combination of terms.

The error terms for each of the calibration parameters are defined as

$$\tilde{\mathbf{b}}(t) = \mathbf{b} - \hat{\mathbf{b}}(t) \quad (2.15)$$

$$\tilde{\mathbf{q}}_g(t) = \mathbf{q}_g \otimes \hat{\mathbf{q}}_g(t)^{-1} \quad (2.16)$$

$$\tilde{\boldsymbol{\gamma}}_I(t) = \boldsymbol{\gamma}_I - \hat{\boldsymbol{\gamma}}_I(t) \quad (2.17)$$

where $\tilde{\boldsymbol{\gamma}}_I(t)$ is a scale factor error vector defined as the difference between the inverted true scale factors and the estimates, written in vector form.

2.2 Lyapunov Stability

All the stability proofs in the following chapters, both for the estimators and controllers, rely on Lyapunov stability arguments. The following theorems, corollaries, and lemmas detail conditions for both asymptotic and exponential convergence of nonautonomous systems.

Theorem 2.1 *Let x be an equilibrium point for $\dot{x}(t) = f(t, x)$, and $D \subset \mathbb{R}^n$ be a domain containing $x = 0$. Let $V : [0, \infty] \times D \rightarrow \mathbb{R}$ be a continuously differentiable function such that*

$$W_1(x) \leq V(t, x) \leq W_2(x)$$

$$\frac{\partial V}{\partial t} + \frac{\partial V}{\partial x} f(t, x) \leq -W_3(x)$$

$\forall t \geq 0, \forall x \in D$ where $W_1(x)$, $W_2(x)$, and $W_3(x)$ are continuous positive definite functions on D . Then, $x = 0$ is uniformly asymptotically stable. [30]

Corollary 2.1 Suppose that all the assumptions of Theorem 2.1 are satisfied with

$$W_1(x) \geq k_1 \|x\|^c, \quad W_2(x) \geq k_2 \|x\|^c, \quad W_3(x) \geq k_3 \|x\|^c$$

for some positive constants k_1 , k_2 , k_3 , and c . Then, $x = 0$ is exponentially stable.

Moreover, if the assumptions hold globally, then $x = 0$ is globally exponentially stable.

[30]

Lemma 2.1 Consider the function $\phi(t)$. If $\phi(t)$ is uniformly continuous and

$\lim_{t \rightarrow \infty} \int_0^\infty \phi(\tau) d\tau$ exists and is finite, then $\lim_{t \rightarrow \infty} \phi(t) = 0$. (Barbalat) [31]

Corollary 2.2 Consider the function $\phi(t)$. If $\phi(t), \dot{\phi}(t) \in \mathcal{L}_\infty$, and $\phi(t) \in \mathcal{L}_p$ for

some $p \in [1, \infty)$, then $\lim_{t \rightarrow \infty} \phi(t) = 0$. [31]

Lemma 2.2 If a scalar function $V(\mathbf{x}, t)$ satisfies the following conditions

$V(\mathbf{x}, t)$ is lower bounded

$\dot{V}(\mathbf{x}, t)$ is negative semi-definite

$\dot{V}(\mathbf{x}, t)$ is uniformly continuous in time

then $\dot{V}(\mathbf{x}, t) \rightarrow 0$ as $t \rightarrow \infty$. [35]

Lemma 2.3 *Consider the differential inequality*

$$\dot{v} \leq -[c - \beta_1(r_0, t)]v + \beta_2(r_0, t) + \rho \quad (2.18)$$

where $v(0) = v_0 \geq 0$, $c > 0$, and $r_0 \geq 0$ are constants, and β_1 and β_2 are class \mathcal{KL} functions. Then there exists a class \mathcal{KL} function β_v and a class \mathcal{K} function γ_v such that

$$v(t) \leq \beta_v(v_0 + r_0, t) + \gamma_v(\rho) \quad (2.19)$$

for all $t \geq 0$. Moreover, if $\beta_i = \alpha_i(r)e^{-\sigma_i t}$, $i = 1, 2$, where $\alpha_i \in \mathcal{K}$ and $\sigma_i > 0$, then there exists $\alpha_v \in \mathcal{K}$ and $\sigma_v > 0$ such that $\beta_v(r, t) = \alpha_v(r)e^{-\sigma_v t}$. [31]

In addition to the above theorems and lemmas, Young's inequality is used throughout the stability proofs. It is given in general form as [31]

$$xy \leq \kappa x^2 + \frac{1}{4\kappa} y^2 \quad (2.20)$$

where $\kappa > 0$. Young's inequality allows a product of variables to be separated into an inequality of the sum of the square of the variables. This inequality is used in the stability proofs to develop bounds on x , for example, given a known upper bound on y .

Finally, the \mathcal{L}_p norms are used in the stability proofs of the following chapters as well as in Corollary 2.2 above. For a function $x(t)$, the \mathcal{L}_p norms, $p \in [1, \infty)$ are defined as [31]

$$\|x(t)\|_p = \begin{cases} (\int_0^\infty |x(t)|^p dt)^{\frac{1}{p}} & p \in [1, \infty) \\ \sup_{t \geq 0} |x(t)| & p = \infty \end{cases}$$

A signal $x(t) \in \mathcal{L}_p$ means the corresponding \mathcal{L}_p norm for $x(t)$ is bounded

$$\|x(t)\|_p < \infty$$

2.3 A Nonlinear Attitude Controller

The attitude dynamics for a rigid spacecraft are given as

$$H\dot{\boldsymbol{\omega}}(t) - S(H\boldsymbol{\omega}(t))\boldsymbol{\omega}(t) = \mathbf{u}(t) \quad (2.21)$$

H is a constant, symmetric inertia matrix and $\mathbf{u}(t)$ is the applied external torque, for example, from attached rocket thrusters. The goal of the control law is to force the actual, measured attitude $\mathbf{q}(t)$ to asymptotically track a (generally) time-varying desired attitude $\mathbf{q}_d(t)$ and angular velocity $\boldsymbol{\omega}_d(t)$, related for consistency by equation 2.3 as

$$\dot{\mathbf{q}}_d(t) = \frac{1}{2}Q(\mathbf{q}_d(t))\boldsymbol{\omega}_d(t) \quad (2.22)$$

It is assumed that $\boldsymbol{\omega}_d(t)$ is bounded and differentiable with $\dot{\boldsymbol{\omega}}_d(t)$ also bounded.

The attitude tracking error is computed with equation 1.4 as

$$\tilde{\mathbf{q}}_c(t) = \begin{bmatrix} \tilde{\boldsymbol{\epsilon}}_c(t) \\ \tilde{\eta}_c(t) \end{bmatrix} = \mathbf{q}(t) \otimes \mathbf{q}_d^{-1}(t) \quad (2.23)$$

Comparing actual and desired rates in a common frame, the rate tracking error is

$$\tilde{\boldsymbol{\omega}}_c(t) = \boldsymbol{\omega}(t) - R(\tilde{\mathbf{q}}_c(t))\boldsymbol{\omega}_d(t) \quad (2.24)$$

where $R(\tilde{\mathbf{q}}_c(t))$ transforms the angular velocity from the desired body frame to the actual body frame. With these definitions, the tracking error kinematically obeys

the differential equation [8]

$$\dot{\tilde{\mathbf{q}}}_c(t) = \frac{1}{2}Q(\tilde{\mathbf{q}}_c(t))\tilde{\boldsymbol{\omega}}_c(t) \quad (2.25)$$

The nonlinear tracking control strategy proposed by Egeland and Godhavn in [32] employs the control law

$$\mathbf{u}(t) = -K_D\mathbf{s}(t) + H\boldsymbol{\alpha}_r(t) - S(H\boldsymbol{\omega}(t))\boldsymbol{\omega}_r(t) \quad (2.26)$$

K_D is any symmetric, positive definite matrix and $\mathbf{s}(t)$ is an error defined as

$$\mathbf{s}(t) = \tilde{\boldsymbol{\omega}}_c(t) + \lambda\tilde{\boldsymbol{\epsilon}}_c(t) = \boldsymbol{\omega}(t) - \boldsymbol{\omega}_r(t) \quad (2.27)$$

where λ is any positive constant. The reference angular velocity $\boldsymbol{\omega}_r(t)$ is computed as

$$\boldsymbol{\omega}_r(t) = R(\tilde{\mathbf{q}}_c(t))\boldsymbol{\omega}_d(t) - \lambda\tilde{\boldsymbol{\epsilon}}_c(t) \quad (2.28)$$

and

$$\boldsymbol{\alpha}_r(t) = \dot{\boldsymbol{\omega}}_r(t) = R(\tilde{\mathbf{q}}_c(t))\dot{\boldsymbol{\omega}}_d(t) - S(\tilde{\boldsymbol{\omega}}_c(t))R(\tilde{\mathbf{q}}_c(t))\boldsymbol{\omega}_d(t) - \lambda Q_1(\tilde{\mathbf{q}}_c(t))\tilde{\boldsymbol{\omega}}_c(t) \quad (2.29)$$

The stability of the closed loop system is analyzed with the Lyapunov function

$$V_c(t) = \frac{1}{2}\mathbf{s}(t)^T H\mathbf{s}(t)$$

The derivative of $V_c(t)$ is

$$\dot{V}_c(t) = \mathbf{s}(t)^T H\dot{\mathbf{s}}(t)$$

Computing the derivative of $\mathbf{s}(t)$ in equation 2.27, and substituting it in $\dot{V}_c(t)$, along with equations 2.26, 2.29, and 2.21, results in

$$\begin{aligned}\dot{V}_c(t) &= \mathbf{s}(t)^T S(H\boldsymbol{\omega}(t))\boldsymbol{\omega}(t) - \mathbf{s}(t)^T K_D \mathbf{s}(t) + \mathbf{s}(t)^T H\boldsymbol{\alpha}_r(t) - \mathbf{s}(t)^T S(H\boldsymbol{\omega}(t))\boldsymbol{\omega}_r(t) \\ &\quad - \mathbf{s}(t)^T H\boldsymbol{\alpha}_r(t)\end{aligned}$$

Since $\mathbf{s}(t) = \boldsymbol{\omega}(t) - \boldsymbol{\omega}_r(t)$, rearranging the terms gives

$$\dot{V}_c(t) = -\mathbf{s}(t)^T K_D \mathbf{s}(t)$$

Therefore by Corollary 2.1, $\mathbf{s}(t)$ goes to zero exponentially fast.

The attitude error, $\tilde{\boldsymbol{\epsilon}}_c(t)$, is bounded by definition. The angular velocity error is also bounded, since $\mathbf{s}(t) = \tilde{\boldsymbol{\omega}}_c(t) + \lambda\tilde{\boldsymbol{\epsilon}}_c(t)$ and both $\mathbf{s}(t)$ and $\tilde{\boldsymbol{\epsilon}}_c(t)$ are bounded.

The squared norm of $\mathbf{s}(t)$ is

$$\|\mathbf{s}(t)\|^2 = \|\tilde{\boldsymbol{\omega}}_c(t)\|^2 + 2\lambda\boldsymbol{\omega}(t)^T \tilde{\boldsymbol{\epsilon}}_c(t) + \lambda^2\|\tilde{\boldsymbol{\epsilon}}_c(t)\|^2 \quad (2.30)$$

Integrating equation 2.30

$$\begin{aligned}\int_0^T \|\mathbf{s}(\tau)\|^2 dt &= \int_0^T \|\tilde{\boldsymbol{\omega}}_c(\tau)\|^2 d\tau \\ &\quad + \lambda^2 \int_0^T \|\tilde{\boldsymbol{\epsilon}}_c(\tau)\|^2 d\tau + 2\lambda \int_0^T \tilde{\boldsymbol{\omega}}_c(\tau)^T \tilde{\boldsymbol{\epsilon}}_c(\tau) d\tau\end{aligned} \quad (2.31)$$

But, $\tilde{\boldsymbol{\omega}}_c(t)^T \tilde{\boldsymbol{\epsilon}}_c(t) = -2\dot{\tilde{\eta}}_c(t)$, so the last term in equation 2.31 becomes $4\lambda[\tilde{\eta}_c(0) - \tilde{\eta}_c(T)]$, which is bounded for all T by $\beta < \infty$. Equation 2.31 is rewritten as

$$\begin{aligned}\int_0^T \|\mathbf{s}(\tau)\|^2 dt - \beta &= \int_0^T \|\tilde{\boldsymbol{\omega}}_c(\tau)\|^2 d\tau \\ &\quad + \lambda^2 \int_0^T \|\tilde{\boldsymbol{\epsilon}}_c(\tau)\|^2 d\tau\end{aligned} \quad (2.32)$$

Since $\mathbf{s}(t) \rightarrow 0$ exponentially fast, $\mathbf{s}(t) \in \mathcal{L}_2$. Therefore the terms on the right side of equation 2.32 must also be in \mathcal{L}_2 .

$$\tilde{\boldsymbol{\omega}}_c(t) \in \mathcal{L}_2, \tilde{\boldsymbol{\varepsilon}}_c(t) \in \mathcal{L}_2$$

Since $\mathbf{s}(t)$ is bounded, $\tilde{\boldsymbol{\omega}}_c(t)$ and $\tilde{\boldsymbol{\varepsilon}}_c(t)$ are also bounded,

$$\tilde{\boldsymbol{\omega}}_c(t), \tilde{\boldsymbol{\varepsilon}}_c(t) \in \mathcal{L}_2 \cap \mathcal{L}_\infty$$

Since $\dot{\tilde{\boldsymbol{\varepsilon}}}_c(t) = \frac{1}{2}[\tilde{\eta}_c(t)\mathbf{I} + S(\tilde{\boldsymbol{\varepsilon}}_c(t))]\tilde{\boldsymbol{\omega}}_c(t)$ and $\tilde{\boldsymbol{\omega}}_c(t)$ is bounded, $\dot{\tilde{\boldsymbol{\varepsilon}}}_c(t)$ is therefore bounded

$$\dot{\tilde{\boldsymbol{\varepsilon}}}_c(t) \in \mathcal{L}_\infty$$

By Lemma 2.1, since $\tilde{\boldsymbol{\varepsilon}}_c(t) \in \mathcal{L}_2 \cap \mathcal{L}_\infty$ and $\dot{\tilde{\boldsymbol{\varepsilon}}}_c(t) \in \mathcal{L}_\infty$, $\|\tilde{\boldsymbol{\varepsilon}}_c(t)\| \rightarrow 0$ as $t \rightarrow \infty$. Since $\boldsymbol{\omega}(t)$, $\boldsymbol{\omega}_d(t)$, $\dot{\boldsymbol{\omega}}(t)$, and $\dot{\boldsymbol{\omega}}_d(t)$ are all bounded, a similar argument establishes that $\|\tilde{\boldsymbol{\omega}}_c(t)\| \rightarrow 0$ as $t \rightarrow \infty$. Asymptotically perfect tracking is obtained with the above control scheme, given noise free measurements of the states $\boldsymbol{\omega}(t)$ and $\mathbf{q}(t)$.

In this work, $\boldsymbol{\omega}(t)$ is not known precisely. Rather, an estimate of $\boldsymbol{\omega}(t)$ is provided, for example, by equations 2.11 through 2.14. Figure 2.2 shows the addition of the nonlinear feedback controller to figure 2.1. The true angular velocity, $\boldsymbol{\omega}(t)$, is not available for feedback into the control algorithm, only $\hat{\boldsymbol{\omega}}(t)$ is available. This work considers the stability of a certainty equivalence substitution of $\hat{\boldsymbol{\omega}}(t)$ into the control law of equation 2.26. With $\hat{\boldsymbol{\omega}}(t)$ replacing $\boldsymbol{\omega}(t)$, the error metric $\mathbf{s}(t)$ becomes

$$\hat{\mathbf{s}}(t) = \hat{\boldsymbol{\omega}}(t) - \boldsymbol{\omega}_r(t)$$

The difference between $\mathbf{s}(t)$ and $\hat{\mathbf{s}}(t)$ is given as

$$\tilde{\mathbf{s}}(t) = \mathbf{s}(t) - \hat{\mathbf{s}}(t) = \boldsymbol{\omega}(t) - \hat{\boldsymbol{\omega}}(t)$$

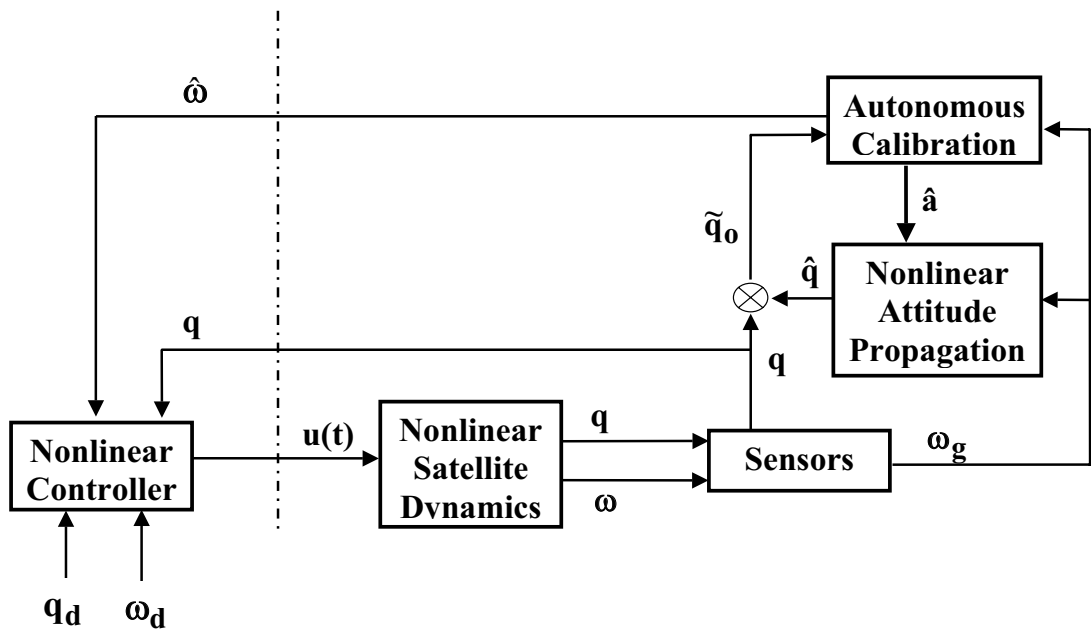


Figure 2.2: Closed Loop Control

In the case of a gyro bias, $\tilde{\mathbf{s}}(t)$ becomes

$$\tilde{\mathbf{s}}(t) = (R(\mathbf{q}_g)\Gamma_I\boldsymbol{\omega}_g(t) - \mathbf{b}) - (R(\mathbf{q}_g)\Gamma_I\boldsymbol{\omega}_g(t) - \hat{\mathbf{b}}(t)) = -\tilde{\mathbf{b}}(t)$$

In the case of a scale factor error, $\tilde{\mathbf{s}}(t)$ becomes

$$\tilde{\mathbf{s}}(t) = (R(\mathbf{q}_g)\Gamma_I\boldsymbol{\omega}_g(t) - \mathbf{b}) - (R(\mathbf{q}_g)\hat{\Gamma}_I(t)\boldsymbol{\omega}_g(t) - \mathbf{b}) = R(\mathbf{q}_g)\tilde{\Gamma}_I(t)\boldsymbol{\omega}_g(t)$$

where $\tilde{\Gamma}_I(t) = \text{diag}\{\tilde{\gamma}_I(t)\}$. Finally, given an alignment error, $\tilde{\mathbf{s}}(t)$ becomes

$$\tilde{\mathbf{s}}(t) = (R(\mathbf{q}_g)\Gamma_I\boldsymbol{\omega}_g(t) - \mathbf{b}) - (R(\hat{\mathbf{q}}_g(t))\Gamma_I\boldsymbol{\omega}_g(t) - \mathbf{b}) = (R(\tilde{\mathbf{q}}_g(t)) - \mathbf{I})R(\hat{\mathbf{q}}_g(t))\Gamma_I\boldsymbol{\omega}_g(t)$$

where $R(\tilde{\mathbf{q}}_g(t)) = R(\mathbf{q}_g)R(\hat{\mathbf{q}}_g(t))^T$. Each of the miscalibrations are first considered individually and then in combinations.

In a nonlinear system there are no guaranteed closed loop stability properties when a stable nonlinear estimator is combined with a stable nonlinear controller, as there are in a linear system. [31] For example, given the following system

$$\dot{x} = u + \theta x^2$$

where θ is unknown. Choose the control law as $u = -x - \hat{\theta}x^2$. $\hat{\theta}$ comes from an estimator designed such that $\hat{\theta}$ is exponentially converging to θ .

$$\tilde{\theta}(t) = \tilde{\theta}(0)e^{-kt}$$

The closed loop equation is therefore

$$\dot{x} = -x + \tilde{\theta}(0)x^2e^{-kt} \tag{2.33}$$

The explicit solution of equation 2.33 is

$$x(t) = \frac{2x(0)}{x(0)\tilde{\theta}(0)e^{-t} + [2 - x(0)\tilde{\theta}(0)]e^t}$$

If $\tilde{\theta}(0)x(0) > 2$, $x(t) = \infty$ in a finite time $t < \infty$. The finite escape time is

$$t_{esc} = \frac{1}{2} \ln \frac{x(0)\tilde{\theta}(0)}{x(0)\tilde{\theta}(0) - 2}$$

Figure 2.3(a) shows the convergence of $\tilde{\theta}$ to zero, and figure 2.3(b) shows $x(t)$ escaping to infinity. Recall from equation 2.21 that quadratic nonlinearities are present in the

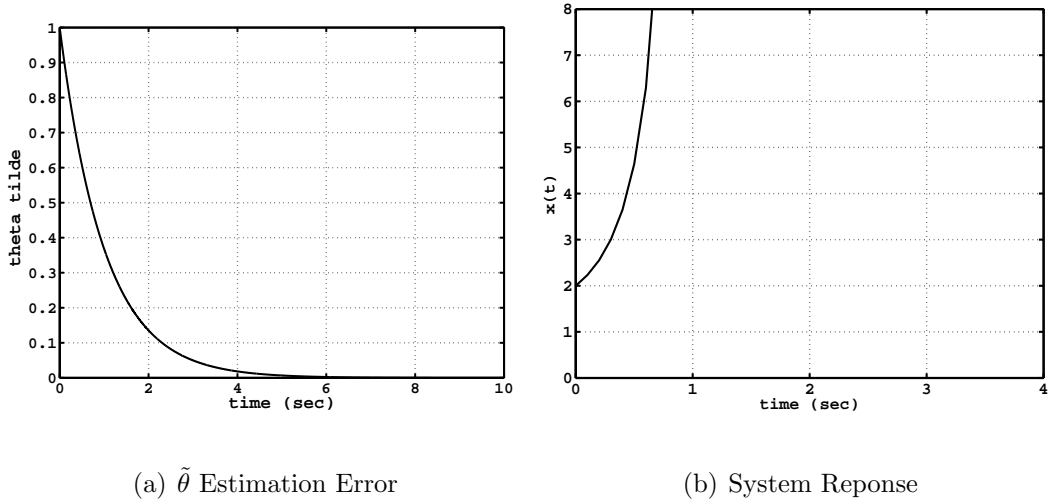


Figure 2.3: Coupled Estimator/Controller Errors With Gyro Bias

rigid body attitude dynamics. The above example illustrates the need to include a closed loop stability analysis when nonlinear estimators and controllers are coupled.

Chapter 3

Gyro Bias Calibration

3.1 Nonlinear Estimator for Constant Gyro Bias

The first estimator presented is the gyro bias estimator. Following the estimator proposed in [27], a state estimator for the attitude and bias is defined as

$$\dot{\hat{\mathbf{q}}}(t) = \frac{1}{2}Q(\hat{\mathbf{q}}(t))R(\tilde{\mathbf{q}}_o(t))^T[\hat{\boldsymbol{\omega}}(t) + k\tilde{\boldsymbol{\varepsilon}}_o(t)\text{sign}(\tilde{\eta}_o(t))] \quad (3.1)$$

$$\dot{\hat{\mathbf{b}}}(t) = -\frac{\alpha}{2}\tilde{\boldsymbol{\varepsilon}}_o(t)\text{sign}(\tilde{\eta}_o(t)) \quad (3.2)$$

where $\hat{\boldsymbol{\omega}}(t)$ is given in 2.12 and is repeated here as

$$\hat{\boldsymbol{\omega}}(t) = \boldsymbol{\omega}_g(t) - \hat{\mathbf{b}}(t) \quad (3.3)$$

Unlike [27], the bias here is considered to be persistent (constant). The scale factor and alignment are assumed known and incorporated into the gyro measurement. The gain k is chosen as a positive constants (note also that 3.2 is scaled by 1 sec^{-2}). Similarly, the learning rate, α , is also a positive constant. Essentially, $\hat{\mathbf{q}}(t)$ is a prediction of the attitude at time t , propagated with the kinematic equation using the measured angular velocity and the current bias estimate. The attitude error

is the relative orientation between the predicted attitude provided by equation 3.1 and the true attitude provided by the measured attitude, $\mathbf{q}(t)$. The attitude error is computed using equation 1.4 as

$$\tilde{\mathbf{q}}_o(t) = \begin{bmatrix} \tilde{\boldsymbol{\varepsilon}}_o(t) \\ \tilde{\eta}_o(t) \end{bmatrix} = \mathbf{q}(t) \otimes \hat{\mathbf{q}}(t)^{-1} \quad (3.4)$$

The term $R(\tilde{\mathbf{q}}_o(t))^T$ in equation 3.1 transforms the angular velocity terms from the body frame to the estimator frame.

The kinematic equation for the attitude error quaternion has the same form as the quaternion kinematic equation in equation 2.3. The angular velocity associated with the attitude error quaternion is the difference between the angular velocity of the body coordinates and the angular velocity of the estimator coordinates (resolved in body coordinates) [36]. Therefore, with equation 2.3, the definition given in equation 2.4, equation 3.1, and noting that $R(\tilde{\mathbf{q}}_o(t))\tilde{\boldsymbol{\varepsilon}}_o(t) = \tilde{\boldsymbol{\varepsilon}}_o(t)$ (since $\tilde{\boldsymbol{\varepsilon}}_o(t)$ points along the eigenaxis of the rotation), the kinematic equation for $\tilde{\mathbf{q}}_o(t)$ is given as

$$\dot{\tilde{\mathbf{q}}}_o(t) = \frac{1}{2} \begin{bmatrix} Q_1(\tilde{\mathbf{q}}_o(t)) \\ -\tilde{\boldsymbol{\varepsilon}}_o(t)^T \end{bmatrix} (-\tilde{\mathbf{b}}(t) - k\tilde{\boldsymbol{\varepsilon}}_o(t)\text{sign}(\tilde{\eta}_o(t))) \quad (3.5)$$

The derivative of $\tilde{\mathbf{b}}(t)$ is determined by differentiating equation 2.15, and substituting equations 3.2 and 2.9.

$$\dot{\tilde{\mathbf{b}}}(t) = \frac{\alpha}{2}\tilde{\boldsymbol{\varepsilon}}_o(t)\text{sign}(\tilde{\eta}_o(t)) \quad (3.6)$$

Note that the equilibrium states for 3.5 and 3.6 are

$$\begin{bmatrix} \tilde{\mathbf{q}}_o(t)^T & \tilde{\mathbf{b}}(t)^T \end{bmatrix} = \begin{bmatrix} 0 & 0 & 0 & \pm 1 & 0 & 0 & 0 \end{bmatrix}$$

Theorem 3.1 For any measured angular velocity, $\boldsymbol{\omega}_g(t)$, the equilibrium states of the system 3.5 and 3.6 are exponentially stable. In particular, $\hat{\mathbf{b}}(t) \rightarrow \mathbf{b}$ exponentially fast from any initial conditions $\hat{\mathbf{q}}(t_0)$ and $\hat{\mathbf{b}}(t_0)$.

Proof: Choose a Lyapunov function as

$$V_o(t) = \frac{1}{2\alpha} \tilde{\mathbf{b}}(t)^T \tilde{\mathbf{b}}(t) + \frac{1}{2} \begin{cases} (\tilde{\eta}_o(t) - 1)^2 + \tilde{\boldsymbol{\varepsilon}}_o(t)^T \tilde{\boldsymbol{\varepsilon}}_o(t) & \tilde{\eta}_o(t) \geq 0 \\ (\tilde{\eta}_o(t) + 1)^2 + \tilde{\boldsymbol{\varepsilon}}_o(t)^T \tilde{\boldsymbol{\varepsilon}}_o(t) & \tilde{\eta}_o(t) < 0 \end{cases}$$

$V_o(t)$ is continuous. The derivative of $V_o(t)$ is

$$\dot{V}_o(t) = \frac{1}{\alpha} \tilde{\mathbf{b}}(t)^T \dot{\tilde{\mathbf{b}}}(t) + \begin{cases} (\tilde{\eta}_o(t) - 1) \dot{\tilde{\eta}}_o(t) + \tilde{\boldsymbol{\varepsilon}}_o(t)^T \dot{\tilde{\boldsymbol{\varepsilon}}}_o(t) & \tilde{\eta}_o(t) \geq 0 \\ (\tilde{\eta}_o(t) + 1) \dot{\tilde{\eta}}_o(t) + \tilde{\boldsymbol{\varepsilon}}_o(t)^T \dot{\tilde{\boldsymbol{\varepsilon}}}_o(t) & \tilde{\eta}_o(t) < 0 \end{cases} \quad (3.7)$$

Noting that $\tilde{\boldsymbol{\varepsilon}}_o(t)^T \dot{\tilde{\boldsymbol{\varepsilon}}}_o(t) + \tilde{\eta}_o(t) \dot{\tilde{\eta}}_o(t) = 0$ (including the left and right derivatives of $\tilde{\eta}_o(t) = 0$), for all t , equation 3.7 is

$$\dot{V}_o(t) = -\frac{k}{2} \tilde{\boldsymbol{\varepsilon}}_o(t)^T \tilde{\boldsymbol{\varepsilon}}_o(t)$$

This establishes that $\tilde{\mathbf{b}}(t)$, $\tilde{\boldsymbol{\varepsilon}}_o(t)$, and $\tilde{\eta}_o(t)$ are globally, uniformly bounded. Moreover, $V_o(t)$ is a continuous, twice differentiable function with

$$\ddot{V}_o(t) = \frac{k}{4} \tilde{\boldsymbol{\varepsilon}}_o(t)^T Q_1(\tilde{\mathbf{q}}_o(t)) [\tilde{\mathbf{b}}(t) + k \tilde{\boldsymbol{\varepsilon}}_o(t) \text{sign}(\tilde{\eta}_o(t))]$$

which is bounded. Lemma 2.1 then shows that $\|\tilde{\boldsymbol{\varepsilon}}_o(t)\| \rightarrow 0$ as $t \rightarrow \infty$.

Since all signals in the estimator are bounded, the system 3.5 and 3.6 can be further analyzed, in the given format, as a linear time-varying system [30] $\dot{\mathbf{x}}(t) =$

$A(t)\mathbf{x}(t)$ where

$$\mathbf{x}(t) = \begin{bmatrix} \tilde{\boldsymbol{\varepsilon}}_o(t) \\ \tilde{\mathbf{b}}(t) \end{bmatrix}$$

$$A(t) = \begin{bmatrix} -\frac{k}{2}\text{sign}(\tilde{\eta}_o(t))Q_1(\tilde{\mathbf{q}}_o(t)) & -\frac{1}{2}Q_1(\tilde{\mathbf{q}}_o(t)) \\ \frac{\alpha}{2}\text{sign}(\tilde{\eta}_o(t))I & 0 \end{bmatrix}$$

where, by virtue of the above Lyapunov analysis, all terms in the matrix $A(t)$ are known to be bounded for all $t \geq t_0$. Rewriting $\dot{V}_o(t)$ as $\dot{V}_o(t) = -\mathbf{x}(t)^T C^T C \mathbf{x}(t) \leq 0$, where $C = \begin{bmatrix} \sqrt{\frac{k}{2}}I & 0 \end{bmatrix}$, Theorem 4.5 and the discussion on pp.626-628 in [30] shows that the equilibrium point $\mathbf{x}(t) = 0$ of this equivalent system is exponentially stable if the pair $(A(t), C)$ is uniformly completely observable (UCO). Since observability properties are unchanged under output feedback [30], $(A(t), C)$ are UCO if the pair $(A(t) - K(t)C, C)$ is uniformly observable for any piecewise, continuous and bounded matrix $K(t)$. Choose $K(t)$ as

$$K(t) = \begin{bmatrix} -\sqrt{\frac{k}{2}}\text{sign}(\tilde{\eta}_o(t))Q_1(\tilde{\mathbf{q}}_o(t)) \\ \sqrt{\frac{\alpha}{2k}}\text{sign}(\tilde{\eta}_o(t))I \end{bmatrix}$$

$K(t)$ is piecewise continuous based on the following properties. Note from the above Lyapunov analysis that $\|\tilde{\boldsymbol{\varepsilon}}_o(t)\| \rightarrow 0$. Since $\|\tilde{\mathbf{q}}_o(t)\|^2 = 1 = \|\tilde{\boldsymbol{\varepsilon}}_o(t)\|^2 + |\tilde{\eta}_o(t)|^2$ for any time, t , there exists a time, $T > 0$, such that $\|\tilde{\eta}_o(t)\| > 0$ for all $t > T$. Since $\tilde{\eta}_o(t)$ therefore cannot pass through zero for $t > T$, $\text{sign}(\tilde{\eta}_o(t))$ is constant for all $t > T$ and, hence, $K(t)$ is a piecewise continuous function of time.

The state transition matrix for the pair $(A(t) - K(t)C, C)$ is

$$\Phi(\tau, t) = \begin{bmatrix} \mathbf{I} & \Sigma(\tau, t) \\ 0 & \mathbf{I} \end{bmatrix} \quad (3.8)$$

where $\Sigma(\tau, t) = -\frac{1}{2} \int_t^\tau Q_1(\tilde{\mathbf{q}}_o(\sigma)) d\sigma$, with $Q_1(\mathbf{q}(t))$ defined in equation 2.4. The observability Grammian is then [33]

$$W(t, t+T) = \int_t^{t+T} \Phi(\tau, t)^T C^T C \Phi(\tau, t) d\tau = \int_t^{t+T} \begin{bmatrix} \frac{k}{2} \mathbf{I} & \frac{k}{2} \Sigma(\tau, t) \\ \frac{k}{2} \Sigma(\tau, t)^T & \frac{k}{2} \Sigma(\tau, t)^T \Sigma(\tau, t) \end{bmatrix} d\tau \quad (3.9)$$

The system is UCO if there exists a $T > 0$ and positive constants $\alpha_1 < \infty, \alpha_2 > 0$ such that, for all $t \geq t_0$, $\alpha_1 \mathbf{I} \geq W(t, t+T) \geq \alpha_2 \mathbf{I}$. Using Lemma 13.4 of [30], this property is assured if $Q_1(\tilde{\mathbf{q}}_o(t))$ and $\frac{d}{dt} Q_1(\tilde{\mathbf{q}}_o(t))$ are bounded, and there exist positive constants T_2, β_1 , and a finite constant β_2 such that, for all $t \geq t_0$,

$$\beta_2 \mathbf{I} \geq \int_t^{t+T_2} Q_1(\tilde{\mathbf{q}}_o(\tau))^T Q_1(\tilde{\mathbf{q}}_o(\tau)) d\tau \geq \beta_1 \mathbf{I} \quad (3.10)$$

$Q_1(\tilde{\mathbf{q}}_o(t))$ is bounded, since all the signals in the estimator are bounded, hence the upper bound in 3.10 is satisfied. Substituting the equality $Q_1(\tilde{\mathbf{q}}_o(t))^T Q_1(\tilde{\mathbf{q}}_o(t)) = \mathbf{I} - \tilde{\mathbf{e}}_o(t) \tilde{\mathbf{e}}_o(t)^T$ into equation 3.10 results in

$$\infty > \beta_2 \mathbf{I} \geq \int_t^{t+T_2} (\mathbf{I} - \tilde{\mathbf{e}}_o(t) \tilde{\mathbf{e}}_o(t)^T) d\tau \geq \beta_1 \mathbf{I} > 0 \quad (3.11)$$

Recall that it has been shown that $\|\tilde{\mathbf{e}}_o(t)\| \rightarrow 0$ asymptotically. Thus, for any $\delta > 0$, there exists a $T_1(\delta) > t_0$ such that $\|\tilde{\mathbf{e}}_o(t)\| < \delta$ for all $t \geq t_0 + T_1$. Taking any $\delta < 1$,

<i>Quaternion</i>	<i>Value</i>	<i>Bias</i>	<i>Value</i>
$\mathbf{q}(t_0)$	$[0, 0, 1, 0]^T$	$\mathbf{b}(t)$	$[0.5, -0.5, 0.5]^T \frac{deg}{sec}$
$\hat{\mathbf{q}}(t_0)$	$[0, 0, 0, 1]^T$	$\hat{\mathbf{b}}(t_0)$	$[0, 0, 0]^T \frac{deg}{sec}$

Table 3.1: Bias Estimator Simulation Initial Conditions

any $T_2 > T_1$, and any \mathbf{z} in \mathbb{R}^3

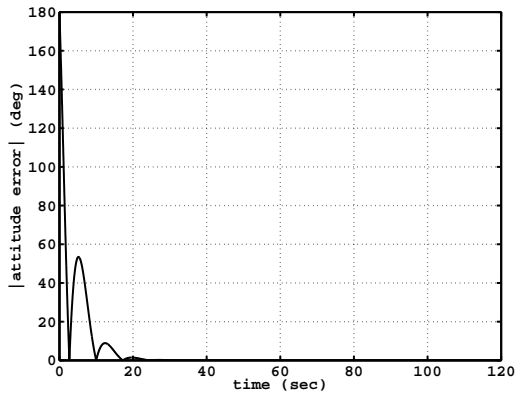
$$\infty > (T_2 - T_1) \|\mathbf{z}\|^2 > \mathbf{z}^T \left[\int_t^{t+T_2} (\mathbf{I} - \tilde{\boldsymbol{\varepsilon}}_o(\tau) \tilde{\boldsymbol{\varepsilon}}_o(\tau)^T) d\tau \right] \mathbf{z} > (1 - \delta^2)(T_2 - T_1) \|\mathbf{z}\|^2 > 0 \quad (3.12)$$

Finally, $\frac{d}{dt} Q_1(\tilde{\mathbf{q}}_o(t)) = \dot{\tilde{\boldsymbol{\varepsilon}}}_o(t) + \dot{\tilde{\boldsymbol{\eta}}}_o(t)$ is bounded, since all the terms in 3.5 are bounded.

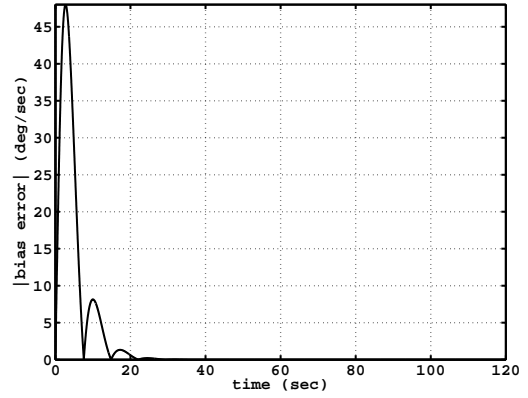
This demonstrates the required UCO property. The PE condition is satisfied for **any** $\boldsymbol{\omega}_g(t)$, and therefore $\tilde{\boldsymbol{\varepsilon}}_o(t)$ and $\tilde{\mathbf{b}}(t)$ approach zero exponentially fast. \square

3.2 Estimator Simulation Results

The gyro bias estimator is tested with a Matlab simulation. Table 3.1 lists the initial conditions for the estimator, as well as the true gyro bias. The gains are chosen as $k = 1$ and $\alpha = 1$. First, the angular velocity is $\boldsymbol{\omega}(t) = [3, -4, 5]$ deg/sec. Figures 3.1(a) and 3.1(b) show that both the attitude prediction error, $\|\tilde{\boldsymbol{\varepsilon}}_o(t)\|$, and the bias estimation error, $\|\tilde{\mathbf{b}}(t)\|$, converge to zero exponentially fast. Figures 3.2(a) and 3.2(b) show the attitude predictions errors and bias estimation errors with $\alpha = 0.5$. The transients are smaller, but the convergence time is slightly longer. Next the

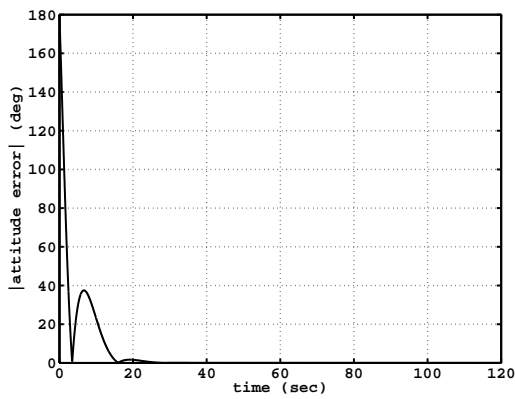


(a) Attitude Prediction Error

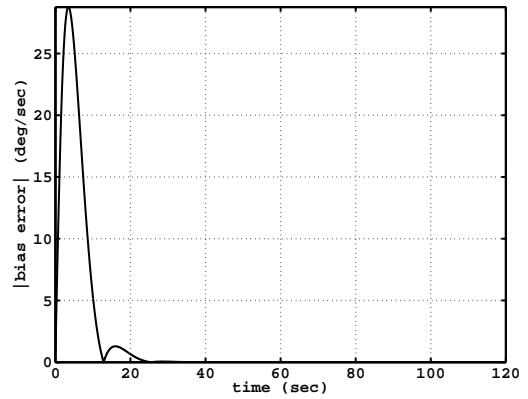


(b) Gyro Bias Estimation Error

Figure 3.1: Gyro Bias Estimator Errors, $\omega(t) = [3, -4, 5]$ deg/sec



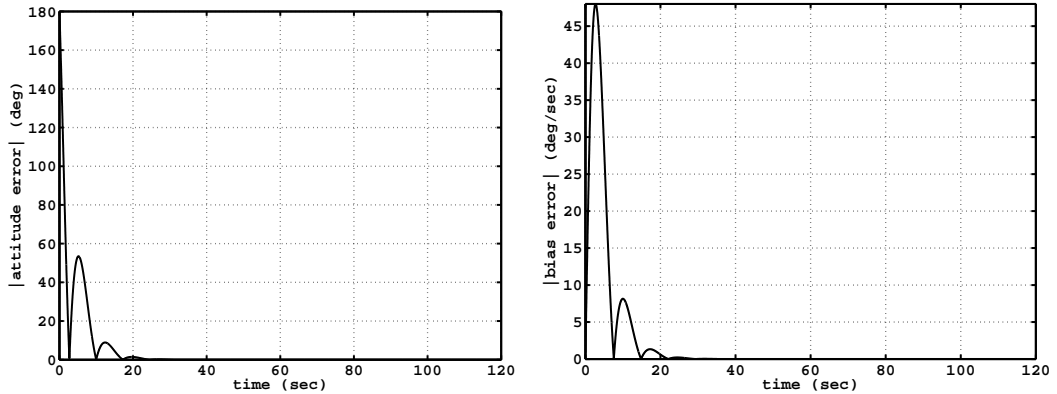
(a) Attitude Prediction Error



(b) Gyro Bias Estimation Error

Figure 3.2: Gyro Bias Estimator Errors with α Reduced, $\omega(t) = [3, -4, 5]$ deg/sec

angular velocity is $\boldsymbol{\omega}(t) = [0, 0, 0]$, with $\alpha = 1$. Figures 3.3(a) and 3.3(b) show that, again, both the attitude prediction error and the bias estimation error converge to zero. Finally, the simulation is repeated with a large gyro bias of $\mathbf{b} = [30, -30, 30]^T$



(a) Attitude Prediction Error

(b) Gyro Bias Estimation Error

Figure 3.3: Gyro Bias Estimation Errors, $\boldsymbol{\omega}(t) = [0, 0, 0]$

deg/sec and a large angular velocity of $\boldsymbol{\omega}(t) = [30, -40, 50]^T$ deg/sec, with $\alpha = 1$. Figure 3.2 shows again that the bias estimation errors converge to zero exponentially fast.

3.3 Closed Loop Stability

The nonlinear tracking control strategy proposed in [32] and summarized in section 2.3 cannot be implemented because exact measurements of the angular velocity $\boldsymbol{\omega}(t)$ are not available. Instead, a certainty equivalence approach is proposed using the estimates $\hat{\boldsymbol{\omega}}(t)$ from equation 3.3 (noise is not considered at this point) generated by

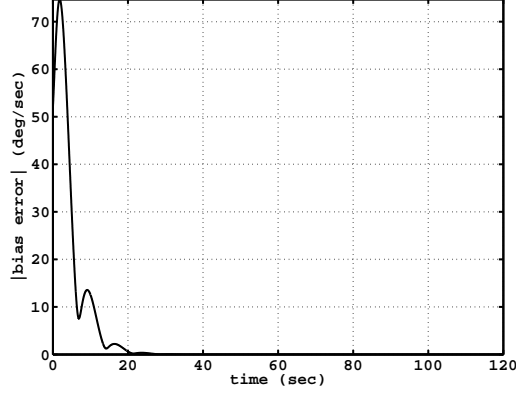


Figure 3.4: Gyro Bias Estimation Errors, $\boldsymbol{\omega}(t) = [30, -40, 50]$ deg/sec

the estimator equations 3.1, 3.2, resulting in

$$\mathbf{u}(t) = -K_D \hat{\mathbf{s}}(t) + H \hat{\boldsymbol{\alpha}}_r(t) - S(H \hat{\boldsymbol{\omega}}(t)) \boldsymbol{\omega}_r(t) \quad (3.13)$$

where, again $\hat{\mathbf{s}}(t) = \hat{\boldsymbol{\omega}}(t) - \boldsymbol{\omega}_r(t)$, $\hat{\boldsymbol{\omega}}_c(t) = \hat{\boldsymbol{\omega}}(t) - R(\tilde{\mathbf{q}}_c(t)) \boldsymbol{\omega}_d(t)$, and

$$\hat{\boldsymbol{\alpha}}_r(t) = R(\tilde{\mathbf{q}}_c(t)) \dot{\boldsymbol{\omega}}_d(t) - S(\hat{\boldsymbol{\omega}}_c(t)) R(\tilde{\mathbf{q}}_c(t)) \boldsymbol{\omega}_d(t) - \lambda Q_1(\tilde{\mathbf{q}}_c(t)) \hat{\boldsymbol{\omega}}_c(t)$$

Substitution of equation 3.13 into equation 2.21, the attitude dynamics, results in

$$H \dot{\boldsymbol{\omega}}(t) - S(H \boldsymbol{\omega}(t)) \boldsymbol{\omega}(t) = -K_D \hat{\mathbf{s}}(t) + H \hat{\boldsymbol{\alpha}}_r(t) - S(H \hat{\boldsymbol{\omega}}(t)) \boldsymbol{\omega}_r(t) \quad (3.14)$$

Since $\mathbf{s}(t) = \boldsymbol{\omega}(t) - \boldsymbol{\omega}_r(t)$, $H \dot{\boldsymbol{\omega}}(t)$ can be written as

$$H \dot{\boldsymbol{\omega}}(t) = H \dot{\mathbf{s}}(t) + H \boldsymbol{\alpha}_r(t)$$

where $\boldsymbol{\alpha}_r(t) = \frac{d}{dt} \boldsymbol{\omega}_r(t)$ is given in equation 2.29. Inserting the expression for $H \dot{\boldsymbol{\omega}}(t)$

into 3.14 gives

$$H \dot{\mathbf{s}}(t) - S(H \boldsymbol{\omega}(t)) \boldsymbol{\omega}(t) = -K_D \hat{\mathbf{s}}(t) + H \hat{\boldsymbol{\alpha}}_r(t) - S(H \hat{\boldsymbol{\omega}}(t)) \boldsymbol{\omega}_r(t) - H \boldsymbol{\alpha}_r(t) \quad (3.15)$$

Recall that $\tilde{\mathbf{s}}(t)$ is defined as

$$\tilde{\mathbf{s}}(t) = \mathbf{s}(t) - \hat{\mathbf{s}}(t) = \boldsymbol{\omega}(t) - \hat{\boldsymbol{\omega}}(t)$$

Substituting $\hat{\boldsymbol{\omega}}(t) = \boldsymbol{\omega}(t) - \tilde{\mathbf{s}}(t)$ into the skew term on the right side of equation 3.15, and adding $K_D \mathbf{s}(t)$ to both sides results in

$$\begin{aligned} H\dot{\mathbf{s}}(t) - S(H\boldsymbol{\omega}(t))\boldsymbol{\omega}(t) + K_D \mathbf{s}(t) &= K_D \mathbf{s}(t) - K_D \hat{\mathbf{s}}(t) \\ &+ H\hat{\boldsymbol{\alpha}}_r(t) - S(H\boldsymbol{\omega}(t) - H\tilde{\mathbf{s}}(t))\boldsymbol{\omega}_r(t) - H\boldsymbol{\alpha}_r(t) \end{aligned} \quad (3.16)$$

Expanding the skew term on the right side, and collecting terms, equation 3.16 becomes

$$\begin{aligned} H\dot{\mathbf{s}}(t) - S(H\boldsymbol{\omega}(t))(\boldsymbol{\omega}(t) - \boldsymbol{\omega}_r(t)) + K_D \mathbf{s}(t) &= K_D \tilde{\mathbf{s}}(t) - H(\boldsymbol{\alpha}_r(t) - \hat{\boldsymbol{\alpha}}_r(t)) \\ &+ S(H\tilde{\mathbf{s}}(t))\boldsymbol{\omega}_r(t) \end{aligned} \quad (3.17)$$

But

$$\tilde{\boldsymbol{\omega}}_c(t) - \hat{\tilde{\boldsymbol{\omega}}}_c(t) = (\boldsymbol{\omega}(t) - R(\tilde{\mathbf{q}}_c(t))\boldsymbol{\omega}_d(t)) - (\hat{\boldsymbol{\omega}}(t) - R(\tilde{\mathbf{q}}_c(t))\boldsymbol{\omega}_d(t)) = \boldsymbol{\omega}(t) - \hat{\boldsymbol{\omega}}(t) = \tilde{\mathbf{s}}(t)$$

and

$$\begin{aligned} \boldsymbol{\alpha}_r(t) - \hat{\boldsymbol{\alpha}}_r(t) &= S(R(\tilde{\mathbf{q}}_c(t))\boldsymbol{\omega}_d(t))(\tilde{\boldsymbol{\omega}}_c(t) - \hat{\tilde{\boldsymbol{\omega}}}_c(t)) - \lambda Q_1(\tilde{\mathbf{q}}_c(t))(\tilde{\boldsymbol{\omega}}_c(t) - \hat{\tilde{\boldsymbol{\omega}}}_c(t)) \\ &= S(R(\tilde{\mathbf{q}}_c(t))\boldsymbol{\omega}_d(t))\tilde{\mathbf{s}}(t) - \lambda Q_1(\tilde{\mathbf{q}}_c(t))\tilde{\mathbf{s}}(t) \end{aligned} \quad (3.18)$$

So, the closed loop dynamics of equation 3.17 become

$$H\dot{\mathbf{s}}(t) - S(H\boldsymbol{\omega}(t))\mathbf{s}(t) + K_D \mathbf{s}(t) = \Delta(\tilde{\mathbf{q}}_c(t), \boldsymbol{\omega}_d(t))\tilde{\mathbf{s}}(t) \quad (3.19)$$

where

$$\Delta(\tilde{\mathbf{q}}_c(t), \boldsymbol{\omega}_d(t)) = -S(\boldsymbol{\omega}_r(t))H - HS(R(\tilde{\mathbf{q}}_c(t))\boldsymbol{\omega}_d(t)) + \lambda H Q_1(\tilde{\mathbf{q}}_c(t)) + K_D$$

The definition of $\boldsymbol{\omega}_r(t)$, the assumption that $\boldsymbol{\omega}_d(t)$ is bounded, and the constraint $\|\tilde{\mathbf{q}}_c(t)\| = 1$ ensure that $\Delta(\tilde{\mathbf{q}}_c(t), \boldsymbol{\omega}_d(t))$ is a bounded matrix over any solution of the coupled dynamics 3.1, 3.2, 2.21, and 3.13.

For gyro bias errors, the error term $\tilde{\mathbf{s}}(t)$ can again be written as

$$\tilde{\mathbf{s}}(t) = \boldsymbol{\omega}(t) - \hat{\boldsymbol{\omega}}(t) = -\tilde{\mathbf{b}}(t)$$

and the closed loop dynamics become

$$H\dot{\mathbf{s}}(t) - S(H\boldsymbol{\omega}(t))\mathbf{s}(t) + K_D\mathbf{s}(t) = -\Delta(\tilde{\mathbf{q}}_c(t), \boldsymbol{\omega}_d(t))\tilde{\mathbf{b}}(t) \quad (3.20)$$

Theorem 3.2 *The control law 3.13 results in global stability and asymptotically perfect tracking, $\|\tilde{\boldsymbol{\varepsilon}}_c(t)\| \rightarrow 0$, $\|\tilde{\boldsymbol{\omega}}_c(t)\| \rightarrow 0$.*

Proof: Using the Lyapunov function from section 2.3 $V_c(t) = \frac{1}{2}\mathbf{s}(t)^T H \mathbf{s}(t)$, the derivative of $V_c(t)$ is

$$\dot{V}_c(t) = -\mathbf{s}(t)^T K_D \mathbf{s}(t) - \mathbf{s}(t)^T \Delta(\tilde{\mathbf{q}}_c(t), \boldsymbol{\omega}_d(t), K_D) \tilde{\mathbf{b}}(t) \quad (3.21)$$

Applying Young's inequality, 3.21 satisfies

$$\dot{V}_c(t) \leq -\frac{k_D}{2}\|\mathbf{s}(t)\|^2 + \frac{\zeta^2}{2k_D}\|\tilde{\mathbf{b}}(t)\|^2 \quad (3.22)$$

where k_D is the smallest eigenvalue of K_D , and

$$\zeta = \sup_{t \geq t_0} \sup_{\|\tilde{\mathbf{q}}_c(t)\|=1} \|\Delta(\tilde{\mathbf{q}}_c(t), \boldsymbol{\omega}_d(t))\| < \infty$$

since all the terms in $\Delta(\tilde{\mathbf{q}}_c(t), \boldsymbol{\omega}_d(t))$ are bounded, as noted above. Since the estimator dynamics 3.1 and 3.2 ensure that $\|\tilde{\mathbf{b}}(t)\|$ is uniformly bounded, the variable $\mathbf{s}(t)$ is also uniformly bounded. This also implies that $\dot{\mathbf{s}}(t)$ is uniformly bounded, since all the terms in the closed-loop dynamics 3.20 are bounded. Moreover, $\mathbf{s}(t) \in \mathcal{L}_2$ since for any $t \geq t_0$

$$\int_{t_0}^t \|\mathbf{s}(\tau)\|^2 d\tau \leq \frac{2}{k_D} [V_c(t) - V_c(t_0)] + \frac{\zeta^2}{k_D^2} \int_{t_0}^t \|\tilde{\mathbf{b}}(\tau)\|^2 d\tau$$

and $\int_{t_0}^t \|\tilde{\mathbf{b}}(\tau)\|^2 d\tau$ is finite for all $t \geq t_0$ since $\|\tilde{\mathbf{b}}(t)\|$ converges exponentially to zero. Thus, by Lemma 2.1, $\mathbf{s}(t) \in \mathcal{L}_\infty \cap \mathcal{L}_2$, $\dot{\mathbf{s}}(t) \in \mathcal{L}_\infty$, implies $\mathbf{s}(t) \rightarrow 0$.

This establishes convergence of $\mathbf{s}(t)$ to zero; now, the convergence of the actual attitude error $\tilde{\boldsymbol{\epsilon}}_c(t)$ is examined. Since $\|\tilde{\boldsymbol{\epsilon}}_c(t)\|$ is bounded by definition, $\mathbf{s}(t) = \tilde{\boldsymbol{\omega}}_c(t) + \lambda \tilde{\boldsymbol{\epsilon}}_c(t) \in \mathcal{L}_\infty$ implies that $\tilde{\boldsymbol{\omega}}_c(t) \in \mathcal{L}_\infty$. This in turn demonstrates that $\dot{\tilde{\boldsymbol{\epsilon}}}_c(t) \in \mathcal{L}_\infty$, since $\dot{\tilde{\boldsymbol{\epsilon}}}_c(t) = \frac{1}{2} Q_1(\tilde{\mathbf{q}}_c(t)) \tilde{\boldsymbol{\omega}}_c(t)$ and both terms on the right are bounded. Finally, $\tilde{\boldsymbol{\epsilon}}_c(t)$ is also in \mathcal{L}_2 since for any $t \geq t_0$

$$\begin{aligned} \int_{t_0}^t \|\tilde{\boldsymbol{\epsilon}}_c(\tau)\|^2 d\tau &= \frac{1}{\lambda^2} \int_{t_0}^t \|\mathbf{s}(\tau)\|^2 d\tau - \frac{2}{\lambda} \int_{t_0}^t \tilde{\boldsymbol{\omega}}_c(\tau)^T \tilde{\boldsymbol{\epsilon}}_c(\tau) d\tau - \int_{t_0}^t \|\tilde{\boldsymbol{\omega}}_c(\tau)\|^2 d\tau \\ \int_{t_0}^t \|\tilde{\boldsymbol{\epsilon}}_c(\tau)\|^2 d\tau &\leq \frac{1}{\lambda^2} \int_{t_0}^t \|\mathbf{s}(\tau)\|^2 d\tau - \frac{2}{\lambda} \int_{t_0}^t \tilde{\boldsymbol{\omega}}_c(\tau)^T \tilde{\boldsymbol{\epsilon}}_c(\tau) d\tau \end{aligned}$$

But, from equation 2.25, $\tilde{\boldsymbol{\omega}}_c(t)^T \tilde{\boldsymbol{\epsilon}}_c(t) = -2\dot{\tilde{\eta}}_c(t)$ resulting in

$$\int_{t_0}^t \|\tilde{\boldsymbol{\epsilon}}_c(\tau)\|^2 d\tau \leq \frac{1}{\lambda^2} \int_{t_0}^t \|\mathbf{s}(\tau)\|^2 d\tau + \frac{4}{\lambda} [\tilde{\eta}_c(t) - \tilde{\eta}_c(t_0)]$$

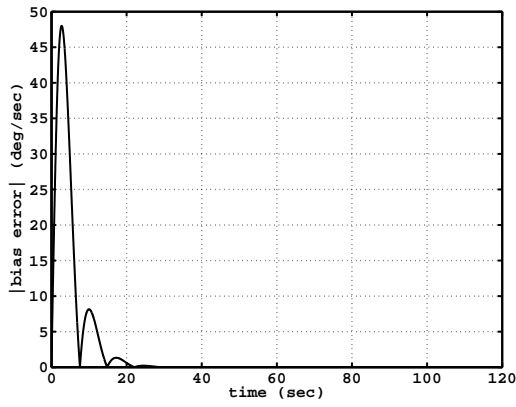
which is finite since $\mathbf{s}(t) \in \mathcal{L}_2$. Hence, $\tilde{\boldsymbol{\epsilon}}_c(t) \in \mathcal{L}_\infty \cap \mathcal{L}_2$, $\dot{\tilde{\boldsymbol{\epsilon}}}_c(t) \in \mathcal{L}_\infty$ and Lemma 2.1 again implies that $\lim_{t \rightarrow \infty} \|\tilde{\boldsymbol{\epsilon}}_c(t)\| = 0$. An equivalent argument establishes that $\lim_{t \rightarrow \infty} \|\tilde{\boldsymbol{\omega}}_c(t)\| = 0$. \square

<i>Quaternion</i>	<i>Value</i>	<i>Bias</i>	<i>Value</i>	<i>Rate</i>	<i>Value</i>
$\mathbf{q}(t_0)$	$[0, 0, 1, 0]^T$	$\mathbf{b}(t)$	$[0.5, -0.5, 0.5]^T \frac{deg}{sec}$	$\boldsymbol{\omega}(t_0)$	$[0, 0, 0]^T \frac{deg}{sec}$
$\hat{\mathbf{q}}(t_0)$	$[0, 0, 0, 1]^T$	$\hat{\mathbf{b}}(t_0)$	$[0, 0, 0]^T \frac{deg}{sec}$	$\boldsymbol{\omega}_d(t_0)$	$[0, 0.063, 0]^T \frac{deg}{sec}$
$\mathbf{q}_d(t_0)$	$[0, 0, 0, 1]^T$				

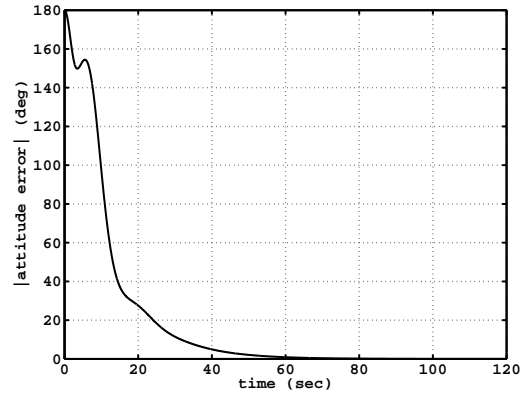
Table 3.2: Bias Estimator Simulation Initial Conditions

3.4 Closed Loop Simulation Results

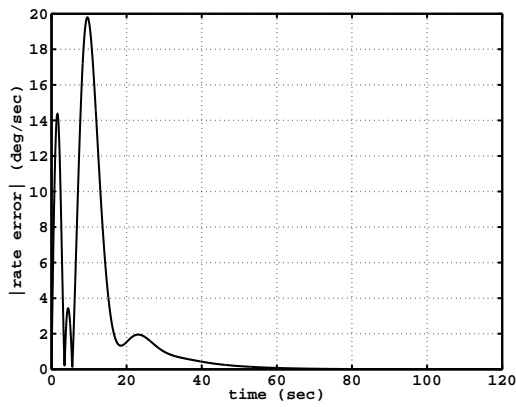
The bias estimator and controller design is tested with a Matlab simulation. The inertia matrix is a diagonal matrix with principal moments of inertia chosen arbitrarily as $[90, 100, 70]$ kg m². The size of the principal moments of inertia is comparable to that of a small satellite. Table 3.2 lists the initial conditions for the estimator and controller, as well as the true gyro bias and true initial angular velocity. The gains are chosen as $k = 1$, $K_D = k_D \mathbf{I}$, $k_D = 6$, and $\lambda = 3$. The desired trajectory is to track a 0.063 deg/sec rotation about the y-axis, a typical 1 rev/orbit rate for a low earth orbit satellite. Figure 3.5(a) shows that $\|\tilde{\mathbf{b}}(t)\|$ converges exponentially to zero. Figure 3.5(b) shows the tracking error, $\|\tilde{\boldsymbol{\epsilon}}_c(t)\|$, converges asymptotically to zero. Figure 3.5(c) similarly shows that the rate tracking errors converge to zero. Without correcting for the bias, the tracking error has a steady state error of approximately 30 degrees, as shown in Figure 3.5(d).



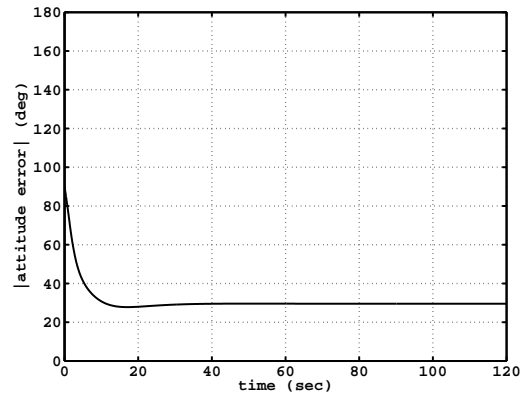
(a) Gyro Bias Estimation Error



(b) Attitude Tracking Error



(c) Rate Tracking Error



(d) Attitude Tracking Error Without Correcting for Bias Estimate

Figure 3.5: Coupled Estimator/Controller Errors With Gyro Bias

3.5 Gyro Noise

The addition of noise to the gyro model is now considered. The gyro reading and bias are given as

$$\boldsymbol{\omega}_g(t) = \boldsymbol{\omega}(t) + \mathbf{b}(t) + \boldsymbol{\nu}(t) \quad (3.23)$$

$$\dot{\mathbf{b}}(t) = \boldsymbol{\nu}_b(t) \quad (3.24)$$

where $\boldsymbol{\nu}(t)$ and $\boldsymbol{\nu}_b(t)$ are zero mean, uniformly bounded, ergodic noise processes with finite variances of $\sigma^2 I_3$ and $\sigma_b^2 I_3$, respectively. The bias is now a 'random walk', and the gyro measurement also has additive noise in addition to the bias. The estimator error equations are now

$$\begin{bmatrix} \dot{\tilde{\mathbf{q}}}_o(t) \\ \dot{\tilde{\mathbf{b}}}(t) \end{bmatrix} = \begin{bmatrix} \frac{1}{2}Q(\tilde{\mathbf{q}}_o(t))(-\tilde{\mathbf{b}}(t) - k\tilde{\boldsymbol{\varepsilon}}_o(t)\text{sign}(\tilde{\eta}_o(t)) - \boldsymbol{\nu}(t)) \\ \frac{1}{2}\tilde{\boldsymbol{\varepsilon}}_o(t)\text{sign}(\tilde{\eta}_o(t)) + \boldsymbol{\nu}_b(t) \end{bmatrix} \quad (3.25)$$

Equation 3.25 is divided into the nominal system of 3.5 and 3.6, without the noise, plus the perturbation

$$\dot{\mathbf{x}}(t) = f(t, \mathbf{x}(t)) + D(t)$$

where, as above,

$$\mathbf{x}(t) = \begin{bmatrix} \tilde{\boldsymbol{\varepsilon}}_o(t) \\ \tilde{\mathbf{b}}(t) \end{bmatrix}$$

and

$$D(t) = \begin{bmatrix} -\frac{1}{2}Q_1(\tilde{\mathbf{q}}_o(t))\boldsymbol{\nu}(t) \\ \boldsymbol{\nu}_b(t) \end{bmatrix}$$

As demonstrated above, the nominal system, $\dot{\mathbf{x}}(t) = f(t, \mathbf{x}(t))$, is exponentially stable. According to the Converse Lyapunov Theorem [30], a Lyapunov function and positive constants c_1 , c_2 , c_3 , and c_4 exist for the nominal system and satisfy the following

$$c_1 \|\mathbf{x}(t)\| \leq V_p(t) \leq c_2 \|\mathbf{x}(t)\|$$

$$\dot{V}_p(t) \leq -c_3 \|\mathbf{x}(t)\|^2$$

$$\left\| \frac{\partial V_p(t)}{\partial \mathbf{x}} \right\| \leq c_4 \|\mathbf{x}(t)\|$$

The nominal system is known, by Theorem 3.1, to be exponentially stable.

Using $V_p(t)$ as the Lyapunov function candidate for the perturbed system, the derivative of $V_p(t)$ along trajectories of the perturbed Lyapunov function satisfy [30]

$$\dot{V}_p(t) \leq -c_3 \|\mathbf{x}(t)\|^2 + \left\| \frac{\partial V_p(t)}{\partial \mathbf{x}}(t) \right\| \|D(t)\|$$

which becomes

$$\dot{V}_p(t) \leq -c_3 \|\mathbf{x}(t)\|^2 + c_4 \|\mathbf{x}(t)\| \|D(t)\| \quad (3.26)$$

Since $D(t)$ is uniformly bounded, the system is globally stable. The state $\mathbf{x}(t)$ converges exponentially to a ball determined by the bound on $D(t)$, and then remains within that ball. [30]

Applying Young's inequality to equation 3.26 results in

$$\dot{V}_p(t) \leq -\frac{c_3}{2} \|\mathbf{x}(t)\|^2 + \frac{c_4^2}{2c_3} \|D(t)\|^2 \leq -\frac{c_3}{2} \|\mathbf{x}(t)\|^2 + \frac{c_4^2}{2c_3} \left(\frac{1}{4} \|\nu(t)\|^2 + \|\nu_b(t)\|^2 \right) \quad (3.27)$$

since $\|Q_1(\tilde{\mathbf{q}}_o(t))\| = 1$. The time average of 3.27 is computed as

$$\frac{1}{T} \int_0^T \|\mathbf{x}^2(\tau)\| d\tau \leq \frac{c_4^2}{c_3^2} \frac{1}{T} \int_0^T \left(\frac{1}{4} \|\nu(\tau)\|^2 + \|\nu_b(\tau)\|^2 \right) d\tau + \frac{2}{c_3 T} [V_p(0) - V_p(T)] \quad (3.28)$$

Taking the limit of 3.28 as $T \rightarrow \infty$

$$\limsup_{T \rightarrow \infty} \frac{1}{T} \int_0^T \|\mathbf{x}(\tau)\|^2 d\tau \leq \lim_{T \rightarrow \infty} \frac{c_4^2}{c_3^2} \frac{1}{T} \int_t^T \left(\frac{1}{4} \|\boldsymbol{\nu}(\tau)\|^2 + \|\nu_b(\tau)\| \right) d\tau$$

The noise processes are ergodic, and therefore the ensemble average is equivalent to the time average [37]. The root mean square (RMS) bound (scaled accordingly for correct units) is given as

$$\|\tilde{\mathbf{b}}(t)\|_{RMS} \leq \|\mathbf{x}(t)\|_{RMS} \leq c \sqrt{\frac{1}{4} \sigma^2 + \sigma_b^2}$$

where the constants are combined into a single constant, $c = \frac{\sqrt{3}c_4}{c_3}$.

The controller analysis is similarly adjusted to account for the noise. Replacing $\boldsymbol{\omega}(t)$ in the analysis in section 3.3 with equation 3.23 results in the following closed loop equation, similar to equation 3.20

$$H\dot{\mathbf{s}}(t) - S(H\boldsymbol{\omega}(t))\mathbf{s}(t) + K_D\mathbf{s}(t) = -\Delta(\tilde{\mathbf{q}}_c(t), \boldsymbol{\omega}_d(t))(\tilde{\mathbf{b}}(t) + \boldsymbol{\nu}(t)) \quad (3.29)$$

The derivative of the Lyapunov function in 3.22 becomes

$$\dot{V}_c(t) \leq -\frac{k_D}{2} \|\mathbf{s}(t)\|^2 + \frac{\zeta^2}{2k_D} (\|\tilde{\mathbf{b}}(t)\|^2 + \|\boldsymbol{\nu}(t)\|^2) \quad (3.30)$$

Thus, from the definition of $V_c(t)$, and recalling from the estimator analysis above that $\|\tilde{\mathbf{b}}(t)\|$ and $\|\boldsymbol{\nu}(t)\|$ are bounded, $\mathbf{s}(t)$ is also seen to be uniformly bounded. Similarly, $\dot{\mathbf{s}}(t)$ is uniformly bounded, since all the terms in 3.29 are bounded. Integrating 3.30

$$\int_0^T \|\mathbf{s}(\tau)\|^2 d\tau \leq \frac{2}{k_D} [V_c(0) - V_c(T)] + \frac{\zeta^2}{k_D^2} \left(\int_0^T \|\tilde{\mathbf{b}}(\tau)\|^2 d\tau + \int_0^T \|\boldsymbol{\nu}(\tau)\|^2 d\tau \right)$$

Substituting $\|\mathbf{s}(t)\|^2 = \|\tilde{\boldsymbol{\omega}}_c(t)\|^2 + 2\lambda\tilde{\boldsymbol{\omega}}_c(t)^T\tilde{\boldsymbol{\epsilon}}_c(t) + \lambda^2\|\tilde{\boldsymbol{\epsilon}}_c(t)\|^2$

$$\begin{aligned} \int_0^T \|\tilde{\boldsymbol{\epsilon}}_c(\tau)\|^2 d\tau &\leq \frac{\zeta^2}{k_D^2\lambda^2} \left(\int_0^T \|\tilde{\mathbf{b}}(\tau)\|^2 d\tau + \int_0^T \|\boldsymbol{\nu}(\tau)\|^2 d\tau \right) + \frac{2}{k_D\lambda^2} [V_c(0) - V_c(T)] \\ &\quad + \frac{4}{\lambda} [\tilde{\eta}(T) - \tilde{\eta}(0)] \end{aligned} \quad (3.31)$$

Computing the time average of 3.31 and taking the limit as $T \rightarrow \infty$

$$\begin{aligned} \limsup_{T \rightarrow \infty} \frac{1}{T} \int_0^T \|\tilde{\boldsymbol{\epsilon}}_c(\tau)\|^2 d\tau &\leq \lim_{T \rightarrow \infty} \frac{\zeta^2}{k_D^2\lambda^2} \frac{1}{T} \left(\int_0^T \|\tilde{\mathbf{b}}(\tau)\|^2 d\tau + \int_0^T \|\boldsymbol{\nu}(\tau)\|^2 d\tau \right) \\ \limsup_{T \rightarrow \infty} \frac{1}{T} \int_0^T \|\tilde{\boldsymbol{\epsilon}}_c(\tau)\|^2 d\tau &\leq \frac{\zeta^2}{k_D^2\lambda^2} [\|\tilde{\mathbf{b}}(t)\|_{RMS}^2 + 3\sigma^2] \end{aligned}$$

The RMS limit of the tracking error is then

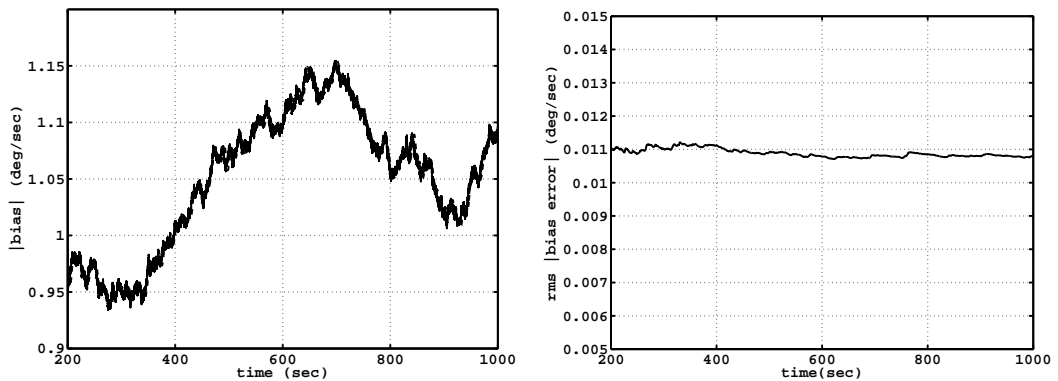
$$\|\tilde{\boldsymbol{\epsilon}}_c(t)\|_{RMS} \leq \frac{\zeta}{k_D\lambda} \left[\left(\frac{c^2}{4} + 3 \right) \sigma^2 + c^2 \sigma_b^2 \right]^{\frac{1}{2}} \quad (3.32)$$

Note that the constants are finite and depend on the spacecraft system properties (for example, gains and inertia).

3.6 Estimator and Closed Loop Simulation Results with Noise

The bias estimator and controller simulation is repeated with the added noise terms. For this example, the standard deviation of the gyro noise is set to 0.004 deg/sec^{1/2} and the bias noise standard deviation is also 0.004 deg/sec^{3/2}. The gyro noise level is that given for a MEMS gyro in [2]. The gyro noise to bias noise ratio is higher than that given for the spacecraft gyros of [5], and represents a gyro with significantly more drift.

First, just the estimator is tested. The initial conditions for the estimator are given in Table 3.1. The gains are $k = 1$ and $\alpha = 1$. The true angular velocity is $\omega(t) = [5, 3, -4]$ deg/sec. Figure 3.6(a) shows the true bias (solid line) and the estimated bias (dashed line). The estimated bias follows the 'random walk' in the true bias, after convergence, to within a ball determined by the variance of the noise. Figure 3.6(b) shows the RMS bias error. The simulation is repeated



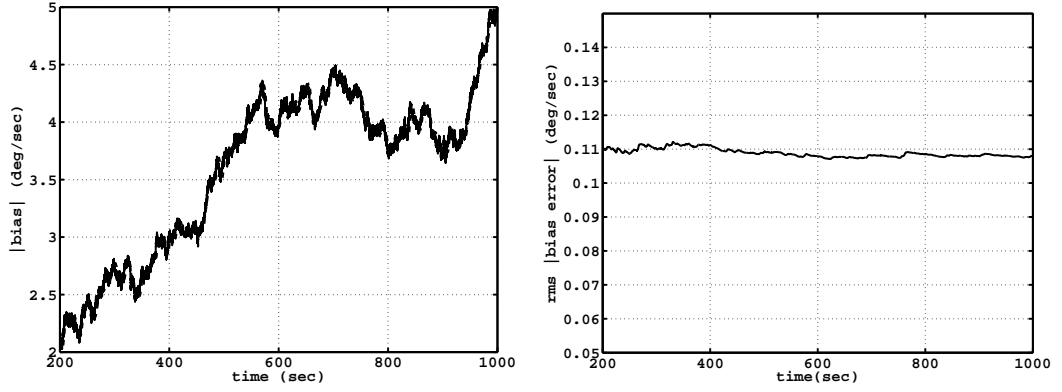
(a) True and Estimated Bias

(b) RMS Bias Estimation Error

Figure 3.6: Gyro Bias Estimation Errors with Added Noise

with the noise standard deviations increased by a factor of ten, $\sigma = 0.04 \text{ deg/sec}^{\frac{1}{2}}$ and $\sigma_b = 0.04 \text{ deg/sec}^{\frac{3}{2}}$. Figure 3.7(a) shows again that the estimated bias follows the 'random walk' in the true bias. Figure 3.7(b) shows the RMS bias estimation error. Here the RMS error is higher, as expected from the increase in the standard deviations of the noise terms.

Next the closed loop system is tested with the added noise terms. The initial conditions for the estimator and controller are given in Table 3.2, the standard devi-



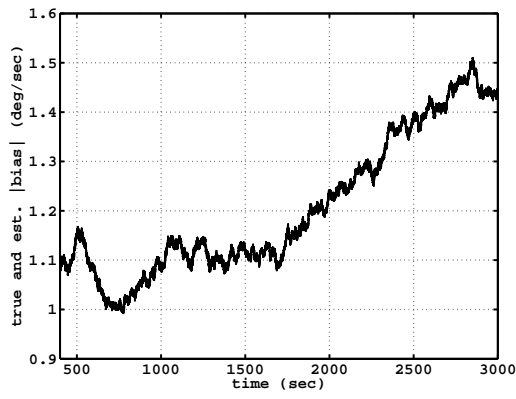
(a) True and Estimated Bias

(b) RMS Bias Estimation Error

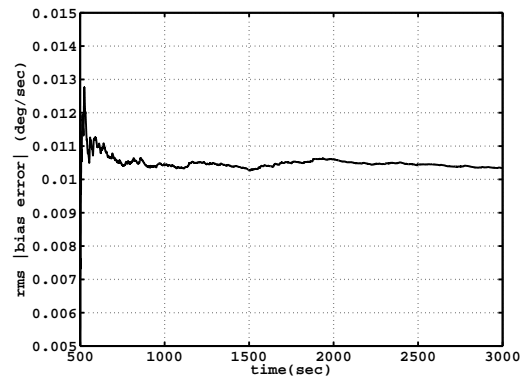
Figure 3.7: Gyro Bias Estimation Errors with Added Noise, Standard Deviations Increased

ations of the noise terms again are $\sigma = 0.004 \text{ deg/sec}^{\frac{1}{2}}$ and the $\sigma_b = 0.004 \text{ deg/sec}^{\frac{3}{2}}$. The gains and initial conditions are the same as in the simulations without noise. Figures 3.8(a) and 3.8(b) show the true gyro bias (solid line), and the estimated gyro bias (dashed line), and the RMS bias error. As with the estimator, the estimated bias follows the 'random walk' in the true bias, after convergence, to within a ball proportional to the standard deviation of the added noise. Figures 3.9(a) and 3.9(b) show the steady state attitude tracking error and the RMS attitude tracking error, while figures 3.10(a) and 3.10(b) show the steady state rate tracking error and the RMS rate tracking error, respectively. Figures 3.11(a) and 3.11(b) show the RMS attitude tracking error with the controller gain, k_D doubled, and similarly with the standard deviations of the noise reduced by half. As compared to the results in figure 3.9(b), in both cases the attitude tracking error is reduced as expected based

on equation 3.32.

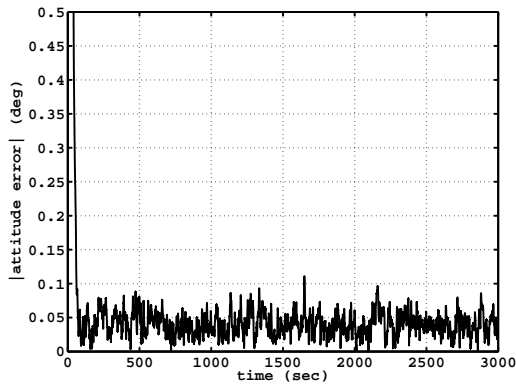


(a) Estimated and True Bias

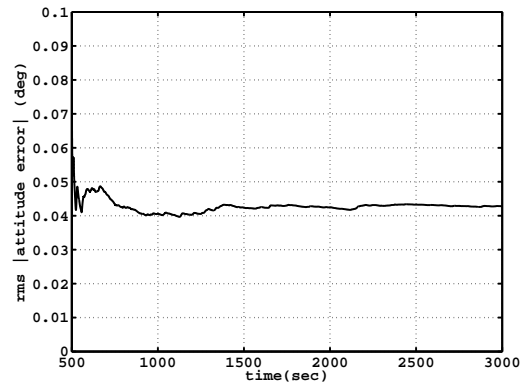


(b) RMS Bias Estimation Error

Figure 3.8: Closed Loop Control with Gyro Bias Error and Added Noise

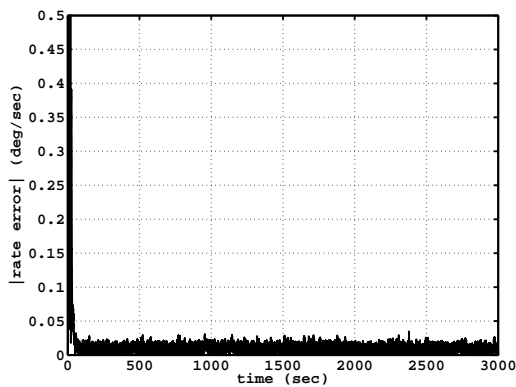


(a) Attitude Tracking Error

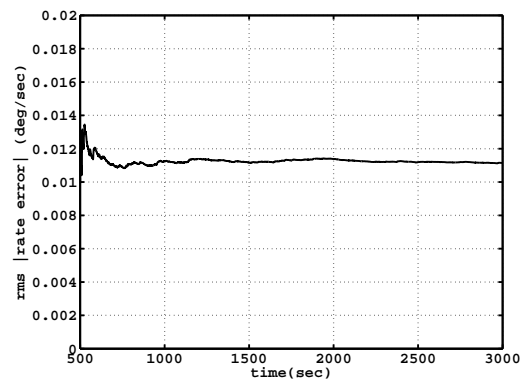


(b) RMS Attitude Tracking Error

Figure 3.9: Closed Loop Control Attitude Tracking Errors with Gyro Bias and Added Noise

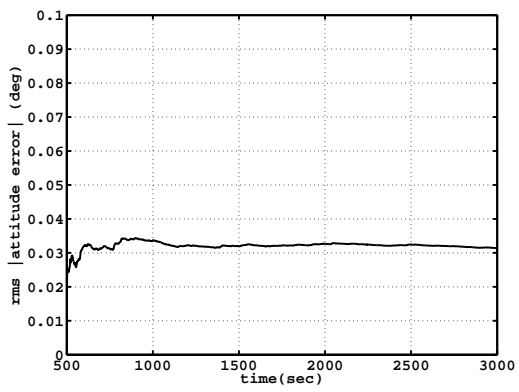


(a) Rate Tracking Error

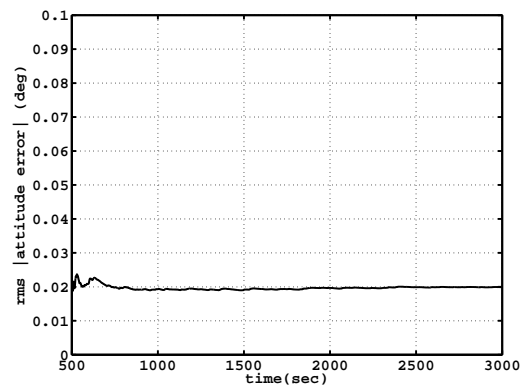


(b) RMS Rate Tracking Error

Figure 3.10: Closed Loop Control Rate Tracking Errors with Gyro Bias and Added Noise



(a) RMS Attitude Tracking Error



(b) RMS Attitude Tracking Error

Figure 3.11: Closed Loop Attitude Tracking Errors with (a) K_D Doubled (b) $\frac{1}{2}\sigma$ and

$\frac{1}{2}\sigma_b$

Chapter 4

Scale Factor Calibration

4.1 Nonlinear Estimator for Constant Scale

Factor

The scale factor estimator is designed similarly to the gyro bias estimator. The attitude prediction is given as

$$\dot{\hat{\mathbf{q}}}(t) = \frac{1}{2}Q(\hat{\mathbf{q}}(t))R(\tilde{\mathbf{q}}_o(t))^T[\hat{\boldsymbol{\omega}}(t) + k\tilde{\boldsymbol{\varepsilon}}_o(t)\text{sign}(\tilde{\eta}_o(t))] \quad (4.1)$$

and the scale factor estimator is

$$\dot{\hat{\gamma}}_{Ii}(t) = \frac{\alpha}{2}\omega_{gi}(t)\tilde{\varepsilon}_{oi}(t)\text{sign}(\tilde{\eta}_o(t)) \quad (4.2)$$

where $\tilde{\varepsilon}_{oi}(t)$ are the three components of $\tilde{\boldsymbol{\varepsilon}}_o(t)$ and $\alpha > 0$. The estimated angular velocity, $\hat{\boldsymbol{\omega}}(t)$, is given in equation 2.14, and is repeated here as

$$\hat{\boldsymbol{\omega}}(t) = \hat{\Gamma}_I(t)\boldsymbol{\omega}_g(t) \quad (4.3)$$

The alignment matrix is assumed known and, without loss of generality, is the identity matrix, $R(\mathbf{q}_g) = \mathbf{I}$. There is no gyro bias error. The estimated scale factor

components, $\hat{\gamma}_{Ii}(t)$ with $i = x, y, z$, are estimates of the inverse of the true scale factor components. The components $\hat{\gamma}_{Ii}(t)$ form the main diagonal of the matrix $\hat{\Gamma}_I(t)$ in equation 4.3. Note that the estimated scale factors, $\hat{\gamma}_{Ii}(t)$, are never inverted in the estimator (or in the controller to follow), so dividing by zero is not a possibility.

The derivatives of the attitude error, $\tilde{\mathbf{q}}_o(t) = \mathbf{q}(t) \otimes \hat{\mathbf{q}}(t)^{-1}$, and the scale factor error components are

$$\dot{\tilde{\mathbf{q}}}_o(t) = \frac{1}{2} \begin{bmatrix} Q_1(\tilde{\mathbf{q}}_o(t)) \\ -\tilde{\boldsymbol{\varepsilon}}_o(t)^T \end{bmatrix} (\Gamma_I \boldsymbol{\omega}_g(t) - \hat{\Gamma}_I(t) \boldsymbol{\omega}_g(t) - k \tilde{\boldsymbol{\varepsilon}}_o(t) \text{sign}(\tilde{\eta}_o(t))) \quad (4.4)$$

$$\dot{\tilde{\gamma}}_{Ii}(t) = -\frac{\alpha}{2} \boldsymbol{\omega}_g(t) \tilde{\varepsilon}_{oi}(t) \text{sign}(\tilde{\eta}_o(t)) \quad (4.5)$$

where again, $i = x, y, z$. Γ_I is a diagonal matrix, containing the inverse of each of the true scale factors, defined as γ_{Ii} , on the main diagonal. Obviously, a zero scale factor would be unacceptable, but unlikely since it would eliminate the use of the gyro data. The scale factor errors are defined as $\tilde{\gamma}_{Ii}(t) = \gamma_{Ii} - \hat{\gamma}_{Ii}(t)$, with $\tilde{\Gamma}_I(t)$ given as

$$\tilde{\Gamma}_I(t) = \begin{bmatrix} \tilde{\gamma}_{Ix}(t) & 0 & 0 \\ 0 & \tilde{\gamma}_{Iy}(t) & 0 \\ 0 & 0 & \tilde{\gamma}_{Iz}(t) \end{bmatrix}$$

The difference in angular velocity terms in equation 4.4 is written as

$$\Gamma_I \boldsymbol{\omega}_g(t) - \hat{\Gamma}_I(t) \boldsymbol{\omega}_g(t) = \tilde{\Gamma}_I(t) \boldsymbol{\omega}_g(t) = \Omega_g(t) \tilde{\boldsymbol{\gamma}}_I(t)$$

where $\Omega_g(t) = \text{diag}\{\boldsymbol{\omega}_g(t)\}$ is a diagonal matrix with the components of $\boldsymbol{\omega}_g(t)$ on the main diagonal and $\tilde{\boldsymbol{\gamma}}_I(t)$ is a vector containing the components $\tilde{\gamma}_{Ii}(t)$. Equation 4.4

is rewritten as

$$\dot{\tilde{\mathbf{q}}}_o(t) = \frac{1}{2} \begin{bmatrix} Q_1(\tilde{\mathbf{q}}_o(t)) \\ -\tilde{\boldsymbol{\varepsilon}}_o(t)^T \end{bmatrix} (\Omega_g(t)\tilde{\gamma}_I(t) - k\tilde{\boldsymbol{\varepsilon}}_o(t)\text{sign}(\tilde{\eta}_o(t))) \quad (4.6)$$

From equation 4.5, the scale factor error components are written in vector form as

$$\dot{\tilde{\gamma}}_I = -\frac{\alpha}{2}\Omega_g(t)\tilde{\boldsymbol{\varepsilon}}_o(t)\text{sign}(\tilde{\eta}_o(t))$$

Note that the equilibrium states for 4.5 and 4.6 are

$$\begin{bmatrix} \tilde{\mathbf{q}}_o(t)^T & \tilde{\gamma}_I(t)^T \end{bmatrix} = \begin{bmatrix} 0 & 0 & 0 & \pm 1 & 0 & 0 & 0 \end{bmatrix}$$

Theorem 4.1 *The equilibrium states of the system 4.5 and 4.6 are globally stable.*

In particular, if the angular velocity, $\boldsymbol{\omega}_g(t)$, is bounded, $\tilde{\boldsymbol{\varepsilon}}_o(t) \rightarrow 0$ asymptotically.

Proof: The proof follows that of the gyro bias estimator. Choose a Lyapunov function as

$$V_o(t) = \frac{1}{2\alpha} \sum_{\omega_{gi}(\dot{t}) \neq 0} \tilde{\gamma}_{Ii}(t)^2 + \frac{1}{2} \begin{cases} (\tilde{\eta}_o(t) - 1)^2 + \tilde{\boldsymbol{\varepsilon}}_o(t)^T \tilde{\boldsymbol{\varepsilon}}_o(t) & \tilde{\eta}_o(t) \geq 0 \\ (\tilde{\eta}_o(t) + 1)^2 + \tilde{\boldsymbol{\varepsilon}}_o(t)^T \tilde{\boldsymbol{\varepsilon}}_o(t) & \tilde{\eta}_o(t) < 0 \end{cases} \quad (4.7)$$

$V_o(t)$ is continuous. Noting that $\tilde{\boldsymbol{\varepsilon}}_o(t)^T \dot{\tilde{\boldsymbol{\varepsilon}}}_o(t) + \tilde{\eta}_o(t)\dot{\tilde{\eta}}_o(t) = 0$, as with the gyro bias analysis, the derivative of $V_o(t)$ (including the left and right derivatives of $\tilde{\eta}_o(t) = 0$) yields, for all t

$$\dot{V}_o(t) = \frac{1}{\alpha} \sum_{\omega_{gi}(\dot{t}) \neq 0} \tilde{\gamma}_{Ii}(t)\dot{\tilde{\gamma}}_{Ii}(t) + \begin{cases} -\dot{\tilde{\eta}}_o(t) & \tilde{\eta}_o(t) \geq 0 \\ \dot{\tilde{\eta}}_o(t) & \tilde{\eta}_o(t) < 0 \end{cases} \quad (4.8)$$

Substituting equation 4.5 and $\dot{\tilde{\eta}}_o(t)$ from equation 4.6 into equation 4.8 results in

$$\dot{V}_o(t) = -\frac{k}{2}\tilde{\boldsymbol{\varepsilon}}_o(t)^T\tilde{\boldsymbol{\varepsilon}}_o(t)$$

This establishes that $\tilde{\boldsymbol{\varepsilon}}_o(t)$, $\tilde{\eta}_o(t)$, and $\tilde{\gamma}_{Ii}(t)$ (those with the corresponding component of $\boldsymbol{\omega}_g(t)$ nonzero), are globally, uniformly bounded. No conclusions yet can be made about the individual components of $\tilde{\gamma}_{Ii}(t)$. This will be analyzed in Theorem 4.2 below.

$V_o(t)$ is a continuous, twice differentiable function with

$$\ddot{V}_o(t) = \frac{k}{2}\tilde{\boldsymbol{\varepsilon}}_o(t)^T Q_1(\tilde{\boldsymbol{q}}_o(t))[-\Omega_g(t)\tilde{\boldsymbol{\gamma}}_I(t) + k\tilde{\boldsymbol{\varepsilon}}_o(t)\text{sign}(\tilde{\eta}_o(t))]$$

where $Q_1(\tilde{\boldsymbol{q}}_o(t))$ is defined in equation 2.4. $\ddot{V}_o(t)$ is bounded, given that $\boldsymbol{\omega}_g(t)$ is bounded. Lemma 2.1 then shows that $\|\tilde{\boldsymbol{\varepsilon}}_o(t)\| \rightarrow 0$ as $t \rightarrow \infty$. \square

Theorem 4.2 *For any bounded, angular velocity, $\boldsymbol{\omega}_g(t)$, that is persistently exciting, the equilibrium states of the system 4.5 and 4.6 are exponentially stable. In particular, $\hat{\boldsymbol{\gamma}}(t) \rightarrow \boldsymbol{\gamma}$ exponentially fast from any initial conditions $\hat{\boldsymbol{q}}(t_0)$ and $\hat{\boldsymbol{\gamma}}(t_0)$.*

Proof: If $\boldsymbol{\omega}_g(t)$ is bounded, all the signals in equations 4.5 and 4.6 are bounded.

The system is, as in the gyro bias case, analyzed as a linear time varying system,

$\dot{\boldsymbol{x}}(t) = A(t)\boldsymbol{x}(t)$. If all the components of $\boldsymbol{\omega}_g(t)$ are nonzero, $A(t)$ is given as

$$A(t) = \begin{bmatrix} -\frac{k}{2}\text{sign}(\tilde{\eta}_o(t))Q_1(\tilde{\boldsymbol{q}}_o(t)) & \frac{1}{2}Q_1(\tilde{\boldsymbol{q}}_o(t))\Omega_g(t) \\ -\frac{\alpha}{2}\text{sign}(\tilde{\eta}_o(t))\Omega_g(t) & 0 \end{bmatrix}$$

The development proceeds like that for the gyro bias in Section 3.1, under the assumption that $\boldsymbol{\omega}_g(t)$ is at least bounded. Rewriting $\dot{V}_o(t)$ as

$$\dot{V}_o(t) = -\mathbf{x}(t)^T C^T C \mathbf{x}(t) \leq 0$$

where $C = \begin{bmatrix} \sqrt{\frac{k}{2}}\mathbf{I} & 0 \end{bmatrix}$, Theorem 4.5 and the discussion on pp.626-628 in [30] shows that the equilibrium point $\mathbf{x}(t) = 0$ of the equivalent system is exponentially stable if the pair $(A(t), C)$ is uniformly completely observable (UCO). Since observability properties are unchanged under output feedback [30], this will be true if the pair $(A(t) - K(t)C, C)$ is uniformly observable for any piecewise, continuous and bounded matrix $K(t)$. Choose $K(t)$ as

$$K(t) = \begin{bmatrix} -\sqrt{\frac{k}{2}}\text{sign}(\tilde{\eta}_o(t))Q_1(\tilde{\mathbf{q}}_o(t)) \\ -\sqrt{\frac{\alpha}{2k}}\text{sign}(\tilde{\eta}_o(t))\Omega_g(t) \end{bmatrix}$$

Note from the above Lyapunov analysis that $\|\tilde{\boldsymbol{\epsilon}}_o(t)\| \rightarrow 0$. Since $\|\tilde{\mathbf{q}}_o(t)\|^2 = 1 = \|\tilde{\boldsymbol{\epsilon}}_o(t)\|^2 + |\tilde{\eta}_o(t)|^2$ for any time, t , there exists a time, $T > 0$, such that $\|\tilde{\eta}_o(t)\| > 0$ for all $t > T$. Since $\tilde{\eta}_o(t)$ can therefore not pass through zero for $t > T$, $\text{sign}(\tilde{\eta}_o(t))$ is constant for all $t > T$ and, hence, $K(t)$ is a piecewise continuous function of time.

Again, the state transition matrix for the pair $(A(t) - K(t)C, C)$ is

$$\Phi(\tau, t) = \begin{bmatrix} \mathbf{I} & \Sigma(\tau, t) \\ 0 & \mathbf{I} \end{bmatrix} \quad (4.9)$$

where $\Sigma(\tau, t) = \frac{1}{2} \int_t^\tau Q_1(\tilde{\mathbf{q}}_o(\sigma))\Omega_g(\sigma)d\sigma$. Repeating equation 3.9, the observability

Grammian is [33]

$$W(t, t+T) = \int_t^{t+T} \Phi(\tau, t)^T C^T C \Phi(\tau, t) d\tau = \int_t^{t+T} \begin{bmatrix} \frac{k}{2} \mathbf{I} & \frac{k}{2} \Sigma(\tau, t) \\ \frac{k}{2} \Sigma(\tau, t)^T & \frac{k}{2} \Sigma(\tau, t)^T \Sigma(\tau, t) \end{bmatrix} d\tau \quad (4.10)$$

The system is UCO if there exists a $T > 0$ and positive constants $\alpha_1 > 0, \alpha_2 > 0$ such that, for all $t \geq t_0$, $\alpha_1 \mathbf{I} \geq W(t, t+T) \geq \alpha_2 \mathbf{I}$. Using Lemma 13.4 of [30], this property is assured if $\boldsymbol{\omega}_g(t)$, $\dot{\boldsymbol{\omega}}_g(t)$, $Q_1(\tilde{\boldsymbol{q}}_o(t))$ and $\frac{d}{dt} Q_1(\tilde{\boldsymbol{q}}_o(t))$ are bounded, and there exist positive constants T_2 , β_1 , and a bounded $\beta_2 < \infty$ such that, for all $t \geq t_0$,

$$\infty > \beta_2 \mathbf{I} \geq \int_t^{t+T_2} \Omega_g(\tau) Q_1(\tilde{\boldsymbol{q}}_o(\tau))^T (\tau) Q_1(\tilde{\boldsymbol{q}}_o(\tau)) \Omega_g(\tau) d\tau \geq \beta_1 \mathbf{I} > 0 \quad (4.11)$$

Substituting $Q_1(\tilde{\boldsymbol{q}}_o(t))^T Q_1(\tilde{\boldsymbol{q}}_o(t)) = \mathbf{I} - \tilde{\boldsymbol{\varepsilon}}_o(t) \tilde{\boldsymbol{\varepsilon}}_o(t)^T$ into equation 4.11 results in

$$\infty > \beta_2 \mathbf{I} \geq \int_t^{t+T_2} \Omega_g(\tau) [\mathbf{I} - \tilde{\boldsymbol{\varepsilon}}_o(\tau) \tilde{\boldsymbol{\varepsilon}}_o(\tau)^T] \Omega_g(\tau) d\tau \geq \beta_1 \mathbf{I} > 0 \quad (4.12)$$

$\tilde{\boldsymbol{\varepsilon}}_o(t)$ is bounded by definition. $\frac{d}{dt} \tilde{\boldsymbol{\varepsilon}}_o(t)$ is also bounded, since the above Lyapunov analysis shows that all the terms in equation 4.6 are bounded, given that $\boldsymbol{\omega}_g(t)$ is bounded. With $\dot{\boldsymbol{\omega}}_g(t)$ bounded, the upper bound in equation 4.12 is satisfied.

To examine the lower bound, again recall that $\|\tilde{\boldsymbol{\varepsilon}}_o(t)\| \rightarrow 0$ asymptotically. Thus, for any $\delta > 0$, there exists a $T_1(\delta) > t_0$ such that $\|\tilde{\boldsymbol{\varepsilon}}_o(t)\| < \delta$ for all $t \geq t_0 + T_1$. Taking any $\delta < 1$ and $T_2 > T_1$

$$\mathbf{I} > \mathbf{I} - \tilde{\boldsymbol{\varepsilon}}_o(t) \tilde{\boldsymbol{\varepsilon}}_o(t)^T > (1 - \delta^2) \mathbf{I} > 0$$

Therefore, for any $\mathbf{z} \in \mathbb{R}^3$

$$\begin{aligned} \mathbf{z}^T \left[\int_t^{t+T_2} \Omega_g(\tau)^2 d\tau \right] \mathbf{z} &> \mathbf{z}^T \left[\int_t^{t+T_2} \Omega_g(\tau) [\mathbf{I} - \tilde{\boldsymbol{\varepsilon}}_o(\tau) \tilde{\boldsymbol{\varepsilon}}_o(\tau)^T] \Omega_g(\tau) \right] \mathbf{z} d\tau \\ &> (1 - \delta^2) \mathbf{z}^T \left[\int_t^{t+T_2} \Omega_g^2 d\tau \right] \mathbf{z} \end{aligned} \quad (4.13)$$

If the following is true

$$\int_t^{t+T_2} \Omega_g(\tau)^2 d\tau = P_{sf} \quad (4.14)$$

where P_{sf} is a bounded, positive definite matrix, then equation 4.13 becomes

$$\infty > \mathbf{z}^T P_{sf} \mathbf{z} > (1 - \delta^2) \mathbf{z}^T P_{sf} \mathbf{z} > 0 \quad (4.15)$$

Equation 4.14 is the persistency of excitation condition for the scale factor estimator.

If each component of $\boldsymbol{\omega}_g(t)$ is persistently exciting, the system is UCO, and both $\tilde{\boldsymbol{\varepsilon}}_o(t)$ and $\tilde{\boldsymbol{\gamma}}_I(t)$ converge to zero exponentially fast.

There are two scenarios to consider in evaluating equation 4.14. The first considers angular velocities that are well behaved and bounded. For example, if the non-zero components of $\boldsymbol{\omega}_g(t)$ are constant, equation 4.11 is satisfied and the system is UCO. If, for example, the components of $\boldsymbol{\omega}_g(t)$ are sinusoidal, equation 4.11 is satisfied and the system is UCO.

The second scenario considers $\boldsymbol{\omega}_g(t)$ that violate equation 4.14. If any component of $\boldsymbol{\omega}_g(t)$ belongs to a class of functions such that [38]

$$\omega_{gi}(t) = \begin{cases} f(t) & t \in [t_i, t'_i] \\ 0 & t \in [t'_i, t_{i+1}] \end{cases} \quad (4.16)$$

where $T_i \equiv |t_{i+1} - t_i|$, $T'_i \equiv |t_{i+1} - t'_i|$, $\{t_i\}$, and $\{t'_i\}$ are all monotonic unbounded sequences of time and $f(t)$ is any piecewise-continuous bounded function. If $T_i \rightarrow \infty$ and $T'_i/T_i \rightarrow 1$ as $t \rightarrow \infty$, then $\omega_g(t)$ is not PE for any finite $T > 0$. The time intervals for which $\omega_{gi}(t) = 0$ get increasingly larger, therefore, any time T_2 will eventually cover an interval where the components of $\omega_g(t)$ are zero for the entire interval. If $\omega_g(t)$ decreases exponentially, the system is not UCO. If $\omega_{gi}(t) = e^{-\alpha t}$, equation 4.14 becomes

$$\int_t^{t+T_2} \Omega_g(\tau)^2 d\tau = \int_t^{t+T_2} e^{-2\alpha t} I d\tau = \frac{1}{2\alpha} e^{-2\alpha t} [1 - e^{-2\alpha T_2}] I \quad (4.17)$$

Equation 4.17 is not positive definite for all $t \geq t_0$. \square

Remark: For situations requiring positive scale factor estimates, a standard projection method such as that described in Chapter 4 of [39] ensures that the estimates remain positive (and smaller than a specified bound, if needed), while retaining all the estimator properties given above.

If the estimates, $\hat{\gamma}_{I_i}(t)$, are constrained to be less than some known upper bound, $\gamma_{iI,max}$, such that

$$\gamma_{iI,max} - \hat{\gamma}_{I_i}(t) > 0$$

and if the estimates are constrained to be positive, $\hat{\gamma}_{I_i}(t) > 0$, equation 4.2 is imple-

<i>Attitude</i>	<i>Value</i>	<i>Scale Factor</i>	<i>Value</i>
$\hat{\mathbf{q}}(t_0)$	$[0, 0, 0, 1]^T$	$\hat{\boldsymbol{\gamma}}(t)$	$[1, 1, 1]^T$
$\mathbf{q}(t_0)$	$[0, 1, 0, 0]^T$	$\boldsymbol{\gamma}_1$	$[3, -5, 4]^T$
		$\boldsymbol{\gamma}_2$	$[\frac{\pi}{180}, -\frac{\pi}{180}, \frac{\pi}{180}]^T$

Table 4.1: Scale Factor Estimator Simulation Initial Conditions

mented as

$$\dot{\hat{\gamma}}_{Ii}(t) = \begin{cases} 0 & \hat{\gamma}_{Ii}(t) > \gamma_{iI,max} \text{ and } \frac{\alpha}{2}\omega_{gi}(t)\tilde{\varepsilon}_{oi}(t)\text{sign}(\tilde{\eta}_o(t)) > 0 \\ 0 & \hat{\gamma}_{Ii}(t) < 0 \text{ and } \frac{\alpha}{2}\omega_{gi}(t)\tilde{\varepsilon}_{oi}(t)\text{sign}(\tilde{\eta}_o(t)) < 0 \\ \frac{\alpha}{2}\omega_{gi}(t)\tilde{\varepsilon}_{oi}(t)\text{sign}(\tilde{\eta}_o(t)) & \text{otherwise} \end{cases}$$

4.2 Estimator Simulation Results

The scale factor estimator is tested for a variety of scenarios. Table 4.1 lists the initial conditions for the estimator, as well as two true scale factors. The first scale factor is arbitrary, while the second represents the possibility of scaling the angular velocity with the incorrect units. Recall that the estimator solves for the inverse scale factor components. All the test cases presented, except the last, use $\boldsymbol{\gamma}_1$ of Table 4.1. The gain is chosen as $k = 0.5$, $\alpha = 1$.

In the first case, the angular velocity is the same as in the gyro bias estimator tests with $\boldsymbol{\omega}_g(t)^T = [3, -4, 5]$ deg/sec. Figure 4.2 shows that the scale factor

estimation errors, $\gamma_I - \hat{\gamma}_I(t)$, converge to zero. Next, the x and y angular velocity

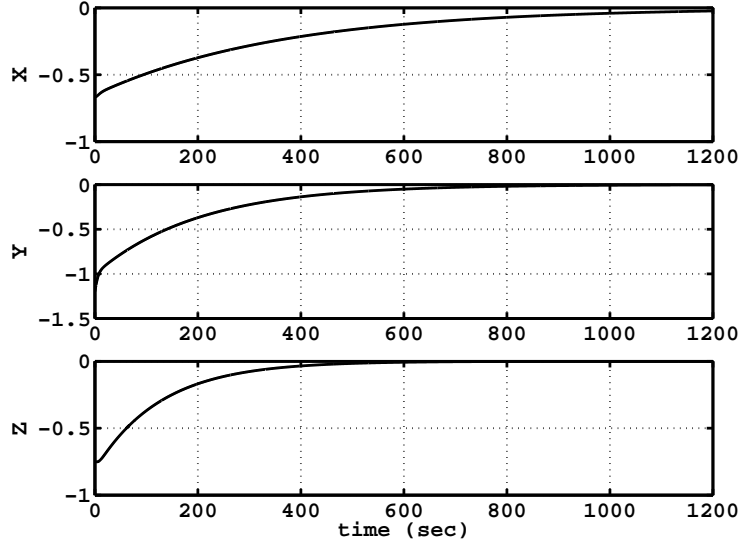


Figure 4.1: Scale Factor Estimation Errors with Constant Angular Velocity

components are as in the first case, but the z component is zero, $\omega_g(t) = [3, -4, 0]$ deg/sec. Figure 4.2 shows that the scale factor estimation errors for the x and y axes converge to zero, but the scale factor estimation error for the z axis is constant. In the third case, the angular velocity components decrease exponentially, $\omega_g(t) = [3, -4, 5]e^{-0.05t}$ deg/sec. Figure 4.2 shows that the scale factor estimation errors do not converge to zero, but rather to constants. Finally, the estimator is tested with γ_2 from Table 4.1. Again, this case represents an extreme case of an incorrect scaling for units. If the angular velocity is output from the gyros in units of rad/sec, but the angular velocity, $\omega(t)$, is needed in deg/sec, the inverse scale factor components must be $\gamma_{Ii} = \frac{180}{\pi}$ (recall equation 1.5). Figure 4.2 shows that the scale factor estimation errors converge to zero. Here the gain is chosen as $k = 5$, $\alpha = 5$.

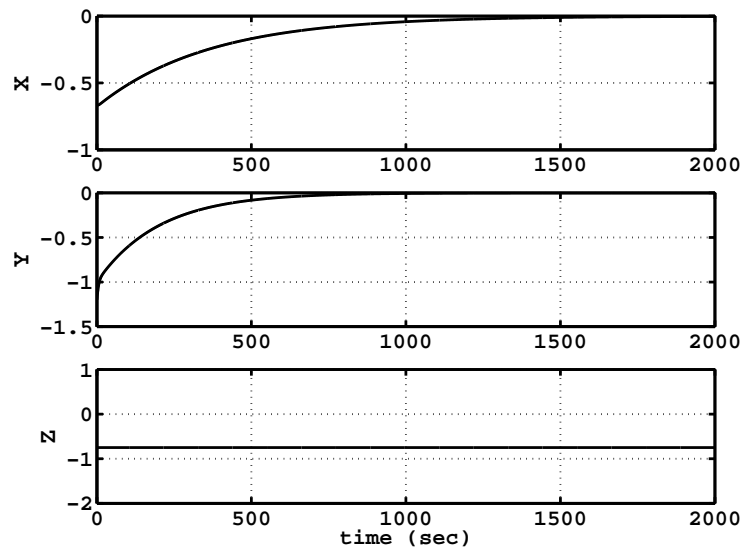


Figure 4.2: Scale Factor Estimation Errors with $\omega_z = 0$

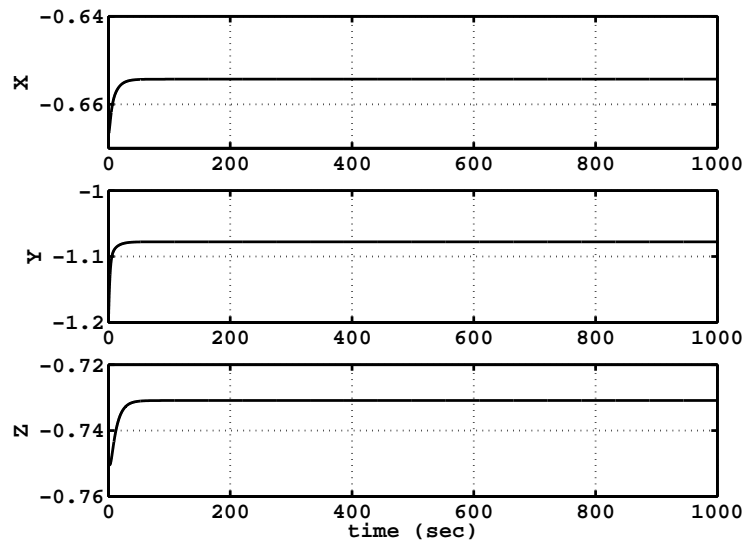


Figure 4.3: Scale Factor Estimation Errors with Exponential Angular Velocity

The angular velocity components are as above $\boldsymbol{\omega}_g(t)^T = [3, -4, 5]$ deg/sec.

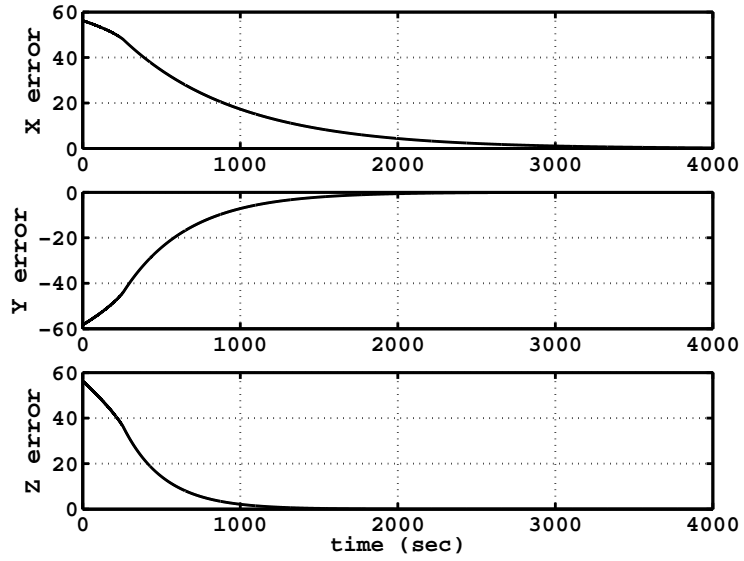


Figure 4.4: Scale Factor Estimation Errors with Large Inverse Scale Factor

4.3 Closed Loop Stability

The closed loop analysis initially proceeds like the gyro bias closed loop analysis.

The control is repeated here as

$$\mathbf{u}(t) = -K_D \hat{\mathbf{s}}(t) + H \hat{\boldsymbol{\alpha}}_r(t) - S(H \hat{\boldsymbol{\omega}}(t)) \boldsymbol{\omega}_r(t) \quad (4.18)$$

The closed loop analysis for the gyro bias, up to equation 3.19, is independent of the specific gyro error. The closed loop equation, given in equation 3.19, is repeated here

$$H \dot{\hat{\mathbf{s}}}(t) - S(H \boldsymbol{\omega}(t)) \hat{\mathbf{s}}(t) + K_D \hat{\mathbf{s}}(t) = \Delta(\tilde{\mathbf{q}}_c(t), \boldsymbol{\omega}_d(t)) \tilde{\mathbf{s}}(t) \quad (4.19)$$

where

$$\begin{aligned}\Delta(\tilde{\mathbf{q}}_c(t), \boldsymbol{\omega}_d(t)) &= -S(\boldsymbol{\omega}_r(t))H - HS(R(\tilde{\mathbf{q}}_c(t))\boldsymbol{\omega}_d(t)) + \lambda H Q_1(\tilde{\mathbf{q}}_c(t)) + K_D \\ &= \Delta'(\tilde{\mathbf{q}}_c(t), \boldsymbol{\omega}_d(t)) + K_D\end{aligned}$$

and the error term $\tilde{\mathbf{s}}(t)$, from section 2.3, is

$$\tilde{\mathbf{s}}(t) = \tilde{\Gamma}_I(t)\boldsymbol{\omega}_g(t) = \Omega_g \tilde{\gamma}_I(t)$$

The closed loop equation can then be written as

$$H\dot{\mathbf{s}}(t) - S(H\boldsymbol{\omega}(t))\mathbf{s}(t) + K_D\mathbf{s}(t) = \Delta(\tilde{\mathbf{q}}_c(t), \boldsymbol{\omega}_d(t))\Omega_g \tilde{\gamma}_I(t) \quad (4.20)$$

The alignment $R(\mathbf{q}_g)$ is assumed to be the identity matrix. Note that the definition of $\boldsymbol{\omega}_r(t)$, the assumption that $\boldsymbol{\omega}_d(t)$ is bounded, and the constraint $\|\tilde{\mathbf{q}}_c(t)\| = 1$ ensure that $\Delta'(\tilde{\mathbf{q}}_c(t), \boldsymbol{\omega}_d(t))$ is a bounded matrix over any solution of the coupled dynamics, equations 4.1, 4.2, 2.21, and 4.18.

Theorem 4.3 *If the scale factors are known to be positive, with a known upper and lower bound on each component (or alternatively, an upper and lower bound on the inverse of each component), with projection implemented in the estimator such that $\hat{\gamma}_I(t)$ is positive and bounded, and if*

$$k_D > \frac{\zeta' \gamma_{I,max} (\gamma_{I,max} + \hat{\gamma}_{I,max}) + 2}{\gamma_{I,max} \hat{\gamma}_{I,max}} > 0$$

where $\gamma_{I,max} = \|\Gamma_I\|$, $\hat{\gamma}_{I,max} = \|\hat{\Gamma}_I(t)\|_{max}$, and

$$\zeta' = \sup_{t \geq t_0} \sup_{\|\tilde{\mathbf{q}}_c(t)\|=1} \|\Delta'(\tilde{\mathbf{q}}_c(t), \boldsymbol{\omega}_d(t))\| < \infty$$

the control law 4.18 results in a stable closed loop system, with $\|\tilde{\mathbf{e}}_c(t)\|$ and $\|\tilde{\boldsymbol{\omega}}_c(t)\|$ uniformly, ultimately bounded.

Proof: Given the Lyapunov function $V_c(t) = \frac{1}{2}\mathbf{s}(t)^T H \mathbf{s}(t)$, the derivative of $V_c(t)$, using equation 4.19, is

$$\dot{V}_c(t) = -\mathbf{s}(t)^T K_D \mathbf{s}(t) + \mathbf{s}(t)^T \Delta(\tilde{\mathbf{q}}_c(t), \boldsymbol{\omega}_d(t))(\mathbf{s}(t) - \hat{\mathbf{s}}(t)) \quad (4.21)$$

or, substituting $\Delta(\tilde{\mathbf{q}}_c(t), \boldsymbol{\omega}_d(t)) = \Delta'(\tilde{\mathbf{q}}_c(t), \boldsymbol{\omega}_d(t)) + K_D$, $\dot{V}_c(t)$ becomes

$$\dot{V}_c(t) = -\mathbf{s}(t)^T K_D \mathbf{s}(t) + \mathbf{s}(t)^T (\Delta'(\tilde{\mathbf{q}}_c(t), \boldsymbol{\omega}_d(t)) + K_D)(\mathbf{s}(t) - \hat{\mathbf{s}}(t)) \quad (4.22)$$

Rewrite $\mathbf{s}(t)$ as

$$\mathbf{s}(t) = \boldsymbol{\omega}(t) - \boldsymbol{\omega}_r(t) = \Gamma_I \boldsymbol{\omega}_g(t) - \boldsymbol{\omega}_r(t)$$

and rewrite $\hat{\mathbf{s}}(t)$ as

$$\hat{\mathbf{s}}(t) = \hat{\boldsymbol{\omega}}(t) - \boldsymbol{\omega}_r(t) = \hat{\Gamma}_I(t) \boldsymbol{\omega}_g(t) - \boldsymbol{\omega}_r(t)$$

Write equation 4.22 as

$$\dot{V}_c(t) = \mathbf{s}(t)^T \Delta'(\tilde{\mathbf{q}}_c(t), \boldsymbol{\omega}_d(t))(\mathbf{s}(t) - \hat{\mathbf{s}}(t)) - \mathbf{s}(t)^T K_D \hat{\mathbf{s}}(t) \quad (4.23)$$

Substitute the expressions for $\mathbf{s}(t)$ and $\hat{\mathbf{s}}(t)$ into equation 4.23, with $K_D = k_d I$, resulting in

$$\begin{aligned}
\dot{V}_c(t) &= (\boldsymbol{\omega}_g(t)^T \Gamma_I - \boldsymbol{\omega}_r(t)^T) \Delta'(\tilde{\mathbf{q}}_c(t), \boldsymbol{\omega}_d(t)) (\Gamma_I - \hat{\Gamma}_I(t)) \boldsymbol{\omega}_g(t) \\
&\quad - k_D (\boldsymbol{\omega}_g(t)^T \Gamma_I - \boldsymbol{\omega}_r(t)^T) (\hat{\Gamma}_I(t) \boldsymbol{\omega}_g(t) - \boldsymbol{\omega}_r(t)) \\
&= \boldsymbol{\omega}_g(t)^T \Gamma_I \Delta'(\tilde{\mathbf{q}}_c(t), \boldsymbol{\omega}_d(t)) (\Gamma_I - \hat{\Gamma}_I(t)) \boldsymbol{\omega}_g(t) \\
&\quad - \boldsymbol{\omega}_r(t)^T \Delta'(\tilde{\mathbf{q}}_c(t), \boldsymbol{\omega}_d(t)) (\Gamma_I - \hat{\Gamma}_I(t)) \boldsymbol{\omega}_g(t) \\
&\quad - k_D \boldsymbol{\omega}_g(t)^T \Gamma_I \hat{\Gamma}_I(t) \boldsymbol{\omega}_g(t) - k_D \boldsymbol{\omega}_r(t)^T \hat{\Gamma}_I(t) \boldsymbol{\omega}_g(t) \\
&\quad - k_D \boldsymbol{\omega}_g(t)^T \Gamma_I \boldsymbol{\omega}_r(t) - k_D \boldsymbol{\omega}_r(t)^T \boldsymbol{\omega}_r(t)
\end{aligned}$$

Rearranging the terms gives

$$\begin{aligned}
\dot{V}_c(t) &= -k_D \boldsymbol{\omega}_g(t)^T \Gamma_I \hat{\Gamma}_I(t) \boldsymbol{\omega}_g(t) - k_D \boldsymbol{\omega}_r(t)^T \boldsymbol{\omega}_r(t) \\
&\quad + \boldsymbol{\omega}_g(t)^T \Gamma_I \Delta'(\tilde{\mathbf{q}}_c(t), \boldsymbol{\omega}_d(t)) (\Gamma_I - \hat{\Gamma}_I(t)) \boldsymbol{\omega}_g(t) \\
&\quad - \boldsymbol{\omega}_r(t)^T \Delta'(\tilde{\mathbf{q}}_c(t), \boldsymbol{\omega}_d(t)) (\Gamma_I - \hat{\Gamma}_I(t)) \boldsymbol{\omega}_g(t) \\
&\quad - k_D \boldsymbol{\omega}_r(t)^T (\Gamma_I + \hat{\Gamma}_I(t)) \boldsymbol{\omega}_g(t)
\end{aligned} \tag{4.24}$$

The scale factors are assumed to be positive, with each component $\gamma_{Ii} > \epsilon$, where ϵ is a known lower bound on the inverse of each component. With projection in the scale factor estimator, the scale factor estimates are also positive with $\hat{\gamma}_{Ii}(t) > \epsilon$.

Let $\hat{\boldsymbol{\gamma}}_{I,max} = \|\hat{\Gamma}_I(t)\|_{max}$, $\boldsymbol{\gamma}_{I,max} = \|\Gamma_I\|$, and

$$\zeta' = \sup_{t \geq t_0} \sup_{\|\tilde{\mathbf{q}}_c(t)\|=1} \|\Delta'(\tilde{\mathbf{q}}_c(t), \boldsymbol{\omega}_d(t))\| < \infty$$

$\dot{V}_c(t)$ is then bounded as

$$\begin{aligned} \dot{V}_c(t) \leq & -k_D \gamma_{I,max} \hat{\gamma}_{I,max} \|\omega_g(t)\|^2 - k_D \|\omega_r(t)\|^2 + k_D (\gamma_{I,max} + \hat{\gamma}_{I,max}) \|\omega_g(t)\| \|\omega_r(t)\| \\ & + \zeta' (\gamma_{I,max} + \hat{\gamma}_{I,max}) \|\omega_g(t)\|^2 + \zeta' (\gamma_{I,max} + \hat{\gamma}_{I,max}) \|\omega_g(t)\| \|\omega_r(t)\| \end{aligned} \quad (4.25)$$

Applying Young's inequality to the terms containing products of $\|\omega_g(t)\|$ and $\|\omega_r(t)\|$ equation 4.25 becomes

$$\begin{aligned} \dot{V}_c(t) \leq & - (k_D \gamma_{I,max} \hat{\gamma}_{I,max} - \zeta' \gamma_{I,max} (\gamma_{I,max} + \hat{\gamma}_{I,max}) - 2) \|\omega_g(t)\|^2 \\ & - (k_D - \frac{1}{4} (\zeta'^2 + k_D^2)) (\gamma_{I,max} + \hat{\gamma}_{I,max})^2 \|\omega_r(t)\|^2 \end{aligned} \quad (4.26)$$

Recall that all the components of the last term are bounded. For the system to be stable, $\dot{V}_c(t) \leq 0$. If

$$k_D > \frac{\zeta' \gamma_{I,max} (\gamma_{I,max} + \hat{\gamma}_{I,max}) + 2}{\gamma_{I,max} \hat{\gamma}_{I,max}} > 0 \quad (4.27)$$

the first term in equation 4.26 is negative. An a priori upper and lower bound is assumed for $\gamma_{I,max}$ and ζ' is bounded by definition. The components of $\hat{\gamma}_I(t)$ are bounded through projection in the estimator, $\hat{\gamma}_I(t) > 0$ and $\|\hat{\gamma}_I(t)\| < \gamma_{I,max}$. Therefore, a bounded k_D exists which satisfies 4.27. If $\|\omega_g(t)\|$ is sufficiently large, $\dot{V}_c(t) < 0$ and the closed loop system is uniformly ultimately bounded. Alternatively, recall that $\mathbf{s}(t) = \boldsymbol{\omega}(t) - \boldsymbol{\omega}_r(t) = \Gamma_I \boldsymbol{\omega}_g(t) - \boldsymbol{\omega}_r(t)$, and $\boldsymbol{\omega}_r(t) = R(\tilde{\mathbf{q}}_c(t)) \boldsymbol{\omega}_d(t) - \lambda \tilde{\boldsymbol{\epsilon}}_c(t)$ is bounded by definition. If $\mathbf{s}(t)$ increases without bound, $\boldsymbol{\omega}_g(t)$ increases without bound. But, eventually $\boldsymbol{\omega}_g(t)$ will be large enough such that $\dot{V}_c(t) < 0$ which implies that $\mathbf{s}(t)$, and $\boldsymbol{\omega}_g(t)$, must remain bounded. If $\mathbf{s}(t)$ is uniformly ultimately bounded,

$\tilde{\boldsymbol{\omega}}_c(t)$ and $\tilde{\boldsymbol{\varepsilon}}_c(t)$ must also be uniformly ultimately bounded since

$$\mathbf{s}(t) = \tilde{\boldsymbol{\omega}}_c(t) + \lambda \tilde{\boldsymbol{\varepsilon}}_c(t)$$

$\tilde{\boldsymbol{\varepsilon}}_c(t)$ is bounded by definition, therefore $\tilde{\boldsymbol{\omega}}_c(t)$ is bounded. \square

Theorem 4.4 *If each component of the angular velocity, $\boldsymbol{\omega}_g(t)$, is persistently exciting, regardless of the magnitude of k_D , such that $k_D > 0$, the control law 4.18 results in a stable closed loop system, with asymptotically perfect tracking, $\|\tilde{\boldsymbol{\varepsilon}}_c(t)\| \rightarrow 0$, $\|\tilde{\boldsymbol{\omega}}_c(t)\| \rightarrow 0$.*

Proof: The convergence of $\mathbf{s}(t)$ to zero depends on the exponential convergence of the scale factor errors, which in turn depends on the angular velocity $\boldsymbol{\omega}_g(t)$ generated by the applied control. Rewriting the error term

$$\mathbf{s}(t) - \hat{\mathbf{s}}(t) = \boldsymbol{\omega}(t) - \hat{\boldsymbol{\omega}}(t) = \tilde{\Gamma}_I(t)\boldsymbol{\omega}_g(t) = \tilde{\Gamma}_I(t)\Gamma\boldsymbol{\omega}(t) = \tilde{\Gamma}_I(t)\Gamma(\mathbf{s}(t) + \boldsymbol{\omega}_r(t))$$

Substituting this into equation 4.22 results in

$$\begin{aligned} \dot{V}_c(t) = & -\mathbf{s}(t)^T K_D \mathbf{s}(t) + \mathbf{s}(t)^T (\Delta'(\tilde{\mathbf{q}}_c(t), \boldsymbol{\omega}_d(t)) + K_D) \tilde{\Gamma}_I(t) \Gamma \mathbf{s}(t) \\ & + \mathbf{s}(t)^T (\Delta'(\tilde{\mathbf{q}}_c(t), \boldsymbol{\omega}_d(t)) + K_D) \tilde{\Gamma}_I(t) \Gamma \boldsymbol{\omega}_r(t) \end{aligned} \quad (4.28)$$

Equation 4.28 is bounded as

$$\dot{V}_c(t) \leq -k_D \|\mathbf{s}(t)\|^2 + (k_D + \zeta') [\gamma_{I,max} \|\tilde{\Gamma}_I(t)\| \|\mathbf{s}(t)\|^2 + \gamma_{I,max} \|\boldsymbol{\omega}_r(t)\| \|\mathbf{s}(t)\| \|\tilde{\Gamma}_I(t)\|] \quad (4.29)$$

Applying Young's inequality to the last term in equation 4.29

$$\dot{V}_c(t) \leq -\left(\frac{k_D}{2} - (k_D + \zeta') \gamma_{I,max} \|\tilde{\Gamma}_I(t)\|\right) \|\mathbf{s}(t)\|^2 + \frac{(k_D + \zeta')^2 \|\boldsymbol{\omega}_r(t)\|^2 \gamma_{I,max}^2}{2k_D} \|\tilde{\Gamma}_I(t)\|^2 \quad (4.30)$$

If the angular velocity, $\boldsymbol{\omega}_g(t)$, in addition to being bounded, satisfies equation 4.14, the system is UCO and the scale factor errors converge to zero exponentially fast. In this case, Lemma 2.3 applies. Since $\tilde{\Gamma}_I(t)$ converges to zero exponentially fast, $V_c(t)$ converges to zero exponentially fast, which means $\mathbf{s}(t)$ converges to zero exponentially fast. With the convergence of $\mathbf{s}(t) \rightarrow 0$, the proof of convergence of the actual attitude and rate errors follows exactly as in the gyro bias analysis of section 3.3. The end result of which is $\lim_{t \rightarrow \infty} \|\tilde{\boldsymbol{\epsilon}}_c(t)\| = 0$ and $\lim_{t \rightarrow \infty} \|\tilde{\boldsymbol{\omega}}_c(t)\| = 0$. \square

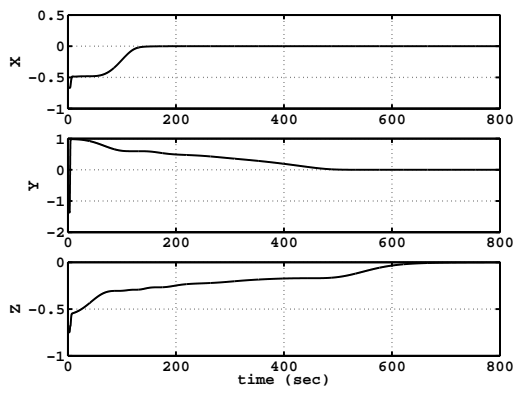
4.4 Closed Loop Simulation Results

The gyro scale factor estimator and controller are tested similarly to the bias estimator and controller. The inertia matrix is the same, a diagonal matrix with principal moments of inertia of $[90, 100, 70]^T$ kg m². Table 4.2 lists the initial conditions for the estimator and controller, as well as the true scale factor. The gains are chosen as $k = 1$, $K_D = k_D I_3$ (where I_3 indicates a 3x3 identity matrix), $k_D = 20$, and $\lambda = 0.1$. Here the initial angular velocity is $\boldsymbol{\omega}(0)^T = [0, 0, 0]$, and the desired angular velocity is constant, $\boldsymbol{\omega}_d(t)^T = [3, 3, 3]$ deg/sec. Figure 4.5(a) shows that the scale factor errors converge to zero. Figures 4.5(b) and 4.5(c) show that both the attitude tracking error and the rate tracking error converge to zero. Note that the y axis scale factor is negative. The y gyro measurement is in the opposite direction from the true y angular rate. The tracking errors converge to zero in this scenario, a simulation of a gyro wired backwards. Figure 4.5(d) shows the tracking attitude error when the

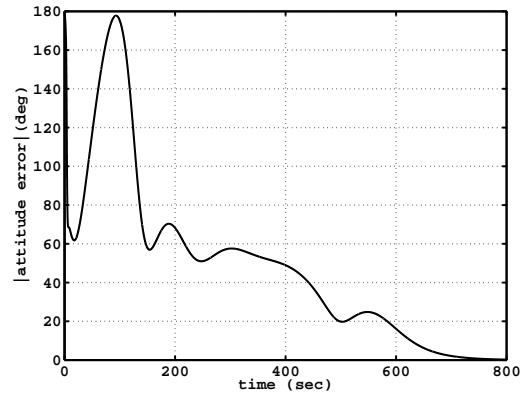
<i>Attitude</i>	<i>Value</i>	<i>Alignment</i>	<i>Value</i>
$\mathbf{q}(t_0)$	$[0, 1, 0, 0]^T$	γ	$[3, -5, 4]^T$
$\hat{\mathbf{q}}(t_0)$	$[0, 0, 0, 1]^T$	$\hat{\gamma}(t_0)$	$[1, 1, 1]^T$
$\mathbf{q}_d(t_0)$	$[0, 0, 0, 1]^T$		

Table 4.2: Scale Factor Estimator/Controller Simulation Initial Conditions

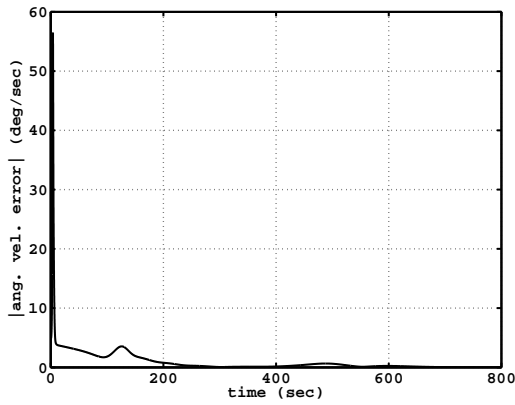
rate is not corrected with the scale factor estimate. The attitude tracking error does not converge to zero.



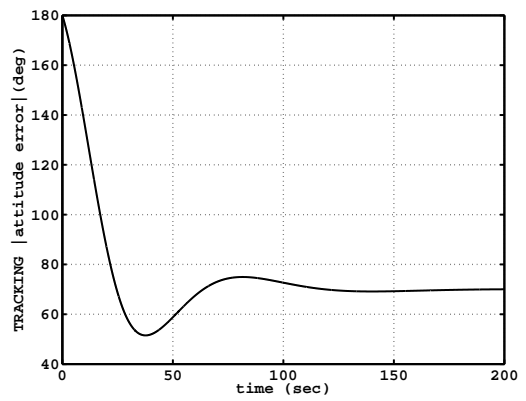
(a) Scale Factor Errors



(b) Attitude Tracking Error



(c) Rate Tracking Error



(d) Attitude Tracking Error without Correcting for Scale Factor

Figure 4.5: Coupled Estimator/Controller Errors with Scale Factor Errors

Chapter 5

Gyro Alignment Calibration

5.1 Nonlinear Estimator for Gyro Alignment

The estimator for the gyro alignment is presented next. Here, the kinematic equations for the attitude estimator quaternion and the alignment estimator quaternion are given as

$$\dot{\hat{\mathbf{q}}}(t) = \frac{1}{2}Q(\hat{\mathbf{q}}(t))R(\tilde{\mathbf{q}}_o(t))^T[\hat{\boldsymbol{\omega}}(t) + k(t)\tilde{\boldsymbol{\varepsilon}}_o(t)\text{sign}(\tilde{\eta}_o(t)) + k_1(t)\text{sign}(\tilde{\boldsymbol{\varepsilon}}_o(t))\text{sign}(\tilde{\eta}_o(t))] \quad (5.1)$$

where

$$\text{sign}(\tilde{\boldsymbol{\varepsilon}}_o(t)) = \begin{bmatrix} \text{sign}(\tilde{\varepsilon}_{o1}(t)) \\ \text{sign}(\tilde{\varepsilon}_{o2}(t)) \\ \text{sign}(\tilde{\varepsilon}_{o3}(t)) \end{bmatrix}$$
$$\dot{\hat{\mathbf{q}}}_g(t) = \frac{1}{2}Q(\hat{\mathbf{q}}_g(t))[(\mathbf{I} - R(\tilde{\mathbf{q}}_o(t)))R(\hat{\mathbf{q}}_g(t))\boldsymbol{\omega}_g(t)] \quad (5.2)$$

where $\hat{\boldsymbol{\omega}}(t)$ is as given in equation 2.13, and is repeated here as

$$\hat{\boldsymbol{\omega}}(t) = R(\hat{\mathbf{q}}_g(t))\boldsymbol{\omega}_g(t)$$

The scale factors (assumed known) are incorporated into $\boldsymbol{\omega}_g(t)$, and there is no bias error. The gains, $k(t)$ and $k_1(t)$, are positive. The quaternion, $\hat{\mathbf{q}}_g(t)$, is the estimated gyro alignment quaternion, transforming from gyro coordinates to an estimated body frame. Again, $\hat{\mathbf{q}}(t)$ is a prediction of the attitude at time, t , propagated by the kinematic equation using the measured angular velocity and the current alignment estimate. The attitude error is as given in equation 3.4 and the alignment error is given in equation 2.16. The term $R(\tilde{\mathbf{q}}_o(t))^T$ in equation 5.1 resolves the angular velocity terms in the estimator frame. The kinematic equation for the attitude error quaternion is

$$\begin{aligned} \dot{\tilde{\mathbf{q}}}_o(t) = \frac{1}{2} \begin{bmatrix} Q_1(\tilde{\mathbf{q}}_o(t)) \\ -\tilde{\boldsymbol{\epsilon}}_o(t)^T \end{bmatrix} & \left(R(\mathbf{q}_g)\boldsymbol{\omega}_g(t) - R(\hat{\mathbf{q}}_g(t))\boldsymbol{\omega}_g(t) - k(t)\tilde{\boldsymbol{\epsilon}}_o(t)\text{sign}(\tilde{\eta}_o(t)) \right. \\ & \left. - k_1(t)\text{sign}(\tilde{\boldsymbol{\epsilon}}_o(t))\text{sign}(\tilde{\eta}_o(t)) \right) \end{aligned} \quad (5.3)$$

Since the true alignment is constant, the angular velocity associated with the kinematic equation for the true alignment quaternion is zero. The kinematic equation for the alignment error quaternion is therefore

$$\dot{\tilde{\mathbf{q}}}_g(t) = \frac{1}{2} \begin{bmatrix} Q_1(\tilde{\mathbf{q}}_g(t)) \\ -\tilde{\boldsymbol{\epsilon}}_g(t)^T \end{bmatrix} [(R(\tilde{\mathbf{q}}_o(t)) - \mathbf{I})R(\hat{\mathbf{q}}_g(t))\boldsymbol{\omega}_g(t)] \quad (5.4)$$

Since $R(\mathbf{q}_g) = R(\tilde{\mathbf{q}}_g(t))R(\hat{\mathbf{q}}_g(t))$, where $R(\tilde{\mathbf{q}}_g(t))$ represents the rotation from the estimated body frame to the actual body frame, 5.3 becomes

$$\dot{\tilde{\mathbf{q}}}_o(t) = \frac{1}{2} \begin{bmatrix} Q_1(\tilde{\mathbf{q}}_o(t)) \\ -\tilde{\boldsymbol{\varepsilon}}_o(t)^T \end{bmatrix} [(R(\tilde{\mathbf{q}}_g(t)) - \mathbf{I})R(\hat{\mathbf{q}}_g(t))\boldsymbol{\omega}_g(t) - k(t)\tilde{\boldsymbol{\varepsilon}}_o(t)\text{sign}(\tilde{\eta}_o(t)) - k_1(t)\text{sign}(\tilde{\boldsymbol{\varepsilon}}_o(t))\text{sign}(\tilde{\eta}_o(t))] \quad (5.5)$$

Note that the equilibrium state for each of the error quaternions, $\tilde{\mathbf{q}}_o(t)$ and $\tilde{\mathbf{q}}_g(t)$, is the identity quaternion, $[0 \ 0 \ 0 \ \pm 1]$.

Theorem 5.1 *If $k(t) \geq 4\|\boldsymbol{\omega}_g(t)\| + k'$ and $k_1(t) \geq 4\|\boldsymbol{\omega}_g(t)\| + k'_1$, where $k' > 0$ and $k'_1 > 0$, the equilibrium states for the system 5.4 and 5.5 are globally stable. In particular, if the angular velocity, $\boldsymbol{\omega}_g(t)$, is bounded, $\tilde{\boldsymbol{\varepsilon}}_o(t) \rightarrow 0$ asymptotically.*

Proof: Choose a Lyapunov function as

$$V_o(t) = \frac{1}{2} \begin{cases} (\tilde{\eta}_o(t) - 1)^2 + \tilde{\boldsymbol{\varepsilon}}_o(t)^T \tilde{\boldsymbol{\varepsilon}}_o(t) & \tilde{\eta}_o(t) \geq 0 \\ (\tilde{\eta}_o(t) + 1)^2 + \tilde{\boldsymbol{\varepsilon}}_o(t)^T \tilde{\boldsymbol{\varepsilon}}_o(t) & \tilde{\eta}_o(t) < 0 \end{cases} + \frac{1}{2} \begin{cases} (\tilde{\eta}_g(t) - 1)^2 + \tilde{\boldsymbol{\varepsilon}}_g(t)^T \tilde{\boldsymbol{\varepsilon}}_g(t) & \tilde{\eta}_g(t) \geq 0 \\ (\tilde{\eta}_g(t) + 1)^2 + \tilde{\boldsymbol{\varepsilon}}_g(t)^T \tilde{\boldsymbol{\varepsilon}}_g(t) & \tilde{\eta}_g(t) < 0 \end{cases} \quad (5.6)$$

The derivative of $V_o(t)$ is (again, as with the gyro bias estimator, including the left and right derivatives of the sign terms, and using $\tilde{\boldsymbol{\varepsilon}}_o(t)^T \dot{\tilde{\boldsymbol{\varepsilon}}}_o(t) + \tilde{\eta}_o(t)\dot{\tilde{\eta}}_o(t) = 0$)

$$\dot{V}_o(t) = \begin{cases} -\dot{\tilde{\eta}}_o(t) & \tilde{\eta}_o(t) \geq 0 \\ \dot{\tilde{\eta}}_o(t) & \tilde{\eta}_o(t) < 0 \end{cases} + \begin{cases} -\dot{\tilde{\eta}}_g(t) & \tilde{\eta}_g(t) \geq 0 \\ \dot{\tilde{\eta}}_g(t) & \tilde{\eta}_g(t) < 0 \end{cases}$$

Substituting for $\dot{\tilde{\eta}}_o(t)$ and $\dot{\tilde{\eta}}_g(t)$ from equations 5.4 and 5.5

$$\begin{aligned} \dot{V}_o(t) = & -\frac{k(t)}{2}\tilde{\epsilon}_o(t)^T\tilde{\epsilon}_o(t) + \frac{1}{2}\tilde{\epsilon}_o(t)^T[(R(\tilde{\mathbf{q}}_g(t)) - \mathbf{I})R(\hat{\mathbf{q}}_g(t))\boldsymbol{\omega}_g(t)\text{sign}(\tilde{\eta}_o(t)) \\ & - k_1(t)\text{sign}(\tilde{\epsilon}_o(t))] + \frac{1}{2}\tilde{\epsilon}_g(t)^T(R(\tilde{\mathbf{q}}_o(t)) - \mathbf{I})R(\hat{\mathbf{q}}_g(t))\boldsymbol{\omega}_g(t)\text{sign}(\tilde{\eta}_g(t)) \end{aligned} \quad (5.7)$$

Substituting equation 2.2 for $R(\tilde{\mathbf{q}}_o(t)) - \mathbf{I}$ into equation 5.7, $\dot{V}_o(t)$ becomes

$$\begin{aligned} \dot{V}_o(t) = & -\tilde{\epsilon}_o(t)^T\tilde{\epsilon}_o(t)\left(\frac{k(t)}{2} - \tilde{\epsilon}_g(t)^TR(\hat{\mathbf{q}}_g(t))\boldsymbol{\omega}_g(t)\text{sign}(\tilde{\eta}_g(t))\right) - \frac{k_1(t)}{2}\|\tilde{\epsilon}_o(t)\|_1 \\ & + \tilde{\epsilon}_g(t)^T(\tilde{\epsilon}_o(t)\tilde{\epsilon}_o(t)^T - \tilde{\eta}_o(t)S(\tilde{\epsilon}_o(t)))R(\hat{\mathbf{q}}_g(t))\boldsymbol{\omega}_g(t)\text{sign}(\tilde{\eta}_g(t)) \\ & + \frac{1}{2}\tilde{\epsilon}_o(t)^T(R(\tilde{\mathbf{q}}_g(t)) - \mathbf{I})R(\hat{\mathbf{q}}_g(t))\boldsymbol{\omega}_g(t)\text{sign}(\tilde{\eta}_o(t)) \end{aligned} \quad (5.8)$$

where $\|\tilde{\epsilon}_o(t)\|_1$ is the one-norm of $\tilde{\epsilon}_o(t)$. $\dot{V}_o(t)$ is bounded as

$$\begin{aligned} \dot{V}_o(t) = & -\|\tilde{\epsilon}_o(t)\|^2\left(\frac{k}{2} - \|\tilde{\epsilon}_g(t)\|\|R(\hat{\mathbf{q}}_g(t))\|\|\boldsymbol{\omega}_g(t)\|\right) - \frac{k_1(t)}{2}\|\tilde{\epsilon}_o(t)\|_1 \\ & \|\tilde{\epsilon}_g(t)\|(\|\tilde{\epsilon}_o(t)\|^2 + |\tilde{\eta}_o(t)|\|\tilde{\epsilon}_o(t)\|\|R(\hat{\mathbf{q}}_g(t))\|\|\boldsymbol{\omega}_g(t)\|) \\ & + \|\tilde{\epsilon}_o(t)\|\|R(\mathbf{q}_g) - \mathbf{I}\|\|R(\hat{\mathbf{q}}_g(t))\|\|\boldsymbol{\omega}_g(t)\| \end{aligned} \quad (5.9)$$

Applying the norms of 2.1, $|\tilde{\eta}_o(t)| \leq 1$, $\|\tilde{\epsilon}_g(t)\| \leq 1$, $\|R(\tilde{\mathbf{q}}_g(t)) - \mathbf{I}\| = 2\|\tilde{\epsilon}_g(t)\| \leq 2$, $\|R(\hat{\mathbf{q}}_g(t))\| = 1$, and utilizing $\|\tilde{\epsilon}_o(t)\| \leq \|\tilde{\epsilon}_o(t)\|_1 \leq \sqrt{3}\|\tilde{\epsilon}_o(t)\|$ [30], equation 5.9 can be written as

$$\dot{V}_o(t) \leq -\|\tilde{\epsilon}_o(t)\|^2\left(\frac{k(t)}{2} - 2\|\boldsymbol{\omega}_g(t)\|\right) - \|\tilde{\epsilon}_o(t)\|\left(\frac{k_1(t)}{2} - 2\|\boldsymbol{\omega}_g(t)\|\right)$$

if $k(t) \geq 4\|\boldsymbol{\omega}_g(t)\| + k'$ and $k_1 \geq 4\|\boldsymbol{\omega}_g(t)\| + k'_1$, where $k' > 0$ and $k'_1 > 0$ then

$$\dot{V}_o(t) \leq -k'\|\tilde{\epsilon}_o(t)\|^2 - k'_1\|\tilde{\epsilon}_o(t)\| \leq -k'\|\tilde{\epsilon}_o(t)\|^2 \quad (5.10)$$

With the added constraint that $\boldsymbol{\omega}_g(t)$ is bounded, $V_o(t)$ is a continuous, twice differentiable function. Lemma 2.1 then shows that $\|\tilde{\epsilon}_o(t)\| \rightarrow 0$ as $t \rightarrow \infty$. \square

Theorem 5.2 For any bounded, angular velocity, $\boldsymbol{\omega}_g(t)$, that is persistently exciting, the equilibrium states of the system 5.4 and 5.5 are exponentially stable. In particular, $\hat{\mathbf{q}}_g(t) \rightarrow \mathbf{q}_g$ exponentially fast from any initial conditions $\hat{\mathbf{q}}_g(t_0)$ and $\hat{\boldsymbol{\eta}}(t_0)$.

Proof: The system given by equations 5.4 and 5.5 is stable. If $\boldsymbol{\omega}_g(t)$ is bounded, all the signals are bounded. As with the gyro bias estimator analysis, the system is cast as a linear time-varying system $\dot{\mathbf{x}}(t) = A(t)\mathbf{x}(t)$ where

$$\mathbf{x}(t) = \begin{bmatrix} \tilde{\boldsymbol{\varepsilon}}_o(t) \\ \tilde{\boldsymbol{\varepsilon}}_g(t) \end{bmatrix}$$

In this case, developing $A(t)$ is more involved. First, the kinematic equation for $\tilde{\boldsymbol{\varepsilon}}_o(t)$ is repeated here as

$$\begin{aligned} \dot{\tilde{\boldsymbol{\varepsilon}}}_o(t) = & \frac{1}{2}Q_1(\tilde{\mathbf{q}}_o(t))[(R(\tilde{\mathbf{q}}_g(t)) - \mathbf{I})R(\hat{\mathbf{q}}_g(t))\boldsymbol{\omega}_g(t) - k\tilde{\boldsymbol{\varepsilon}}_o(t)\text{sign}(\tilde{\eta}_o(t)) \\ & - k_1\text{sign}(\tilde{\boldsymbol{\varepsilon}}_o(t))\text{sign}(\tilde{\eta}_o(t))] \end{aligned} \quad (5.11)$$

Substituting for $R(\tilde{\mathbf{q}}_g(t)) - \mathbf{I}$ from equation 2.2 and rearranging terms, equation 5.11 becomes

$$\begin{aligned} \dot{\tilde{\boldsymbol{\varepsilon}}}_o(t) = & -\frac{1}{2}Q_1(\tilde{\mathbf{q}}_o(t))\text{sign}(\tilde{\eta}_o(t))[k\tilde{\boldsymbol{\varepsilon}}_o(t) + k_1\text{sign}(\tilde{\boldsymbol{\varepsilon}}_o(t))] \\ & - Q_1(\tilde{\mathbf{q}}_o(t))[(R(\hat{\mathbf{q}}_g(t))\boldsymbol{\omega}_g(t))\tilde{\boldsymbol{\varepsilon}}_g(t)^T - (\tilde{\boldsymbol{\varepsilon}}_g(t)^T R(\hat{\mathbf{q}}_g(t))\boldsymbol{\omega}_g(t))\mathbf{I} \\ & - \tilde{\eta}_g(t)S(R(\hat{\mathbf{q}}_g(t))\boldsymbol{\omega}_g(t))]\tilde{\boldsymbol{\varepsilon}}_g(t) \end{aligned} \quad (5.12)$$

Rewrite $\text{sign}(\tilde{\boldsymbol{\varepsilon}}_o(t))$ as

$$\text{sign}(\tilde{\boldsymbol{\varepsilon}}_o(t)) = \begin{bmatrix} \frac{1}{|\tilde{\varepsilon}_{o1}(t)|} & 0 & 0 \\ 0 & \frac{1}{|\tilde{\varepsilon}_{o2}(t)|} & 0 \\ 0 & 0 & \frac{1}{|\tilde{\varepsilon}_{o3}(t)|} \end{bmatrix} \tilde{\boldsymbol{\varepsilon}}_o(t) = E(\tilde{\boldsymbol{\varepsilon}}_o(t))\tilde{\boldsymbol{\varepsilon}}_o(t) \quad (5.13)$$

Note that if any component of $\tilde{\boldsymbol{\varepsilon}}_o(t)$ is zero, the corresponding component in equation 5.13 is identically zero, given the definition of the sign function in equation 2.1. There is no possibility of dividing by zero. Equation 5.13 is used for the demonstration of the proof only. Equation 5.13 is substituted into equation 5.12 resulting in

$$\begin{aligned}\dot{\tilde{\boldsymbol{\varepsilon}}}_o(t) = & -\frac{1}{2}Q_1(\tilde{\boldsymbol{q}}_o(t))\text{sign}(\tilde{\eta}_o(t))[k + k_1E(\tilde{\boldsymbol{\varepsilon}}_o(t))]\tilde{\boldsymbol{\varepsilon}}_o(t) \\ & - Q_1(\tilde{\boldsymbol{q}}_o(t))[(R(\hat{\boldsymbol{q}}_g(t))\boldsymbol{\omega}_g(t))\tilde{\boldsymbol{\varepsilon}}_g(t)^T - (\tilde{\boldsymbol{\varepsilon}}_g(t)^T R(\hat{\boldsymbol{q}}_g(t))\boldsymbol{\omega}_g(t))\mathbf{I}] \\ & - \tilde{\eta}_g(t)S(R(\hat{\boldsymbol{q}}_g(t))\boldsymbol{\omega}_g(t))\tilde{\boldsymbol{\varepsilon}}_g(t)\end{aligned}\quad (5.14)$$

The kinematic equation for $\tilde{\boldsymbol{\varepsilon}}_g(t)$ is

$$\dot{\tilde{\boldsymbol{\varepsilon}}}_g(t) = \frac{1}{2}Q_1(\tilde{\boldsymbol{q}}_g(t))(R(\tilde{\boldsymbol{q}}_o(t)) - \mathbf{I})R(\hat{\boldsymbol{q}}_g(t))\boldsymbol{\omega}_g(t)\quad (5.15)$$

Again, substituting for $R(\tilde{\boldsymbol{q}}_o(t)) - \mathbf{I}$ from equation 2.2 and rearranging terms, equation 5.15 becomes

$$\begin{aligned}\dot{\tilde{\boldsymbol{\varepsilon}}}_g(t) = & -Q_1(\tilde{\boldsymbol{q}}_g(t))[(R(\hat{\boldsymbol{q}}_g(t))\boldsymbol{\omega}_g(t))\tilde{\boldsymbol{\varepsilon}}_o(t)^T - (\tilde{\boldsymbol{\varepsilon}}_o(t)^T R(\hat{\boldsymbol{q}}_g(t))\boldsymbol{\omega}_g(t))\mathbf{I}] \\ & - \tilde{\eta}_o(t)S(R(\hat{\boldsymbol{q}}_g(t))\boldsymbol{\omega}_g(t))\tilde{\boldsymbol{\varepsilon}}_o(t)\end{aligned}\quad (5.16)$$

From equations 5.14 and 5.16, the matrix $A(t)$ is written as

$$A(t) = \begin{bmatrix} A_{11}(t) & A_{12}(t) \\ A_{21}(t) & 0 \end{bmatrix}$$

where

$$\begin{aligned}A_{11}(t) = & -\frac{1}{2}Q_1(\tilde{\boldsymbol{q}}_o(t))\text{sign}(\tilde{\eta}_o(t))[k + k_1E(\tilde{\boldsymbol{\varepsilon}}_o(t))] \\ A_{12}(t) = & -Q_1(\tilde{\boldsymbol{q}}_o(t))[(R(\hat{\boldsymbol{q}}_g(t))\boldsymbol{\omega}_g(t))\tilde{\boldsymbol{\varepsilon}}_g(t)^T \\ & - (\tilde{\boldsymbol{\varepsilon}}_g(t)^T R(\hat{\boldsymbol{q}}_g(t))\boldsymbol{\omega}_g(t))\mathbf{I} - \tilde{\eta}_g(t)S(R(\hat{\boldsymbol{q}}_g(t))\boldsymbol{\omega}_g(t))]\end{aligned}$$

$$A_{21}(t) = -Q_1(\tilde{\mathbf{q}}_g(t))[(R(\hat{\mathbf{q}}_g(t))\boldsymbol{\omega}_g(t))\tilde{\boldsymbol{\varepsilon}}_o(t)^T \\ - (\tilde{\boldsymbol{\varepsilon}}_o(t)^T R(\hat{\mathbf{q}}_g(t))\boldsymbol{\omega}_g(t))\mathbf{I} - \tilde{\eta}_o(t)S(R(\hat{\mathbf{q}}_g(t))\boldsymbol{\omega}_g(t))]$$

Following the proof for the gyro bias estimator, $\dot{V}_o(t)$ is rewritten as $\dot{V}_o(t) \leq -\mathbf{x}(t)^T C^T C \mathbf{x}(t) \leq 0$, where $C = [\sqrt{k'} \ 0]$. Again, theorem 4.5 and the discussion on pp.626-628 in [30] shows that the equilibrium point $\mathbf{x}(t) = 0$ of this equivalent system is exponentially stable if the pair $(A(t), C)$ is uniformly completely observable (UCO). Since observability properties are unchanged under output feedback [30], this will be true if the pair $(A(t) - K(t)C, C)$ is uniformly observable for any piecewise, continuous and bounded matrix $K(t)$. $K(t)$ is chosen as

$$K(t) = \begin{bmatrix} \frac{1}{\sqrt{k'}} A_{11}(t) \\ \frac{1}{\sqrt{k'}} A_{21}(t) \end{bmatrix}$$

With $\boldsymbol{\omega}_g(t)$ bounded, applying the same arguments as with the gyro bias estimator, $K(t)$ is a piecewise continuous function of time.

The state transition matrix for the pair $(A(t) - K(t)C, C)$ is given in 3.8 where here

$$\Sigma(\tau, t) = \int_t^\tau A_{12}(\sigma) d\sigma$$

The observability Grammian is

$$W(t, t+T) = \int_t^{t+T} \Phi(\tau, t)^T C^T C \Phi(\tau, t) d\tau \\ = \int_t^{t+T} \begin{bmatrix} k' \mathbf{I} & k' \Sigma(\tau, t) \\ k' \Sigma(\tau, t)^T & k' \Sigma(\tau, t)^T \Sigma(\tau, t) \end{bmatrix} d\tau \quad (5.17)$$

The system is UCO if there exists a $T > 0$ and positive constants $\alpha_1 > 0, \alpha_2 > 0$ such that, for all $t \geq t_0$, $\alpha_1 \mathbf{I} \geq W(t, t+T) \geq \alpha_2 \mathbf{I}$. Proceeding similarly to 3.10 for the gyro bias estimator proof, this is assured if $A_{12}(t)$ and $\frac{d}{dt}A_{12}(t)$ are bounded, and there exist positive constants T_2, β_1 , and β_2 such that, for all $t \geq t_0$

$$\beta_2 \mathbf{I} \geq \int_t^{t+T_2} A_{12}(\tau)^T A_{12}(\tau) d\tau \geq \beta_1 \mathbf{I} \quad (5.18)$$

Rewrite $A_{12}(t)$ as $A_{12}(t) = -Q_1(\tilde{\mathbf{q}}_o(t))B(t)$, where

$$B(t) = (R(\hat{\mathbf{q}}_g(t))\boldsymbol{\omega}_g(t))\tilde{\boldsymbol{\epsilon}}_g(t)^T - (\tilde{\boldsymbol{\epsilon}}_g(t)^T R(\hat{\mathbf{q}}_g(t))\boldsymbol{\omega}_g(t))\mathbf{I} - \tilde{\eta}_g(t)S(R(\hat{\mathbf{q}}_g(t))\boldsymbol{\omega}_g(t))$$

The integral 5.18 becomes

$$\beta_2 \mathbf{I} \geq \int_t^{t+T_2} B(\tau)^T Q_1(\tilde{\mathbf{q}}_o(\tau))^T Q_1(\tilde{\mathbf{q}}_o(\tau)) B(\tau) d\tau \geq \beta_1 \mathbf{I} \quad (5.19)$$

$Q_1(\tilde{\mathbf{q}}_o(t))$ is bounded by definition, since it contains elements of the quaternion, $\tilde{\mathbf{q}}_o(t)$. $\frac{d}{dt}Q_1(\tilde{\mathbf{q}}_o(t))$ is also bounded, since the above Lyapunov analysis shows that all the terms in equation 5.5 are bounded, given that $\boldsymbol{\omega}_g(t)$ is bounded. With $\dot{\boldsymbol{\omega}}_g(t)$ bounded, the upper bound in equation 5.19 is satisfied.

To examine the lower bound, as with the gyro bias estimator, again recall that $\|\tilde{\boldsymbol{\epsilon}}_o(t)\| \rightarrow 0$ asymptotically. Thus, for any $\delta > 0$, there exists a $T_1(\delta) > t_0$ such that $\|\tilde{\boldsymbol{\epsilon}}_o(t)\| < \delta$ for all $t \geq t_0 + T_1$. Taking any $\delta < 1$ and $T_2 > T_1$ and using

$Q_1(\tilde{\mathbf{q}}_o(t))^T Q_1(\tilde{\mathbf{q}}_o(t)) = \mathbf{I} - \tilde{\boldsymbol{\varepsilon}}_o(t)\tilde{\boldsymbol{\varepsilon}}_o(t)^T$, for any $z \in \mathbb{R}^3$

$$\begin{aligned}
& \mathbf{z}^T \left[\int_t^{t+T_2} B(\tau)^T Q_1(\tilde{\mathbf{q}}_o(\tau))^T Q_1(\tilde{\mathbf{q}}_o(\tau)) B(\tau) d\tau \right] \mathbf{z} \\
&= \mathbf{z}^T \left[\int_t^{t+T_2} B(\tau) (\mathbf{I} - \tilde{\boldsymbol{\varepsilon}}_o(t)\tilde{\boldsymbol{\varepsilon}}_o(t)^T) B(\tau) d\tau \right] \mathbf{z} \\
&\geq \mathbf{z}^T \left[\int_t^{t+T_2} B(\tau) (\mathbf{I} - \delta^2 \mathbf{I}) B(\tau) d\tau \right] \mathbf{z} \\
&\geq (1 - \delta^2) \mathbf{z}^T \left[\int_t^{t+T_2} B(\tau)^T B(\tau) d\tau \right] \mathbf{z}
\end{aligned} \tag{5.20}$$

If the following is true, for all $t \geq t_0 + T_1$

$$\mathbf{z}^T \left[\int_t^{t+T_2} B(\tau)^T B(\tau) d\tau \right] \mathbf{z} > 0 \tag{5.21}$$

then equation 5.18 is satisfied and the system is UCO.

Rewrite $B(t)$ as

$$\begin{aligned}
B(t) &= S(\tilde{\boldsymbol{\varepsilon}}_g(t)) S(R(\hat{\mathbf{q}}_g(t)) \boldsymbol{\omega}_g(t)) - \tilde{\eta}_g(t) S(R(\hat{\mathbf{q}}_g(t)) \boldsymbol{\omega}_g(t)) \\
&= (S(\tilde{\boldsymbol{\varepsilon}}_g(t)) - \tilde{\eta}_g(t) \mathbf{I}) S(R(\hat{\mathbf{q}}_g(t)) \boldsymbol{\omega}_g(t))
\end{aligned} \tag{5.22}$$

Because of the skew symmetric matrices, $B(t)$ is singular. Using $B(t)$ from equation 5.22, $B(t)^T B(t)$ is

$$\begin{aligned}
B(t)^T B(t) &= S(R(\hat{\mathbf{q}}_g(t)) \boldsymbol{\omega}_g(t)) (S(\tilde{\boldsymbol{\varepsilon}}_g(t)) + \tilde{\eta}_g(t) \mathbf{I}) (S(\tilde{\boldsymbol{\varepsilon}}_g(t)) - \tilde{\eta}_g(t) \mathbf{I}) S(R(\hat{\mathbf{q}}_g(t)) \boldsymbol{\omega}_g(t)) \\
&= S(R(\hat{\mathbf{q}}_g(t)) \boldsymbol{\omega}_g(t)) (S(\tilde{\boldsymbol{\varepsilon}}_g(t)) S(\tilde{\boldsymbol{\varepsilon}}_g(t)) - \tilde{\eta}_g(t)^2 \mathbf{I}) S(R(\hat{\mathbf{q}}_g(t)) \boldsymbol{\omega}_g(t)) \\
&= S(R(\hat{\mathbf{q}}_g(t)) \boldsymbol{\omega}_g(t)) (\tilde{\boldsymbol{\varepsilon}}_g(t) \tilde{\boldsymbol{\varepsilon}}_g(t)^T - \mathbf{I}) S(R(\hat{\mathbf{q}}_g(t)) \boldsymbol{\omega}_g(t)) \\
&= R(\hat{\mathbf{q}}_g(t)) S(\boldsymbol{\omega}_g(t))^T (\mathbf{I} - \tilde{\boldsymbol{\varepsilon}}_{gR}(t) \tilde{\boldsymbol{\varepsilon}}_{gR}(t)^T) S(\boldsymbol{\omega}_g(t)) R(\hat{\mathbf{q}}_g(t))^T
\end{aligned} \tag{5.23}$$

where $\tilde{\boldsymbol{\varepsilon}}_{gR}(t) = R(\hat{\mathbf{q}}_g(t))^T \tilde{\boldsymbol{\varepsilon}}_g(t)$, note that $\|\tilde{\boldsymbol{\varepsilon}}_{gR}(t)\| = \|\tilde{\boldsymbol{\varepsilon}}_g(t)\|$.

Substituting equation 5.23 into equation 5.21 gives

$$\mathbf{z}^T \left[\int_t^{t+T_2} R(\hat{\mathbf{q}}_g(\tau)) S(\boldsymbol{\omega}_g(t))^T (\mathbf{I} - \tilde{\boldsymbol{\epsilon}}_{gR}(t) \tilde{\boldsymbol{\epsilon}}_{gR}(t)^T) S(\boldsymbol{\omega}_g(t)) R(\hat{\mathbf{q}}_g(\tau))^T d\tau \right] \mathbf{z} \quad (5.24)$$

Let $\mathbf{y} = R(\hat{\mathbf{q}}_g(t))^T \mathbf{z}$. The transformation matrix $R(\hat{\mathbf{q}}_g(t))$ is nonsingular, so equation 5.24 can be evaluated equivalently as

$$\mathbf{y}^T \left[\int_t^{t+T_2} S(\boldsymbol{\omega}_g(t))^T (\mathbf{I} - \tilde{\boldsymbol{\epsilon}}_{gR}(t) \tilde{\boldsymbol{\epsilon}}_{gR}(t)^T) S(\boldsymbol{\omega}_g(t)) d\tau \right] \mathbf{y} \quad (5.25)$$

for any $\mathbf{y} \in \mathbb{R}^3$. Next, the matrix in the middle of equation 5.25, $[\mathbf{I} - \tilde{\boldsymbol{\epsilon}}_{gR}(t) \tilde{\boldsymbol{\epsilon}}_{gR}(t)^T]$ is evaluated.

If a component of $\|\tilde{\boldsymbol{\epsilon}}_g(t)\| = 1$, a component of $\tilde{\boldsymbol{\epsilon}}_{gR}(t)$ could equal 1. In that case equation 5.25 will not be positive definite for any $\boldsymbol{\omega}_g(t)$. However, if $\|\tilde{\boldsymbol{\epsilon}}_g(t)\| = 1$ at t_0 , it cannot remain there. This is shown with the following lemma.

Lemma 5.1 *If $\hat{\mathbf{q}}(t_0)$ is initialized such that $\hat{\mathbf{q}}(t_0) = \mathbf{q}(t_0)$, $\|\tilde{\boldsymbol{\epsilon}}_g(t)\| < 1$ for all $t \geq t_0$.*

Proof: The derivative of the Lyapunov function, again, satisfies

$$\dot{V}_o(t) \leq -k' \|\tilde{\boldsymbol{\epsilon}}_o(t)\|^2$$

$\dot{V}_o(t)$ is integrated as

$$V_o(t) \leq V_o(t_0) - k' \int_{t_0}^t \tilde{\boldsymbol{\epsilon}}_o(\tau)^T \tilde{\boldsymbol{\epsilon}}_o(\tau) d\tau \quad (5.26)$$

The Lyapunov function is therefore decreasing with time, $V_o(t) < V_o(t_0)$. At t_0 , the portion of $V_o(t_0)$ due to $\tilde{\mathbf{q}}_o(t_0)$ is a minimum if $\|\tilde{\boldsymbol{\epsilon}}_o(t_0)\| = 0$. Since $\tilde{\mathbf{q}}_o(t_0)$ is known,

$\|\tilde{\boldsymbol{\varepsilon}}_o(t_0)\|$ can be set such that $\|\tilde{\boldsymbol{\varepsilon}}_o(t_0)\| = 0$. Substituting for $V_o(t)$ and $V_o(t_0)$ from equation 5.6 gives

$$\begin{aligned}
& \frac{1}{2} \left\{ \begin{array}{l} (\tilde{\eta}_o(t) - 1)^2 + \tilde{\boldsymbol{\varepsilon}}_o(t)^T \tilde{\boldsymbol{\varepsilon}}_o(t) \quad \tilde{\eta}_o(t) \geq 0 \\ (\tilde{\eta}_o(t) + 1)^2 + \tilde{\boldsymbol{\varepsilon}}_o(t)^T \tilde{\boldsymbol{\varepsilon}}_o(t) \quad \tilde{\eta}_o(t) < 0 \end{array} \right. \\
& + \frac{1}{2} \left\{ \begin{array}{l} (\tilde{\eta}_g(t) - 1)^2 + \tilde{\boldsymbol{\varepsilon}}_g(t)^T \tilde{\boldsymbol{\varepsilon}}_g(t) \quad \tilde{\eta}_g(t) \geq 0 \\ (\tilde{\eta}_g(t) + 1)^2 + \tilde{\boldsymbol{\varepsilon}}_g(t)^T \tilde{\boldsymbol{\varepsilon}}_g(t) \quad \tilde{\eta}_g(t) < 0 \end{array} \right. \\
& < \frac{1}{2} \left\{ \begin{array}{l} (\tilde{\eta}_g(t_0) - 1)^2 + \tilde{\boldsymbol{\varepsilon}}_g(t_0)^T \tilde{\boldsymbol{\varepsilon}}_g(t_0) \quad \tilde{\eta}_g(t_0) \geq 0 \\ (\tilde{\eta}_g(t_0) + 1)^2 + \tilde{\boldsymbol{\varepsilon}}_g(t_0)^T \tilde{\boldsymbol{\varepsilon}}_g(t_0) \quad \tilde{\eta}_g(t_0) < 0 \end{array} \right. \\
& + \frac{1}{2} \left\{ \begin{array}{l} (\tilde{\eta}_o(t_0) - 1)^2 + \tilde{\boldsymbol{\varepsilon}}_o(t_0)^T \tilde{\boldsymbol{\varepsilon}}_o(t_0) \quad \tilde{\eta}_o(t_0) \geq 0 \\ (\tilde{\eta}_o(t_0) + 1)^2 + \tilde{\boldsymbol{\varepsilon}}_o(t_0)^T \tilde{\boldsymbol{\varepsilon}}_o(t_0) \quad \tilde{\eta}_o(t_0) < 0 \end{array} \right.
\end{aligned} \tag{5.27}$$

Substituting $\tilde{\boldsymbol{\varepsilon}}_o(t_0) = 0$ (which means $\tilde{\eta}_o(t_0) = \pm 1$) equation 5.27 becomes

$$\begin{aligned}
& \frac{1}{2} \left\{ \begin{array}{l} (\tilde{\eta}_o(t) - 1)^2 + \tilde{\boldsymbol{\varepsilon}}_o(t)^T \tilde{\boldsymbol{\varepsilon}}_o(t) \quad \tilde{\eta}_o(t) \geq 0 \\ (\tilde{\eta}_o(t) + 1)^2 + \tilde{\boldsymbol{\varepsilon}}_o(t)^T \tilde{\boldsymbol{\varepsilon}}_o(t) \quad \tilde{\eta}_o(t) < 0 \end{array} \right. \\
& + \frac{1}{2} \left\{ \begin{array}{l} (\tilde{\eta}_g(t) - 1)^2 + \tilde{\boldsymbol{\varepsilon}}_g(t)^T \tilde{\boldsymbol{\varepsilon}}_g(t) \quad \tilde{\eta}_g(t) \geq 0 \\ (\tilde{\eta}_g(t) + 1)^2 + \tilde{\boldsymbol{\varepsilon}}_g(t)^T \tilde{\boldsymbol{\varepsilon}}_g(t) \quad \tilde{\eta}_g(t) < 0 \end{array} \right. \\
& < \frac{1}{2} \left\{ \begin{array}{l} (\tilde{\eta}_g(t_0) - 1)^2 + \tilde{\boldsymbol{\varepsilon}}_g(t_0)^T \tilde{\boldsymbol{\varepsilon}}_g(t_0) \quad \tilde{\eta}_g(t_0) \geq 0 \\ (\tilde{\eta}_g(t_0) + 1)^2 + \tilde{\boldsymbol{\varepsilon}}_g(t_0)^T \tilde{\boldsymbol{\varepsilon}}_g(t_0) \quad \tilde{\eta}_g(t_0) < 0 \end{array} \right.
\end{aligned}$$

Expanding the quaternion terms results in

$$1 + \begin{cases} -\tilde{\eta}_g(t) & \tilde{\eta}_g(t) \geq 0 \\ \tilde{\eta}_g(t) & \tilde{\eta}_g(t) < 0 \end{cases} + 1 + \begin{cases} -\tilde{\eta}_o(t) & \tilde{\eta}_o(t) \geq 0 \\ \tilde{\eta}_o(t) & \tilde{\eta}_o(t) < 0 \end{cases} < 1 + \begin{cases} -\tilde{\eta}_g(t_0) & \tilde{\eta}_g(t_0) \geq 0 \\ \tilde{\eta}_g(t_0) & \tilde{\eta}_g(t_0) < 0 \end{cases}$$

Rearranging the terms again, gives

$$|\tilde{\eta}_g(t)| > |\tilde{\eta}_g(t_0)| + 1 - |\tilde{\eta}_o(t)|$$

Since $|\tilde{\eta}_o(t)| \leq 1$ and $|\tilde{\eta}_g(t)| \leq 1$, the following is true

$$1 \geq |\tilde{\eta}_g(t)| > |\tilde{\eta}_g(t_0)|$$

Since $|\tilde{\eta}_g(t)|$ is greater than $|\tilde{\eta}_g(t_0)|$, equivalently

$$\|\tilde{\boldsymbol{\varepsilon}}_g(t)\| < \|\tilde{\boldsymbol{\varepsilon}}_g(t_0)\| \quad (5.28)$$

If $\|\tilde{\boldsymbol{\varepsilon}}_g(t_0)\| = 1$, $\|\tilde{\boldsymbol{\varepsilon}}_g(t)\| < 1$. \square

Equation 5.25 can now be evaluated with $\|\tilde{\boldsymbol{\varepsilon}}_g(t)\| < 1$. The norm of $\tilde{\boldsymbol{\varepsilon}}_{gR}(t)$ is again $\|\tilde{\boldsymbol{\varepsilon}}_{gR}(t)\| = \|\tilde{\boldsymbol{\varepsilon}}_g(t)\|$. Choose $\delta_g < 1$, and let $\|\tilde{\boldsymbol{\varepsilon}}_{gR}(t)\| = \delta_g < 1$. Therefore,

$$\mathbf{I} - \tilde{\boldsymbol{\varepsilon}}_{gR}(t)\tilde{\boldsymbol{\varepsilon}}_{gR}(t)^T \geq (1 - \delta_g^2)\mathbf{I} \quad (5.29)$$

Substitute equation 5.29 into equation 5.25. Now, if the following is true

$$(1 - \delta_g)^2 \mathbf{y}^T \left[\int_t^{t+T_2} S(\boldsymbol{\omega}_g(\tau))^T S(\boldsymbol{\omega}_g(\tau)) d\tau \right] \mathbf{y} > 0 \quad (5.30)$$

or equivalently, if the following matrix is positive definite

$$\int_t^{t+T_2} S(\boldsymbol{\omega}_g(\tau))^T S(\boldsymbol{\omega}_g(\tau)) d\tau > 0 \quad (5.31)$$

equation 5.21 is satisfied.

The skew symmetric matrix $S(\boldsymbol{\omega}_g(t))$ is singular for any time, t . The matrix $S(\boldsymbol{\omega}_g(t))S(\boldsymbol{\omega}_g(t))$ is therefore singular for any time, t . In order to satisfy the PE condition, the angular velocity must change directions sufficiently over the time interval T_2 , such that the integral 5.31 is positive definite. An example of an angular velocity that satisfies the PE condition is

$$\boldsymbol{\omega}_g(t)^T = [\sin \vartheta t \ 1 \ 0]$$

and $T_2 = \frac{2\pi}{\vartheta}$. Substituting $\boldsymbol{\omega}_g(t)$ into equation 5.25, and evaluating the integral results in

$$\int_t^{t+T_2} S(\boldsymbol{\omega}_g(\tau))^T S(\boldsymbol{\omega}_g(\tau)) d\tau = \frac{\pi}{\vartheta} \begin{bmatrix} 2 & 0 & 0 \\ 0 & 1 & 0 \\ 0 & 0 & 3 \end{bmatrix}$$

which is positive definite. Equation 5.21 is satisfied, the system is persistently exciting, and the alignment errors converge to zero exponentially fast.

If the angular velocity is constant, the PE condition will not be satisfied. Evaluating equation 5.31 with $\boldsymbol{\omega}_g(t)^T = [a, \ b, \ c]$, for example, gives

$$\begin{aligned} & \int_t^{t+T_2} S(\boldsymbol{\omega}_g(\tau))^T S(\boldsymbol{\omega}_g(\tau)) d\tau \\ &= \begin{bmatrix} 0 & -c & b \\ c & 0 & -a \\ -b & a & 0 \end{bmatrix} \begin{bmatrix} 0 & -c & b \\ c & 0 & -a \\ -b & a & 0 \end{bmatrix} (T_2 - T_1) \end{aligned}$$

<i>Attitude</i>	<i>Value</i>	<i>Alignment</i>	<i>Value</i>
$\mathbf{q}(t_0)$	$[0, 1, 0, 0]^T$	\mathbf{q}_g	$[0, 0, 1, 0]^T$
$\hat{\mathbf{q}}(t_0)$	$[0, 0, 0, 1]^T$	$\hat{\mathbf{q}}_g(t)$	$[0, 0, 0, 1]^T$

Table 5.1: Alignment Estimation Simulation Initial Conditions

which is singular (the determinants of the skew symmetric matrices are zero), and therefore not positive definite. The system is not PE for a constant angular velocity.

□

5.2 Estimation Simulation Results

The gyro alignment estimator is tested similarly to the bias estimator. Table 5.1 lists the initial quaternions for the estimator, as well as the true alignment. In the first case, the angular velocity is constant, with $\boldsymbol{\omega}(t)^T = [3, -4, 5]$ deg/sec. The gains are chosen as $k' = 1$, $k'_1 = 0.01$. Figure 5.2 shows that the alignment estimation errors converge to a constant, since a constant angular velocity does not meet the PE condition. Next, the angular velocity is time varying. The angular velocity is chosen as $\boldsymbol{\omega}(t)^T = [\sin \vartheta t, 1, 0]$ deg/sec, where $\vartheta = 5$ deg/sec. The gains are chosen as $k' = 0.001$ and $k'_1 = 0.1$. Figure 5.2 shows that the alignment estimation errors converge to zero.

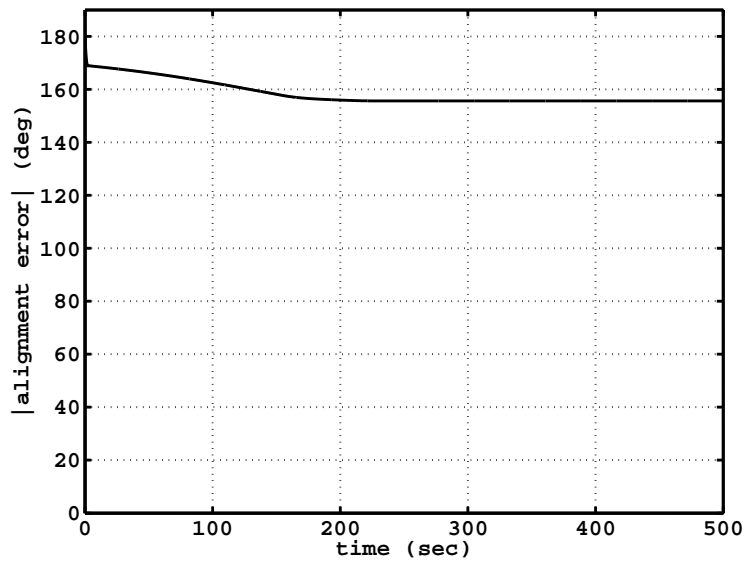


Figure 5.1: Alignment Estimation with Constant Angular Velocity

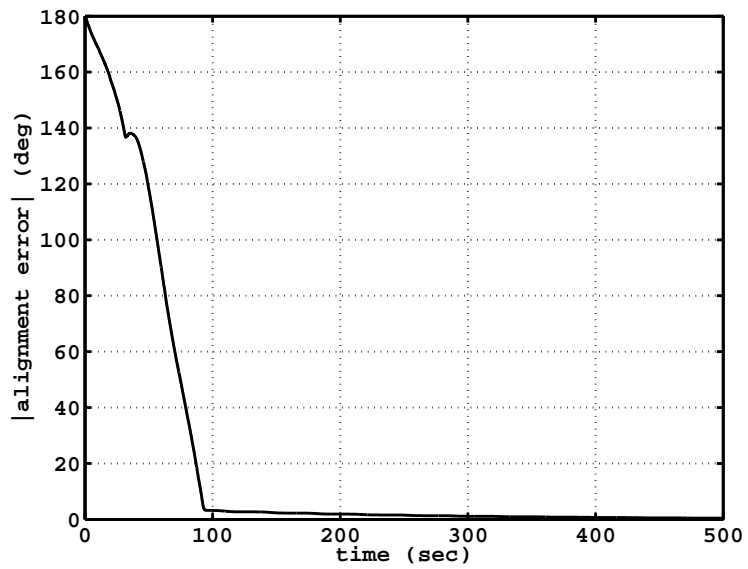


Figure 5.2: Alignment Estimation with PE Angular Velocity

5.3 Closed Loop Stability

As in Section 3.3, a certainty equivalence approach is proposed in utilizing the non-linear tracking algorithm in [32]. Here the estimates $\hat{\boldsymbol{\omega}}(t)$ of 2.13, generated by the estimator equations 5.1 and 5.2 are used to generate the control. Again, the control is given as

$$\mathbf{u}(t) = -K_D \hat{\mathbf{s}}(t) + H \hat{\boldsymbol{\alpha}}_r(t) - S(H \hat{\boldsymbol{\omega}}(t)) \boldsymbol{\omega}_r(t) \quad (5.32)$$

The closed loop analysis from Section 3.3, up to equation 3.20, is independent of the specific gyro error. As with the scale factor, the closed loop equation, given in equation 3.20, is repeated here

$$H \dot{\mathbf{s}}(t) - S(H \boldsymbol{\omega}(t)) \mathbf{s}(t) + K_D \mathbf{s}(t) = \Delta(\tilde{\mathbf{q}}_c(t), \boldsymbol{\omega}_d(t)) \tilde{\mathbf{s}}(t) \quad (5.33)$$

where

$$\begin{aligned} \Delta(\tilde{\mathbf{q}}_c(t), \boldsymbol{\omega}_d(t)) &= -S(\boldsymbol{\omega}_r(t))H - HS(R(\tilde{\mathbf{q}}_c(t))\boldsymbol{\omega}_d(t)) + \lambda H Q_1(\tilde{\mathbf{q}}_c(t)) + K_D \\ &= \Delta'(\tilde{\mathbf{q}}_c(t), \boldsymbol{\omega}_d(t)) + K_D \end{aligned}$$

and the error term $\tilde{\mathbf{s}}(t)$ is

$$\tilde{\mathbf{s}}(t) = \mathbf{s}(t) - \hat{\mathbf{s}}(t) = \boldsymbol{\omega}(t) - \hat{\boldsymbol{\omega}}(t)$$

Note that the definition of $\boldsymbol{\omega}_r(t)$, the assumption the $\boldsymbol{\omega}_d(t)$ is bounded, and the constraint $\|\tilde{\mathbf{q}}_c(t)\| = 1$ ensure that $\Delta'(\tilde{\mathbf{q}}_c(t), \boldsymbol{\omega}_d(t))$ is a bounded matrix over any solution of the coupled dynamics 5.1, 5.2, 2.21, and 5.32.

Theorem 5.3 *If the gyro alignment rotation angle is less than 90 degrees and*

$$k_D > 2\zeta' + 2$$

where $\zeta' = \sup_{t \geq t_0} \sup_{\|\tilde{\mathbf{q}}_c(t)\|=1} \|\Delta'(\tilde{\mathbf{q}}_c(t), \boldsymbol{\omega}_r(t))\| < \infty$, the control law 5.32 results in a stable closed loop system, with $\|\tilde{\boldsymbol{\epsilon}}_c(t)\|$ and $\|\tilde{\boldsymbol{\omega}}_c(t)\|$ uniformly, ultimately bounded.

Proof: Using the Lyapunov function $V_c(t) = \frac{1}{2} \mathbf{s}(t)^T H \mathbf{s}(t)$, the derivative of $V_c(t)$ is

$$\dot{V}_c(t) = -\mathbf{s}(t)^T K_D \mathbf{s}(t) + \mathbf{s}(t)^T \Delta(\tilde{\mathbf{q}}_c(t), \boldsymbol{\omega}_d(t)) \tilde{\mathbf{s}}(t) \quad (5.34)$$

or substituting for $\Delta(\tilde{\mathbf{q}}_c(t), \boldsymbol{\omega}_d(t))$

$$\dot{V}_c(t) = -\mathbf{s}(t)^T K_D \mathbf{s}(t) + \mathbf{s}(t)^T (\Delta'(\tilde{\mathbf{q}}_c(t), \boldsymbol{\omega}_d(t)) + K_D) \tilde{\mathbf{s}}(t) \quad (5.35)$$

$\dot{V}_c(t)$ is rewritten in terms of $\boldsymbol{\omega}_g(t)$ and $\boldsymbol{\omega}_r(t)$. Rewrite $\mathbf{s}(t)$ as

$$\mathbf{s}(t) = \boldsymbol{\omega}(t) - \boldsymbol{\omega}_r(t) = R(\mathbf{q}_g) \boldsymbol{\omega}_g(t) - \boldsymbol{\omega}_r(t) = R(\tilde{\mathbf{q}}_g(t)) R(\hat{\mathbf{q}}_g(t)) \boldsymbol{\omega}_g(t) - \boldsymbol{\omega}_r(t)$$

and rewrite $\hat{\mathbf{s}}(t)$ as

$$\hat{\mathbf{s}}(t) = \hat{\boldsymbol{\omega}}(t) - \boldsymbol{\omega}_r(t) = R(\hat{\mathbf{q}}_g(t)) \boldsymbol{\omega}_g(t) - \boldsymbol{\omega}_r(t)$$

Expanding 5.35 gives

$$\dot{V}_c(t) = \mathbf{s}(t)^T \Delta'(\tilde{\mathbf{q}}_c(t), \boldsymbol{\omega}_d(t)) (\mathbf{s}(t) - \hat{\mathbf{s}}(t)) - \mathbf{s}^T K_D \hat{\mathbf{s}}(t) \quad (5.36)$$

Substitute the expressions for $\mathbf{s}(t)$ and $\hat{\mathbf{s}}(t)$ into equation 5.36, letting $K_D = k_D I$,

resulting in

$$\begin{aligned} \dot{V}_c(t) = & (\boldsymbol{\omega}_g(t)^T R(\hat{\mathbf{q}}_g(t))^T R(\tilde{\mathbf{q}}_g(t))^T \\ & - \boldsymbol{\omega}_r(t)^T \Delta'(\tilde{\mathbf{q}}_c(t), \boldsymbol{\omega}_d(t)) (R(\tilde{\mathbf{q}}_g(t)) - \mathbf{I}) R(\hat{\mathbf{q}}_g(t)) \boldsymbol{\omega}_g(t) \\ & - k_D (\boldsymbol{\omega}_g(t)^T R(\hat{\mathbf{q}}_g(t))^T R(\tilde{\mathbf{q}}_g(t))^T - \boldsymbol{\omega}_r(t)^T) (R(\hat{\mathbf{q}}_g(t)) \boldsymbol{\omega}_g(t) - \boldsymbol{\omega}_r(t)) \end{aligned} \quad (5.37)$$

Expanding the terms in equation 5.37 gives

$$\begin{aligned}
\dot{V}_c(t) &= -k_D(R(\hat{\mathbf{q}}_g(t))\boldsymbol{\omega}_g(t))^T R(\tilde{\mathbf{q}}_g(t))^T (R(\hat{\mathbf{q}}_g(t))\boldsymbol{\omega}_g(t)) + k_D\boldsymbol{\omega}_r(t)^T R(\hat{\mathbf{q}}_g(t))\boldsymbol{\omega}_g(t) \\
&\quad + k_D\boldsymbol{\omega}_g(t)^T R(\hat{\mathbf{q}}_g(t))^T R(\tilde{\mathbf{q}}_g(t))^T \boldsymbol{\omega}_r(t) - k_D\boldsymbol{\omega}_r(t)^T \boldsymbol{\omega}_r(t) \\
&\quad \boldsymbol{\omega}_g(t)^T R(\hat{\mathbf{q}}_g(t))^T R(\tilde{\mathbf{q}}_g(t))^T \Delta'(\tilde{\mathbf{q}}_c(t), \boldsymbol{\omega}_d(t))(R(\tilde{\mathbf{q}}_g(t)) - \mathbf{I})R(\hat{\mathbf{q}}_g(t))\boldsymbol{\omega}_g(t) \\
&\quad - \boldsymbol{\omega}_r(t)^T \Delta'(\tilde{\mathbf{q}}_c(t), \boldsymbol{\omega}_d(t))(R(\tilde{\mathbf{q}}_g(t)) - \mathbf{I})R(\hat{\mathbf{q}}_g(t))\boldsymbol{\omega}_g(t)
\end{aligned} \tag{5.38}$$

The first term in equation 5.38 is negative if $R(\tilde{\mathbf{q}}_g(t))$ is positive definite. Recall that

$$\begin{aligned}
R(\tilde{\mathbf{q}}_g(t)) &= (\tilde{\eta}_g(t)^2 - \tilde{\boldsymbol{\varepsilon}}_g(t)^T \tilde{\boldsymbol{\varepsilon}}_g(t))\mathbf{I} + 2\tilde{\boldsymbol{\varepsilon}}_g(t)\tilde{\boldsymbol{\varepsilon}}_g(t)^T - 2\tilde{\eta}_g(t)S(\tilde{\boldsymbol{\varepsilon}}_g(t)) \\
&= (1 - 2\tilde{\boldsymbol{\varepsilon}}_g(t)^T \tilde{\boldsymbol{\varepsilon}}_g(t))\mathbf{I} + 2\tilde{\boldsymbol{\varepsilon}}_g(t)\tilde{\boldsymbol{\varepsilon}}_g(t)^T - 2\tilde{\eta}_g(t)S(\tilde{\boldsymbol{\varepsilon}}_g(t))
\end{aligned}$$

If

$$1 - 2\|\tilde{\boldsymbol{\varepsilon}}_g(t)\|^2 > 0$$

or $\|\tilde{\boldsymbol{\varepsilon}}_g(t)\|^2 < \frac{1}{2}$, $R(\tilde{\mathbf{q}}_g(t))$ (and equivalently $R(\tilde{\mathbf{q}}_g(t))^T$) is positive definite.

The terms in equation 5.38 are bounded as

$$\begin{aligned}
\dot{V}_c(t) &\leq -k_D\|\boldsymbol{\omega}_g(t)\|^2 + 2k_D\|\boldsymbol{\omega}_g(t)\|\|\boldsymbol{\omega}_r(t)\| - k_D\|\boldsymbol{\omega}_r(t)\|^2 \\
&\quad + 2\zeta'\|\boldsymbol{\omega}_g(t)\|^2 + 2\zeta'\|\boldsymbol{\omega}_g(t)\|\|\boldsymbol{\omega}_r(t)\|
\end{aligned} \tag{5.39}$$

where $\|R(\hat{\mathbf{q}}_g(t))\| = 1$ and

$$\zeta' = \sup_{t \geq t_0} \sup_{\|\tilde{\mathbf{q}}_c(t)\|=1} \|\Delta'(\tilde{\mathbf{q}}_c(t), \boldsymbol{\omega}_r(t))\| < \infty$$

Applying Young's inequality to the terms with the product of $\|\boldsymbol{\omega}_g(t)\|$ and $\|\boldsymbol{\omega}_r(t)\|$,

$\dot{V}_c(t)$ becomes

$$\dot{V}_c(t) \leq -(k_D - 2\zeta' - 2)\|\boldsymbol{\omega}_g(t)\|^2 - (k_D - \frac{1}{2}k_D^2 - \frac{1}{2}\zeta'^2)\|\boldsymbol{\omega}_r(t)\|^2 \tag{5.40}$$

If

$$k_D > 2\zeta' + 2 \quad (5.41)$$

and $\boldsymbol{\omega}_g(t)$ is sufficiently large, $\dot{V}_c(t) < 0$. If $\mathbf{s}(t)$ increases without bound, $\boldsymbol{\omega}_g(t)$ increases without bounded. But eventually $\boldsymbol{\omega}_g(t)$ will be large enough such that $\dot{V}_c(t) < 0$ which implies that $\mathbf{s}(t)$, and $\boldsymbol{\omega}_g(t)$, must remain bounded.

Again, in order to satisfy equation 5.41,

$$1 - 2\|\tilde{\boldsymbol{\epsilon}}_g(t)\|^2 > 0$$

or $\|\tilde{\boldsymbol{\epsilon}}_g(t)\|^2 < \frac{1}{2}$. Recalling the definition of the quaternion, this requires

$$|\phi|_{\tilde{\mathbf{q}}_g(t)} < 90 \text{ degrees}$$

where $\phi_{\tilde{\mathbf{q}}_g(t)}$ is the rotation angle in the alignment error quaternion $\tilde{\mathbf{q}}_g(t)$. Lemma 5.1 shows that $\|\tilde{\boldsymbol{\epsilon}}_g(t)\| < \|\tilde{\boldsymbol{\epsilon}}_g(t_0)\|$. If $\|\tilde{\boldsymbol{\epsilon}}_g(t_0)\|^2 < \frac{1}{2}$, $\|\tilde{\boldsymbol{\epsilon}}_g(t)\|^2 < \frac{1}{2}$. From equation 1.4, if $\hat{\mathbf{q}}_g(t_0)^T = [0 \ 0 \ 0 \ 1]$, $\tilde{\mathbf{q}}_g(t_0) = \mathbf{q}_g$. The rotation angle of $\tilde{\mathbf{q}}_g(t)$ at t_0 equals the rotation angle of \mathbf{q}_g , which must, therefore, be known a priori to be less than 90 degrees. With k_D as given in equation 5.41 and $|\phi|_{\tilde{\mathbf{q}}_g(t)} < 90$ degrees, the closed loop system is uniformly ultimately bounded. This implies that $\tilde{\boldsymbol{\omega}}_c(t)$ and $\tilde{\boldsymbol{\epsilon}}_c(t)$ are uniformly, ultimately bounded. \square

Theorem 5.4 *If the angular velocity $\boldsymbol{\omega}_g(t)$ is persistently exciting, regardless of the magnitude of k_D , such that $k_D > 0$, the control law 5.32 results in global stability and asymptotically perfect tracking, $\|\tilde{\boldsymbol{\epsilon}}_c(t)\| \rightarrow 0$, $\|\tilde{\boldsymbol{\omega}}_c(t)\| \rightarrow 0$.*

Proof: The convergence of $\mathbf{s}(t)$ to zero depends on the exponential convergence of the alignment errors, which in turn depends on the angular velocity $\boldsymbol{\omega}_g(t)$ generated by the applied control. Rewriting the error term

$$\mathbf{s}(t) - \hat{\mathbf{s}}(t) = \boldsymbol{\omega}(t) - \hat{\boldsymbol{\omega}}(t) = (\mathbf{I} - R(\tilde{\mathbf{q}}_g(t)))\boldsymbol{\omega}(t) = (\mathbf{I} - R(\tilde{\mathbf{q}}_g(t)))(\mathbf{s}(t) + \boldsymbol{\omega}_r(t))$$

Substituting this into equation 5.35 results in

$$\begin{aligned} \dot{V}_c(t) = & -\mathbf{s}(t)^T K_D \mathbf{s}(t) + \mathbf{s}(t)^T (\Delta'(\tilde{\mathbf{q}}_c(t), \boldsymbol{\omega}_d(t)) + K_D) (\mathbf{I} - R(\tilde{\mathbf{q}}_g(t))) \mathbf{s}(t) \\ & + \mathbf{s}(t)^T (\Delta'(\tilde{\mathbf{q}}_c(t), \boldsymbol{\omega}_d(t)) + K_D) (\mathbf{I} - R(\tilde{\mathbf{q}}_g(t))) \boldsymbol{\omega}_r(t) \end{aligned} \quad (5.42)$$

Equation 5.42 is bounded as

$$\dot{V}_c(t) \leq -k_D \|\mathbf{s}(t)\|^2 + 2(k_D + \zeta') \|\tilde{\boldsymbol{\epsilon}}_g(t)\| \|\mathbf{s}(t)\|^2 + 2(k_D + \zeta') \|\boldsymbol{\omega}_r(t)\| \|\mathbf{s}(t)\| \|\tilde{\boldsymbol{\epsilon}}_g(t)\| \quad (5.43)$$

Applying Young's inequality to the last term in equation 5.43

$$\dot{V}_c(t) \leq -\left(\frac{k_D}{2} - 2(k_D + \zeta') \|\tilde{\boldsymbol{\epsilon}}_g(t)\|\right) \|\mathbf{s}(t)\|^2 + \frac{(k_D + \zeta')^2 \|\boldsymbol{\omega}_r(t)\|^2}{2k_D} \|\tilde{\boldsymbol{\epsilon}}_g(t)\|^2 \quad (5.44)$$

If the angular velocity, $\boldsymbol{\omega}_g(t)$ satisfies equation 5.21, the system is UCO and the alignment errors, $\tilde{\boldsymbol{\epsilon}}_g(t)$, converge to zero exponentially fast. In this case, Lemma 2.3 applies and $V_c(t)$ converges to zero exponentially fast, which means $\mathbf{s}(t)$ converges to zero exponentially fast. With the convergence of $\mathbf{s}(t) \rightarrow 0$, the proof of convergence of the actual attitude and rate errors follows exactly as in the gyro bias analysis of section 3.3. The end result of which is $\lim_{t \rightarrow \infty} \|\tilde{\boldsymbol{\epsilon}}_c(t)\| = 0$ and $\lim_{t \rightarrow \infty} \|\tilde{\boldsymbol{\omega}}_c(t)\| = 0$.

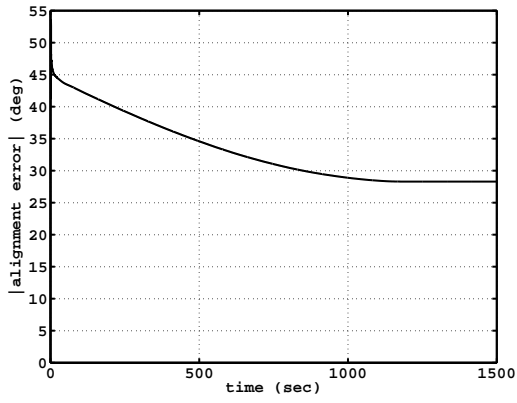
□

<i>Attitude</i>	<i>Value</i>	<i>Alignment</i>	<i>Value</i>
$\mathbf{q}(t_0)$	$[0, 1, 0, 0]^T$	\mathbf{q}_g	$[0.24, 0.24, 0.24, 0.91]$
$\hat{\mathbf{q}}(t_0)$	$[0, 0, 0, 1]^T$	$\hat{\mathbf{q}}_g(t)$	$[0, 0, 0, 1]$
$\mathbf{q}_d(t_0)$	$[0, 0, 0, 1]^T$		

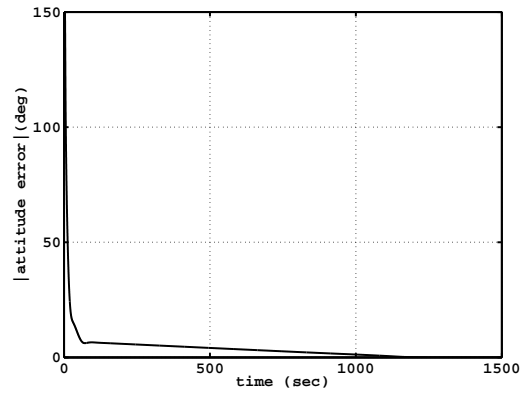
Table 5.2: Alignment Estimator and Controller Simulation Initial Conditions

5.4 Closed Loop Simulation Results

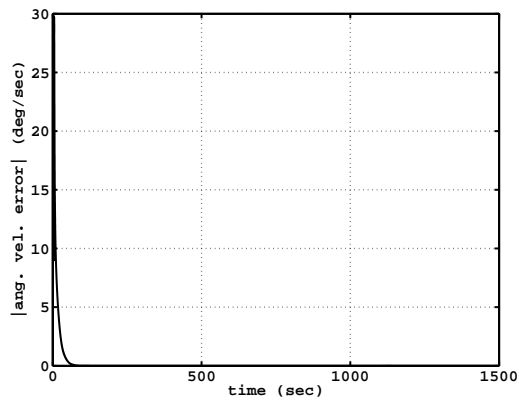
The gyro alignment estimator and controller are tested similarly to the bias estimator and controller. The inertia matrix is the same, a diagonal matrix with principal moments of inertia of $[90, 100, 70]^T$ kg m². Table 5.2 lists the initial conditions for the estimator and controller, as well as the true gyro alignment. The gains are chosen as $k' = 0.001$, $k'_1 = 0.1$, $K_D = k_D I_3$ (where I_3 indicates a 3x3 identity matrix), $k_D = 20$, and $\lambda = 3$. The initial angular velocity is $\boldsymbol{\omega}(0)^T = [0, 0, 0]$. The gyro coordinate frame is rotated by 45 degrees. In the first case, the desired angular velocity is constant, $\boldsymbol{\omega}_d(t)^T = [3, -4, 5]$ deg/sec. Figure 5.3(a) shows that the alignment errors converge to a constant. Figure 5.3(b) shows the attitude tracking error and figure 5.3(c) shows the rate tracking error. Both converge nearly to zero, despite the error in the alignment. The analysis shows that the tracking errors are at least upper bounded. In this case, the actual errors are very close to zero. Next, the desired angular velocity changes direction, similarly to that used above to test



(a) Alignment Estimation Error



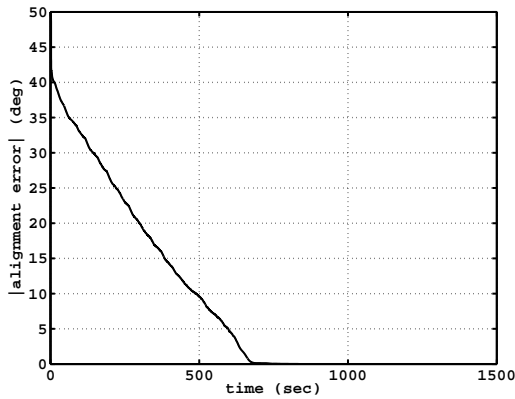
(b) Attitude Tracking Error



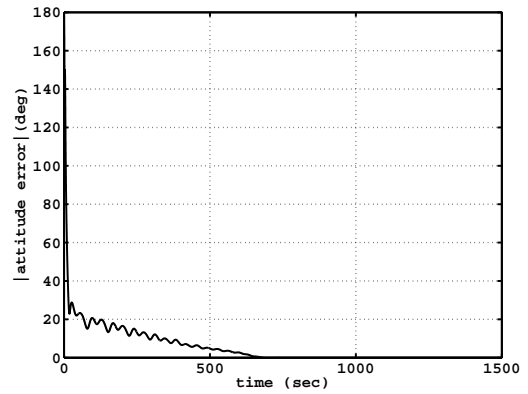
(c) Rate Tracking Error

Figure 5.3: Closed Loop Alignment Estimator/Controller with Constant $\omega_a(t)$

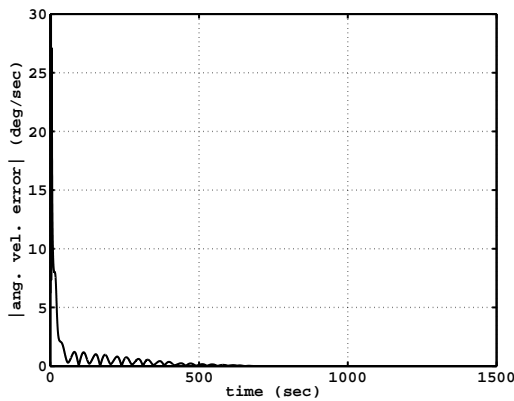
just the estimator, $\omega_d(t)^T = 5[\sin \vartheta t, 1, 0]$ deg/sec, with $\vartheta = 5$ deg/sec. Here, all the errors converge to zero. Figure 5.4(a) shows that the alignment errors converge to zero. Figures 5.4(b) and 5.4(c) show that attitude and rate tracking errors converge to zero. Figure 5.4(d) shows the attitude tracking error when the gyro rate is not corrected with the estimated alignment.



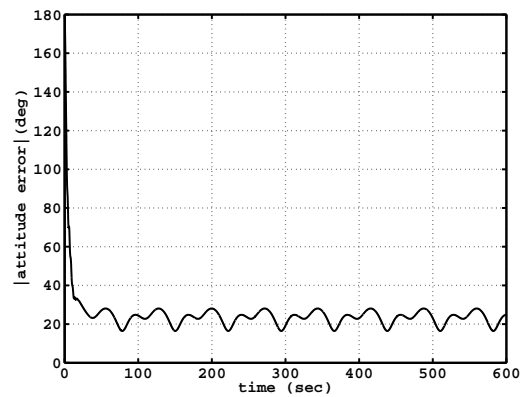
(a) Alignment Estimation Error



(b) Attitude Tracking Error



(c) Rate Tracking Error



(d) Attitude Tracking Error Without Correcting for Alignment

Figure 5.4: Closed Loop Alignment Estimator/Controller with PE $\omega_d(t)$

Chapter 6

Combined Parameter Estimation

Different combinations of the estimators developed in the previous chapters are analyzed next. The stability of the combined estimators is discussed, along with an analysis of the resulting closed loop systems. First the scale factor and gyro bias are combined. Then the alignment and gyro bias are combined. Finally, all three calibration components are combined.

6.1 Scale Factor and Gyro Bias Estimator

The scale factor estimator and the gyro bias estimator equations are

$$\dot{\hat{\mathbf{b}}} = -\frac{\alpha_b}{2}\tilde{\boldsymbol{\varepsilon}}_o(t)\text{sign}(\tilde{\eta}_o(t)) \quad (6.1)$$

$$\dot{\hat{\gamma}}_{Ii}(t) = \frac{\alpha_\gamma}{2}\omega_{gi}(t)\tilde{\varepsilon}_{oi}(t)\text{sign}(\tilde{\eta}_o(t)) \quad (6.2)$$

where, again, $\tilde{\varepsilon}_{oi}(t)$ are the three elements of $\tilde{\boldsymbol{\varepsilon}}_o(t)$, $\alpha_b > 0$, and $\alpha_\gamma > 0$. The attitude estimator given in equation 3.1 is repeated here

$$\dot{\hat{\mathbf{q}}}(t) = \frac{1}{2}Q(\hat{\mathbf{q}}(t))R(\tilde{\mathbf{q}}_o(t))^T[\hat{\boldsymbol{\omega}}(t) + k\tilde{\boldsymbol{\varepsilon}}_o(t)\text{sign}(\tilde{\eta}_o(t))] \quad (6.3)$$

The estimated angular velocity, $\hat{\boldsymbol{\omega}}(t)$, is now

$$\hat{\boldsymbol{\omega}}(t) = \hat{\Gamma}_I(t)\boldsymbol{\omega}_g(t) - \hat{\mathbf{b}}(t) \quad (6.4)$$

Recall from equation 1.5 that the effective gyro bias in the body frame is defined as $\mathbf{b}(t) = R(\mathbf{q}_g)\Gamma_I\mathbf{b}_g(t)$, where $\mathbf{b}_g(t)$ is the true gyro bias in the gyro frame. The alignment matrix is assumed known, and, without loss of generality, is taken as the identity matrix, $R(\mathbf{q}_g) = \mathbf{I}$. As in Section 4.1, the estimated scale factor components, $\hat{\gamma}_{Ii}(t)$ with $i = x, y, z$, are estimates of the inverse of the true scale factor components and the components $\hat{\gamma}_{Ii}(t)$ form the main diagonal of the matrix $\hat{\Gamma}_I(t)$ in equation 6.4.

The derivatives of the attitude error, $\tilde{\mathbf{q}}_o(t)$, scale factor error components, and gyro bias error are

$$\begin{aligned} \dot{\tilde{\mathbf{q}}}_o(t) &= \frac{1}{2} \begin{bmatrix} Q_1(\tilde{\mathbf{q}}_o(t)) \\ -\tilde{\boldsymbol{\varepsilon}}_o(t)^T \end{bmatrix} (\Gamma_I\boldsymbol{\omega}_g(t) - \mathbf{b}(t) - \hat{\Gamma}_I(t)\boldsymbol{\omega}_g(t) + \hat{\mathbf{b}}(t) - k\tilde{\boldsymbol{\varepsilon}}_o(t)\text{sign}(\tilde{\eta}_o(t))) \\ &= \frac{1}{2} \begin{bmatrix} Q_1(\tilde{\mathbf{q}}_o(t)) \\ -\tilde{\boldsymbol{\varepsilon}}_o(t)^T \end{bmatrix} (\Omega_g(t)\tilde{\boldsymbol{\gamma}}_I(t) - \tilde{\mathbf{b}}(t) - k\tilde{\boldsymbol{\varepsilon}}_o(t)\text{sign}(\tilde{\eta}_o(t))) \end{aligned} \quad (6.5)$$

$$\dot{\tilde{\mathbf{b}}}(t) = \frac{\alpha_b}{2}\tilde{\boldsymbol{\varepsilon}}_o(t)\text{sign}(\tilde{\eta}_o(t)) \quad (6.6)$$

$$\dot{\tilde{\gamma}}_{Ii}(t) = -\frac{\alpha_\gamma}{2}\omega_{gi}(t)\tilde{\boldsymbol{\varepsilon}}_{oi}(t)\text{sign}(\tilde{\eta}_o(t)) \quad (6.7)$$

where again, as in Section 4.1, $\Omega_g(t)$ is a diagonal matrix with the components of $\boldsymbol{\omega}_g(t)$ on the main diagonal, the scale factor errors are $\tilde{\gamma}_{Ii}(t) = \gamma_{Ii} - \hat{\gamma}_{Ii}(t)$, and $\tilde{\boldsymbol{\gamma}}_I(t)$

is a vector containing the components $\tilde{\gamma}_{I_i}(t)$. Note that the equilibrium states for 6.5, 6.6, and 6.7 are

$$\begin{bmatrix} \tilde{\mathbf{q}}_o(t)^T & \tilde{\mathbf{b}}(t)^T & \tilde{\gamma}_{I_i}(t)^T \end{bmatrix} = \begin{bmatrix} 0 & 0 & 0 & \pm 1 & 0 & 0 & 0 & 0 & 0 & 0 \end{bmatrix}$$

Theorem 6.1 *The equilibrium states of the system 6.5, 6.6, and 6.7 are globally stable. If the angular velocity, $\boldsymbol{\omega}_g(t)$, is bounded, $\tilde{\boldsymbol{\epsilon}}_o(t) \rightarrow 0$ asymptotically.*

Proof: The proof follows that of the gyro bias estimator. Choose a Lyapunov function as

$$V_o(t) = \frac{1}{2\alpha_b} \tilde{\mathbf{b}}(t)^T \tilde{\mathbf{b}}(t) + \frac{1}{2\alpha_\gamma} \sum_{\omega_{g_i}(t) \neq 0} \tilde{\gamma}_{I_i}(t)^2 + \frac{1}{2} \begin{cases} (\tilde{\eta}_o(t) - 1)^2 + \tilde{\boldsymbol{\epsilon}}_o(t)^T \tilde{\boldsymbol{\epsilon}}_o(t) & \tilde{\eta}_o(t) \geq 0 \\ (\tilde{\eta}_o(t) + 1)^2 + \tilde{\boldsymbol{\epsilon}}_o(t)^T \tilde{\boldsymbol{\epsilon}}_o(t) & \tilde{\eta}_o(t) < 0 \end{cases} \quad (6.8)$$

$V_o(t)$ is continuous. Noting that $\tilde{\boldsymbol{\epsilon}}_o(t)^T \dot{\tilde{\boldsymbol{\epsilon}}}_o(t) + \tilde{\eta}_o(t) \dot{\tilde{\eta}}_o(t) = 0$, as with the gyro bias and scale factor analysis, the derivative of $V_o(t)$ (including the left and right derivatives of $\tilde{\eta}_o(t) = 0$) yields, for all t

$$\dot{V}_o(t) = \frac{1}{\alpha_b} \tilde{\mathbf{b}}(t) \dot{\tilde{\mathbf{b}}}(t) + \frac{1}{\alpha_\gamma} \sum_{\omega_{g_i}(t) \neq 0} \tilde{\gamma}_{I_i}(t) \dot{\tilde{\gamma}}_{I_i}(t) + \begin{cases} -\dot{\tilde{\eta}}_o(t) & \tilde{\eta}_o(t) \geq 0 \\ \dot{\tilde{\eta}}_o(t) & \tilde{\eta}_o(t) < 0 \end{cases} \quad (6.9)$$

Substituting equations 6.6 and 6.7 and $\dot{\tilde{\eta}}_o(t)$ from equation 6.5 into equation 6.9 results in

$$\dot{V}_o(t) = -\frac{k}{2} \tilde{\boldsymbol{\epsilon}}_o(t)^T \tilde{\boldsymbol{\epsilon}}_o(t)$$

This establishes that $\tilde{\boldsymbol{\epsilon}}_o(t)$, $\tilde{\eta}_o(t)$, $\tilde{\mathbf{b}}(t)$, and $\tilde{\gamma}_{I_i}(t)$ are globally, uniformly bounded.

$V_o(t)$ is a continuous, twice differentiable function with

$$\ddot{V}_o(t) = \frac{k}{2} \tilde{\boldsymbol{\varepsilon}}_o(t)^T Q_1(\tilde{\boldsymbol{q}}_o(t)) [\tilde{\boldsymbol{b}}(t) - \Omega_g(t) \tilde{\boldsymbol{\gamma}}_I(t) + k \tilde{\boldsymbol{\varepsilon}}_o(t) \text{sign}(\tilde{\eta}_o(t))]$$

where $Q_1(\tilde{\boldsymbol{q}}_o(t))$ is defined in equation 2.4. $\ddot{V}_o(t)$ is bounded, given that $\boldsymbol{\omega}_g(t)$ is bounded. Lemma 2.1 then shows that $\|\tilde{\boldsymbol{\varepsilon}}_o(t)\| \rightarrow 0$ as $t \rightarrow \infty$. \square

Theorem 6.2 *For any bounded, angular velocity, $\boldsymbol{\omega}_g(t)$, that is persistently exciting, the equilibrium states of the system 6.5, 6.6, and 6.7 are exponentially stable. In particular, $\hat{\boldsymbol{b}}(t) \rightarrow \boldsymbol{b}(t)$ and $\hat{\boldsymbol{\gamma}}(t) \rightarrow \boldsymbol{\gamma}$ exponentially fast from any initial conditions $\hat{\boldsymbol{q}}(t_0)$, $\hat{\boldsymbol{b}}(t_0)$, and $\hat{\boldsymbol{\gamma}}(t_0)$.*

Proof: If $\boldsymbol{\omega}_g(t)$ is bounded, all the signals in equations 6.5, 6.6, and 6.7 are bounded. The system is, as in the gyro bias and scale factor case, analyzed as a linear time varying system, $\dot{\boldsymbol{x}}(t) = A(t)\boldsymbol{x}(t)$, where $\boldsymbol{x}(t)^T = [\tilde{\boldsymbol{\varepsilon}}_o(t), \tilde{\boldsymbol{\gamma}}_I(t), \tilde{\boldsymbol{b}}(t)]$. $A(t)$ is given as

$$A(t) = \begin{bmatrix} -\frac{k}{2} \text{sign}(\tilde{\eta}_o(t)) Q_1(\tilde{\boldsymbol{q}}_o(t)) & \frac{1}{2} Q_1(\tilde{\boldsymbol{q}}_o(t)) \Omega_g(t) & -\frac{1}{2} Q_1(\tilde{\boldsymbol{q}}_o(t)) \\ -\frac{\alpha_\gamma}{2} \text{sign}(\tilde{\eta}_o(t)) \Omega_g(t) & 0 & 0 \\ \frac{\alpha_b}{2} \text{sign}(\tilde{\eta}_o(t)) \mathbf{I} & 0 & 0 \end{bmatrix}$$

The development proceeds like that for the gyro bias and scale factor in Sections 3.1 and 4.1, under the assumption that $\boldsymbol{\omega}_g(t)$ is at least bounded. Again $\dot{V}_o(t)$ is

written as $\dot{V}_o(t) = -\mathbf{x}(t)^T C^T C \mathbf{x}(t) \leq 0$, where $C = \begin{bmatrix} \sqrt{\frac{k}{2}}\mathbf{I} & 0 & 0 \end{bmatrix}$. Choose $K(t)$ as

$$K(t) = \begin{bmatrix} -\sqrt{\frac{k}{2}}\text{sign}(\tilde{\eta}_o(t))Q_1(\tilde{\mathbf{q}}_o(t)) \\ -\sqrt{\frac{\alpha_\gamma}{2k}}\text{sign}(\tilde{\eta}_o(t))\Omega_g(t) \\ \sqrt{\frac{\alpha_b}{2k}}\text{sign}(\tilde{\eta}_o(t))\mathbf{I} \end{bmatrix}$$

As with the gyro bias and scale factor observers, $K(t)$ is a piecewise continuous function of time. The matrix $A(t) - K(t)C$ is then

$$A(t) - K(t)C = \begin{bmatrix} 0 & \frac{1}{2}Q_1(\tilde{\mathbf{q}}_o(t))\Omega_g(t) & -\frac{1}{2}Q_1(\tilde{\mathbf{q}}_o(t)) \\ 0 & 0 & 0 \\ 0 & 0 & 0 \end{bmatrix}$$

Here, the state transition matrix for the pair $(A(t) - K(t)C, C)$ is

$$\Phi(\tau, t) = \begin{bmatrix} \mathbf{I} & \Sigma(\tau, t) \\ 0 & \mathbf{I}_6 \end{bmatrix} \quad (6.10)$$

where \mathbf{I}_6 is a 6x6 identity matrix, and

$$\Sigma(\tau, t) = \begin{bmatrix} \frac{1}{2} \int_t^\tau Q_1(\tilde{\mathbf{q}}_o(\sigma))\Omega_g(\sigma)d\sigma & -\frac{1}{2} \int_t^\tau Q_1(\tilde{\mathbf{q}}_o(\sigma))d\sigma \end{bmatrix}$$

The observability Grammian is given in equation 3.9, and is repeated here as

$$W(t, t+T) = \int_t^{t+T} \Phi(\tau, t)^T C^T C \Phi(\tau, t) d\tau = \int_t^{t+T} \begin{bmatrix} \frac{k}{2}\mathbf{I} & \frac{k}{2}\Sigma(\tau, t) \\ \frac{k}{2}\Sigma(\tau, t)^T & \frac{k}{2}\Sigma(\tau, t)^T \Sigma(\tau, t) \end{bmatrix} d\tau \quad (6.11)$$

The system is UCO if there exists a $T > 0$ and positive constants $\alpha_1 > 0, \alpha_2 > 0$ such that, for all $t \geq t_0$, $\alpha_1 \mathbf{I} \geq W(t, t+T) \geq \alpha_2 \mathbf{I}$. Using Lemma 13.4 of [30], this

property is assured if $\boldsymbol{\omega}_g(t)$, $\dot{\boldsymbol{\omega}}_g(t)$, $Q_1(\tilde{\boldsymbol{q}}_o(t))$ and $\frac{d}{dt}Q_1(\tilde{\boldsymbol{q}}_o(t))$ are bounded, and there exist positive constants T_2 , β_1 , β_2 such that, for all $t \geq t_0$,

$$\begin{aligned} & \beta_2 \mathbf{I} \geq \\ & \int_t^{t+T_2} \begin{bmatrix} \Omega_g(\tau) Q_1(\tilde{\boldsymbol{q}}_o(\tau))^T (\tau) Q_1(\tilde{\boldsymbol{q}}_o(\tau)) \Omega_g(\tau) & \Omega_g(\tau) Q_1(\tilde{\boldsymbol{q}}_o(\tau))^T Q_1(\tilde{\boldsymbol{q}}_o(\tau)) \\ Q_1(\tilde{\boldsymbol{q}}_o(\tau))^T (\tau) Q_1(\tilde{\boldsymbol{q}}_o(\tau)) \Omega_g(\tau) & Q_1(\tilde{\boldsymbol{q}}_o(\tau))^T Q_1(\tilde{\boldsymbol{q}}_o(\tau)) \end{bmatrix} d\tau \\ & \geq \beta_1 \mathbf{I} \end{aligned} \tag{6.12}$$

$Q_1(\tilde{\boldsymbol{q}}_o(t))$ is bounded by definition, since it contains elements of the quaternion, $\tilde{\boldsymbol{q}}_o(t)$. $\frac{d}{dt}Q_1(\tilde{\boldsymbol{q}}_o(t))$ is also bounded, since the above Lyapunov analysis shows that all the terms in equation 6.5 are bounded, given that $\boldsymbol{\omega}_g(t)$ is bounded. With $\dot{\boldsymbol{\omega}}_g(t)$ bounded, the upper bound in equation 6.12 is satisfied.

To examine the lower bound, first substitute $Q_1(\tilde{\boldsymbol{q}}_o(t))^T Q_1(\tilde{\boldsymbol{q}}_o(t)) = \mathbf{I} - \tilde{\boldsymbol{\epsilon}}_o(t) \tilde{\boldsymbol{\epsilon}}_o(t)^T$ into equation 6.12

$$\begin{aligned} & \int_t^{t+T_2} \begin{bmatrix} \Omega_g(\tau) (\mathbf{I} - \tilde{\boldsymbol{\epsilon}}_o(\tau) \tilde{\boldsymbol{\epsilon}}_o(\tau)^T) \Omega_g(\tau) & \Omega_g(\tau) (\mathbf{I} - \tilde{\boldsymbol{\epsilon}}_o(\tau) \tilde{\boldsymbol{\epsilon}}_o(\tau)^T) \\ (\mathbf{I} - \tilde{\boldsymbol{\epsilon}}_o(\tau) \tilde{\boldsymbol{\epsilon}}_o(\tau)^T) \Omega_g(\tau) & \mathbf{I} - \tilde{\boldsymbol{\epsilon}}_o(\tau) \tilde{\boldsymbol{\epsilon}}_o(\tau)^T \end{bmatrix} d\tau \\ & \geq \beta_1 \mathbf{I} \end{aligned} \tag{6.13}$$

Recall that $\|\tilde{\boldsymbol{\epsilon}}_o(t)\| \rightarrow 0$ asymptotically. Thus, for any $\delta > 0$, there exists a $T_1(\delta) > t_0$ such that $\|\tilde{\boldsymbol{\epsilon}}_o(t)\| < \delta$ for all $t \geq t_0 + T_1$. Taking any $\delta < 1$ and $T_2 > T_1$,

$\mathbf{I} - \tilde{\boldsymbol{\varepsilon}}_o(t)\tilde{\boldsymbol{\varepsilon}}_o(t)^T > (1 - \delta^2)\mathbf{I}$, the matrix inside the integral in equation 6.13 becomes

$$\begin{aligned} & \begin{bmatrix} \Omega_g(\tau)[\mathbf{I} - \tilde{\boldsymbol{\varepsilon}}_o(\tau)\tilde{\boldsymbol{\varepsilon}}_o(\tau)^T]\Omega_g(\tau) & \Omega_g(\tau)(\mathbf{I} - \tilde{\boldsymbol{\varepsilon}}_o(\tau)\tilde{\boldsymbol{\varepsilon}}_o(\tau)^T) \\ (\mathbf{I} - \tilde{\boldsymbol{\varepsilon}}_o(\tau)\tilde{\boldsymbol{\varepsilon}}_o(\tau)^T)\Omega_g(\tau) & (\mathbf{I} - \tilde{\boldsymbol{\varepsilon}}_o(\tau)\tilde{\boldsymbol{\varepsilon}}_o(\tau)^T) \end{bmatrix} \\ & > (1 - \delta^2) \begin{bmatrix} \Omega_g(\tau)^2 & \Omega_g(\tau) \\ \Omega_g(\tau) & \mathbf{I} \end{bmatrix} \end{aligned} \quad (6.14)$$

The system is UCO if the following is true, for any $\mathbf{z} \in \mathbb{R}^6$,

$$(1 - \delta^2)\mathbf{z}^T \left[\int_t^{t+T_2} \begin{bmatrix} \Omega_g(\tau)^2 & \Omega_g(\tau) \\ \Omega_g(\tau) & \mathbf{I} \end{bmatrix} d\tau \right] \mathbf{z} \geq 0 \quad (6.15)$$

Since $(1 - \delta^2) > 0$, the following must then be true

$$\mathbf{z}^T \left[\int_t^{t+T_2} \begin{bmatrix} \Omega_g(\tau)^2 & \Omega_g(\tau) \\ \Omega_g(\tau) & \mathbf{I} \end{bmatrix} d\tau \right] \mathbf{z} \quad (6.16)$$

Equation 6.16 establishes a persistency of excitation condition. If equation 6.16 is satisfied, the system is UCO, and $\tilde{\boldsymbol{\varepsilon}}_o(t)$, $\tilde{\mathbf{b}}(t)$, and $\tilde{\boldsymbol{\gamma}}_I(t)$ converge to zero exponentially fast.

Equation 6.16 will not be satisfied if the angular velocity is zero or constant. If the angular velocity is constant, for example $\boldsymbol{\omega}_g(t) = [a, b, c]$, the matrix in equation

6.16 becomes

$$\begin{bmatrix} a^2 & 0 & 0 & a & 0 & 0 \\ 0 & b^2 & 0 & 0 & b & 0 \\ 0 & 0 & c^2 & 0 & 0 & c \\ a & 0 & 0 & 1 & 0 & 0 \\ 0 & b & 0 & 0 & 1 & 0 \\ 0 & 0 & c & 0 & 0 & 1 \end{bmatrix} \quad (6.17)$$

The determinant of the matrix in equation 6.17 is zero, the matrix is not positive definite. The PE condition is not satisfied with a constant angular velocity. The angular velocity must therefore change with time in such a way as to satisfy the PE condition of equation 6.16. An example of an angular velocity that does satisfy the PE condition is $\boldsymbol{\omega}_g(t)^T = \sin \vartheta t [1, 1, 1]$. In this case, the matrix in equation 6.16 becomes

$$\int_t^{t+T_2} \begin{bmatrix} (\sin \vartheta \tau)^2 \mathbf{I} & \sin \vartheta \tau \mathbf{I} \\ \sin \vartheta \tau \mathbf{I} & \mathbf{I} \end{bmatrix} d\tau \quad (6.18)$$

Evaluating the integral in equation 6.18

$$\begin{bmatrix} \left(\frac{\tau}{2} - \frac{1}{4\vartheta} \sin 2\vartheta \tau \right) \mathbf{I} & -\frac{1}{\vartheta} \cos \vartheta \tau \mathbf{I} \\ -\frac{1}{\vartheta} \cos \vartheta \tau \mathbf{I} & \tau \mathbf{I} \end{bmatrix}_{t, t+T_2} \quad (6.19)$$

Let $T_2 = \frac{2\pi}{\vartheta}$, equation 6.19 is then

$$\mathbf{z}^T \begin{bmatrix} \frac{\pi}{\vartheta} \mathbf{I} & 0 \\ 0 & \frac{2\pi}{\vartheta} \mathbf{I} \end{bmatrix}$$

<i>Attitude</i>	<i>Value</i>	<i>Bias</i>	<i>Value</i>	<i>Scale Factor</i>	<i>Value</i>
$\mathbf{q}(t_0)$	$[0, 0, 1, 0]^T$	$\mathbf{b}(t)$	$[0.5, -0.5, 0.5]^T \frac{deg}{sec}$	γ	$[3, -5, 4]^T$
$\hat{\mathbf{q}}(t_0)$	$[0, 0, 0, 1]^T$	$\hat{\mathbf{b}}(t)$	$[0, 0, 0]$	$\hat{\gamma}(t)$	$[1, 1, 1]^T$

Table 6.1: Scale Factor and Bias Estimator Simulation Initial Conditions

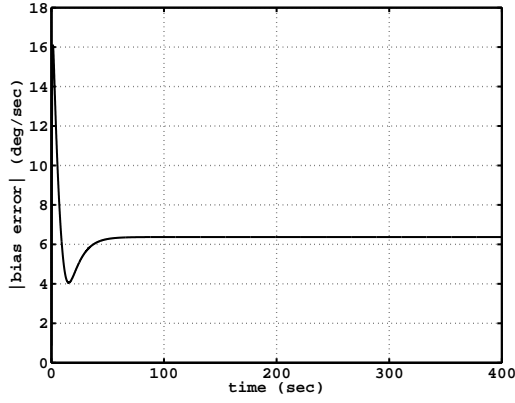
which is positive definite. The system is UCO and $\tilde{\boldsymbol{\varepsilon}}_o(t)$, $\tilde{\mathbf{b}}(t)$, and $\tilde{\boldsymbol{\gamma}}_I(t)$ converge to zero exponentially fast. \square

Remark: For situations requiring positive scale factor estimates, or scale factor estimates confined to a specified region, a standard projection method such as that described in Chapter 4 of [39] ensures that the estimates remain positive or within a specified bound, while retaining all the estimator properties given above. See the discussion in Section 4.1.

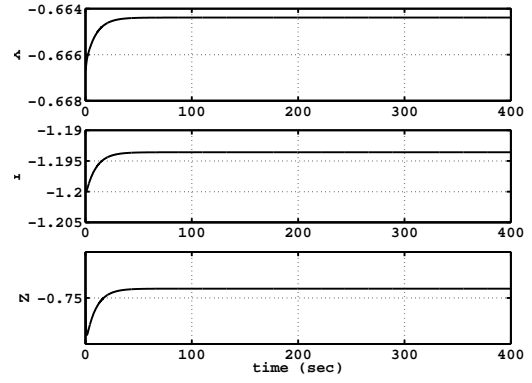
6.2 Estimator Simulation Results

The combined bias and scale factor estimator is tested for three scenarios. Table 6.1 lists the initial conditions for the estimator, as well as the true scale factor. The gains are chosen as $k = 5$ and $\vartheta = 1$.

In the first case, the angular velocity is constant, $\boldsymbol{\omega}_g(t)^T = [3, -4, 5]$ deg/sec. Figures 6.1(a) and 6.1(b) show that the bias and scale factor estimation errors do not converge to zero. In the second case, the angular velocity components are sinusoidal, as in equation 6.18, with $\vartheta = 5$ deg/sec. Figures 6.2(a) and 6.2(b) show that the



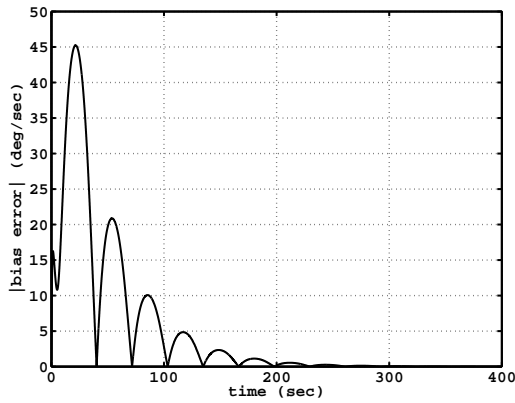
(a) Bias Estimation Error



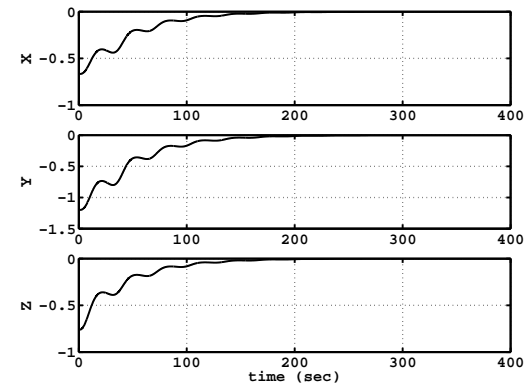
(b) Scale Factor Estimation Error

Figure 6.1: Bias and Scale Factor Estimation Errors with Constant Angular Velocity

bias and scale factor estimation errors also converge to zero.



(a) Bias Estimation Error



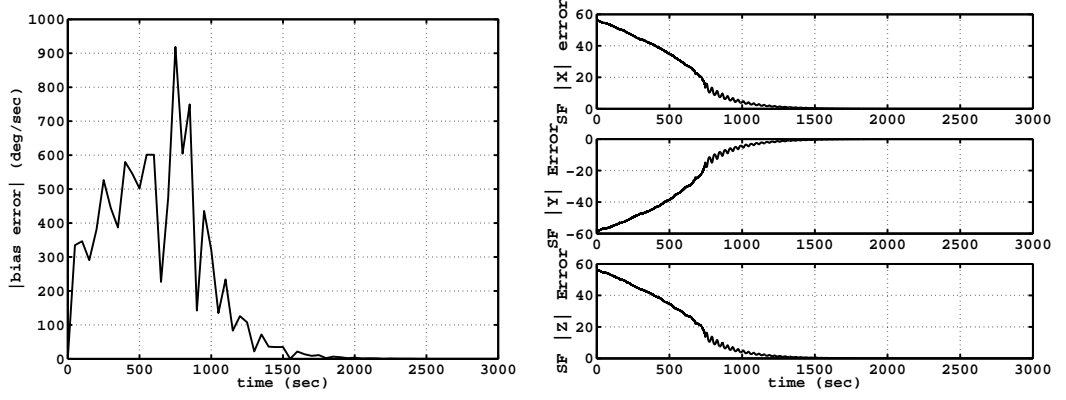
(b) Scale Factor Estimation Error

Figure 6.2: Bias and Scale Factor Estimation Errors with Sinusoidal Angular Velocity

Finally, as with the scale factor estimator, the combined scale factor and bias estimator is tested with the scale factors

$$\gamma = \left[\frac{\pi}{180}, -\frac{\pi}{180}, \frac{\pi}{180} \right]^T$$

and the bias as given above. Figures 6.3(a) and 6.3(b) show that the bias estimation errors and the scale factor estimation errors converge to zero. Again, this represents an extreme case of scaling the angular velocity with incorrect units.



(a) Bias Estimation Error

(b) Scale Factor Estimation Error

Figure 6.3: Bias and Scale Factor Estimator Errors with Large Inverse Scale Factor

6.3 Closed Loop Stability

The closed loop analysis initially proceeds like that in Section 3.3. The control is repeated here as

$$\mathbf{u}(t) = -K_D \hat{\mathbf{s}}(t) + H \hat{\boldsymbol{\alpha}}_r(t) - S(H \hat{\boldsymbol{\omega}}(t)) \boldsymbol{\omega}_r(t) \quad (6.20)$$

The closed loop analysis for the gyro bias, up to equation 3.19, is independent of the specific gyro error. The closed loop equation, given in equation 3.19, is repeated here

$$H \dot{\mathbf{s}}(t) - S(H \boldsymbol{\omega}(t)) \mathbf{s}(t) + K_D \mathbf{s}(t) = \Delta(\tilde{\mathbf{q}}_c(t), \boldsymbol{\omega}_d(t)) \tilde{\mathbf{s}}(t) \quad (6.21)$$

where again

$$\Delta(\tilde{\mathbf{q}}_c(t), \boldsymbol{\omega}_d(t)) = \Delta'(\tilde{\mathbf{q}}_c(t), \boldsymbol{\omega}_d(t)) + K_D$$

Note that the definition of $\boldsymbol{\omega}_r(t)$, the assumption that $\boldsymbol{\omega}_d(t)$ is bounded, and the constraint $\|\tilde{\mathbf{q}}_c(t)\| = 1$ ensure that $\Delta'(\tilde{\mathbf{q}}_c(t), \boldsymbol{\omega}_d(t))$ is a bounded matrix over any solution of the coupled dynamics, equations 6.1, 6.2, 6.3, 2.21, and 6.20.

Theorem 6.3 *If the scale factors are known to be positive, with a known upper and lower bound on each component, with projection implemented in the estimator such that $\hat{\gamma}_I(t)$ has a known upper and lower bound, and if*

$$k_D > \frac{\zeta'(\gamma_{I,max} + \hat{\gamma}_{I,max}) + 7}{\gamma_{I,max} \hat{\gamma}_{I,max}} > 0$$

where $\gamma_{I,max} = \|\Gamma_I\|$, $\hat{\gamma}_{I,max} = \|\hat{\Gamma}_I(t)\|_{max}$, and

$$\zeta' = \sup_{t \geq t_0} \sup_{\|\tilde{\mathbf{q}}_c(t)\|=1} \|\Delta'(\tilde{\mathbf{q}}_c(t), \boldsymbol{\omega}_d(t))\| < \infty$$

the control law 6.20 results in a stable closed loop system, with $\|\tilde{\boldsymbol{\varepsilon}}_c(t)\|$ and $\|\tilde{\boldsymbol{\omega}}_c(t)\|$ uniformly, ultimately bounded.

Proof: The Lyapunov proof proceeds identically to that for the scale factor in 4.3, except for the addition of the bias terms. $\dot{V}_c(t)$ is rewritten in terms of $\boldsymbol{\omega}_g(t)$ and $\boldsymbol{\omega}_r(t)$. Rewrite $\mathbf{s}(t)$ as

$$\mathbf{s}(t) = \boldsymbol{\omega}(t) - \boldsymbol{\omega}_r(t) = \Gamma_I \boldsymbol{\omega}_g(t) - \mathbf{b} - \boldsymbol{\omega}_r(t)$$

and rewrite $\hat{\mathbf{s}}(t)$ as

$$\hat{\mathbf{s}}(t) = \hat{\boldsymbol{\omega}}(t) - \boldsymbol{\omega}_r(t) = \hat{\Gamma}_I(t) \boldsymbol{\omega}_g(t) - \hat{\mathbf{b}}(t) - \boldsymbol{\omega}_r(t)$$

$\dot{V}_c(t)$ from equation 4.22 is expanded as

$$\dot{V}_c(t) = \mathbf{s}(t)^T \Delta'(\tilde{\mathbf{q}}_c(t), \boldsymbol{\omega}_d(t))(\mathbf{s}(t) - \hat{\mathbf{s}}(t)) - \mathbf{s}^T K_D \hat{\mathbf{s}}(t) \quad (6.22)$$

Substituting the expressions for $\mathbf{s}(t)$ and $\hat{\mathbf{s}}(t)$ into equation 6.22, along with $K_D = k_D \mathbf{I}$, results in (the arguments of $\Delta'(\tilde{\mathbf{q}}_c(t), \boldsymbol{\omega}_d(t))$ and the argument of time are omitted for clarity)

$$\begin{aligned} \dot{V}_c(t) &= (\boldsymbol{\omega}_g^T \Gamma_I - \mathbf{b}^T - \boldsymbol{\omega}_r^T) \Delta'((\Gamma_I - \hat{\Gamma}_I) \boldsymbol{\omega}_g(t) - (\mathbf{b} - \hat{\mathbf{b}})) \\ &\quad - k_D (\boldsymbol{\omega}_g^T \Gamma_I - \mathbf{b}^T - \boldsymbol{\omega}_r^T) (\hat{\Gamma}_I \boldsymbol{\omega}_g - \hat{\mathbf{b}} - \boldsymbol{\omega}_r) \\ \dot{V}_c(t) &= \boldsymbol{\omega}_g^T \Gamma_I \Delta'(\Gamma_I - \hat{\Gamma}_I) \boldsymbol{\omega}_g - \boldsymbol{\omega}_g^T \Gamma_I \Delta'(\mathbf{b} - \hat{\mathbf{b}}) - \mathbf{b}^T \Delta'(\Gamma_I - \hat{\Gamma}_I) \boldsymbol{\omega}_g \\ &\quad + \mathbf{b}^T \Delta'(\mathbf{b} - \hat{\mathbf{b}}) - \boldsymbol{\omega}_r^T \Delta'(\Gamma_I - \hat{\Gamma}_I) \boldsymbol{\omega}_g + \boldsymbol{\omega}_r^T \Delta'(\mathbf{b} - \hat{\mathbf{b}}) \\ &\quad - k_D \boldsymbol{\omega}_g^T \Gamma_I \hat{\Gamma}_I \boldsymbol{\omega}_g + k_D \boldsymbol{\omega}_g^T \Gamma_I \hat{\mathbf{b}} + k_D \boldsymbol{\omega}_g^T \Gamma_I \boldsymbol{\omega}_r \\ &\quad + k_D \mathbf{b}^T \hat{\Gamma}_I \boldsymbol{\omega}_g - k_D \mathbf{b}^T \hat{\mathbf{b}} - k_D \mathbf{b}^T \boldsymbol{\omega}_r + k_D \boldsymbol{\omega}_r^T \hat{\Gamma}_I \boldsymbol{\omega}_g(t) \\ &\quad - k_D \boldsymbol{\omega}_r^T \hat{\mathbf{b}} - k_D \boldsymbol{\omega}_r^T \boldsymbol{\omega}_r \end{aligned}$$

The above expression is bounded as (again, without the time argument)

$$\begin{aligned} \dot{V}_c(t) &\leq -k_D \gamma_{I,max} \hat{\gamma}_{I,max} \|\boldsymbol{\omega}_g\|^2 - k_D \|\boldsymbol{\omega}_r\|^2 + \zeta' \gamma_{I,max} (\gamma_{I,max} + \hat{\gamma}_{I,max}) \|\boldsymbol{\omega}_g\|^2 \\ &\quad + \zeta' \gamma_{I,max} \|\boldsymbol{\omega}_g\| (\|\mathbf{b}\| + \|\hat{\mathbf{b}}\|) + \zeta' (\gamma_{I,max} + \hat{\gamma}_{I,max}) \|\boldsymbol{\omega}_g\| \|\mathbf{b}\| \\ &\quad + \zeta' (\gamma_{I,max} + \hat{\gamma}_{I,max}) \|\boldsymbol{\omega}_g\| \|\boldsymbol{\omega}_r\| + k_D \gamma_{I,max} \|\boldsymbol{\omega}_g\| \|\hat{\mathbf{b}}\| \\ &\quad + k_D \gamma_{I,max} \|\boldsymbol{\omega}_g\| \|\boldsymbol{\omega}_r\| + k_D \hat{\gamma}_{I,max} \|\boldsymbol{\omega}_g\| \|\mathbf{b}\| + k_D \hat{\gamma}_{I,max} \|\boldsymbol{\omega}_g\| \|\boldsymbol{\omega}_r\| \\ &\quad + f_1(\|\mathbf{b}\|, \|\hat{\mathbf{b}}\|, \|\boldsymbol{\omega}_r\|, k_D, \zeta') \end{aligned} \quad (6.23)$$

Applying Young's inequality to equation 6.23 results in

$$\begin{aligned}
\dot{V}_c(t) &\leq - (k_D \gamma_{I,max} \hat{\gamma}_{I,max} - \zeta' \gamma_{I,max} (\gamma_{I,max} + \hat{\gamma}_{I,max}) - 7) \|\omega_g(t)\|^2 \\
&\quad - (k_D - \frac{1}{4}(k_D^2 + \zeta'^2)) (\gamma_{I,max} + \hat{\gamma}_{I,max})^2 \|\omega_r(t)\|^2 \\
&\quad + f_2(\|\mathbf{b}\|, \|\hat{\mathbf{b}}\|, \|\omega_r\|, \gamma_{I,max}, \hat{\gamma}_{I,max}, k_D, \zeta')
\end{aligned} \tag{6.24}$$

where f_1 and f_2 are both positive, bounded functions. For the system to be stable, $\dot{V}_c(t) \leq 0$. If the scale factor factors and the scale factor estimates are both positive and upper and lower bounded, and if

$$k_D > \frac{\zeta'(\gamma_{I,max} + \hat{\gamma}_{I,max}) + 7}{\gamma_{I,max} \hat{\gamma}_{I,max}} > 0 \tag{6.25}$$

the first term in equation 6.24 is negative. From the estimator analysis, $\gamma_{I,max}$, $\hat{\gamma}_{I,max}$, \mathbf{b} , and $\hat{\mathbf{b}}(t)$ are all bounded, and ζ' is bounded by definition. A known upper and lower bound on $\gamma_{I,max}$ is assumed a priori. Projection in the estimator ensures an upper and lower bound for $\hat{\gamma}_{I,max}$.

The above analysis establishes that a bounded k_D exists which satisfies 6.25. If $\|\omega_g(t)\|$ is sufficiently large, $\dot{V}_c(t) < 0$ and the closed loop system is uniformly ultimately bounded. Alternatively, recall that $\mathbf{s}(t) = \omega(t) - \omega_r(t) = \Gamma_I \omega_g(t) - \mathbf{b} - \omega_r(t)$. If $\mathbf{s}(t)$ increases without bound, $\omega_g(t)$ increases without bound. But, eventually $\omega_g(t)$ will be large enough such that $\dot{V}_c(t) < 0$ which implies that $\mathbf{s}(t)$, and $\omega_g(t)$, must remain bounded. If $\mathbf{s}(t)$ is uniformly ultimately bounded, $\tilde{\omega}_c(t)$ and $\tilde{\mathbf{e}}_c(t)$ must also be uniformly ultimately bounded since

$$\mathbf{s}(t) = \tilde{\omega}_c(t) + \lambda \tilde{\mathbf{e}}_c(t)$$

$\tilde{\boldsymbol{\varepsilon}}_c(t)$ is bounded by definition, therefore $\tilde{\boldsymbol{\omega}}_c(t)$ is bounded. \square

Theorem 6.4 *If the angular velocity, $\boldsymbol{\omega}_g(t)$, is persistently exciting, regardless of the specific magnitude of $k_D > 0$, the control law 6.20 results in a stable closed loop system, with asymptotically perfect tracking, $\|\tilde{\boldsymbol{\varepsilon}}_c(t)\| \rightarrow 0$, $\|\tilde{\boldsymbol{\omega}}_c(t)\| \rightarrow 0$.*

Proof: The convergence of $\mathbf{s}(t)$ to zero depends on the exponential convergence of the scale factor and bias errors, which in turn depends on the angular velocity $\boldsymbol{\omega}_g(t)$ generated by the applied control. Rewriting the error term

$$\mathbf{s}(t) - \hat{\mathbf{s}}(t) = \boldsymbol{\omega}(t) - \hat{\boldsymbol{\omega}}(t) = \tilde{\Gamma}_I(t)\boldsymbol{\omega}_g(t) - \tilde{\mathbf{b}}(t) \quad (6.26)$$

From equation 1.1, $\boldsymbol{\omega}_g(t)$ can be written as

$$\boldsymbol{\omega}_g(t) = \Gamma(\boldsymbol{\omega}(t) + \mathbf{b})$$

Substituting $\boldsymbol{\omega}(t) = \mathbf{s}(t) + \boldsymbol{\omega}_r(t)$ into the expression for $\boldsymbol{\omega}_g(t)$, equation 6.26 is then

$$\mathbf{s}(t) - \hat{\mathbf{s}}(t) = \tilde{\Gamma}_I(t)\Gamma(\mathbf{s}(t) + \boldsymbol{\omega}_r(t) + \mathbf{b}) - \tilde{\mathbf{b}}(t)$$

Substituting this into equation 4.22 results in

$$\begin{aligned} \dot{V}_c(t) = & -\mathbf{s}(t)^T K_D \mathbf{s}(t) + \mathbf{s}(t)^T (\Delta'(\tilde{\mathbf{q}}_c(t), \boldsymbol{\omega}_d(t)) + K_D) \tilde{\Gamma}_I(t) \Gamma \mathbf{s}(t) \\ & + \mathbf{s}(t)^T (\Delta'(\tilde{\mathbf{q}}_c(t), \boldsymbol{\omega}_d(t)) + K_D) \tilde{\Gamma}_I(t) \Gamma \boldsymbol{\omega}_r(t) \\ & + \mathbf{s}(t)^T (\Delta'(\tilde{\mathbf{q}}_c(t), \boldsymbol{\omega}_d(t)) + K_D) \tilde{\Gamma}_I(t) \Gamma \mathbf{b} + \mathbf{s}(t)^T (\Delta'(\tilde{\mathbf{q}}_c(t), \boldsymbol{\omega}_d(t)) + K_D) \tilde{\mathbf{b}}(t) \end{aligned} \quad (6.27)$$

Equation 6.27 is bounded as

$$\begin{aligned}
\dot{V}_c(t) &\leq -k_D \|\mathbf{s}(t)\|^2 + (k_D + \zeta') \|\tilde{\Gamma}_I(t)\| \gamma_{I,max} \|\mathbf{s}(t)\|^2 \\
&\quad + (k_D + \zeta') \gamma_{I,max} \|\boldsymbol{\omega}_r(t)\| \|\mathbf{s}(t)\| \|\tilde{\Gamma}_I(t)\| \\
&\quad + (k_D + \zeta') \gamma_{I,max} \|\mathbf{b}\| \|\mathbf{s}(t)\| \|\tilde{\Gamma}_I(t)\| + (k_D + \zeta') \|\mathbf{s}(t)\| \|\tilde{\mathbf{b}}(t)\|
\end{aligned} \tag{6.28}$$

Applying Young's inequality to the last three terms in equation 6.28

$$\begin{aligned}
\dot{V}_c(t) &\leq -\left(\frac{k_D}{2} - (k_D + \zeta') \gamma_{I,max} \|\tilde{\Gamma}_I(t)\|\right) \|\mathbf{s}(t)\|^2 \\
&\quad + \frac{3(k_D + \zeta')^2 \gamma_{I,max}^2}{2k_D} (\|\boldsymbol{\omega}_r(t)\|^2 + \|\mathbf{b}\|^2) \|\tilde{\Gamma}_I(t)\|^2 + \frac{3(k_D + \zeta')^2}{2k_D} \|\tilde{\mathbf{b}}(t)\|^2
\end{aligned} \tag{6.29}$$

If the angular velocity, $\boldsymbol{\omega}_g(t)$, in addition to being bounded, satisfies equation 6.16, the system is UCO and the scale factor and bias errors converge to zero exponentially fast. In this case, Lemma 2.3 applies. Since $\|\tilde{\Gamma}_I(t)\|$ and $\|\tilde{\mathbf{b}}(t)\|$ converge to zero exponentially fast, $V_c(t)$ converges to zero exponentially fast, which means $\mathbf{s}(t)$ converges to zero exponentially fast. With the convergence of $\mathbf{s}(t) \rightarrow 0$, the proof of convergence of the actual attitude and rate errors follows exactly as in the gyro bias analysis of section 3.3. The end result of which is $\lim_{t \rightarrow \infty} \|\tilde{\boldsymbol{\epsilon}}_c(t)\| = 0$ and $\lim_{t \rightarrow \infty} \|\tilde{\boldsymbol{\omega}}_c(t)\| = 0$. \square

6.4 Closed Loop Simulation Results

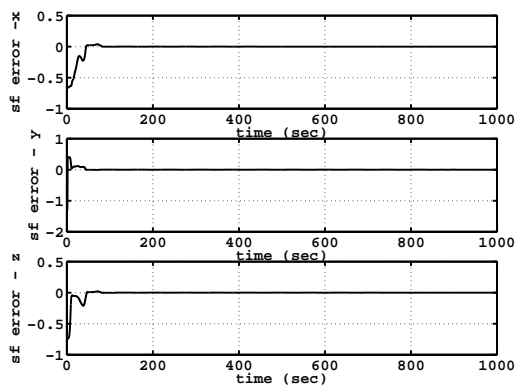
The combined gyro scale factor/bias estimator and controller are tested similarly to the bias estimator and controller. The inertia matrix is the same, a diagonal matrix with principal moments of inertia of $[90, 100, 70]^T$ kg m². Table 6.2 lists the initial conditions for the estimator and controller, as well as the true scale factor. The gains

<i>Attitude</i>	<i>Value</i>	<i>Scale Factor</i>	<i>Value</i>	<i>Bias</i>	<i>Value</i>
$\mathbf{q}(t_0)$	$[0, 1, 0, 0]^T$	γ	$[3, -5, 4]^T$	\mathbf{b}	$[0.5, -0.5, 0.5]^T \frac{\text{deg}}{\text{sec}}$
$\hat{\mathbf{q}}(t_0)$	$[0, 0, 0, 1]^T$	$\hat{\gamma}(t)$	$[1, 1, 1]^T$	$\hat{\mathbf{b}}(t)$	$[0, 0, 0]^T$
$\mathbf{q}_d(t_0)$	$[0, 0, 0, 1]^T$				

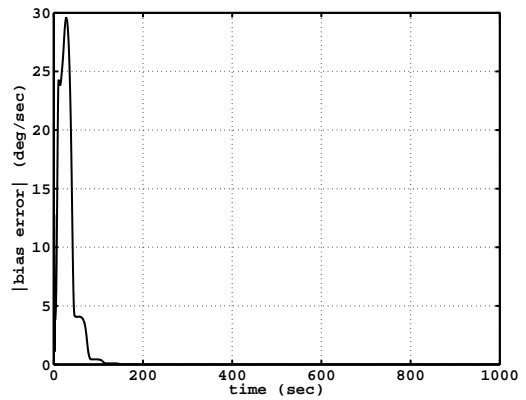
Table 6.2: Scale Factor and Bias Estimator/Controller Simulation Initial Conditions

are chosen as $k = 5$, $K_D = k_D I_3$ (where I_3 indicates a 3x3 identity matrix), $\alpha_b = 1$, $\alpha_\gamma = 1$, $k_D = 10$, and $\lambda = 3$. Here the initial angular velocity is $\boldsymbol{\omega}(0)^T = [0, 0, 0]$, and the desired angular velocity is sinusoidal, $\boldsymbol{\omega}_d(t)^T = [\sin \vartheta t, \sin \vartheta t, \sin \vartheta t]$ where $\vartheta = 5$ deg/sec.

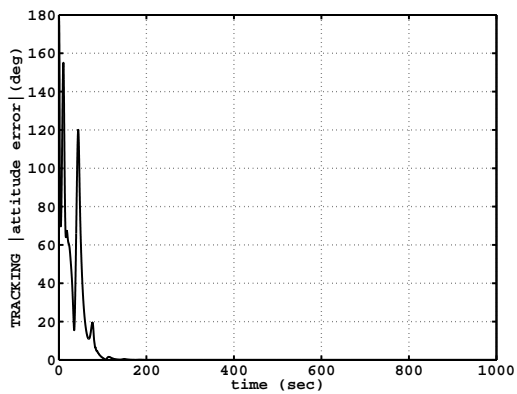
Figures 6.4(a) and 6.4(b) show that the scale factor and bias errors converge to zero. Figures 6.4(c) and 6.4(d) show that both the tracking attitude error and the tracking angular velocity error converge to zero.



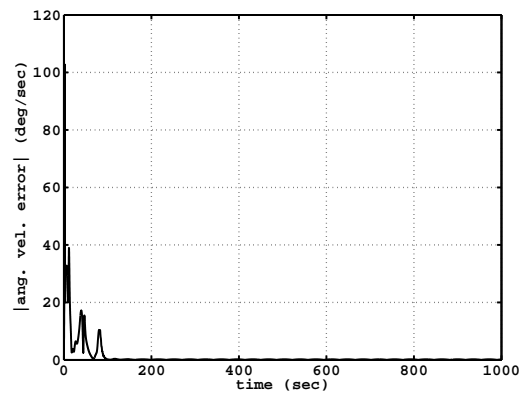
(a) Scale Factor Errors



(b) Bias Errors



(c) Tracking Attitude Error



(d) Tracking Rate Error

Figure 6.4: Coupled Estimator/Controller Errors with Scale Factor and Bias Errors

6.5 Alignment and Gyro Bias Estimator

The estimators for the gyro alignment and gyro bias are combined next. Here, the kinematic equations for the predicted attitude quaternion and the estimated alignment quaternion are given as

$$\dot{\hat{\mathbf{q}}}(t) = \frac{1}{2}Q(\hat{\mathbf{q}}(t))R(\tilde{\mathbf{q}}_o(t))^T[\hat{\boldsymbol{\omega}}(t) + k(t)\tilde{\boldsymbol{\varepsilon}}_o(t)\text{sign}(\tilde{\eta}_o(t)) + k_1(t)\text{sign}(\tilde{\boldsymbol{\varepsilon}}_o(t))\text{sign}(\tilde{\eta}_o(t))] \quad (6.30)$$

$$\dot{\hat{\mathbf{q}}}_g(t) = \frac{1}{2}Q(\hat{\mathbf{q}}_g(t))[(I - R(\tilde{\mathbf{q}}_o(t)))R(\hat{\mathbf{q}}_g(t))\boldsymbol{\omega}_g(t)] \quad (6.31)$$

where $\hat{\boldsymbol{\omega}}(t)$ is now

$$\hat{\boldsymbol{\omega}}(t) = R(\hat{\mathbf{q}}_g(t))\boldsymbol{\omega}_g(t) - \hat{\mathbf{b}}(t)$$

The gyro bias estimator is, again

$$\dot{\hat{\mathbf{b}}}(t) = -\frac{\alpha_b}{2}\tilde{\boldsymbol{\varepsilon}}_o(t)\text{sign}(\tilde{\eta}_o(t)) \quad (6.32)$$

The scale factors (assumed known) are incorporated into $\boldsymbol{\omega}_g(t)$. The gains, $k(t)$, $k_1(t)$, and α_b , are positive. The quaternion, $\hat{\mathbf{q}}_g(t)$, is the estimated gyro alignment quaternion, transforming from gyro coordinates to an estimated body frame. Again, $\hat{\mathbf{q}}(t)$ is a prediction of the attitude at time, t , propagated by the kinematic equation using the measured angular velocity and the current alignment and gyro bias estimates. The attitude error is as given in equation 3.4 and the alignment error is given in equation 2.16. The term $R(\tilde{\mathbf{q}}_o(t))^T$ in equation 6.30 resolves the angular velocity terms in the estimator frame. The kinematic equation for the attitude error

quaternion, recalling equations 5.3 and 5.5 from Section 5.1, is

$$\begin{aligned}
\dot{\tilde{\mathbf{q}}}_o(t) &= \frac{1}{2} \begin{bmatrix} Q_1(\tilde{\mathbf{q}}_o(t)) \\ -\tilde{\boldsymbol{\varepsilon}}_o(t)^T \end{bmatrix} (R(\mathbf{q}_g)\boldsymbol{\omega}_g(t) - \mathbf{b}(t) - R(\hat{\mathbf{q}}_g(t))\boldsymbol{\omega}_g(t) + \tilde{\mathbf{b}}(t) \\
&\quad - k(t)\tilde{\boldsymbol{\varepsilon}}_o(t)\text{sign}(\tilde{\eta}_o(t)) - k_1(t)\text{sign}(\tilde{\boldsymbol{\varepsilon}}_o(t))\text{sign}(\tilde{\eta}_o(t))) \\
&= \frac{1}{2} \begin{bmatrix} Q_1(\tilde{\mathbf{q}}_o(t)) \\ -\tilde{\boldsymbol{\varepsilon}}_o(t)^T \end{bmatrix} (R(\tilde{\mathbf{q}}_g(t)) - \mathbf{I})R(\hat{\mathbf{q}}_g(t))\boldsymbol{\omega}_g(t) - \tilde{\mathbf{b}}(t) \\
&\quad - k(t)\tilde{\boldsymbol{\varepsilon}}_o(t)\text{sign}(\tilde{\eta}_o(t)) - k_1(t)\text{sign}(\tilde{\boldsymbol{\varepsilon}}_o(t))\text{sign}(\tilde{\eta}_o(t)))
\end{aligned} \tag{6.33}$$

The kinematic equation for the alignment error quaternion is given in equation 5.4, repeated here as

$$\dot{\tilde{\mathbf{q}}}_g(t) = \frac{1}{2} \begin{bmatrix} Q_1(\tilde{\mathbf{q}}_g(t)) \\ -\tilde{\boldsymbol{\varepsilon}}_g(t)^T \end{bmatrix} [(R(\tilde{\mathbf{q}}_o(t)) - \mathbf{I})R(\hat{\mathbf{q}}_g(t))\boldsymbol{\omega}_g(t)] \tag{6.34}$$

Finally, the derivative of the gyro bias error is

$$\dot{\tilde{\mathbf{b}}}(t) = \frac{\alpha_b}{2} \tilde{\boldsymbol{\varepsilon}}_o(t)\text{sign}(\tilde{\eta}_o(t)) \tag{6.35}$$

Note that the equilibrium state for each of the error quaternions, $\tilde{\mathbf{q}}_o(t)$ and $\tilde{\mathbf{q}}_g(t)$, is the identity quaternion, $[0 \ 0 \ 0 \ \pm 1]$. The equilibrium state for the gyro bias is $\tilde{\mathbf{b}}(t)^T = [0 \ 0 \ 0]$.

Theorem 6.5 *If $k(t) \geq \|\boldsymbol{\omega}_g(t)\| + k'$ and $k_1(t) \geq 4\|\boldsymbol{\omega}_g(t)\| + k'_1$, where $k' > 0$ and $k'_1 > 0$, the equilibrium states for the system 6.33, 6.34, and 6.35 are globally stable.*

In particular, if the angular velocity, $\boldsymbol{\omega}_g(t)$, is bounded, $\tilde{\boldsymbol{\varepsilon}}_o(t) \rightarrow 0$ asymptotically.

Proof: Chose a Lyapunov function as

$$V_o(t) = \frac{1}{2\alpha_b} \tilde{\mathbf{b}}(t)^T \tilde{\mathbf{b}}(t) + \frac{1}{2} \begin{cases} (\tilde{\eta}_o(t) - 1)^2 + \tilde{\boldsymbol{\varepsilon}}_o(t)^T \tilde{\boldsymbol{\varepsilon}}_o(t) & \tilde{\eta}_o(t) \geq 0 \\ (\tilde{\eta}_o(t) + 1)^2 + \tilde{\boldsymbol{\varepsilon}}_o(t)^T \tilde{\boldsymbol{\varepsilon}}_o(t) & \tilde{\eta}_o(t) < 0 \end{cases} \quad (6.36)$$

$$+ \frac{1}{2} \begin{cases} (\tilde{\eta}_g(t) - 1)^2 + \tilde{\boldsymbol{\varepsilon}}_g(t)^T \tilde{\boldsymbol{\varepsilon}}_g(t) & \tilde{\eta}_g(t) \geq 0 \\ (\tilde{\eta}_g(t) + 1)^2 + \tilde{\boldsymbol{\varepsilon}}_g(t)^T \tilde{\boldsymbol{\varepsilon}}_g(t) & \tilde{\eta}_g(t) < 0 \end{cases}$$

The derivative of $V_o(t)$ is (again, including the left and right derivatives of the sign terms, and using $\tilde{\boldsymbol{\varepsilon}}_o(t)^T \dot{\tilde{\boldsymbol{\varepsilon}}}_o(t) + \tilde{\eta}_o(t) \dot{\tilde{\eta}}_o(t) = 0$)

$$\dot{V}_o(t) = \frac{1}{\alpha_b} \tilde{\mathbf{b}}(t)^T \dot{\tilde{\mathbf{b}}}(t) + \begin{cases} -\dot{\tilde{\eta}}_o(t) & \tilde{\eta}_o(t) \geq 0 \\ \dot{\tilde{\eta}}_o(t) & \tilde{\eta}_o(t) < 0 \end{cases} + \begin{cases} -\dot{\tilde{\eta}}_g(t) & \tilde{\eta}_g(t) \geq 0 \\ \dot{\tilde{\eta}}_g(t) & \tilde{\eta}_g(t) < 0 \end{cases}$$

Substituting for $\dot{\tilde{\eta}}_o(t)$, $\dot{\tilde{\eta}}_g(t)$, and $\dot{\tilde{\mathbf{b}}}(t)$ from equations 6.33, 6.34 and 6.35

$$\begin{aligned} \dot{V}_o(t) = & -\frac{k(t)}{2} \tilde{\boldsymbol{\varepsilon}}_o(t)^T \tilde{\boldsymbol{\varepsilon}}_o(t) + \frac{1}{2} \tilde{\boldsymbol{\varepsilon}}_o(t)^T [(R(\tilde{\mathbf{q}}_g(t)) - \mathbf{I})R(\hat{\mathbf{q}}_g(t))\boldsymbol{\omega}_g(t)\text{sign}(\tilde{\eta}_o(t)) \\ & - k_1(t)\text{sign}(\tilde{\boldsymbol{\varepsilon}}_o(t))] + \frac{1}{2} \tilde{\boldsymbol{\varepsilon}}_g(t)^T [(R(\tilde{\mathbf{q}}_o(t)) - \mathbf{I})R(\hat{\mathbf{q}}_g(t))\boldsymbol{\omega}_g(t)\text{sign}(\tilde{\eta}_g(t))] \end{aligned} \quad (6.37)$$

Equation 6.37 is the same as equation 5.7, since the bias terms cancel. The derivative is then bounded in the same manner, resulting in equation 5.1, repeated here

$$\dot{V}_o(t) \leq -k'\|\tilde{\boldsymbol{\varepsilon}}_o(t)\|^2 - k'_1\|\tilde{\boldsymbol{\varepsilon}}_o(t)\| \leq -k'\|\tilde{\boldsymbol{\varepsilon}}_o(t)\|^2 \quad (6.38)$$

where $k(t) = 4\|\boldsymbol{\omega}_g(t)\| + k'$ and $k_1 = 4\|\boldsymbol{\omega}_g(t)\| + k'_1$, where $k' > 0$ and $k'_1 > 0$. With the added constraint that $\boldsymbol{\omega}_g(t)$ is bounded, $V_o(t)$ is a continuous, twice differentiable function. Lemma 2.1 then shows that $\|\tilde{\boldsymbol{\varepsilon}}_o(t)\| \rightarrow 0$ as $t \rightarrow \infty$. \square

Theorem 6.6 For any bounded, angular velocity, $\boldsymbol{\omega}_g(t)$, that is persistently exciting, the equilibrium states of the system 6.33, 6.34, and 6.35 are exponentially stable. In particular, $\hat{\mathbf{q}}_g(t) \rightarrow \mathbf{q}_g$ and $\hat{\mathbf{b}}(t) \rightarrow \mathbf{b}(t)$ exponentially fast from any initial conditions $\hat{\mathbf{q}}_g(t_0)$, $\hat{\mathbf{b}}(t_0)$, and $\hat{\mathbf{q}}(t_0)$.

Proof: The system given by equations 6.33, 6.34, and 6.35 is stable. If $\boldsymbol{\omega}_g(t)$ is bounded, all the signals are bounded. As with the gyro bias estimator analysis, the system is cast as a linear time-varying system $\dot{\mathbf{x}}(t) = A(t)\mathbf{x}(t)$ where

$$\mathbf{x}(t) = \begin{bmatrix} \tilde{\boldsymbol{\epsilon}}_o(t) \\ \tilde{\boldsymbol{\epsilon}}_g(t) \\ \tilde{\mathbf{b}}(t) \end{bmatrix}$$

Developing $A(t)$ is the same as in the alignment estimator, with added terms for the bias error. Here $A(t)$ is

$$A(t) = \begin{bmatrix} A_{11}(t) & A_{12}(t) & -\frac{1}{2}Q_1(\tilde{\mathbf{q}}_o(t)) \\ A_{21}(t) & 0 & 0 \\ \frac{\alpha b}{2}\text{sign}(\tilde{\eta}_o(t))\mathbf{I} & 0 & 0 \end{bmatrix}$$

where again

$$A_{11}(t) = -\frac{1}{2}Q_1(\tilde{\mathbf{q}}_o(t))\text{sign}(\tilde{\eta}_o(t))[k + k_1E(\tilde{\boldsymbol{\epsilon}}_o(t))]$$

$$A_{12}(t) = -Q_1(\tilde{\mathbf{q}}_o(t))[(R(\hat{\mathbf{q}}_g(t))\boldsymbol{\omega}_g(t))\tilde{\boldsymbol{\epsilon}}_g(t)^T \\ - (\tilde{\boldsymbol{\epsilon}}_g(t)^T R(\hat{\mathbf{q}}_g(t))\boldsymbol{\omega}_g(t))\mathbf{I} - \tilde{\eta}_g(t)S(R(\hat{\mathbf{q}}_g(t))\boldsymbol{\omega}_g(t))]$$

$$A_{21}(t) = -Q_1(\tilde{\mathbf{q}}_g(t))[(R(\hat{\mathbf{q}}_g(t))\boldsymbol{\omega}_g(t))\tilde{\boldsymbol{\epsilon}}_o(t)^T \\ - (\tilde{\boldsymbol{\epsilon}}_o(t)^T R(\hat{\mathbf{q}}_g(t))\boldsymbol{\omega}_g(t))\mathbf{I} - \tilde{\eta}_o(t)S(R(\hat{\mathbf{q}}_g(t))\boldsymbol{\omega}_g(t))]$$

where $E(\tilde{\boldsymbol{\varepsilon}}_o(t))$ is defined in equation 5.13. See section 5.1 for definitions of the other terms above.

Following the proof for the gyro bias and alignment estimators, $\dot{V}_o(t)$ is rewritten as $\dot{V}_o(t) \leq -\boldsymbol{x}(t)^T C^T C \boldsymbol{x}(t) \leq 0$, where $C = [\sqrt{k'}\mathbf{I} \ 0 \ 0]$. Here $K(t)$ is chosen as

$$K(t) = \begin{bmatrix} \frac{1}{\sqrt{k'}} A_{11}(t) \\ \frac{1}{\sqrt{k'}} A_{21}(t) \\ \frac{\alpha_b}{2\sqrt{k'}} \text{sign}(\tilde{\eta}_o(t)) \mathbf{I} \end{bmatrix}$$

With $\boldsymbol{\omega}_g(t)$ bounded, applying the same arguments as with the gyro bias and alignment estimators, $K(t)$ is a piecewise continuous function of time.

The state transition matrix for the pair $(A(t) - K(t)C, C)$ is

$$\Phi(\tau, t) = \begin{bmatrix} \mathbf{I} & \Sigma(\tau, t) \\ 0 & \mathbf{I}_6 \end{bmatrix} \quad (6.39)$$

where \mathbf{I}_6 is a 6x6 identity matrix and

$$\Sigma(\tau, t) = \begin{bmatrix} \int_t^\tau A_{12}(\sigma) d\sigma & -\frac{1}{2} \int_t^\tau Q_1(\tilde{\boldsymbol{q}}_o(\sigma)) d\sigma \end{bmatrix}$$

The observability Grammian is

$$\begin{aligned} W(t, t+T) &= \int_t^{t+T} \Phi(\tau, t)^T C^T C \Phi(\tau, t) d\tau \\ &= \int_t^{t+T} \begin{bmatrix} k' \mathbf{I} & k' \Sigma(\tau, t) \\ k' \Sigma(\tau, t)^T & k' \Sigma(\tau, t)^T \Sigma(\tau, t) \end{bmatrix} d\tau \end{aligned} \quad (6.40)$$

The system is UCO if there exists a $T > 0$ and positive constants $\alpha_1 > 0, \alpha_2 > 0$ such that, for all $t \geq t_0$, $\alpha_1 \mathbf{I} \geq W(t, t+T) \geq \alpha_2 \mathbf{I}$. Proceeding similarly to 3.10 for

the gyro bias estimator proof, this is assured if $Q_1(\tilde{\mathbf{q}}_o(t))$, $\frac{d}{dt}Q_1(\tilde{\mathbf{q}}_o(t))$, $A_{12}(t)$ and $\frac{d}{dt}A_{12}(t)$ are bounded, and there exist positive constants T_2 , β_1 , and β_2 such that, for all $t \geq t_0$

$$\begin{aligned} \beta_2 \mathbf{I} &\geq \int_t^{t+T_2} \begin{bmatrix} A_{12}(\tau)^T A_{12}(\tau) & -\frac{1}{2} A_{12}(\tau)^T Q_1(\tilde{\mathbf{q}}_o(\tau)) \\ -\frac{1}{2} Q_1(\tilde{\mathbf{q}}_o(\tau))^T A_{12}(\tau) & \frac{1}{4} Q_1(\tilde{\mathbf{q}}_o(\tau))^T Q_1(\tilde{\mathbf{q}}_o(\tau)) \end{bmatrix} d\tau \\ &> \beta_1 \mathbf{I} \end{aligned} \quad (6.41)$$

As with the alignment analysis, rewrite $A_{12}(t)$ as $A_{12}(t) = -Q_1(\tilde{\mathbf{q}}_o(t))B(t)$, where again

$$B(t) = (R(\hat{\mathbf{q}}_g(t))\boldsymbol{\omega}_g(t))\tilde{\boldsymbol{\varepsilon}}_g(t)^T - (\tilde{\boldsymbol{\varepsilon}}_g(t)^T R(\hat{\mathbf{q}}_g(t))\boldsymbol{\omega}_g(t))\mathbf{I} - \tilde{\eta}_g(t)S(R(\hat{\mathbf{q}}_g(t))\boldsymbol{\omega}_g(t))$$

or as in equation 5.22, $B(t)$ is

$$\begin{aligned} B(t) &= S(\tilde{\boldsymbol{\varepsilon}}_g(t))S(R(\hat{\mathbf{q}}_g(t))\boldsymbol{\omega}_g(t)) - \tilde{\eta}_g(t)S(R(\hat{\mathbf{q}}_g(t))\boldsymbol{\omega}_g(t)) \\ &= (S(\tilde{\boldsymbol{\varepsilon}}_g(t)) - \tilde{\eta}_g(t)\mathbf{I})S(R(\hat{\mathbf{q}}_g(t))\boldsymbol{\omega}_g(t)) \end{aligned} \quad (6.42)$$

The integral 6.41 becomes

$$\begin{aligned} \beta_2 \mathbf{I} &\geq \int_t^{t+T_2} \begin{bmatrix} B(\tau)^T Q_1(\tilde{\mathbf{q}}_o(\tau))^T Q_1(\tilde{\mathbf{q}}_o(\tau)) B(\tau) & -\frac{1}{2} B(\tau)^T Q_1(\tilde{\mathbf{q}}_o(\tau))^T Q_1(\tilde{\mathbf{q}}_o(\tau)) \\ -\frac{1}{2} Q_1(\tilde{\mathbf{q}}_o(\tau))^T Q_1(\tilde{\mathbf{q}}_o(\tau)) B(\tau) & \frac{1}{4} Q_1(\tilde{\mathbf{q}}_o(\tau))^T Q_1(\tilde{\mathbf{q}}_o(\tau)) \end{bmatrix} d\tau \\ &> \beta_1 \mathbf{I} \end{aligned} \quad (6.43)$$

$Q_1(\tilde{\mathbf{q}}_o(t))$ is bounded by definition, since it contains elements of the quaternion, $\tilde{\mathbf{q}}_o(t)$. $\frac{d}{dt}Q_1(\tilde{\mathbf{q}}_o(t))$ is also bounded, since the above Lyapunov analysis shows that all

the terms in equation 6.33 are bounded, given that $\boldsymbol{\omega}_g(t)$ is bounded. With $\dot{\boldsymbol{\omega}}_g(t)$ bounded, the upper bound in equation 6.43 is satisfied.

To examine the lower bound, substitute $Q_1(\tilde{\boldsymbol{q}}_o(t))^T Q_1(\tilde{\boldsymbol{q}}_o(t)) = \mathbf{I} - \tilde{\boldsymbol{\varepsilon}}_o(t)\tilde{\boldsymbol{\varepsilon}}_o(t)^T$ into equation 6.43

$$\int_t^{t+T_2} \begin{bmatrix} B(\tau)^T [\mathbf{I} - \tilde{\boldsymbol{\varepsilon}}_o(\tau)\tilde{\boldsymbol{\varepsilon}}_o(\tau)^T] B(\tau) & -\frac{1}{2}B(\tau)^T [\mathbf{I} - \tilde{\boldsymbol{\varepsilon}}_o(\tau)\tilde{\boldsymbol{\varepsilon}}_o(\tau)^T] \\ -\frac{1}{2}[\mathbf{I} - \tilde{\boldsymbol{\varepsilon}}_o(\tau)\tilde{\boldsymbol{\varepsilon}}_o(\tau)^T] B(\tau) & \frac{1}{4}[\mathbf{I} - \tilde{\boldsymbol{\varepsilon}}_o(\tau)\tilde{\boldsymbol{\varepsilon}}_o(\tau)^T] \end{bmatrix} d\tau \quad (6.44)$$

$$> \beta_1 \mathbf{I}$$

Since $\|\tilde{\boldsymbol{\varepsilon}}_o(t)\| \rightarrow 0$ asymptotically, for any $\delta > 0$, there exists a $T_1(\delta) > t_0$ such that $\|\tilde{\boldsymbol{\varepsilon}}_o(t)\| < \delta$ for all $t \geq t_0 + T_1$. Taking any $\delta < 1$ and $T_2 > T_1$, $\mathbf{I} - \tilde{\boldsymbol{\varepsilon}}_o(t)\tilde{\boldsymbol{\varepsilon}}_o(t)^T > (1 - \delta^2)\mathbf{I}$. The matrix inside equation 6.44 can then be written as

$$\begin{bmatrix} B(\tau)^T [\mathbf{I} - \tilde{\boldsymbol{\varepsilon}}_o(\tau)\tilde{\boldsymbol{\varepsilon}}_o(\tau)^T] B(\tau) & -\frac{1}{2}B(\tau)^T [\mathbf{I} - \tilde{\boldsymbol{\varepsilon}}_o(\tau)\tilde{\boldsymbol{\varepsilon}}_o(\tau)^T] \\ -\frac{1}{2}[\mathbf{I} - \tilde{\boldsymbol{\varepsilon}}_o(\tau)\tilde{\boldsymbol{\varepsilon}}_o(\tau)^T] B(\tau) & \frac{1}{4}[\mathbf{I} - \tilde{\boldsymbol{\varepsilon}}_o(\tau)\tilde{\boldsymbol{\varepsilon}}_o(\tau)^T] \end{bmatrix} \quad (6.45)$$

$$> (1 - \delta^2) \begin{bmatrix} B(\tau)^T B(\tau) & -\frac{1}{2}B(\tau)^T \\ -\frac{1}{2}B(\tau) & \frac{1}{4} \end{bmatrix}$$

Since $1 - \delta^2 > 0$, the system is UCO if, for any $\mathbf{z} \in \mathbb{R}^6$, the following is true

$$\mathbf{z}^T \left[\int_t^{t+T_2} \begin{bmatrix} B(\tau)^T B(\tau) & -\frac{1}{2}B(\tau)^T \\ -\frac{1}{2}B(\tau) & \frac{1}{4}\mathbf{I} \end{bmatrix} d\tau \right] \mathbf{z} > 0 \quad (6.46)$$

If equation 6.46 is positive, then equation 6.41 is satisfied and the system is UCO. This establishes the persistency of excitation condition for the combined alignment and gyro bias estimators.

The analysis of equation 6.46 proceeds as in the alignment estimator analysis in section 5.1. $B(t)$ is singular for any given time. In order for the term $B(t)^T B(t)$ to be positive definite, the angular velocity must change directions. Repeating equation 5.23, $B(t)^T B(t)$ is

$$\begin{aligned} B(t)^T B(t) &= R(\hat{\mathbf{q}}_g(t))S(\boldsymbol{\omega}_g(t))^T(\mathbf{I} - \tilde{\boldsymbol{\epsilon}}_{gR}(t)\tilde{\boldsymbol{\epsilon}}_{gR}(t)^T)S(\boldsymbol{\omega}_g(t))R(\hat{\mathbf{q}}_g(t))^T \\ &= R(\hat{\mathbf{q}}_g(t))[S(\boldsymbol{\omega}_g(t))^T S(\boldsymbol{\omega}_g(t)) - S(\tilde{\boldsymbol{\epsilon}}_{gR}(t))\boldsymbol{\omega}_g(t)\boldsymbol{\omega}_g(t)^T S(\tilde{\boldsymbol{\epsilon}}_{gR}(t))]R(\hat{\mathbf{q}}_g(t))^T \end{aligned} \quad (6.47)$$

where $\tilde{\boldsymbol{\epsilon}}_{gR}(t) = R(\hat{\mathbf{q}}_g(t))^T \tilde{\boldsymbol{\epsilon}}_g(t)$.

A constant angular velocity will not satisfy the PE condition given by equation 6.46. As shown in Section 5.1, the matrix $B(t)^T B(t)$ is singular at any time, t . If the angular velocity is constant, $B(t)^T B(t)$ integrated over any time interval T_2 will not be positive definite. If the integration of $B(t)^T B(t)$ is not positive definite, the matrix in equation 6.46 will not be positive definite.

An example of an angular velocity that will satisfy the PE condition is $\boldsymbol{\omega}_g(t) = [\sin \vartheta t, \cos \vartheta t, 0]^T$. The upper left submatrix in equation 6.46 is evaluated with this $\boldsymbol{\omega}_g(t)$ first.

$$\int_t^{t+T_2} B(\tau)^T B(\tau) d\tau$$

Substituting equation 6.47 into the integral gives

$$\int_t^{t+T_2} R(\hat{\mathbf{q}}_g(\tau))[S(\boldsymbol{\omega}_g(\tau))^T S(\boldsymbol{\omega}_g(\tau)) - S(\tilde{\boldsymbol{\epsilon}}_{gR}(\tau))\boldsymbol{\omega}_g(\tau)\boldsymbol{\omega}_g(\tau)^T S(\tilde{\boldsymbol{\epsilon}}_{gR}(\tau))]R(\hat{\mathbf{q}}_g(\tau))^T d\tau$$

If, for any $\mathbf{z} \in \mathbb{R}^3$

$$\begin{aligned} & \mathbf{z} \left[\int_t^{t+T_2} R(\hat{\mathbf{q}}_g(\tau)) [S(\boldsymbol{\omega}_g(\tau))^T S(\boldsymbol{\omega}_g(\tau)) \right. \\ & \quad \left. - S(\tilde{\boldsymbol{\epsilon}}_{gR}(t)) \boldsymbol{\omega}_g(\tau) \boldsymbol{\omega}_g(\tau)^T S(\tilde{\boldsymbol{\epsilon}}_{gR}(t))] R(\hat{\mathbf{q}}_g(\tau))^T d\tau \right] \mathbf{z} > 0 \end{aligned} \quad (6.48)$$

the upper left matrix in equation 6.46 is positive definite. Since $R(\hat{\mathbf{q}}_g(t))$ is nonsingular, let $\mathbf{y} = R(\hat{\mathbf{q}}_g(t))^T \mathbf{z}$ where $\mathbf{y} \in \mathbb{R}^3$. Equation 6.48 is then

$$\mathbf{y}^T \left[\int_t^{t+T_2} (S(\boldsymbol{\omega}_g(\tau))^T S(\boldsymbol{\omega}_g(\tau)) - S(\tilde{\boldsymbol{\epsilon}}_{gR}(t)) \boldsymbol{\omega}_g(\tau) \boldsymbol{\omega}_g(\tau)^T S(\tilde{\boldsymbol{\epsilon}}_{gR}(t))) d\tau \right] \mathbf{y} \quad (6.49)$$

Since $\tilde{\boldsymbol{\epsilon}}_o(t) \rightarrow 0$ asymptotically, the derivative of $\tilde{\boldsymbol{\epsilon}}_g(t)$, which is proportional to $\tilde{\boldsymbol{\epsilon}}_o(t)$ through $R(\tilde{\mathbf{q}}_o(t))$, will be approaching zero, as will the derivative of $R(\hat{\mathbf{q}}_g(t))$, through $\hat{\mathbf{q}}_g(t)$, (see equations 6.34 and 6.33). The integration in equation 6.49 is performed with $\tilde{\boldsymbol{\epsilon}}_g(t)$ and $R(\hat{\mathbf{q}}_g(t))$ (nearly) constant (recall that $\tilde{\boldsymbol{\epsilon}}_{gR}(t) = R(\hat{\mathbf{q}}_g(t))^T \tilde{\boldsymbol{\epsilon}}_g(t)$). With $\boldsymbol{\omega}_g(t)$ given above and $T_2 = \frac{2\pi}{\vartheta}$, equation 6.49 becomes

$$\begin{aligned} & \frac{\pi}{\vartheta} \mathbf{y}^T \begin{bmatrix} 2 - \tilde{\epsilon}_{gR,2}^2 - \tilde{\epsilon}_{gR,3}^2 & \tilde{\epsilon}_{gR,1} \tilde{\epsilon}_{gR,2} & \tilde{\epsilon}_{gR,1} \tilde{\epsilon}_{gR,3} \\ \tilde{\epsilon}_{gR,1} \tilde{\epsilon}_{gR,2} & 2 - \tilde{\epsilon}_{gR,1}^2 - \tilde{\epsilon}_{gR,3}^2 & \tilde{\epsilon}_{gR,2} \tilde{\epsilon}_{gR,3} \\ \tilde{\epsilon}_{gR,1} \tilde{\epsilon}_{gR,3} & \tilde{\epsilon}_{gR,2} \tilde{\epsilon}_{gR,3} & 2 - \tilde{\epsilon}_{gR,1}^2 - \tilde{\epsilon}_{gR,2}^2 \end{bmatrix} \mathbf{y} \\ & = \frac{\pi}{\vartheta} \mathbf{y}^T \begin{bmatrix} 1 + \tilde{\eta}_{gR}^2 + \tilde{\epsilon}_{gR,1}^2 & \tilde{\epsilon}_{gR,1} \tilde{\epsilon}_{gR,2} & \tilde{\epsilon}_{gR,1} \tilde{\epsilon}_{gR,3} \\ \tilde{\epsilon}_{gR,1} \tilde{\epsilon}_{gR,2} & 1 + \tilde{\eta}_{gR}^2 + \tilde{\epsilon}_{gR,2}^2 & \tilde{\epsilon}_{gR,2} \tilde{\epsilon}_{gR,3} \\ \tilde{\epsilon}_{gR,1} \tilde{\epsilon}_{gR,3} & \tilde{\epsilon}_{gR,2} \tilde{\epsilon}_{gR,3} & 1 + \tilde{\eta}_{gR}^2 + \tilde{\epsilon}_{gR,3}^2 \end{bmatrix} \mathbf{y} > 0 \end{aligned} \quad (6.50)$$

If $\|\tilde{\boldsymbol{\epsilon}}_g(t)\| = \|\tilde{\boldsymbol{\epsilon}}_{gR}(t)\| = 1$ for all $t \geq t_0$, the PE condition above would not be satisfied, since $\mathbf{I} - \tilde{\boldsymbol{\epsilon}}_g(t) \tilde{\boldsymbol{\epsilon}}_g(t)^T$ in equation 6.47 would be singular for all t . However, $\|\tilde{\boldsymbol{\epsilon}}_g(t)\| = 1$ is equivalent to an alignment rotational error of 180 degrees. For the

estimate of the alignment to remain 180 degrees away from the actual alignment requires that the fourth element of $\tilde{\mathbf{q}}_g(t)$, $\tilde{\eta}_g = \cos(\frac{\tilde{\phi}}{2})$, remain at zero for all $t \geq t_0$. If $\tilde{\eta}_g$ of $\tilde{\mathbf{q}}_g(t)$ does not change from zero, then $\|\tilde{\boldsymbol{\varepsilon}}_g(t)\|$ remains at $\|\tilde{\boldsymbol{\varepsilon}}_g(t)\| = 1$. For this to be true, the derivative of $\tilde{\eta}_g$ in equation 6.34 must be zero. If the attitude prediction error $\tilde{\boldsymbol{\varepsilon}}_o(t)$ is not zero, $R(\tilde{\mathbf{q}}_o(t)) - \mathbf{I}$ in equation 6.34 will not be zero. For $\dot{\tilde{\eta}}_g = 0$, the angular velocity term in equation 6.34 must remain perpendicular to $\tilde{\boldsymbol{\varepsilon}}_g$ for all time. But, the angular velocity $\boldsymbol{\omega}_g(t)$ is changing direction continuously, $\tilde{\boldsymbol{\varepsilon}}_o(t)$ is also changing continuously (converging to zero). Until $\tilde{\boldsymbol{\varepsilon}}_o(t)$ converges identically to zero, $(R(\tilde{\mathbf{q}}_o(t)) - \mathbf{I})R(\hat{\mathbf{q}}_g(t))\boldsymbol{\omega}_g(t)$ will not be zero and shouldn't remain perpendicular to $\tilde{\boldsymbol{\varepsilon}}_g(t)$ for all $t > t_0$ since it changes direction. As long as $\|\tilde{\boldsymbol{\varepsilon}}_g(t)\| \neq 1$, the PE condition is satisfied and the errors converge to zero exponentially fast.

The lower left submatrix (which is equivalent to the upper right submatrix) is now evaluated with $\boldsymbol{\omega}_g(t)$ and $T_2 = \frac{2\pi}{\vartheta}$, and letting $R(\hat{\mathbf{q}}_g(t))$ and $\tilde{\boldsymbol{\varepsilon}}_g(t)$ be treated as (nearly) constant,

$$\int_t^{t+T_2} B(\tau)d\tau = \int_t^{t+T_2} (S(\tilde{\boldsymbol{\varepsilon}}_g(t)) - \tilde{\eta}_g(t)\mathbf{I})R(\hat{\mathbf{q}}_g(\tau))S(\boldsymbol{\omega}_g(\tau))R(\hat{\mathbf{q}}_g(\tau))^T d\tau = 0 \quad (6.51)$$

Finally, the lower right submatrix becomes

$$\int_t^{t+T_2} \frac{1}{4}\mathbf{I}d\tau = \frac{\pi}{2\vartheta}\mathbf{I}$$

Since the diagonal matrices in equation 6.46 are positive definite, and the off diagonal matrices are zero, the matrix in equation 6.46 is positive definite. The system is UCO and the alignment and bias errors converge to zero exponentially fast. \square

Remark: For situations requiring a bounded alignment angle estimate, a standard projection method such as that described in Chapter 4 of [39] ensures that the estimated angle remains within a specified bound, while retaining all the estimator properties given above.

The angle $\hat{\phi}_g$ is computed from the quaternion components, as given in equation 1.2. Depending on the desired range, $\hat{\phi}_g$ can either be computed as $\hat{\phi}_g = 2 \cos^{-1}(\hat{\eta}_g)$, or

$$\hat{\phi}_g = 2 \tan^{-1} \frac{\hat{\varepsilon}_{gi}}{\hat{e}_{gi} \hat{\eta}_g}$$

where $\hat{\varepsilon}_{gi}$ is a component of $\hat{\varepsilon}_g$ and \hat{e}_{gi} is the corresponding component of the unit rotation vector. If the size of the estimated angle, $\hat{\phi}_g$, is constrained to be less than some known upper bound, $\phi_{g,max}$, such that

$$|\phi_{g,max}| - |\hat{\phi}_g| \geq 0$$

equation 6.31 is implemented as

$$\dot{\hat{\eta}}_g(t) = \begin{cases} 0 & |\hat{\phi}_g| \geq \phi_{g,max} \text{ and } \dot{\hat{\eta}}_g(t) < 0 \\ -\frac{1}{2} \tilde{\varepsilon}_g(t)^T (I - R(\tilde{\mathbf{q}}_o(t))) R(\hat{\mathbf{q}}_g(t)) \boldsymbol{\omega}_g(t) & \text{otherwise} \end{cases}$$

6.6 Estimator Simulation Results

The combined gyro alignment and bias estimator is tested similarly to the bias estimator. Table 6.3 lists the initial quaternions and gyro bias for the estimator, as well as the true alignment and gyro bias. In the first case, the angular velocity is con-

<i>Attitude</i>	<i>Value</i>	<i>Alignment</i>	<i>Value</i>	<i>Bias</i>	<i>Value</i>
$\mathbf{q}(t_0)$	$[0, 0, 1, 0]^T$	\mathbf{q}_g	$[0, 0, 1, 0]^T$	$\mathbf{b}(t)$	$[0.5, -0.5, 0.5]^T \frac{deg}{sec}$
$\hat{\mathbf{q}}(t_0)$	$[0, 0, 0, 1]^T$	$\hat{\mathbf{q}}_g(t)$	$[0, 0, 0, 1]^T$	$\hat{\mathbf{b}}(t)$	$[0, 0, 0]^T$

Table 6.3: Alignment and Gyro Bias Estimator Simulation Initial Conditions

stant, with $\boldsymbol{\omega}_g(t)^T = [3, -4, 5]$ deg/sec. The gains are chosen as $k' = 0.1$, $k'_1 = 0.1$, and $\alpha_b = 1$. Figures 6.5(a) and 6.5(b) show that the alignment and bias estimation errors converge to constants, since a constant angular velocity does not meet the PE condition required for equation 6.46. Next, the angular velocity is time varying.

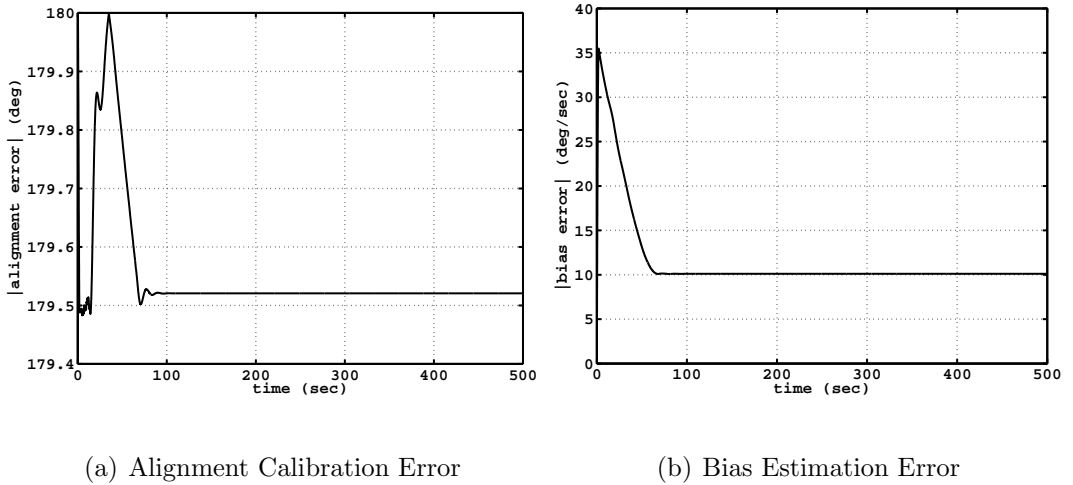
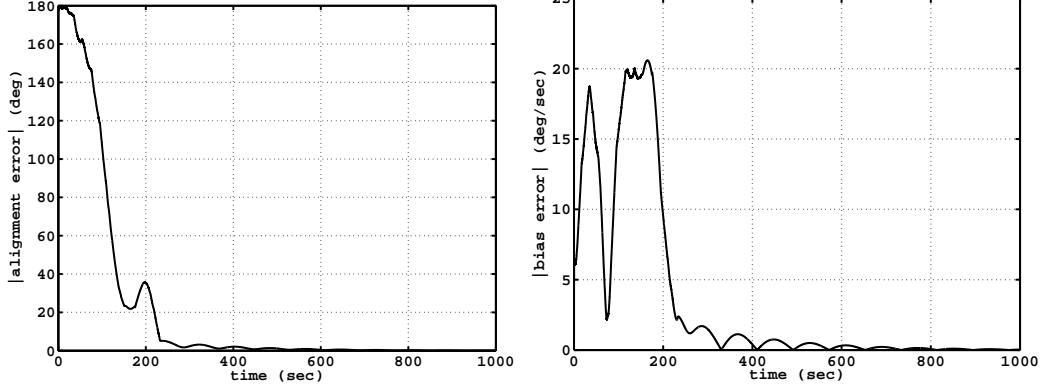


Figure 6.5: Alignment and Gyro Bias Estimation with Constant Angular Velocity

The angular velocity is chosen as $\boldsymbol{\omega}_g(t)^T = [\sin \vartheta t, \cos \vartheta t, 0]$ deg/sec, where $\vartheta = 5$ deg/sec. Figures 6.6(a) and 6.6(b) show that the alignment estimation errors and the bias estimation errors converge to zero.



(a) Alignment Calibration Error

(b) Bias Estimation Error

Figure 6.6: Alignment and Gyro Bias Estimator with PE Angular Velocity

6.7 Closed Loop Stability

As in Section 3.3, a certainty equivalence approach is proposed in utilizing the non-linear tracking algorithm in [32]. Here the estimates $\hat{\boldsymbol{\omega}}(t)$ of 2.13, generated by the estimator equations 6.30, 6.31, and 6.32 are used to generate the control. Again, the control is given as

$$\mathbf{u}(t) = -K_D \hat{\mathbf{s}}(t) + H \hat{\boldsymbol{\alpha}}_r(t) - S(H \hat{\boldsymbol{\omega}}(t)) \boldsymbol{\omega}_r(t) \quad (6.52)$$

The closed loop analysis for the gyro bias, up to equation 3.20, is independent of the specific gyro error. The closed loop equation, given in equation 3.20, is repeated here

$$H \dot{\mathbf{s}}(t) - S(H \boldsymbol{\omega}(t)) \mathbf{s}(t) + K_D \mathbf{s}(t) = \Delta(\tilde{\mathbf{q}}_c(t), \boldsymbol{\omega}_d(t)) \tilde{\mathbf{s}}(t) \quad (6.53)$$

where

$$\Delta(\tilde{\mathbf{q}}_c(t), \boldsymbol{\omega}_d(t)) = \Delta'(\tilde{\mathbf{q}}_c(t), \boldsymbol{\omega}_d(t)) + K_D$$

and the error term $\tilde{\mathbf{s}}(t)$ is again

$$\tilde{\mathbf{s}}(t) = \mathbf{s}(t) - \hat{\mathbf{s}}(t) = \boldsymbol{\omega}(t) - \hat{\boldsymbol{\omega}}(t)$$

Note that the definition of $\boldsymbol{\omega}_r(t)$, the assumption that $\boldsymbol{\omega}_d(t)$ is bounded, and the constraint $\|\tilde{\mathbf{q}}_c(t)\| = 1$ ensure that $\Delta'(\tilde{\mathbf{q}}_c(t), \boldsymbol{\omega}_d(t))$ is a bounded matrix over any solution of the coupled dynamics 6.30, 6.31, 6.32, 2.21, and 6.52.

Theorem 6.7 *If the gyro alignment rotation angle is between ± 45 degrees, with projection implemented in the observer such that $|\hat{\phi}|_g \leq 45$ degrees, and*

$$k_D > 2\zeta' + 6$$

where $\zeta' = \sup_{t \geq t_0} \sup_{\|\tilde{\mathbf{q}}_c(t)\|=1} \|\Delta'(\tilde{\mathbf{q}}_c(t), \boldsymbol{\omega}_r(t))\| < \infty$, the control law 6.52 results in a stable closed loop system, with $\|\tilde{\boldsymbol{\varepsilon}}_c(t)\|$ and $\|\tilde{\boldsymbol{\omega}}_c(t)\|$ uniformly, ultimately bounded.

Proof: Using the Lyapunov function $V_c(t) = \frac{1}{2}\mathbf{s}(t)^T H \mathbf{s}(t)$, the derivative of $V_c(t)$ is

$$\dot{V}_c(t) = -\mathbf{s}(t)^T K_D \mathbf{s}(t) + \mathbf{s}(t)^T \Delta(\tilde{\mathbf{q}}_c(t), \boldsymbol{\omega}_d(t)) \tilde{\mathbf{s}}(t) \quad (6.54)$$

or substituting for $\Delta(\tilde{\mathbf{q}}_c(t), \boldsymbol{\omega}_d(t))$

$$\dot{V}_c(t) = -\mathbf{s}(t)^T K_D \mathbf{s}(t) + \mathbf{s}(t)^T (\Delta'(\tilde{\mathbf{q}}_c(t), \boldsymbol{\omega}_d(t)) + K_D) \tilde{\mathbf{s}}(t) \quad (6.55)$$

$\dot{V}_c(t)$ is rewritten in terms of $\boldsymbol{\omega}_g(t)$ and $\boldsymbol{\omega}_r(t)$. Rewrite $\mathbf{s}(t)$ as

$$\mathbf{s}(t) = \boldsymbol{\omega}(t) - \boldsymbol{\omega}_r(t) = R(\tilde{\mathbf{q}}_g(t))R(\hat{\mathbf{q}}_g(t))\boldsymbol{\omega}_g(t) - \mathbf{b} - \boldsymbol{\omega}_r(t)$$

and rewrite $\hat{\mathbf{s}}(t)$ as

$$\hat{\mathbf{s}}(t) = \hat{\boldsymbol{\omega}}(t) - \boldsymbol{\omega}_r(t) = R(\hat{\mathbf{q}}_g(t))\boldsymbol{\omega}_g(t) - \hat{\mathbf{b}}(t) - \boldsymbol{\omega}_r(t)$$

From equation 6.55, $\dot{V}_c(t)$ is written as

$$\dot{V}_c(t) = \mathbf{s}(t)^T \Delta'(\tilde{\mathbf{q}}_c(t), \boldsymbol{\omega}_d(t))(\mathbf{s}(t) - \hat{\mathbf{s}}(t)) - \mathbf{s}(t)^T K_D \hat{\mathbf{s}}(t) \quad (6.56)$$

Substitute the expressions for $\mathbf{s}(t)$ and $\hat{\mathbf{s}}(t)$ into equation 6.56, letting $K_D = k_D I$, resulting in (the arguments are omitted for clarity)

$$\begin{aligned} \dot{V}_c(t) &= (\boldsymbol{\omega}_g^T R(\hat{\mathbf{q}}_g)^T R(\tilde{\mathbf{q}}_g)^T - \mathbf{b}^T - \boldsymbol{\omega}_r^T) \Delta'((R(\tilde{\mathbf{q}}_g) - \mathbf{I})R(\hat{\mathbf{q}}_g)\boldsymbol{\omega}_g - (\mathbf{b} - \hat{\mathbf{b}})) \\ &\quad - k_D (\boldsymbol{\omega}_g^T R(\hat{\mathbf{q}}_g)^T R(\tilde{\mathbf{q}}_g)^T - \mathbf{b}^T - \boldsymbol{\omega}_r^T) (R(\hat{\mathbf{q}}_g)\boldsymbol{\omega}_g - \hat{\mathbf{b}} - \boldsymbol{\omega}_r) \\ \dot{V}_c(t) &= -k_D \boldsymbol{\omega}_g^T R(\hat{\mathbf{q}}_g)^T R(\tilde{\mathbf{q}}_g)^T R(\hat{\mathbf{q}}_g)\boldsymbol{\omega}_g + k_D \boldsymbol{\omega}_g^T R(\hat{\mathbf{q}}_g)^T R(\tilde{\mathbf{q}}_g)^T R(\hat{\mathbf{q}}_g)\hat{\mathbf{b}} \\ &\quad + k_D \boldsymbol{\omega}_g^T R(\hat{\mathbf{q}}_g)^T R(\tilde{\mathbf{q}}_g)^T \boldsymbol{\omega}_r + k_D \mathbf{b}^T R(\hat{\mathbf{q}}_g)\boldsymbol{\omega}_g(t) - k_D \mathbf{b}^T \hat{\mathbf{b}} \\ &\quad - k_D \mathbf{b}^T \boldsymbol{\omega}_r + k_D \boldsymbol{\omega}_r^T R(\hat{\mathbf{q}}_g)\boldsymbol{\omega}_g - k_D \boldsymbol{\omega}_r^T \hat{\mathbf{b}} - k_D \boldsymbol{\omega}_r^T \boldsymbol{\omega}_r \\ &\quad \boldsymbol{\omega}_g^T R(\hat{\mathbf{q}}_g)^T R(\tilde{\mathbf{q}}_g)^T \Delta'(R(\tilde{\mathbf{q}}_g) - \mathbf{I})R(\hat{\mathbf{q}}_g)\boldsymbol{\omega}_g - \boldsymbol{\omega}_g^T R(\hat{\mathbf{q}}_g)^T R(\tilde{\mathbf{q}}_g)^T \Delta'(\mathbf{b} - \hat{\mathbf{b}}) \\ &\quad - \mathbf{b}^T \Delta'(R(\tilde{\mathbf{q}}_g) - \mathbf{I})R(\hat{\mathbf{q}}_g)\boldsymbol{\omega}_g + \mathbf{b}^T \Delta'(\mathbf{b} - \hat{\mathbf{b}}) \\ &\quad - \boldsymbol{\omega}_r^T \Delta'(R(\tilde{\mathbf{q}}_g) - \mathbf{I})R(\hat{\mathbf{q}}_g)\boldsymbol{\omega}_g + \boldsymbol{\omega}_r^T \Delta'(\mathbf{b} - \hat{\mathbf{b}}) \end{aligned} \quad (6.57)$$

If $R(\tilde{\mathbf{q}}_g(t))$ is positive definite, the above terms are bounded as

$$\begin{aligned} \dot{V}_c(t) &\leq -k_D \|\boldsymbol{\omega}_g\|^2 - k_D \|\boldsymbol{\omega}_r\|^2 + 2\zeta' \|\boldsymbol{\omega}_g\|^2 \\ &\quad + \zeta' \|\boldsymbol{\omega}_g\| (\|\mathbf{b}\| + \|\hat{\mathbf{b}}\|) + 2\zeta' \|\boldsymbol{\omega}_g\| \|\mathbf{b}\| + 2\zeta' \|\boldsymbol{\omega}_g\| \|\boldsymbol{\omega}_r\| \\ &\quad + k_D \|\boldsymbol{\omega}_g\| \|\hat{\mathbf{b}}\| + 2k_D \|\boldsymbol{\omega}_g\| \|\boldsymbol{\omega}_r\| + k_D \|\boldsymbol{\omega}_g(t)\| \|\mathbf{b}\| \\ &\quad + f_1(\|\mathbf{b}\|, \|\hat{\mathbf{b}}\|, \|\boldsymbol{\omega}_r\|, \zeta', k_D) \end{aligned}$$

where f_1 is a positive, bounded function. Applying Young's inequality gives

$$\begin{aligned}
\dot{V}_c(t) &\leq - (k_D - 2\zeta' - 6)\|\boldsymbol{\omega}_g(t)\|^2 \\
&\quad - (k_D - \frac{1}{2}(k_D^2 + \zeta'^2))\|\boldsymbol{\omega}_r(t)\|^2 \\
&\quad + \frac{1}{4}(3\zeta'^2 + k_D^2)\|\mathbf{b}\|^2 + \frac{1}{4}(\zeta'^2 + k_D^2)\|\hat{\mathbf{b}}(t)\|^2 \\
&\quad + f_2(\|\mathbf{b}\|, \|\hat{\mathbf{b}}(t)\|, \|\boldsymbol{\omega}_r(t)\|, \zeta', k_D)
\end{aligned} \tag{6.58}$$

where f_2 is a positive, bounded function. Again, the first term in equation 6.57 is negative if $R(\tilde{\mathbf{q}}_g(t))$ is positive definite, or $|\tilde{\phi}|_g < 90$ degrees. In order to assure this, the alignment angle must known to be within ± 45 degrees, and the estimated alignment angle must be bounded, through projection, to be within ± 45 degrees. This ensures that the alignment error angle is within ± 90 degrees. If

$$k_D > 2\zeta' + 6 \tag{6.59}$$

and $\boldsymbol{\omega}_g(t)$ is sufficiently large, $\dot{V}_c(t) < 0$. If $\mathbf{s}(t)$ increases without bound, $\boldsymbol{\omega}_g(t)$ increases without bound. But eventually $\boldsymbol{\omega}_g(t)$ will be large enough such that $\dot{V}_c(t) < 0$ which implies that $\mathbf{s}(t)$, and $\boldsymbol{\omega}_g(t)$, must remain bounded. \square

Theorem 6.8 *If the angular velocity $\boldsymbol{\omega}_g(t)$ is persistently exciting, regardless of the specific magnitude of $k_D > 0$, the control law 6.52 results in global stability and asymptotically perfect tracking, $\|\tilde{\boldsymbol{\epsilon}}_c(t)\| \rightarrow 0$, $\|\tilde{\boldsymbol{\omega}}_c(t)\| \rightarrow 0$, .*

Proof: The convergence of $\mathbf{s}(t)$ to zero depends on the exponential convergence of the bias and alignment errors, which in turn depends on the angular velocity $\boldsymbol{\omega}_g(t)$

generated by the applied control. Rewriting the error term

$$\mathbf{s}(t) - \hat{\mathbf{s}}(t) = \boldsymbol{\omega}(t) - \hat{\boldsymbol{\omega}}(t) = (R(\tilde{\mathbf{q}}_g(t)) - \mathbf{I})R(\hat{\mathbf{q}}_g(t))\boldsymbol{\omega}_g(t) - \tilde{\mathbf{b}}(t) \quad (6.60)$$

From equation 1.1, $\boldsymbol{\omega}_g(t)$ is written as

$$\boldsymbol{\omega}_g(t) = R(\mathbf{q}_g)^T(\boldsymbol{\omega}(t) + \mathbf{b})$$

Substituting the expression $\boldsymbol{\omega}(t) = \mathbf{s}(t) + \boldsymbol{\omega}_r(t)$ into the expression for $\boldsymbol{\omega}_g(t)$, equation 6.60 becomes

$$\mathbf{s}(t) - \hat{\mathbf{s}}(t) = (R(\tilde{\mathbf{q}}_g(t)) - \mathbf{I})R(\hat{\mathbf{q}}_g(t))R(\mathbf{q}_g)^T(\mathbf{s}(t) + \boldsymbol{\omega}_r(t) + \mathbf{b}) - \tilde{\mathbf{b}}(t)$$

Substituting $R(\mathbf{q}_g) = R(\tilde{\mathbf{q}}_g(t))R(\hat{\mathbf{q}}_g(t))$

$$\mathbf{s}(t) - \hat{\mathbf{s}}(t) = (\mathbf{I} - R(\tilde{\mathbf{q}}_g(t))^T)(\mathbf{s}(t) + \boldsymbol{\omega}_r(t) + \mathbf{b}) - \tilde{\mathbf{b}}(t)$$

Substituting this into equation 6.55 results in

$$\begin{aligned} \dot{V}_c(t) = & -\mathbf{s}(t)^T K_D \mathbf{s}(t) + \mathbf{s}(t)^T (\Delta'(\tilde{\mathbf{q}}_c(t), \boldsymbol{\omega}_d(t)) + K_D) (\mathbf{I} - R(\tilde{\mathbf{q}}_g(t))^T) \mathbf{s}(t) \\ & + \mathbf{s}(t)^T (\Delta'(\tilde{\mathbf{q}}_c(t), \boldsymbol{\omega}_d(t)) + K_D) (\mathbf{I} - R(\tilde{\mathbf{q}}_g(t))^T) \boldsymbol{\omega}_r(t) \\ & + \mathbf{s}(t)^T (\Delta'(\tilde{\mathbf{q}}_c(t), \boldsymbol{\omega}_d(t)) + K_D) (\mathbf{I} - R(\tilde{\mathbf{q}}_g(t))^T) \mathbf{b} \\ & - \mathbf{s}(t)^T (\Delta'(\tilde{\mathbf{q}}_c(t), \boldsymbol{\omega}_d(t)) + K_D) \tilde{\mathbf{b}}(t) \end{aligned} \quad (6.61)$$

Equation 6.61 is bounded as

$$\begin{aligned} \dot{V}_c(t) \leq & -k_D \|\mathbf{s}(t)\|^2 + 2(k_D + \zeta') \|\tilde{\boldsymbol{\epsilon}}_g(t)\| \|\mathbf{s}(t)\|^2 \\ & + 2(k_D + \zeta') (\|\boldsymbol{\omega}_r(t)\| \|\mathbf{s}(t)\| \|\tilde{\boldsymbol{\epsilon}}_g(t)\| + \|\mathbf{b}\| \|\mathbf{s}(t)\| \|\tilde{\boldsymbol{\epsilon}}_g(t)\|) \\ & + (k_D + \zeta') \|\mathbf{s}(t)\| \|\tilde{\mathbf{b}}(t)\| \end{aligned} \quad (6.62)$$

Applying Young's inequality to the last three terms in equation 6.62

$$\begin{aligned} \dot{V}_c(t) \leq & -\left(\frac{k_D}{2} - 2(k_D + \zeta')\|\tilde{\boldsymbol{\epsilon}}_g(t)\|\right)\|\mathbf{s}(t)\|^2 \\ & + 6\frac{(k_D + \zeta')^2}{k_D}(\|\boldsymbol{\omega}_r(t)\|^2 + \|\mathbf{b}\|^2)\|\tilde{\boldsymbol{\epsilon}}_g(t)\|^2 \\ & + \frac{3(k_D + \zeta')^2}{2k_D}\|\tilde{\mathbf{b}}(t)\|^2 \end{aligned} \quad (6.63)$$

If the angular velocity, $\boldsymbol{\omega}_g(t)$, in addition to being bounded, satisfies equation 6.46, the system is UCO and the alignment errors, $\tilde{\boldsymbol{\epsilon}}_g(t)$, and the bias errors, $\tilde{\mathbf{b}}(t)$, converge to zero exponentially fast. In this case, Lemma 2.3 applies. Since $\|\tilde{\boldsymbol{\epsilon}}_g(t)\| \rightarrow 0$ and $\|\tilde{\mathbf{b}}(t)\| \rightarrow 0$ exponentially fast, $V_c(t)$ converges to zero exponentially fast. Therefore $\mathbf{s}(t)$ converges to zero exponentially fast. With the convergence of $\mathbf{s}(t) \rightarrow 0$, the proof of convergence of the actual attitude and rate errors follows exactly as in the gyro bias analysis of section 3.3. The end result of which is $\lim_{t \rightarrow \infty} \|\tilde{\boldsymbol{\epsilon}}_c(t)\| = 0$ and $\lim_{t \rightarrow \infty} \|\tilde{\boldsymbol{\omega}}_c(t)\| = 0$. \square

6.8 Closed Loop Simulation Results

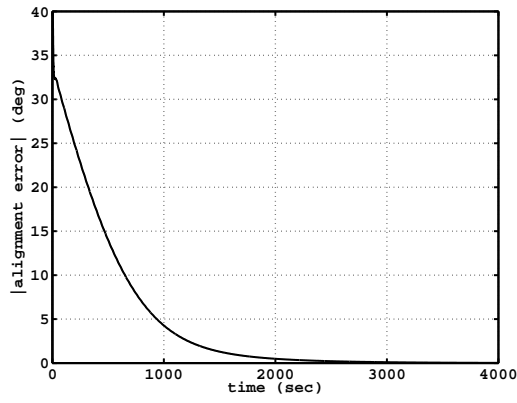
The gyro alignment and bias estimator and controller are tested similarly to the bias estimator and controller. The inertia matrix is the same, a diagonal matrix with principal moments of inertia of $[90, 100, 70]^T$ kg m². Table 6.4 lists the initial conditions for the estimator and controller, as well as the true gyro alignment and bias. The gains are chosen as $k' = 5$, $k'_1 = 0.1$, $K_D = k_D I_3$ (where I_3 indicates a 3x3 identity matrix), $\alpha_b = 1$, $k_D = 20$, and $\lambda = 3$. The initial angular velocity is $\boldsymbol{\omega}(0)^T = [0, 0, 0]$. The gyro coordinate frame is rotated by 45 degrees from the body

<i>Attitude</i>	<i>Value</i>	<i>Component</i>	<i>Value</i>	<i>Bias</i>	<i>Value</i>
$\mathbf{q}(t_0)$	$[0, 1, 0, 0]^T$	\mathbf{q}_g	$[0, 0, 0.38, 0.92]$	\mathbf{b}	$[0.5, -0.5, 0.5]^T \frac{deg}{sec}$
$\hat{\mathbf{q}}(t_0)$	$[0, 0, 0, 1]^T$	$\hat{\mathbf{q}}_g(t)$	$[0, 0, 0, 1]^T$	$\hat{\mathbf{b}}(t)$	$[0, 0, 0]^T$
$\mathbf{q}_d(t_0)$	$[0, 0, 0, 1]^T$				

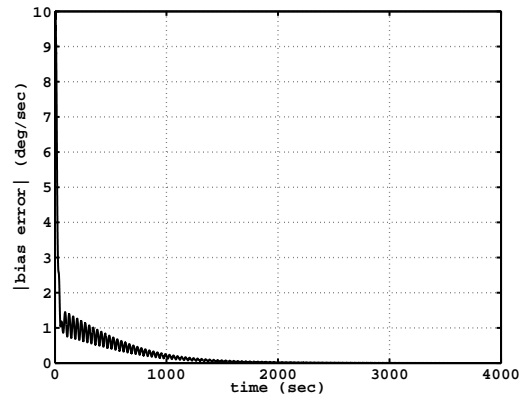
Table 6.4: Alignment and Bias Estimator/ Controller Simulation Initial Conditions

frame, about the z-axis. The desired angular velocity changes direction and is given as $\boldsymbol{\omega}_d(t)^T = 5[\sin \vartheta t, \cos \vartheta t, 0]$ deg/sec, with $\vartheta = 10$ deg/sec.

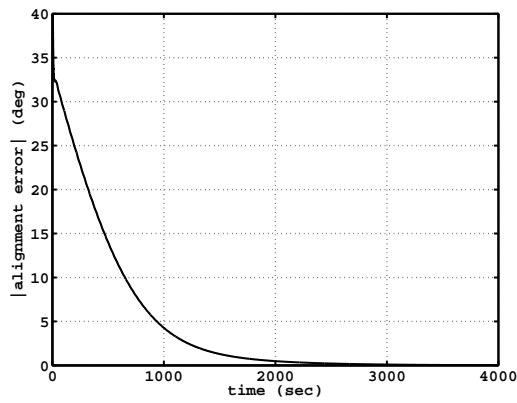
Figures 6.7(a) and 6.7(b) show that the alignment and bias estimation errors converge to zero. Figures 6.7(c) and 6.7(d) show that the attitude and rate tracking errors, respectively, converge to zero also.



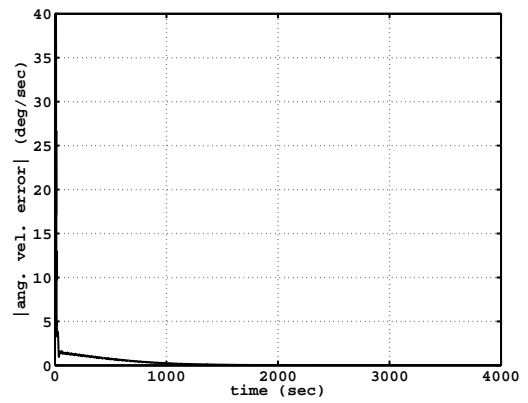
(a) Alignment Calibration Error



(b) Bias Estimation Error



(c) Attitude Tracking Error



(d) Rate Tracking Error

Figure 6.7: Coupled Estimator/Controller Errors with Alignment and Bias Errors

6.9 Alignment, Scale Factor, and Gyro Bias Estimator

Finally, the estimators for the gyro alignment, scale factor and bias are combined.

The kinematic equations for the attitude estimator quaternion and the alignment estimator quaternion are again given as

$$\dot{\hat{\mathbf{q}}}(t) = \frac{1}{2}Q(\hat{\mathbf{q}}(t))R(\tilde{\mathbf{q}}_o(t))^T[\hat{\boldsymbol{\omega}}(t) + k(t)\tilde{\boldsymbol{\varepsilon}}_o(t)\text{sign}(\tilde{\eta}_o(t)) + k_1(t)\text{sign}(\tilde{\boldsymbol{\varepsilon}}_o(t))\text{sign}(\tilde{\eta}_o(t))] \quad (6.64)$$

$$\dot{\hat{\mathbf{q}}}_g(t) = \frac{1}{2}Q(\hat{\mathbf{q}}_g(t))[(I - R(\tilde{\mathbf{q}}_o(t)))R(\hat{\mathbf{q}}_g(t))\boldsymbol{\omega}_g(t)] \quad (6.65)$$

where $\hat{\boldsymbol{\omega}}(t)$ is now

$$\hat{\boldsymbol{\omega}}(t) = R(\hat{\mathbf{q}}_g(t))\hat{\Gamma}_I(t)\boldsymbol{\omega}_g(t) - \hat{\mathbf{b}}(t)$$

The scale factor and gyro bias observers are

$$\dot{\hat{\boldsymbol{\gamma}}}_I(t) = \frac{\alpha_\gamma}{2}\Omega_g(t)R(\hat{\mathbf{q}}_g(t))^T\tilde{\boldsymbol{\varepsilon}}_o(t)\text{sign}(\tilde{\eta}_o(t)) \quad (6.66)$$

$$\dot{\hat{\mathbf{b}}}(t) = -\frac{\alpha_b}{2}\tilde{\boldsymbol{\varepsilon}}_o(t)\text{sign}(\tilde{\eta}_o(t)) \quad (6.67)$$

where $\alpha_\gamma > 0$, $\alpha_b > 0$, and $\Omega_g(t)$ is a matrix with $\boldsymbol{\omega}_g(t)$ on the main diagonal and $\hat{\Gamma}_I(t)$ is a diagonal matrix with the estimated scale factor inverse components on the main diagonal. The same components make up the vector $\hat{\boldsymbol{\gamma}}_I(t)$. Note that the scale factor term is written here as a vector, rather than the component terms, due to the addition of the matrix $R(\hat{\mathbf{q}}_g(t))^T$ in the scale factor estimator. The gains, $k(t)$ and $k_1(t)$, are positive. The quaternion, $\hat{\mathbf{q}}_g(t)$, is the estimated gyro alignment quaternion, transforming from gyro coordinates to an estimated body frame. Again,

$\hat{\mathbf{q}}(t)$ is a prediction of the attitude at time, t , propagated by the kinematic equation using the measured angular velocity and the current alignment, scale factor, and gyro bias estimates. The attitude error is as given in equation 3.4 and the alignment error is given in equation 2.16. The term $R(\tilde{\mathbf{q}}_o(t))^T$ in equation 6.64 resolves the angular velocity terms in the estimator frame. The kinematic equation for the attitude error quaternion is

$$\begin{aligned} \dot{\tilde{\mathbf{q}}}_o(t) = \frac{1}{2} \begin{bmatrix} Q_1(\tilde{\mathbf{q}}_o(t)) \\ -\tilde{\boldsymbol{\varepsilon}}_o(t)^T \end{bmatrix} & (R(\mathbf{q}_g)\Gamma_I\boldsymbol{\omega}_g(t) - \mathbf{b}(t) - R(\hat{\mathbf{q}}_g(t))\hat{\Gamma}_I(t)\boldsymbol{\omega}_g(t) + \hat{\mathbf{b}}(t) \\ & - k(t)\tilde{\boldsymbol{\varepsilon}}_o(t)\text{sign}(\tilde{\eta}_o(t)) - k_1(t)\text{sign}(\tilde{\boldsymbol{\varepsilon}}_o(t))\text{sign}(\tilde{\eta}_o(t))) \end{aligned} \quad (6.68)$$

Rewriting the angular velocity terms, with $R(\mathbf{q}_g) = R(\tilde{\mathbf{q}}_g(t))R(\hat{\mathbf{q}}_g(t))$, and $\tilde{\boldsymbol{\gamma}}_I(t) = \boldsymbol{\gamma}_I - \hat{\boldsymbol{\gamma}}_I(t)$ gives

$$\begin{aligned} R(\mathbf{q}_g)\Gamma_I\boldsymbol{\omega}_g(t) - R(\hat{\mathbf{q}}_g(t))\hat{\Gamma}_I(t)\boldsymbol{\omega}_g(t) &= (R(\tilde{\mathbf{q}}_g(t)) - \mathbf{I})R(\hat{\mathbf{q}}_g(t))\Omega_g(t)\boldsymbol{\gamma}_I \\ &+ R(\hat{\mathbf{q}}_g(t))\Omega_g(t)\tilde{\boldsymbol{\gamma}}_I(t) \end{aligned}$$

Substituting this into equation 6.68

$$\begin{aligned} \dot{\tilde{\mathbf{q}}}_o(t) = \frac{1}{2} \begin{bmatrix} Q_1(\tilde{\mathbf{q}}_o(t)) \\ -\tilde{\boldsymbol{\varepsilon}}_o(t)^T \end{bmatrix} & (R(\tilde{\mathbf{q}}_g(t)) - \mathbf{I})R(\hat{\mathbf{q}}_g(t))\Omega_g(t)\boldsymbol{\gamma}_I + R(\hat{\mathbf{q}}_g(t))\Omega_g(t)\tilde{\boldsymbol{\gamma}}_I(t) - \tilde{\mathbf{b}}(t) \\ & - k(t)\tilde{\boldsymbol{\varepsilon}}_o(t)\text{sign}(\tilde{\eta}_o(t)) - k_1(t)\text{sign}(\tilde{\boldsymbol{\varepsilon}}_o(t))\text{sign}(\tilde{\eta}_o(t))) \end{aligned} \quad (6.69)$$

The kinematic equation for the alignment error quaternion is again

$$\dot{\tilde{\mathbf{q}}}_g(t) = \frac{1}{2} \begin{bmatrix} Q_1(\tilde{\mathbf{q}}_g(t)) \\ -\tilde{\boldsymbol{\varepsilon}}_g(t)^T \end{bmatrix} [(R(\tilde{\mathbf{q}}_o(t)) - \mathbf{I})R(\hat{\mathbf{q}}_g(t))\boldsymbol{\omega}_g(t)] \quad (6.70)$$

Finally, the derivatives of the scale factor error and the gyro bias error are

$$\dot{\tilde{\boldsymbol{\gamma}}}_I(t) = -\frac{\alpha_\gamma}{2}\Omega_g(t)R(\hat{\mathbf{q}}_g(t))^T\tilde{\boldsymbol{\varepsilon}}_o(t)\text{sign}(\tilde{\eta}_o(t)) \quad (6.71)$$

$$\dot{\tilde{\mathbf{b}}}(t) = \frac{\alpha_b}{2}\tilde{\boldsymbol{\varepsilon}}_o(t)\text{sign}(\tilde{\eta}_o(t)) \quad (6.72)$$

Note that the equilibrium state for each of the error quaternions, $\tilde{\mathbf{q}}_o(t)$ and $\tilde{\mathbf{q}}_g(t)$, is the identity quaternion, $[0 \ 0 \ 0 \ \pm 1]$. The equilibrium states for the scale factor and bias are $\tilde{\boldsymbol{\gamma}}_I(t)^T = [0 \ 0 \ 0]$ and $\tilde{\mathbf{b}}(t)^T = [0 \ 0 \ 0]$, respectively.

Theorem 6.9 *If $k(t) \geq 4\|\boldsymbol{\omega}_g(t)\| + k'$ and $k_1(t) \geq 4\|\boldsymbol{\omega}_g(t)\|\|\boldsymbol{\gamma}_I\|_{max} + k'_1$, where $k' > 0$ and $k'_1 > 0$, and $\|\boldsymbol{\gamma}_I\|_{max}$ is a known upper bound on the norm of the inverse scale factor components, the equilibrium states for the system 6.69, 6.70, 6.71 and 6.72 and are globally stable. In particular, if the angular velocity, $\boldsymbol{\omega}_g(t)$, is bounded, $\tilde{\boldsymbol{\varepsilon}}_o(t) \rightarrow 0$ asymptotically.*

Proof: Choose a Lyapunov function as

$$\begin{aligned} V_o(t) = & \frac{1}{2\alpha_b}\tilde{\mathbf{b}}(t)^T\tilde{\mathbf{b}}(t) + \frac{1}{2\alpha_\gamma}\tilde{\boldsymbol{\gamma}}_I(t)^T\tilde{\boldsymbol{\gamma}}_I(t) + \\ & \frac{1}{2} \begin{cases} (\tilde{\eta}_o(t) - 1)^2 + \tilde{\boldsymbol{\varepsilon}}_o(t)^T\tilde{\boldsymbol{\varepsilon}}_o(t) & \tilde{\eta}_o(t) \geq 0 \\ (\tilde{\eta}_o(t) + 1)^2 + \tilde{\boldsymbol{\varepsilon}}_o(t)^T\tilde{\boldsymbol{\varepsilon}}_o(t) & \tilde{\eta}_o(t) < 0 \end{cases} \\ & + \frac{1}{2} \begin{cases} (\tilde{\eta}_g(t) - 1)^2 + \tilde{\boldsymbol{\varepsilon}}_g(t)^T\tilde{\boldsymbol{\varepsilon}}_g(t) & \tilde{\eta}_g(t) \geq 0 \\ (\tilde{\eta}_g(t) + 1)^2 + \tilde{\boldsymbol{\varepsilon}}_g(t)^T\tilde{\boldsymbol{\varepsilon}}_g(t) & \tilde{\eta}_g(t) < 0 \end{cases} \end{aligned} \quad (6.73)$$

The derivative of $V_o(t)$ is (again, including the left and right derivatives of the sign terms, and using $\tilde{\boldsymbol{\varepsilon}}_o(t)^T \dot{\tilde{\boldsymbol{\varepsilon}}}_o(t) + \tilde{\eta}_o(t) \dot{\tilde{\eta}}_o(t) = 0$)

$$\dot{V}_o(t) = \frac{1}{\alpha_b} \tilde{\boldsymbol{b}}(t)^T \dot{\tilde{\boldsymbol{b}}}(t) + \frac{1}{\alpha_\gamma} \tilde{\boldsymbol{\gamma}}_I(t)^T \dot{\tilde{\boldsymbol{\gamma}}}_I(t) + \begin{cases} -\dot{\tilde{\eta}}_o(t) & \tilde{\eta}_o(t) \geq 0 \\ \dot{\tilde{\eta}}_o(t) & \tilde{\eta}_o(t) < 0 \end{cases} + \begin{cases} -\dot{\tilde{\eta}}_g(t) & \tilde{\eta}_g(t) \geq 0 \\ \dot{\tilde{\eta}}_g(t) & \tilde{\eta}_g(t) < 0 \end{cases}$$

Substituting for $\dot{\tilde{\eta}}_o(t)$, $\dot{\tilde{\eta}}_g(t)$, and $\dot{\tilde{\boldsymbol{\gamma}}}_I(t)$, and $\dot{\tilde{\boldsymbol{b}}}(t)$ from equations 6.69, 6.70, 6.71, and 6.72

$$\begin{aligned} \dot{V}_o(t) = & -\frac{k(t)}{2} \tilde{\boldsymbol{\varepsilon}}_o(t)^T \tilde{\boldsymbol{\varepsilon}}_o(t) + \frac{1}{2} \tilde{\boldsymbol{\varepsilon}}_o(t)^T [(R(\tilde{\boldsymbol{q}}_g(t)) - I)R(\hat{\boldsymbol{q}}_g(t))\boldsymbol{\Omega}_g(t)\boldsymbol{\gamma}_I \text{sign}(\tilde{\eta}_o(t)) \\ & - k_1(t) \text{sign}(\tilde{\boldsymbol{\varepsilon}}_o(t))] + \frac{1}{2} \tilde{\boldsymbol{\varepsilon}}_g(t)^T (R(\tilde{\boldsymbol{q}}_o(t)) - I)R(\hat{\boldsymbol{q}}_g(t))\boldsymbol{\omega}_g(t) \text{sign}(\tilde{\eta}_g(t)) \end{aligned} \quad (6.74)$$

Equation 6.74 is the same as equation 5.7, except for the addition of $\boldsymbol{\gamma}_I$ in the second term, since the terms with $\tilde{\boldsymbol{b}}(t)$ and $\tilde{\boldsymbol{\gamma}}_I(t)$ cancel. The derivative is bounded in the same manner, resulting in

$$\dot{V}_o(t) \leq -\|\tilde{\boldsymbol{\varepsilon}}_o(t)\|^2 \left(\frac{k(t)}{2} - 2\|\boldsymbol{\omega}_g(t)\| \right) - \|\tilde{\boldsymbol{\varepsilon}}_o(t)\| \left(\frac{k_1(t)}{2} - 2\|\boldsymbol{\omega}_g(t)\| \|\boldsymbol{\gamma}_I\| \right)$$

If $k(t) \geq 4\|\boldsymbol{\omega}_g(t)\| + k'$ and $k_1 \geq 4\|\boldsymbol{\omega}_g(t)\| \|\boldsymbol{\gamma}_I\|_{max} + k'_1$, where $k' > 0$ and $k'_1 > 0$, and $\|\boldsymbol{\gamma}_I\|_{max}$ is a known upper bound on the norm of the inverse scale factors.

$$\dot{V}_o(t) \leq -k' \|\tilde{\boldsymbol{\varepsilon}}_o(t)\|^2 - k'_1 \|\tilde{\boldsymbol{\varepsilon}}_o(t)\| \leq -k' \|\tilde{\boldsymbol{\varepsilon}}_o(t)\|^2 \quad (6.75)$$

With the added constraint that $\boldsymbol{\omega}_g(t)$ is bounded, $V_o(t)$ is a continuous, twice differentiable function. Lemma 2.1 then shows that $\|\tilde{\boldsymbol{\varepsilon}}_o(t)\| \rightarrow 0$ as $t \rightarrow \infty$. \square

Theorem 6.10 *For any bounded, angular velocity, $\boldsymbol{\omega}_g(t)$, that is persistently exciting, the equilibrium states of the system 6.69, 6.70, 6.71 and 6.72 are exponentially stable. In particular, $\hat{\mathbf{q}}_g(t) \rightarrow \mathbf{q}_g$, $\hat{\boldsymbol{\gamma}}(t) \rightarrow \boldsymbol{\gamma}$, and $\hat{\mathbf{b}}(t) \rightarrow \mathbf{b}(t)$ exponentially fast from any initial conditions $\hat{\mathbf{q}}_g(t_0)$, $\hat{\boldsymbol{\gamma}}(t_0)$, $\hat{\mathbf{b}}(t_0)$, and $\hat{\boldsymbol{\gamma}}(t_0)$.*

Proof: The system given by equations 6.69, 6.70, 6.71 and 6.72 is stable. If $\boldsymbol{\omega}_g(t)$ is bounded, all the signals are bounded. As with the gyro bias estimator analysis, the system is cast as a linear time-varying system $\dot{\mathbf{x}}(t) = A(t)\mathbf{x}(t)$ where

$$\mathbf{x}(t) = \begin{bmatrix} \tilde{\boldsymbol{\varepsilon}}_o(t) \\ \tilde{\boldsymbol{\varepsilon}}_g(t) \\ \tilde{\boldsymbol{\gamma}}_I(t) \\ \tilde{\mathbf{b}}(t) \end{bmatrix}$$

Developing $A(t)$ is similar to that for the alignment estimator, with added terms for the scale factor and bias errors. Here $A(t)$ is

$$A(t) = \begin{bmatrix} A_{11}(t) & A'_{12}(t) & \frac{1}{2}Q_1(\tilde{\mathbf{q}}_o(t))R(\hat{\mathbf{q}}_g(t))\Omega_g(t) & -\frac{1}{2}Q_1(\tilde{\mathbf{q}}_o(t)) \\ A_{21}(t) & 0 & 0 & 0 \\ -\frac{\alpha_\gamma}{2}\Omega_g(t)R(\hat{\mathbf{q}}_g(t))^T\text{sign}(\tilde{\boldsymbol{\eta}}_o(t)) & 0 & 0 & 0 \\ \frac{\alpha_b}{2}\text{sign}(\tilde{\boldsymbol{\eta}}_o(t)) & 0 & 0 & 0 \end{bmatrix}$$

where

$$\begin{aligned} A'_{12}(t) = & -Q_1(\tilde{\mathbf{q}}_o(t))[(R(\hat{\mathbf{q}}_g(t))\Omega_g(t)\boldsymbol{\gamma}_I)\tilde{\boldsymbol{\varepsilon}}_g(t)^T \\ & - (\tilde{\boldsymbol{\varepsilon}}_g(t)^T R(\hat{\mathbf{q}}_g(t))\Omega_g(t)\boldsymbol{\gamma}_I)\mathbf{I} - \tilde{\boldsymbol{\eta}}_g(t)S(R(\hat{\mathbf{q}}_g(t))\Omega_g(t)\boldsymbol{\gamma}_I)] \end{aligned}$$

$A_{11}(t)$ and $A_{21}(t)$ are the same as in section 5.1

Following the proof for the gyro bias, scale factor, and alignment observers, $\dot{V}_o(t)$ is rewritten as $\dot{V}_o(t) \leq -\mathbf{x}(t)^T C^T C \mathbf{x}(t) \leq 0$, where $C = \begin{bmatrix} \sqrt{k'}\mathbf{I} & 0 & 0 & 0 \end{bmatrix}$.

Choose $K(t)$ as

$$K(t) = \begin{bmatrix} \frac{1}{\sqrt{k'}} A_{11}(t) \\ \frac{1}{\sqrt{k'}} A_{21}(t) \\ -\frac{\alpha_\gamma}{2\sqrt{k'}} \Omega_g(t) R(\hat{\mathbf{q}}_g(t))^T \text{sign}(\tilde{\eta}_o(t)) \\ \frac{\alpha_b}{2\sqrt{k'}} \text{sign}(\tilde{\eta}_o(t)) \end{bmatrix}$$

With $\boldsymbol{\omega}_g(t)$ bounded, applying the same arguments as with the gyro bias, alignment, and scale factor observers, $K(t)$ is a piecewise continuous function of time.

The state transition matrix for the pair $(A(t) - K(t)C, C)$ is

$$\Phi(\tau, t) = \begin{bmatrix} \mathbf{I} & \Sigma(\tau, t) \\ 0 & \mathbf{I}_9 \end{bmatrix}$$

where \mathbf{I}_9 is a 9x9 identity matrix and

$$\Sigma(\tau, t) = \begin{bmatrix} \int_t^\tau A'_{12}(\sigma) d\sigma & \frac{1}{2} \int_t^\tau Q_1(\tilde{\mathbf{q}}_o(\sigma)) R(\hat{\mathbf{q}}_g(\tau)) \Omega_g(\tau) d\sigma & -\frac{1}{2} \int_t^\tau Q_1(\tilde{\mathbf{q}}_o(\sigma)) d\sigma \end{bmatrix}$$

The observability Grammian is

$$\begin{aligned} W(t, t+T) &= \int_t^{t+T} \Phi(\tau, t)^T C^T C \Phi(\tau, t) d\tau \\ &= \int_t^{t+T} \begin{bmatrix} k'\mathbf{I} & k'\Sigma(\tau, t) \\ k'\Sigma(\tau, t)^T & k'\Sigma(\tau, t)^T \Sigma(\tau, t) \end{bmatrix} d\tau \end{aligned} \quad (6.76)$$

Proceeding similarly to 3.10 for the gyro bias estimator proof, the system is UCO if $Q_1(\tilde{\mathbf{q}}_o(t))$, $\frac{d}{dt}Q_1(\tilde{\mathbf{q}}_o(t))$, $A'_{12}(t)$ and $\frac{d}{dt}A'_{12}(t)$ are bounded, and there exist positive

constants T_2 , β_1 , and β_2 such that, for all $t \geq t_0$ (time and the argument of $Q_1(\tilde{\mathbf{q}}_o(t))$ are not included for clarity)

$$\begin{aligned}
& \beta_2 \mathbf{I} \geq \\
& \int_t^{t+T_2} \begin{bmatrix} A'_{12}{}^T A'_{12} & \frac{1}{2} A'_{12}{}^T Q_1 R(\hat{\mathbf{q}}_g) \Omega_g & -\frac{1}{2} A'_{12}{}^T Q_1 \\ \frac{1}{2} \Omega_g R(\hat{\mathbf{q}}_g)^T Q_1^T A'_{12} & \frac{1}{4} \Omega_g R(\hat{\mathbf{q}}_g)^T Q_1^T Q_1 R(\hat{\mathbf{q}}_g) \Omega_g & -\frac{1}{4} \Omega_g R(\hat{\mathbf{q}}_g)^T Q_1^T Q_1 \\ -\frac{1}{2} Q_1^T A'_{12} & -\frac{1}{4} Q_1^T Q_1 R(\hat{\mathbf{q}}_g) \Omega_g & \frac{1}{4} Q_1^T Q_1 \end{bmatrix} d\tau \\
& \geq \beta_1 \mathbf{I}
\end{aligned} \tag{6.77}$$

Again, rewrite $A'_{12}(t)$ as $A'_{12}(t) = -Q_1(\tilde{\mathbf{q}}_o(t))B(t)$, where here $B(t)$ is

$$\begin{aligned}
B(t) &= (R(\hat{\mathbf{q}}_g(t))\Omega_g(t)\gamma_I)\tilde{\boldsymbol{\varepsilon}}_g(t)^T - (\tilde{\boldsymbol{\varepsilon}}_g(t)^T R(\hat{\mathbf{q}}_g(t))\Omega_g(t)\gamma_I)\mathbf{I} \\
&\quad - \tilde{\eta}_g(t)S(R(\hat{\mathbf{q}}_g(t))\Omega_g(t)\gamma_I) \\
&= S(\tilde{\boldsymbol{\varepsilon}}_g(t))S(R(\hat{\mathbf{q}}_g(t))\Omega_g(t)\gamma_I) - \tilde{\eta}_g(t)S(R(\hat{\mathbf{q}}_g(t))\Omega_g(t)\gamma_I) \\
&= (S(\tilde{\boldsymbol{\varepsilon}}_g(t)) - \tilde{\eta}_g(t)\mathbf{I})S(R(\hat{\mathbf{q}}_g(t))\Gamma_I\boldsymbol{\omega}_g(t))
\end{aligned}$$

The integral 6.77 becomes

$$\beta_2 \mathbf{I} \geq \int_t^{t+T_2} M'(\tau) d\tau \geq \beta_1 \mathbf{I} \tag{6.78}$$

where

$$M'(t) = \begin{bmatrix} B^T Q_1^T Q_1 B & -\frac{1}{2} B^T Q_1^T Q_1 R(\hat{\mathbf{q}}_g) \Omega_g & \frac{1}{2} B^T Q_1^T Q_1 \\ -\frac{1}{2} \Omega_g R(\hat{\mathbf{q}}_g)^T Q_1^T Q_1 B & \frac{1}{4} \Omega_g R(\hat{\mathbf{q}}_g)^T Q_1^T Q_1 R(\hat{\mathbf{q}}_g) \Omega_g & -\frac{1}{4} \Omega_g R(\hat{\mathbf{q}}_g)^T Q_1^T Q_1 \\ \frac{1}{2} Q_1^T Q_1 B & -\frac{1}{4} Q_1^T Q_1 R(\hat{\mathbf{q}}_g) \Omega_g & \frac{1}{4} Q_1^T Q_1 \end{bmatrix}$$

$Q_1(\tilde{\mathbf{q}}_o(t))$ is bounded by definition, since it contains elements of the quaternion, $\tilde{\mathbf{q}}_o(t)$. $\frac{d}{dt}Q_1(\tilde{\mathbf{q}}_o(t))$ is also bounded, since the above Lyapunov analysis shows that all the terms in equation 6.69 are bounded, given that $\boldsymbol{\omega}_g(t)$ is bounded. With $\dot{\boldsymbol{\omega}}_g(t)$ bounded, the upper bound in equation 6.78 is satisfied.

Next the lower bound is considered. First, $Q_1(\tilde{\mathbf{q}}_o(t))^T Q_1(\tilde{\mathbf{q}}_o(t))$ in $M'(t)$ is replaced with $Q_1(\tilde{\mathbf{q}}_o(t))^T Q_1(\tilde{\mathbf{q}}_o(t)) = \mathbf{I} - \tilde{\boldsymbol{\varepsilon}}_o(t)\tilde{\boldsymbol{\varepsilon}}_o(t)^T$. Since $\|\tilde{\boldsymbol{\varepsilon}}_o(t)\| \rightarrow 0$ asymptotically, for any $\delta > 0$, there exists a $T_1(\delta) > t_0$ such that $\|\tilde{\boldsymbol{\varepsilon}}_o(t)\| < \delta$ for all $t \geq t_0 + T_1$. Taking any $\delta < 1$ and $T_2 > T_1$, $\mathbf{I} - \tilde{\boldsymbol{\varepsilon}}_o(t)\tilde{\boldsymbol{\varepsilon}}_o(t)^T > (1 - \delta^2)\mathbf{I}$. Therefore $M'(t) > (1 - \delta^2)M(t)$ where $M(t)$ is given as (again, time is omitted for clarity)

$$M(t) = \begin{bmatrix} B^T B & -\frac{1}{2}B^T R(\hat{\mathbf{q}}_g)\Omega_g & \frac{1}{2}B^T \\ -\frac{1}{2}\Omega_g R(\hat{\mathbf{q}}_g)^T B & \frac{1}{4}\Omega_g^2 & -\frac{1}{4}\Omega_g R(\hat{\mathbf{q}}_g)^T \\ \frac{1}{2}B & -\frac{1}{4}R(\hat{\mathbf{q}}_g)\Omega_g & \frac{1}{4}\mathbf{I} \end{bmatrix} \quad (6.79)$$

If the following is true, for any $\mathbf{z} \in \mathbb{R}^9$,

$$\mathbf{z}^T \left[\int_t^{t+T_2} M(\tau) d\tau \right] \mathbf{z} \geq 0 \quad (6.80)$$

the system is UCO. This establishes the persistency of excitation condition for the combined alignment, scale factor, and gyro bias estimation.

In order to satisfy equation 6.80, the integral of $M(t)$ over the interval T_2 must be positive definite. Let

$$P = \begin{bmatrix} P_{11} & -\frac{1}{2}P_{12} & \frac{1}{2}P_{13} \\ -\frac{1}{2}P_{12}^T & \frac{1}{4}P_{22} & -\frac{1}{4}P_{23} \\ \frac{1}{2}P_{13}^T & -\frac{1}{4}P_{23}^T & \frac{1}{4}P_{33} \end{bmatrix}$$

where

$$P = \int_t^{t+T_2} M(\tau) d\tau \quad (6.81)$$

In both Sections 5.1 and 6.5, a constant angular velocity did not satisfy the PE conditions when the alignment is estimated. A constant angular velocity did not satisfy the PE conditions in Section 6.1 when the scale factor and bias are estimated together. In this case, when all three parameters are estimated, a constant angular velocity will again not satisfy the PE condition of equation 6.80. Therefore, the PE condition will be evaluated only with

$$\boldsymbol{\omega}_g(t)^T = [\cos \vartheta t, \sin \vartheta t, \cos 2\vartheta t]$$

and $T_2 = \frac{2\pi}{\vartheta}$. First, the matrix P_{11} is evaluated as

$$\begin{aligned} P_{11} &= \int_t^{t+T_2} B(\tau)^T B(\tau) d\tau \\ &= \int_t^{t+T_2} (S(R(\hat{\mathbf{q}}_g(\tau))\Gamma_I \boldsymbol{\omega}_g(\tau))(S(\tilde{\boldsymbol{\epsilon}}_g) + \tilde{\eta}_g \mathbf{I})(S(\tilde{\boldsymbol{\epsilon}}_g) \\ &\quad - \tilde{\eta}_g \mathbf{I})S(R(\hat{\mathbf{q}}_g(\tau))\Gamma_I \boldsymbol{\omega}_g(\tau))) d\tau \\ &= \int_t^{t+T_2} S(R(\hat{\mathbf{q}}_g(\tau))\Gamma_I \boldsymbol{\omega}_g(\tau))(\tilde{\boldsymbol{\epsilon}}_g \tilde{\boldsymbol{\epsilon}}_g^T - \mathbf{I})S(R(\hat{\mathbf{q}}_g(\tau))\Gamma_I \boldsymbol{\omega}_g(\tau)) d\tau \\ &= \int_t^{t+T_2} R(\hat{\mathbf{q}}_g(\tau))S(\tilde{\boldsymbol{\epsilon}}_{gR})[\Gamma_I \boldsymbol{\omega}_g(\tau)\boldsymbol{\omega}_g(\tau)^T \Gamma_I]S(\tilde{\boldsymbol{\epsilon}}_{gR})R(\hat{\mathbf{q}}_g(\tau))^T \\ &\quad - [R(\hat{\mathbf{q}}_g(\tau))\Gamma_I \boldsymbol{\omega}_g(\tau)\boldsymbol{\omega}_g(\tau)^T \Gamma_I R(\hat{\mathbf{q}}_g(\tau))^T - \boldsymbol{\omega}_g(\tau)^T \Gamma_I^2 \boldsymbol{\omega}_g(\tau)\mathbf{I}] d\tau \end{aligned}$$

Recall that $\tilde{\boldsymbol{\epsilon}}_o(t) \rightarrow 0$ asymptotically. As above, at some time $T_1(\delta) > t_0$, $\|\tilde{\boldsymbol{\epsilon}}_o(t)\| < \delta$. The derivatives of $\tilde{\boldsymbol{\epsilon}}_{gR}(t)$ and $R(\hat{\mathbf{q}}_g(t))$ are directly proportional to the attitude prediction error. As $\tilde{\boldsymbol{\epsilon}}_o(t) \rightarrow 0$, the derivatives of $\tilde{\boldsymbol{\epsilon}}_{gR}(t)$ and $R(\hat{\mathbf{q}}_g(t))$ will converge to zero. The integration of P_{11} and the remaining matrices, is performed for some time

$t > T_1$, such that the derivatives are close to zero, and therefore the terms $\tilde{\boldsymbol{\varepsilon}}_{gR}(t)$ and $R(\hat{\boldsymbol{q}}_g(t))$ are treated as being nearly constant. Recall also that Γ_I is constant.

P_{11} is then

$$\begin{aligned}
P_{11} &= R(\hat{\boldsymbol{q}}_g)S(\tilde{\boldsymbol{\varepsilon}}_{gR})\Gamma_I\left[\int_t^{t+T_2}\boldsymbol{\omega}_g(\tau)\boldsymbol{\omega}_g(\tau)^T d\tau\right]\Gamma_I S(\tilde{\boldsymbol{\varepsilon}}_{gR})R(\hat{\boldsymbol{q}}_g)^T \\
&\quad - R(\hat{\boldsymbol{q}}_g)\Gamma_I\left[\int_t^{t+T_2}\boldsymbol{\omega}_g(\tau)\boldsymbol{\omega}_g(\tau)^T d\tau\right]\Gamma_I R(\hat{\boldsymbol{q}}_g)^T \\
&\quad + R(\hat{\boldsymbol{q}}_g)\left[\int_t^{t+T_2}\boldsymbol{\omega}_g(\tau)^T\Gamma_I^2\boldsymbol{\omega}_g(\tau)d\tau\right]R(\hat{\boldsymbol{q}}_g)^T \\
&= \frac{\pi}{\vartheta}R(\hat{\boldsymbol{q}}_g(t))\left[S(\tilde{\boldsymbol{\varepsilon}}_{gR})\Gamma_I^2S(\tilde{\boldsymbol{\varepsilon}}_{gR}) - \Gamma_I^2 + \|\boldsymbol{\gamma}_I\|^2\mathbf{I}\right]R(\hat{\boldsymbol{q}}_g)^T
\end{aligned}$$

where $S(R(\hat{\boldsymbol{q}}_g)^T\tilde{\boldsymbol{\varepsilon}}_g) = R(\hat{\boldsymbol{q}}_g)^T S(\tilde{\boldsymbol{\varepsilon}}_g)R(\hat{\boldsymbol{q}}_g)$ [7], and again $\tilde{\boldsymbol{\varepsilon}}_{gR} = R(\hat{\boldsymbol{q}}_g)^T\tilde{\boldsymbol{\varepsilon}}_g$. The next matrix to be evaluated is P_{12} .

$$\begin{aligned}
P_{12} &= \int_t^{t+T_2} B(\tau)^T R(\hat{\boldsymbol{q}}_g(\tau))\Omega_g(\tau)d\tau \\
&= \int_t^{t+T_2} S(R(\hat{\boldsymbol{q}}_g(\tau))\Gamma_I\boldsymbol{\omega}_g(\tau))(S(\tilde{\boldsymbol{\varepsilon}}_g) + \tilde{\eta}_g\mathbf{I})R(\hat{\boldsymbol{q}}_g)\Omega_g(\tau)d\tau \\
&= \int_t^{t+T_2} R(\hat{\boldsymbol{q}}_g(\tau))S(\Gamma_I\boldsymbol{\omega}_g(\tau))R(\hat{\boldsymbol{q}}_g(\tau))^T(S(\tilde{\boldsymbol{\varepsilon}}_g) + \tilde{\eta}_g\mathbf{I})R(\hat{\boldsymbol{q}}_g(\tau))\Omega_g(\tau)d\tau \\
&= \int_t^{t+T_2} R(\hat{\boldsymbol{q}}_g(\tau))(S(\Gamma_I\boldsymbol{\omega}_g(\tau))S(\tilde{\boldsymbol{\varepsilon}}_{gR})\Omega_g(\tau) + \tilde{\eta}_gS(\Gamma_I\boldsymbol{\omega}_g(\tau))\Omega_g(t))d\tau
\end{aligned}$$

Again, treating $R(\hat{\boldsymbol{q}}_g(t))$ and $\tilde{\boldsymbol{\varepsilon}}_{gR}(t)$ as (nearly) constant, substituting $\boldsymbol{\omega}_g(t)$ from above into P_{12} results in

$$P_{12} = \frac{\pi}{\vartheta}R(\hat{\boldsymbol{q}}_g) \begin{bmatrix} 0 & \tilde{\boldsymbol{\varepsilon}}_{gR,1} & \tilde{\boldsymbol{\varepsilon}}_{gR,1} \\ \tilde{\boldsymbol{\varepsilon}}_{gR,2} & 0 & \tilde{\boldsymbol{\varepsilon}}_{gR,2} \\ \tilde{\boldsymbol{\varepsilon}}_{gR,3} & \tilde{\boldsymbol{\varepsilon}}_{gR,3} & 0 \end{bmatrix} \Gamma_I$$

where $\tilde{\varepsilon}_{gR,1}$, $\tilde{\varepsilon}_{gR,2}$, and $\tilde{\varepsilon}_{gR,3}$ are the components of $\tilde{\varepsilon}_{gR}$. Next P_{13} is evaluated. With $R(\hat{\mathbf{q}}_g(t))$ and $\tilde{\varepsilon}_{gR}(t)$ (nearly) constant, and $\omega_g(t)$ above, P_{13} is

$$P_{13} = \int_t^{t+T_2} B(\tau)^T d\tau = \frac{1}{2} \int_t^{t+T_2} S(R(\hat{\mathbf{q}}_g)\Gamma_I\omega_g(\tau))(S(\tilde{\varepsilon}_g) + \tilde{\eta}_g\mathbf{I})d\tau = 0$$

Similarly, the remaining matrices are evaluated as

$$\begin{aligned} P_{22} &= \int_t^{t+T_2} \Omega_g(\tau)^2 d\tau = \frac{\pi}{\vartheta} \mathbf{I} \\ P_{23} &= \int_t^{t+T_2} \Omega_g(\tau) R(\hat{\mathbf{q}}_g) d\tau = 0 \\ P_{33} &= \int_t^{t+T_2} \mathbf{I} d\tau = \frac{2\pi}{\vartheta} \end{aligned}$$

P is now given as

$$P = \begin{bmatrix} P_{11} & -\frac{1}{2}P_{12} & 0 \\ -\frac{1}{2}P_{12}^T & \frac{1}{4}P_{22} & 0 \\ 0 & 0 & \frac{1}{4}P_{33} \end{bmatrix}$$

Next, let

$$P' = \frac{\pi}{\vartheta} \begin{bmatrix} P'_{11} & -\frac{1}{2}P'_{12} & 0 \\ -\frac{1}{2}P'_{12}^T & \frac{1}{4}\mathbf{I} & 0 \\ 0 & 0 & \frac{1}{2}\mathbf{I} \end{bmatrix}$$

where the submatrices of P' are the same as those of P , with $\frac{\pi}{\vartheta}$ factored out. Let

$$P_{UL} = \begin{bmatrix} P'_{11} & -\frac{1}{2}P'_{12} \\ -\frac{1}{2}P'_{12}^T & \frac{1}{4}\mathbf{I} \end{bmatrix}$$

P_{33} is positive definite, since it is diagonal with positive elements on the diagonal. If

P_{UL} is positive definite, then P is positive definite. Let

$$D = F(P_{UL})F^T \tag{6.82}$$

where

$$F = \begin{bmatrix} \mathbf{I} & 2P'_{12} \\ 0 & \mathbf{I} \end{bmatrix}$$

The matrix D is then

$$D = \begin{bmatrix} P'_{11} - P'_{12}P'_{12}{}^T & 0 \\ 0 & \frac{1}{4}\mathbf{I} \end{bmatrix}$$

The matrix $P'_{11} - P'_{12}P'_{12}{}^T$ is computed as

$$\begin{aligned} P'_{11} - P'_{12}P'_{12}{}^T &= R(\hat{\mathbf{q}}_g)[S(\tilde{\boldsymbol{\varepsilon}}_{gR}(t))\Gamma_I^2 S(\tilde{\boldsymbol{\varepsilon}}_{gR}(t)) \\ &\quad - \Gamma_I^2 + \|\boldsymbol{\gamma}_I\|^2 \mathbf{I} \\ &\quad - \begin{bmatrix} 0 & \tilde{\varepsilon}_{gR,1} & \tilde{\varepsilon}_{gR,1} \\ \tilde{\varepsilon}_{gR,2} & 0 & \tilde{\varepsilon}_{gR,2} \\ \tilde{\varepsilon}_{gR,3} & \tilde{\varepsilon}_{gR,3} & 0 \end{bmatrix} \Gamma_I^2 \begin{bmatrix} 0 & \tilde{\varepsilon}_{gR,2} & \tilde{\varepsilon}_{gR,3} \\ \tilde{\varepsilon}_{gR,1} & 0 & \tilde{\varepsilon}_{gR,3} \\ \tilde{\varepsilon}_{gR,1} & \tilde{\varepsilon}_{gR,2} & 0 \end{bmatrix}] R(\hat{\mathbf{q}}_g)^T \\ &= R(\hat{\mathbf{q}}_g) \begin{bmatrix} d'_{11} & 0 & 0 \\ 0 & d'_{22} & 0 \\ 0 & 0 & d'_{33} \end{bmatrix} R(\hat{\mathbf{q}}_g)^T \\ &= R(\hat{\mathbf{q}}_g) D'_u R(\hat{\mathbf{q}}_g)^T \end{aligned}$$

where

$$d'_{11} = \gamma_{Iy}^2 (1 - \tilde{\varepsilon}_{gR,1}^2 - \tilde{\varepsilon}_{gR,3}^2) + \gamma_{Iz}^2 (1 - \tilde{\varepsilon}_{gR,1}^2 - \tilde{\varepsilon}_{gR,2}^2)$$

$$d'_{22} = \gamma_{Ix}^2 (1 - \tilde{\varepsilon}_{gR,2}^2 - \tilde{\varepsilon}_{gR,3}^2) + \gamma_{Iz}^2 (1 - \tilde{\varepsilon}_{gR,1}^2 - \tilde{\varepsilon}_{gR,2}^2)$$

$$d'_{33} = \gamma_{Ix}^2 (1 - \tilde{\varepsilon}_{gR,2}^2 - \tilde{\varepsilon}_{gR,3}^2) + \gamma_{Iy}^2 (1 - \tilde{\varepsilon}_{gR,1}^2 - \tilde{\varepsilon}_{gR,3}^2)$$

The matrix D'_u is diagonal. The elements on the main diagonal are all positive, except if a component of $\tilde{\boldsymbol{\varepsilon}}_{gR}$ is 1. Recall that $\tilde{\boldsymbol{\varepsilon}}_{gR} = R(\hat{\boldsymbol{q}}_g)^T \tilde{\boldsymbol{\varepsilon}}_g$. If the steady state error is such that $\|\tilde{\boldsymbol{\varepsilon}}_g\| = 1$, a component of $\tilde{\boldsymbol{\varepsilon}}_{gR}$ could be 1.

From equation 6.82, D is written as

$$D = R(\hat{\boldsymbol{q}}_g)_6 D' R(\hat{\boldsymbol{q}}_g)_6^T = \begin{bmatrix} R(\hat{\boldsymbol{q}}_g) & 0 \\ 0 & R(\hat{\boldsymbol{q}}_g) \end{bmatrix} \begin{bmatrix} D'_u & 0 \\ 0 & \frac{1}{4}\mathbf{I} \end{bmatrix} \begin{bmatrix} R(\hat{\boldsymbol{q}}_g)^T & 0 \\ 0 & R(\hat{\boldsymbol{q}}_g)^T \end{bmatrix}$$

or

$$D' = R(\hat{\boldsymbol{q}}_g)_6^T F (P_{UL}) F^T R(\hat{\boldsymbol{q}}_g)_6$$

Let $F' = R(\hat{\boldsymbol{q}}_g)_6^T F$. Since both $R(\hat{\boldsymbol{q}}_g)_6$ and F are non-singular, F' is non-singular, P_{UL} can be written as

$$P_{UL} = F'^{-1} D' F'^{-T}$$

For any $\boldsymbol{z} \in \mathbb{R}^6$, if

$$\boldsymbol{z}^T P_{UL} \boldsymbol{z} > 0 \tag{6.83}$$

P_{UL} is positive definite. Let $\boldsymbol{y} = F'^{-1} \boldsymbol{z}$. Equation 6.83 is then written as

$$\boldsymbol{z}^T P_{UL} \boldsymbol{z} = \boldsymbol{y}^T D' \boldsymbol{y} > 0$$

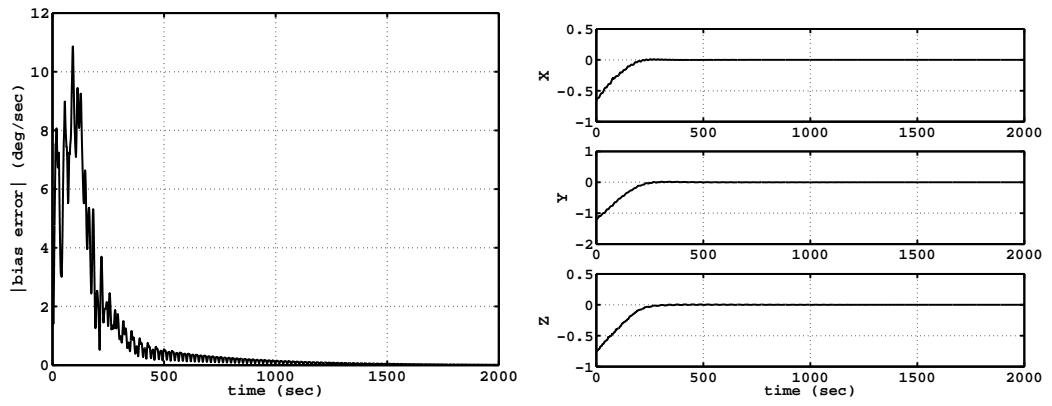
Therefore, P_{UL} is positive definite. Since P_{33} is also positive definite, P is positive definite. Equation 6.80 is satisfied and the system is UCO, the alignment, scale factor, and bias errors all converge to zero exponentially fast.

If $\|\tilde{\boldsymbol{\varepsilon}}_g(t)\| = \|\tilde{\boldsymbol{\varepsilon}}_{gR}(t)\| = 1$ for all $t \geq t_0$, the PE condition above would not be satisfied. Following the same argument as that at the end of Section 6.5, $\|\tilde{\boldsymbol{\varepsilon}}_g(t)\| = 1$

is equivalent to an alignment rotational error of 180 degrees. For the estimate of the alignment to remain 180 degrees away from the actual alignment, the fourth element of $\tilde{\mathbf{q}}_g(t)$, $\tilde{\eta}_g = \cos(\frac{\tilde{\phi}}{2})$, must remain at zero for all $t \geq t_0$. If $\tilde{\eta}_g$ of $\tilde{\mathbf{q}}_g(t)$ does not change from zero, then $\|\tilde{\boldsymbol{\varepsilon}}_g(t)\|$ remains at $\|\tilde{\boldsymbol{\varepsilon}}_g(t)\| = 1$. For this to be true, the derivative of $\tilde{\eta}_g$ in equation 6.70 must be zero. If the attitude prediction error $\tilde{\boldsymbol{\varepsilon}}_o(t)$ is not zero, $R(\tilde{\mathbf{q}}_o(t)) - \mathbf{I}$ in equation 6.70 will not be zero. For $\dot{\tilde{\eta}}_g = 0$, the angular velocity term in equation 6.70 must remain perpendicular to $\tilde{\boldsymbol{\varepsilon}}_g$ for all $t > t_0$. But, the angular velocity $\boldsymbol{\omega}_g(t)$ is changing direction continuously, $\tilde{\boldsymbol{\varepsilon}}_o(t)$ is also changing continuously (converging to zero). Until $\tilde{\boldsymbol{\varepsilon}}_o(t)$ converges identically to zero, $(R\mathbf{t}_o - \mathbf{I})R(\hat{\mathbf{q}}_g(t))\boldsymbol{\omega}_g(t)$ will not be zero and should not remain perpendicular to $\tilde{\boldsymbol{\varepsilon}}_g(t)$ for all $t > t_0$. As long as $\|\tilde{\boldsymbol{\varepsilon}}_g(t)\| \neq 1$, the PE condition is satisfied and the errors converge to zero exponentially fast. \square

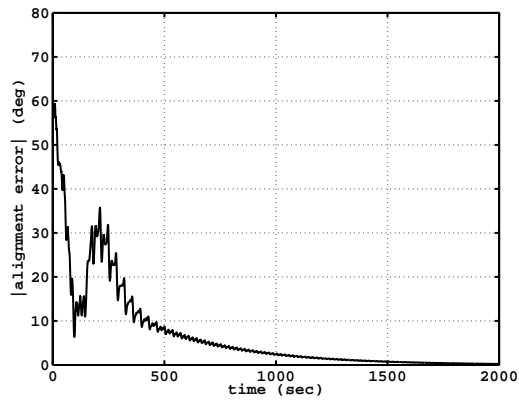
6.10 Estimator Simulation Results

The combined gyro bias, scale factor, and alignment parameter estimation is tested similarly to the bias estimator. Table 6.5 lists the initial quaternions, scale factor and gyro bias for the estimator, as well as the true alignment, scale factor, and gyro bias. The angular velocity is $\boldsymbol{\omega}_g(t)^T = [\cos \vartheta t, \sin \vartheta t, \cos 2\vartheta t]$ rad/sec, where $\vartheta = 10$ deg/sec. The gains are chosen as $k' = 5$, $k'_1 = 0.01$, $\alpha_b = 1$, and $\alpha_\gamma = 1$. Figures 6.8(a), 6.8(b), and 6.8(c) show that the bias, scale factor, and alignment estimation errors converge to zero.



(a) Bias Estimation Error

(b) Scale Factor Estimation Error



(c) Alignment Estimation Error

Figure 6.8: Combined Estimators with PE Angular Velocity

<i>Attitude</i>	<i>Value</i>	<i>Variable</i>	<i>Value</i>
$\mathbf{q}(t_0)$	$[0, 1, 0, 0]^T$	\mathbf{q}_g	$[0.34, 0.34, 0.34, 0.81]^T$
$\hat{\mathbf{q}}(t_0)$	$[0, 0, 0, 1]^T$	$\hat{\mathbf{q}}_g(t)$	$[0, 0, 0, 1]^T$
$\boldsymbol{\gamma}(t_0)$	$[3, -5, 4]^T$	$\hat{\boldsymbol{\gamma}}_I(t_0)$	$[1, 1, 1]^T$
$\mathbf{b}(t)$	$[0.5, -0.5, 0.5]^T \frac{deg}{sec}$	$\hat{\mathbf{b}}(t)$	$[0, 0, 0]^T$

Table 6.5: Alignment, Scale Factor, and Gyro Bias Estimator Simulation Initial Conditions

6.11 Closed Loop Stability

As in Section 3.3, a certainty equivalence approach is proposed in utilizing the non-linear tracking algorithm in [32]. Here the estimates $\hat{\boldsymbol{\omega}}(t)$ of 2.13, generated by the estimator equations 6.64, 6.65, 6.66 and 6.67 are used to generate the control. Again, the control is given as

$$\mathbf{u}(t) = -K_D \hat{\mathbf{s}}(t) + H \hat{\boldsymbol{\alpha}}_r(t) - S(H \hat{\boldsymbol{\omega}}(t)) \boldsymbol{\omega}_r(t) \quad (6.84)$$

The closed loop analysis for the gyro bias, up to equation 3.20, is independent of the specific gyro error. The closed loop equation, given in equation 3.20, is repeated here

$$H \dot{\mathbf{s}}(t) - S(H \boldsymbol{\omega}(t)) \mathbf{s}(t) + K_D \mathbf{s}(t) = \Delta(\tilde{\mathbf{q}}_c(t), \boldsymbol{\omega}_d(t)) \tilde{\mathbf{s}}(t) \quad (6.85)$$

where

$$\Delta(\tilde{\mathbf{q}}_c(t), \boldsymbol{\omega}_d(t)) = \Delta'(\tilde{\mathbf{q}}_c(t), \boldsymbol{\omega}_d(t)) + K_D$$

as with all the previous closed loop analysis, the error term $\tilde{\mathbf{s}}(t)$ is

$$\tilde{\mathbf{s}}(t) = \mathbf{s}(t) - \hat{\mathbf{s}}(t) = \boldsymbol{\omega}(t) - \hat{\boldsymbol{\omega}}(t)$$

Note that the definition of $\boldsymbol{\omega}_r(t)$, the assumption the $\boldsymbol{\omega}_d(t)$ is bounded, and the constraint $\|\tilde{\mathbf{q}}_c(t)\| = 1$ ensure that $\Delta'(\tilde{\mathbf{q}}_c(t), \boldsymbol{\omega}_d(t))$ is a bounded matrix over any solution of the coupled dynamics 6.64, 6.65, 6.66, 6.67, 2.21, and 6.84.

Theorem 6.11 *If the gyro alignment rotation angle is less than 45 degrees, if the scale factors are known to be positive, with a known upper and lower bound on each component, with projection implemented in the estimators such that $\hat{\gamma}_I(t)$ has a known upper and lower bound and $|\hat{\phi}|_g < 45$ degrees, and if*

$$k_D > \frac{\zeta'(\gamma_{I,max} + \hat{\gamma}_{I,max}) + 8}{\gamma_{I,max} \hat{\gamma}_{I,max}} > 0$$

where $\gamma_{I,max} = \|\Gamma_I\|$ and $\hat{\gamma}_{I,max} = \|\hat{\Gamma}_I(t)\|$ and

$$\zeta' = \sup_{t \geq t_0} \sup_{\|\tilde{\mathbf{q}}_c(t)\|=1} \|\Delta'(\tilde{\mathbf{q}}_c(t), \boldsymbol{\omega}_d(t))\| < \infty$$

the control law 6.84 results in a stable closed loop system, with $\|\tilde{\boldsymbol{\varepsilon}}_c(t)\|$ and $\|\tilde{\boldsymbol{\omega}}_c(t)\|$ uniformly, ultimately bounded.

Proof: Using the Lyapunov function $V_c(t) = \frac{1}{2} \mathbf{s}(t)^T H \mathbf{s}(t)$, the derivative of $V_c(t)$ is

$$\dot{V}_c(t) = -\mathbf{s}(t)^T K_D \mathbf{s}(t) + \mathbf{s}(t)^T \Delta(\tilde{\mathbf{q}}_c(t), \boldsymbol{\omega}_d(t)) \tilde{\mathbf{s}}(t) \quad (6.86)$$

or substituting for $\Delta(\tilde{\mathbf{q}}_c(t), \boldsymbol{\omega}_d(t))$

$$\dot{V}_c(t) = -\mathbf{s}(t)^T K_D \mathbf{s}(t) + \mathbf{s}(t)^T (\Delta'(\tilde{\mathbf{q}}_c(t), \boldsymbol{\omega}_d(t)) + K_D) \tilde{\mathbf{s}}(t) \quad (6.87)$$

$\dot{V}_c(t)$ is now rewritten in terms of $\boldsymbol{\omega}_g(t)$ and $\boldsymbol{\omega}_r(t)$. First, $\dot{V}_c(t)$ from equation 6.87 is written as

$$\dot{V}_c(t) = \mathbf{s}(t)^T \Delta'(\tilde{\mathbf{q}}_c(t), \boldsymbol{\omega}_d(t))(\mathbf{s}(t) - \hat{\mathbf{s}}(t)) - \mathbf{s}(t)^T K_D \hat{\mathbf{s}}(t) \quad (6.88)$$

Rewrite $\mathbf{s}(t)$ as

$$\mathbf{s}(t) = \boldsymbol{\omega}(t) - \boldsymbol{\omega}_r(t) = R(\tilde{\mathbf{q}}_g(t))R(\hat{\mathbf{q}}_g(t))\Gamma_I \boldsymbol{\omega}_g(t) - \mathbf{b} - \boldsymbol{\omega}_r(t)$$

and rewrite $\hat{\mathbf{s}}(t)$ as

$$\hat{\mathbf{s}}(t) = \hat{\boldsymbol{\omega}}(t) - \boldsymbol{\omega}_r(t) = R(\hat{\mathbf{q}}_g(t))\hat{\Gamma}_I(t)\boldsymbol{\omega}_g(t) - \hat{\mathbf{b}} - \boldsymbol{\omega}_r(t)$$

Substitute the expressions for $\mathbf{s}(t)$ and $\hat{\mathbf{s}}(t)$ into equation 6.88, letting $K_D = k_D I$, resulting in (the arguments of $\Delta'(\tilde{\mathbf{q}}_c(t), \boldsymbol{\omega}_d(t))$ and the time argument are omitted for clarity)

$$\begin{aligned} \dot{V}_c(t) &= (\boldsymbol{\omega}_g^T \Gamma_I R(\hat{\mathbf{q}}_g)^T R(\tilde{\mathbf{q}}_g)^T - \mathbf{b}^T - \boldsymbol{\omega}_r^T) \Delta'((R(\tilde{\mathbf{q}}_g)R(\hat{\mathbf{q}}_g)\Gamma_I - R(\hat{\mathbf{q}}_g)\hat{\Gamma}_I)\boldsymbol{\omega}_g - (\mathbf{b} - \hat{\mathbf{b}})) \\ &\quad - k_D (\boldsymbol{\omega}_g^T \Gamma_I R(\hat{\mathbf{q}}_g)^T R(\tilde{\mathbf{q}}_g)^T - \mathbf{b}^T - \boldsymbol{\omega}_r^T) (R(\hat{\mathbf{q}}_g)\hat{\Gamma}_I \boldsymbol{\omega}_g - \hat{\mathbf{b}} - \boldsymbol{\omega}_r) \\ &= \boldsymbol{\omega}_g^T \Gamma_I R(\hat{\mathbf{q}}_g)^T R(\tilde{\mathbf{q}}_g)^T \Delta'(R(\tilde{\mathbf{q}}_g)R(\hat{\mathbf{q}}_g)\Gamma_I - R(\hat{\mathbf{q}}_g)\hat{\Gamma}_I(t))\boldsymbol{\omega}_g \\ &\quad - \mathbf{b}^T \Delta'(R(\tilde{\mathbf{q}}_g)R(\hat{\mathbf{q}}_g)\Gamma_I - R(\hat{\mathbf{q}}_g)\hat{\Gamma}_I(t))\boldsymbol{\omega}_g - \boldsymbol{\omega}_r^T \Delta'(R(\tilde{\mathbf{q}}_g)R(\hat{\mathbf{q}}_g)\Gamma_I - R(\hat{\mathbf{q}}_g)\hat{\Gamma}_I(t))\boldsymbol{\omega}_g \\ &\quad - \boldsymbol{\omega}_g^T \Gamma_I R(\hat{\mathbf{q}}_g)^T R(\tilde{\mathbf{q}}_g)^T \Delta'(\mathbf{b} - \hat{\mathbf{b}}) - (\mathbf{b}^T - \boldsymbol{\omega}_r^T) \Delta'(\mathbf{b} - \hat{\mathbf{b}}) \\ &\quad - k_D \boldsymbol{\omega}_g^T \Gamma_I R(\hat{\mathbf{q}}_g)^T R(\tilde{\mathbf{q}}_g)^T R(\hat{\mathbf{q}}_g)\hat{\Gamma}_I(t)\boldsymbol{\omega}_g - k_D \boldsymbol{\omega}_r^T \boldsymbol{\omega}_r + k_D \boldsymbol{\omega}_g^T \Gamma_I R(\hat{\mathbf{q}}_g)^T R(\tilde{\mathbf{q}}_g)^T \hat{\mathbf{b}} \\ &\quad + k_D \boldsymbol{\omega}_g^T \Gamma_I R(\hat{\mathbf{q}}_g)^T R(\tilde{\mathbf{q}}_g)^T \boldsymbol{\omega}_r + k_D \mathbf{b}^T R(\hat{\mathbf{q}}_g)\hat{\Gamma}_I(t)\boldsymbol{\omega}_g + k_D \boldsymbol{\omega}_r^T R(\hat{\mathbf{q}}_g)\hat{\Gamma}_I(t)\boldsymbol{\omega}_g \\ &\quad - k_D (\mathbf{b}^T (\hat{\mathbf{b}} + \boldsymbol{\omega}_r) + \boldsymbol{\omega}_r^T \hat{\mathbf{b}}) \end{aligned}$$

If Γ_I and $\hat{\Gamma}_I(t)$ are both positive, and if $R(\tilde{\mathbf{q}}_g(t))$ is positive definite, meaning the rotation angle of $\tilde{\mathbf{q}}_g(t)$ is less than 90 degrees, $\dot{V}_c(t)$ is bounded as (again, the time argument is omitted for clarity)

$$\begin{aligned}\dot{V}_c(t) &\leq -k_D \gamma_{I,max} \hat{\gamma}_{I,max} \|\boldsymbol{\omega}_g\|^2 - k_D \|\boldsymbol{\omega}_r\|^2 + k_D \gamma_{I,max} \|\boldsymbol{\omega}_g\| \|\hat{\mathbf{b}}\| \\ &\quad + k_D \gamma_{I,max} \|\boldsymbol{\omega}_g\| \|\boldsymbol{\omega}_r\| + k_D \hat{\gamma}_{I,max} \|\boldsymbol{\omega}_g\| \|\mathbf{b}\| + k_D \hat{\gamma}_{I,max} \|\boldsymbol{\omega}_g\| \|\boldsymbol{\omega}_r\| \\ &\quad + \zeta' \gamma_{I,max} (\gamma_{I,max} + \hat{\gamma}_{I,max}) \|\boldsymbol{\omega}_g\|^2 + \zeta' (\gamma_{I,max} + \hat{\gamma}_{I,max}) \|\boldsymbol{\omega}_g\| \|\mathbf{b}\| \\ &\quad + \zeta' (\gamma_{I,max} + \hat{\gamma}_{I,max}) \|\boldsymbol{\omega}_g\| \|\boldsymbol{\omega}_r\| + \zeta' \gamma_{I,max} \|\boldsymbol{\omega}_g\| (\|\mathbf{b}\| + \|\hat{\mathbf{b}}\|) \\ &\quad + f_1(\|\mathbf{b}\|, \|\hat{\mathbf{b}}\|, \|\boldsymbol{\omega}_r\|, k_D, \zeta')\end{aligned}$$

Applying Young's inequality to the products containing $\|\boldsymbol{\omega}_g(t)\|$ results in

$$\begin{aligned}\dot{V}_c(t) &\leq -(k_D \gamma_{I,max} \hat{\gamma}_{I,max} - \gamma_{I,max} (\gamma_{I,max} + \hat{\gamma}_{I,max}) - 8) \|\boldsymbol{\omega}_g(t)\|^2 \\ &\quad - (k_D - \frac{1}{4}(k_D^2 + \zeta'^2) (\gamma_{I,max} + \hat{\gamma}_{I,max})^2) \|\boldsymbol{\omega}_r(t)\|^2 \\ &\quad + f_2(\|\mathbf{b}\|, \|\hat{\mathbf{b}}(t)\|, \|\boldsymbol{\omega}_r(t)\|, k_D, \zeta')\end{aligned}$$

where $f_1(\|\mathbf{b}\|, \|\hat{\mathbf{b}}(t)\|, \|\boldsymbol{\omega}_r(t)\|, k_D, \zeta')$ and $f_2(\|\mathbf{b}\|, \|\hat{\mathbf{b}}(t)\|, \|\boldsymbol{\omega}_r(t)\|, k_D, \zeta')$ are both positive, bounded functions. If

$$k_D > \frac{\gamma_{I,max} (\gamma_{I,max} + \hat{\gamma}_{I,max}) + 8}{\gamma_{I,max} \hat{\gamma}_{I,max}}$$

and $\boldsymbol{\omega}_g(t)$ is sufficiently large, $\dot{V}_c(t) < 0$. If $\mathbf{s}(t)$ increases without bound, $\boldsymbol{\omega}_g(t)$ increases without bound. Eventually $\boldsymbol{\omega}_g(t)$ will be large enough such that $\dot{V}_c(t) < 0$, which implies that $\boldsymbol{\omega}_g(t)$ and $\mathbf{s}(t)$ must remain bounded.

Theorem 6.12 *If the angular velocity $\boldsymbol{\omega}_g(t)$ is persistently exciting, regardless of the specific magnitude of $k_D > 0$, the control law 6.84 results in global stability and*

asymptotically perfect tracking, $\|\tilde{\mathbf{e}}_c(t)\| \rightarrow 0, \|\tilde{\boldsymbol{\omega}}_c(t)\| \rightarrow 0$, if the angular velocity $\boldsymbol{\omega}_g(t)$ is persistently exciting.

Proof: The convergence of $\mathbf{s}(t)$ to zero depends on the exponential convergence of the bias, scale factor, and alignment errors, which in turn depends on the angular velocity $\boldsymbol{\omega}_g(t)$ generated by the applied control. Rewriting the error term

$$\mathbf{s}(t) - \hat{\mathbf{s}}(t) = (R(\tilde{\mathbf{q}}_g(t)) - \mathbf{I})R(\hat{\mathbf{q}}_g(t))\Gamma_I\boldsymbol{\omega}_g(t) + R(\hat{\mathbf{q}}_g(t))\tilde{\Gamma}_I(t)\boldsymbol{\omega}_g(t) - \tilde{\mathbf{b}}(t) \quad (6.89)$$

From equation 1.1, $\boldsymbol{\omega}_g(t)$ is written as

$$\boldsymbol{\omega}_g(t) = \Gamma_I R(\mathbf{q}_g)^T(\boldsymbol{\omega}(t) + \mathbf{b})$$

Substituting the expression for $\boldsymbol{\omega}(t) = \mathbf{s}(t) + \boldsymbol{\omega}_r(t)$ into the expression for $\boldsymbol{\omega}_g(t)$, equation 6.89 becomes

$$\begin{aligned} \mathbf{s}(t) - \hat{\mathbf{s}}(t) &= (R(\tilde{\mathbf{q}}_g(t)) - \mathbf{I})R(\hat{\mathbf{q}}_g(t))\Gamma_I^2 R(\mathbf{q}_g)^T(\mathbf{s}(t) + \boldsymbol{\omega}_r(t) + \mathbf{b}) \\ &\quad + R(\hat{\mathbf{q}}_g(t))\tilde{\Gamma}_I(t)\Gamma_I R(\mathbf{q}_g)^T(\mathbf{s}(t) + \boldsymbol{\omega}_r(t) + \mathbf{b}) - \tilde{\mathbf{b}}(t) \end{aligned}$$

Substituting this into equation 6.87 results in

$$\begin{aligned} \dot{V}_c(t) &= -\mathbf{s}(t)^T K_D \mathbf{s}(t) \\ &\quad + \mathbf{s}(t)^T (\Delta'(\tilde{\mathbf{q}}_c(t), \boldsymbol{\omega}_d(t)) + K_D)(\mathbf{I} - R(\tilde{\mathbf{q}}_g(t)))R(\hat{\mathbf{q}}_g(t))\Gamma_I^2 R(\mathbf{q}_g)^T \mathbf{s}(t) \\ &\quad + \mathbf{s}(t)^T (\Delta'(\tilde{\mathbf{q}}_c(t), \boldsymbol{\omega}_d(t)) + K_D)(\mathbf{I} - R(\tilde{\mathbf{q}}_g(t)))R(\hat{\mathbf{q}}_g(t))\Gamma_I^2 R(\mathbf{q}_g)^T (\boldsymbol{\omega}_r(t) + \mathbf{b}) \\ &\quad + \mathbf{s}(t)^T (\Delta'(\tilde{\mathbf{q}}_c(t), \boldsymbol{\omega}_d(t)) + K_D)R(\hat{\mathbf{q}}_g(t))\tilde{\Gamma}_I(t)\Gamma_I R(\mathbf{q}_g)^T \mathbf{s}(t) \\ &\quad + \mathbf{s}(t)^T (\Delta'(\tilde{\mathbf{q}}_c(t), \boldsymbol{\omega}_d(t)) + K_D)R(\hat{\mathbf{q}}_g(t))\tilde{\Gamma}_I(t)\Gamma_I R(\mathbf{q}_g)^T (\boldsymbol{\omega}_r(t) + \mathbf{b}) \\ &\quad - \mathbf{s}(t)^T (\Delta'(\tilde{\mathbf{q}}_c(t), \boldsymbol{\omega}_d(t)) + K_D)\tilde{\mathbf{b}}(t) \end{aligned} \quad (6.90)$$

Equation 6.90 is bounded as

$$\begin{aligned}
\dot{V}_c(t) &\leq -k_D \|\mathbf{s}(t)\|^2 + 2(k_D + \zeta') (\|\tilde{\boldsymbol{\varepsilon}}_g(t)\| \gamma_{I,max}^2 + \|\tilde{\Gamma}_I(t)\| \gamma_{I,max}) \|\mathbf{s}(t)\|^2 \\
&\quad + 2(k_D + \zeta') \|\mathbf{s}(t)\| (\|\boldsymbol{\omega}_r(t)\| + \|\mathbf{b}\|) \|\tilde{\boldsymbol{\varepsilon}}_g(t)\| \\
&\quad + (k_D + \zeta') \|\mathbf{s}(t)\| (\|\boldsymbol{\omega}_r(t)\| + \|\mathbf{b}\|) \|\tilde{\Gamma}_I(t)\| \\
&\quad + (k_D + \zeta') \|\mathbf{s}(t)\| \|\tilde{\mathbf{b}}(t)\|
\end{aligned} \tag{6.91}$$

Applying Young's inequality to the last three terms in equation 6.91

$$\begin{aligned}
\dot{V}_c(t) &\leq -\left(\frac{k_D}{2} - 2(k_D + \zeta') (\|\tilde{\boldsymbol{\varepsilon}}_g(t)\| \gamma_{I,max}^2 + \|\tilde{\Gamma}_I(t)\|)\right) \|\mathbf{s}(t)\|^2 \\
&\quad + 3 \frac{(k_D + \zeta')^2}{k_D} (\|\boldsymbol{\omega}_r(t)\| + \|\mathbf{b}\|)^2 \|\tilde{\boldsymbol{\varepsilon}}_g(t)\|^2 \\
&\quad + \frac{3(k_D + \zeta')^2}{2k_D} (\|\boldsymbol{\omega}_r(t)\| + \|\mathbf{b}\|)^2 \|\tilde{\Gamma}_I(t)\|^2 \\
&\quad + \frac{3(k_D + \zeta')^2}{2k_D} \|\tilde{\mathbf{b}}(t)\|^2
\end{aligned} \tag{6.92}$$

If the angular velocity, $\boldsymbol{\omega}_g(t)$, in addition to being bounded, satisfies equation 6.80, the system is UCO and the alignment errors, $\tilde{\boldsymbol{\varepsilon}}_g(t)$, scale factor errors, $\tilde{\Gamma}_I(t)$, and the bias errors, $\tilde{\mathbf{b}}(t)$, converge to zero exponentially fast. In this case, Lemma 2.3 applies. Since $\|\tilde{\boldsymbol{\varepsilon}}_g(t)\| \rightarrow 0$, $\|\tilde{\gamma}_I(t)\| \rightarrow 0$, and $\|\tilde{\mathbf{b}}(t)\| \rightarrow 0$ exponentially fast, $V_c(t)$ converges to zero exponentially fast, which means $\mathbf{s}(t)$ converges to zero exponentially fast. With the convergence of $\mathbf{s}(t) \rightarrow 0$, the proof of convergence of the actual attitude and rate errors follows exactly as in the gyro bias analysis of section 3.3. The end result of which is $\lim_{t \rightarrow \infty} \|\tilde{\boldsymbol{\varepsilon}}_c(t)\| = 0$ and $\lim_{t \rightarrow \infty} \|\tilde{\boldsymbol{\omega}}_c(t)\| = 0$. \square

<i>Attitude</i>	<i>Value</i>	<i>Variable</i>	<i>Value</i>	<i>Variable</i>	<i>Value</i>
$\mathbf{q}(t_0)$	$[0, 1, 0, 0]^T$	\mathbf{q}_g	$[0, 0, 0.38, 0.92]$	γ	$[3, 5, 4]^T$
$\hat{\mathbf{q}}(t_0)$	$[0, 0, 0, 1]^T$	$\hat{\mathbf{q}}_g(t)$	$[0, 0, 0, 1]$	$\hat{\gamma}(t)$	$[1, 1, 1]^T$
$\mathbf{q}_d(t_0)$	$[0, 0, 0, 1]^T$	\mathbf{b}	$[0.5, -0.5, 0.5] \frac{deg}{sec}$		
		$\hat{\mathbf{b}}(t)$	$[0, 0, 0]$		

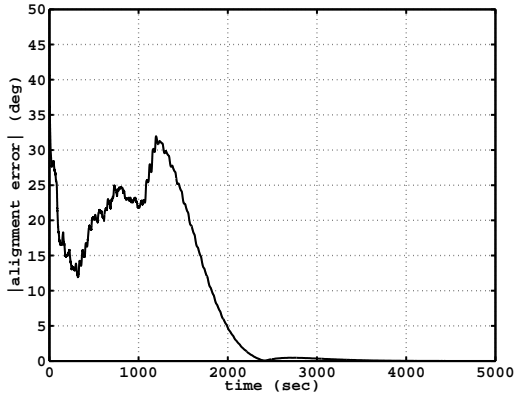
Table 6.6: Alignment, Scale Factor and Bias Estimator/ Controller Simulation Initial Conditions

6.12 Closed Loop Simulation Results

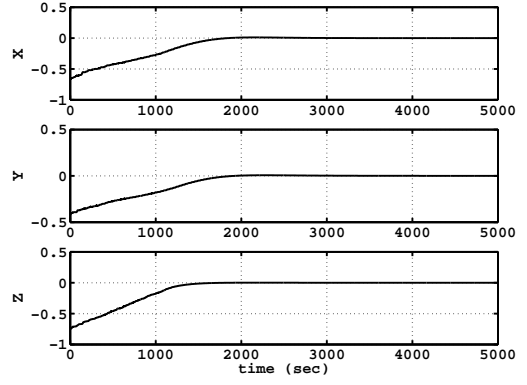
The gyro alignment, scale factor, and bias estimator and controller are tested similarly to the bias estimator and controller. The inertia matrix is the same, a diagonal matrix with principal moments of inertia of $[90, 100, 70]^T$ kg m². Table 6.6 lists the initial conditions for the estimator and controller, as well as the true gyro alignment, scale factor, and bias. The gains are chosen as $k' = 5$, $k'_1 = 0.1$, $K_D = k_D I_3$ (where I_3 indicates a 3x3 identity matrix), $\alpha_b = 1$, $\alpha_\gamma = 1$, $k_D = 20$, and $\lambda = 3$. The initial angular velocity is $\boldsymbol{\omega}(0)^T = [0, 0, 0]$. The gyro coordinate frame is rotated by 45 degrees from the body frame, about the z-axis. The desired angular velocity changes direction and is given as $\boldsymbol{\omega}_d(t)^T = 5[\cos \vartheta t, \sin \vartheta t, \sin 2\vartheta t]$ deg/sec, with $\vartheta = 10$ deg/sec.

Figures 6.9(a), 6.9(b) and 6.9(c) show that the alignment, scale factor and

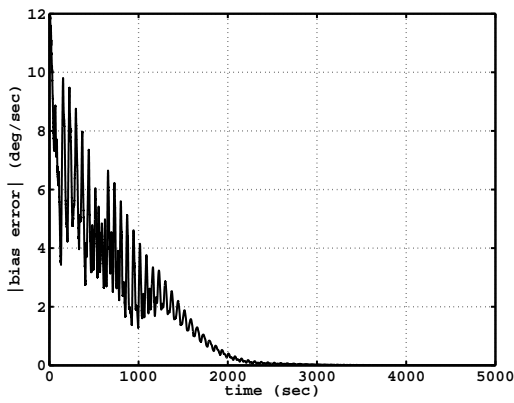
bias errors, respectively, converge to zero. Figures 6.9(d) and 6.9(e) show that the attitude and rate tracking errors, respectively, converge to zero also.



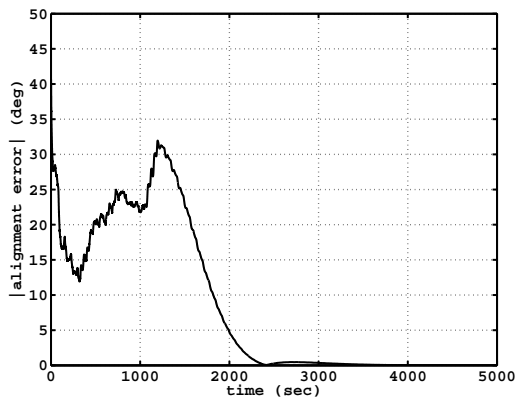
(a) Alignment Error



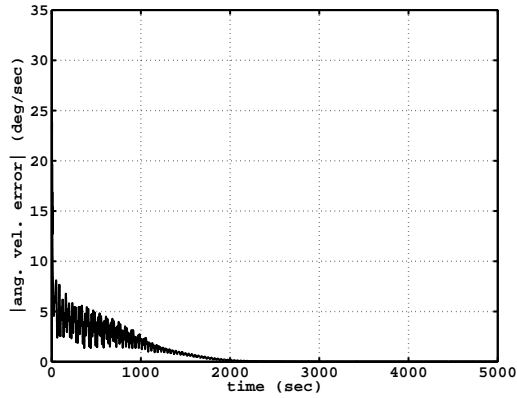
(b) Scale Factor Error



(c) Bias Error



(d) Attitude Tracking Error



(e) Rate Tracking Error

Figure 6.9: Coupled Estimator/Controller Errors with Alignment, Scale Factor, and Bias Errors

Chapter 7

Comparison to a Pseudo-Linear Kalman Filter

The three gyro calibration observers are each compared to a pseudo-linear Kalman filter designed to estimate gyro calibration parameters. The pseudo-linear Kalman filter is presented by Bar-Itzhack in [13]. Like the nonlinear observers, the pseudo-linear approach is based on the quaternion kinematic equation given in equation 2.3, repeated here

$$\dot{\mathbf{q}}(t) = \begin{bmatrix} \dot{\hat{\epsilon}}(t) \\ \dot{\eta}(t) \end{bmatrix} = \frac{1}{2}Q(\mathbf{q}(t))\boldsymbol{\omega}(t)$$

From Section 1.1.2, equation 1.8 gives the measured angular velocity as

$$\boldsymbol{\omega}_g(t) = (\mathbf{I} + K)(\mathbf{I} + M)^T\boldsymbol{\omega}(t) + \mathbf{b} = \boldsymbol{\omega}(t) + \Delta\boldsymbol{\omega}(t)$$

where again K is a diagonal matrix of small scale factor errors and M is a matrix with small alignment errors in the off diagonal terms. Rearranging the terms, and separating the calibration errors and including noise, gives

$$\boldsymbol{\omega}(t) = \boldsymbol{\omega}_g(t) - \Delta\boldsymbol{\omega}(t) - \mathbf{v}_\omega(t) \quad (7.1)$$

where $\boldsymbol{\omega}_g(t)$ is the measured angular velocity, $\Delta\boldsymbol{\omega}(t)$ is the error in the angular velocity, and $\mathbf{v}_\omega(t)$ is a zero-mean white noise process.

As shown in Section 1.1.2, the error term $\Delta\boldsymbol{\omega}(t)$ is modelled as a sum of error terms due to errors in each of the three calibration parameters

$$\Delta\boldsymbol{\omega}(t) = \Delta\boldsymbol{\omega}^m(t) + \Delta\boldsymbol{\omega}^k(t) + \Delta\boldsymbol{\omega}^b \quad (7.2)$$

The first term, $\Delta\boldsymbol{\omega}^m(t)$, is the error due to an alignment error and is defined as

$$\Delta\boldsymbol{\omega}^m(t) = \Omega^m \mathbf{m}$$

where Ω^m is a matrix composed of the angular velocity, and \mathbf{m} is a vector of small alignment errors

$$\mathbf{m}^T = [m_{xy} \ m_{xz} \ m_{yx} \ m_{yz} \ m_{zx} \ m_{zy}]$$

m_{ij} is a misalignment angle, defined as the projection of the i -gyro sensitive axis on the j body axis. The misalignment angles are assumed to be small. The second term in equation 7.2 is the error due to a scale factor error, defined as

$$\Delta\boldsymbol{\omega}^k(t) = \Omega^k \mathbf{k}$$

where again Ω^k is a matrix composed of the angular velocity, and \mathbf{k} is a vector of scale factor errors. The third error term is the error due to a gyro bias, written simply as

$$\Delta\boldsymbol{\omega}^b = I_3 \mathbf{b}$$

where \mathbf{b} is a vector of gyro biases.

The calibration terms are combined as

$$\Delta\boldsymbol{\omega}(t) = G(\boldsymbol{\omega}(t))\mathbf{x} \quad (7.3)$$

where

$$G(\boldsymbol{\omega}(t)) = [\Omega^m \ \Omega^k \ \mathbf{I}]$$

and \mathbf{x} is a 12x1 vector containing the alignment error angles, m_{ij} , the scale factor errors, k_i , and the bias \mathbf{b} .

The kinematic equation for the quaternion can be written as

$$\dot{\mathbf{q}}(t) = \frac{1}{2}Q(\mathbf{q})\boldsymbol{\omega}(t) = \frac{1}{2}\Omega(t)\mathbf{q}(t)$$

where here

$$\Omega(t) = \begin{bmatrix} 0 & \omega_z & -\omega_y & \omega_x \\ -\omega_z & 0 & \omega_x & \omega_y \\ \omega_y & -\omega_x & 0 & \omega_z \\ -\omega_x & -\omega_y & -\omega_z & 0 \end{bmatrix}$$

Using equations 7.1 and 7.3, $\Omega(t)$ is written as

$$\Omega(t) = \Omega_g(t) - \Delta\Omega - \Omega_{noise} \quad (7.4)$$

where the terms in equation 7.4 are defined similarly to $\Omega(t)$ above with the corresponding components in place of the components of $\boldsymbol{\omega}(t)$. Substituting equation 7.4 into the kinematic equation, rearranging the terms, and using equation 7.3 gives

$$\dot{\mathbf{q}}(t) = \frac{1}{2}\Omega_g\mathbf{q} - \frac{1}{2}QG(\boldsymbol{\omega}(t))\mathbf{x} - \frac{1}{2}Q\boldsymbol{\nu}_\omega(t) \quad (7.5)$$

The calibration components, \mathbf{x} are modelled as

$$\dot{\mathbf{x}} = \boldsymbol{\nu}_x \quad (7.6)$$

where $\boldsymbol{\nu}_x$ is a zero mean noise.

The pseudo-linear Kalman filter estimates a quaternion, along with the calibration states. The augmented state equation is formed from equations 7.5 and

$$7.6 \quad \begin{bmatrix} \dot{\mathbf{q}} \\ \dot{\mathbf{x}} \end{bmatrix} = \begin{bmatrix} \frac{1}{2}\Omega_g & \frac{1}{2}QG(\boldsymbol{\omega}(t)) \\ 0 & 0 \end{bmatrix} \begin{bmatrix} \mathbf{q} \\ \mathbf{x} \end{bmatrix} + \begin{bmatrix} \boldsymbol{\nu}_q \\ \boldsymbol{\nu}_x \end{bmatrix} \quad (7.7)$$

where $\boldsymbol{\nu}_q = \frac{1}{2}Q\boldsymbol{\nu}_\omega$. The estimated quaternion, $\hat{\mathbf{q}}$ is used in forming Q in equation 7.7.

The estimated angular velocity, $\hat{\boldsymbol{\omega}}$ computed using the estimates of the calibration parameters, is used in forming G in equation 7.7. Using estimates in the dynamics matrix is why this method is referred to as a 'pseudo-linear' Kalman filter.

The measurement model in the pseudo-linear Kalman filter is based on a measured quaternion and is simply

$$\mathbf{q}_m = \begin{bmatrix} \mathbf{I} & 0 \end{bmatrix} \begin{bmatrix} \mathbf{q} \\ \mathbf{x} \end{bmatrix} \quad (7.8)$$

Equations 7.7 and 7.8 form the dynamics and measurement equations for the pseudo-linear Kalman filter, respectively. Note that the pseudo-linear Kalman filter relies on the kinematic equation, as do the nonlinear estimators presented previously. Both approaches assume the calibration components are constant, and both utilize an estimate, or prediction, of the actual attitude. The significant difference occurs in the treatment of the calibration errors. The pseudo-linear filter development is based on small calibration errors. Even though the bias is not explicitly assumed to be small in the development of the pseudo-linear filter, it must be relatively small since it is

multiplied by the estimate of the attitude and angular velocity in equation 7.7.

First, each of the nonlinear estimators is compared to the pseudo-linear Kalman filter, set up to estimate one calibration component at a time. For example, the bias estimator is compared to the pseudo-linear Kalman filter set up to estimate the quaternion and the gyro bias. The alignment and scale factor errors are not considered. The estimated angular velocity in both the pseudo-linear Kalman filter and the gyro bias observer is

$$\hat{\boldsymbol{\omega}}(t) = \boldsymbol{\omega}_g(t) - \hat{\mathbf{b}}(t)$$

The error between the estimated and true bias from both algorithms is computed as

$$\mathbf{e}_b(t) = \mathbf{b} - \hat{\mathbf{b}}(t)$$

The two algorithms are compared without added noise.

The scale factor estimator is compared to the pseudo-linear Kalman filter set up to estimate the quaternion and the scale factor errors. In this case the estimated angular velocity in the pseudo-linear Kalman filter is

$$\hat{\boldsymbol{\omega}}(t) = \boldsymbol{\omega}_g(t) - \hat{K}(t)\boldsymbol{\omega}_g(t) = (I - \hat{K}(t))\boldsymbol{\omega}_g(t)$$

where $\hat{K}(t)$ is a matrix with the estimated scale factor errors, $\hat{\mathbf{k}}$, on the main diagonal.

The estimated angular velocity in the scale factor estimator is

$$\hat{\boldsymbol{\omega}}(t) = \hat{\Gamma}_I(t)\boldsymbol{\omega}_g(t)$$

The true angular velocity is given as

$$\boldsymbol{\omega}(t) = \Gamma_I\boldsymbol{\omega}_g(t)$$

where Γ_I is the inverse of the scale factor matrix. In comparing the pseudo-linear Kalman filter to the scale factor estimator, the errors are computed as

$$E_{PL}^{sf}(t) = \Gamma_I - (I - \hat{K}(t))$$

$$E_{NL}^{sf}(t) = \Gamma_I - \hat{\Gamma}_I(t)$$

where PL is the pseudo-linear result and NL is the nonlinear scale factor estimator result.

The alignment estimator is compared to the pseudo-linear Kalman filter set up to estimate the attitude quaternion and the alignment angles. In this case, the estimated angular velocity in the pseudo-linear Kalman filter is

$$\hat{\omega}(t) = \omega_g(t) - \hat{M}(t)\omega_g(t) = (I - \hat{M}(t))\omega_g(t)$$

where \hat{M} is matrix containing the estimated alignment angles, $\hat{\mathbf{m}}$. The estimated angular velocity in the alignment estimator is

$$\hat{\omega}(t) = R(\hat{\mathbf{q}}_g(t))\omega_g(t)$$

and the true angular velocity is

$$\omega(t) = R(\mathbf{q}_g)\omega_g(t)$$

where $R(\mathbf{q}_g)$ is the true alignment matrix. In comparing the pseudo-linear Kalman filter to the alignment estimator, an error matrix is computed as

$$E_{PL}^m(t) = R(\mathbf{q}_g) - (I - \hat{M}(t))$$

$$E_{NL}^m(t) = R(\mathbf{q}_g) - R(\hat{\mathbf{q}}_g(t))$$

The nonlinear estimators are then combined, and compared to the pseudo-linear Kalman filter set up to estimate all three calibration components. The estimated angular velocity in the pseudo-linear Kalman filter is

$$\hat{\boldsymbol{\omega}}(t) = \boldsymbol{\omega}_g(t) - \hat{M}(t)\boldsymbol{\omega}_g(t) - \hat{K}(t)\boldsymbol{\omega}_g(t) - \hat{\mathbf{b}}(t)$$

The estimated angular velocity in the nonlinear estimator is given in equation 2.11 and is repeated here as

$$\hat{\boldsymbol{\omega}}(t) = R(\hat{\mathbf{q}}_g(t))\hat{\Gamma}_I(t)\boldsymbol{\omega}_g(t) - \hat{\mathbf{b}}(t)$$

The error terms for the bias error, scale factor error, and the alignment are as given above.

7.1 Comparison of Gyro Bias Estimation

The same Matlab simulation used to test the gyro bias estimator is used in the comparison of the gyro bias estimator and the pseudo-linear Kalman filter. The initial quaternions and true rate are

$$\mathbf{q}(t_0) = \hat{\mathbf{q}}(t_0) = [0 \ 0 \ 0 \ 1]^T, \quad \boldsymbol{\omega}(t) = [3, -4, 5]\text{deg/sec}$$

except for the last case. In the last case, the rate is $\boldsymbol{\omega}(t) = [30, -40, 50]$ rad/sec. Table 7.1 compares the norm of the error as a percentage of the norm of the actual bias for the two algorithms for several tests with different added biases and no added

<i>Bias (deg/sec)</i>	<i>% Error Nonlinear</i>	<i>% Error Linear</i>
$[0.005, -0.005, 0.005]^T$	$1E - 12$	$1E - 11$
$[0.05, -0.05, 0.05]^T$	$1E - 13$	$1E - 11$
$[0.5, -0.5, 0.5]^T$	$9E - 15$	$1E - 11$
$[2, -2, 2]^T$	$2E - 14$	$1E - 11$
$[0.5, -0.5, 0.5]^T, \ \boldsymbol{\omega}_g(t)\ = 70 \text{ deg/sec}$	$2E - 13$	3

Table 7.1: Bias Estimation Comparison

noise. Results are given after 500 seconds. In all the test cases, both algorithms use the same data and both are run at 20 Hz. Both algorithms produce accurate bias estimates as long as the rates are relatively small. With a very large angular velocity, the linear approach does not estimate the bias well. The bias errors from the nonlinear estimator are smaller in each case.

7.2 Comparison of Scale Factor Estimation

The initial quaternions and true rate in the scale factor comparison are

$$\mathbf{q}(t_0) = \hat{\mathbf{q}}(t_0) = [0 \ 0 \ 0 \ 1]^T, \quad \boldsymbol{\omega}(t) = [3, -4, 5] \text{deg/sec}$$

The true scale factor matrix is defined as

$$\Gamma = \begin{bmatrix} 1 + k_x & 0 & 0 \\ 0 & 1 + k_y & 0 \\ 0 & 0 & 1 + k_z \end{bmatrix}$$

In each of the cases presented, k_i is increased. The norm of the scale factor error for each algorithm is computed as

$$e_{sf}^{PL} = \sqrt{\sum (diag(E_{PL}^{sf}(t)^T E_{PL}^{sf}(t)))}$$

$$e_{sf}^{NL} = \sqrt{\sum (diag(E_{NL}^{sf}(t)^T E_{NL}^{sf}(t)))}$$

Table 7.2 compares the error, again as a percentage of the norm of Γ_I . The results are given after 4000 seconds. In the first three cases, the angular velocity is increased from $\|\boldsymbol{\omega}_g(t)\| = 7$ deg/sec, to $\|\boldsymbol{\omega}_g(t)\| = 7$ rad/sec, to $\|\boldsymbol{\omega}_g(t)\| = 70$ rad/sec in the third case. In the fourth case, the angular velocity is again $\|\boldsymbol{\omega}_g(t)\| = 7$ deg/sec and the scale factor is increased by a factor of two. The final case, represents the extreme case of using erroneous units. When k_i is small and the angular velocity is small, both algorithms have a small error. However, as the scale factor error increases or the angular velocity increases, the error in the pseudolinear Kalman filter estimate increases. In the final case, the pseudolinear Kalman filter cannot estimate the large scale factor error.

<i>Scale factor, k_i</i>	<i>% Error Nonlinear</i>	<i>% Error Linear</i>
$1E - 04, \ \boldsymbol{\omega}_g(t)\ = 7 \text{ deg/sec}$	$2E - 10$	$2E - 06$
$1E - 04, \ \boldsymbol{\omega}_g(t)\ = 7 \text{ rad/sec}$	$2E - 14$	$5E - 04$
$1E - 04, \ \boldsymbol{\omega}_g(t)\ = 70 \text{ rad/sec}$	$1E - 13$	3
$1E - 02, \ \boldsymbol{\omega}_g(t)\ = 7 \text{ deg/sec}$	$5E - 13$	$1E - 2$
$\frac{\pi}{180} - 1, \ \boldsymbol{\omega}_g(t)\ = 7 \text{ deg/sec}$	$8E - 09$	169

Table 7.2: Scale Factor Estimation Comparison

7.3 Comparison of Misalignment Estimation

The initial quaternions in the alignment comparison are

$$\mathbf{q}(t_0) = \hat{\mathbf{q}}(t_0) = [0 \ 0 \ 0 \ 1]^T$$

The angular velocity is the same as that used to test the alignment estimator

$$\boldsymbol{\omega}_g(t)^T = [\sin \vartheta t, 1, 0]$$

where $\vartheta = 5$ deg/sec. The true gyro alignment quaternion is defined using equation 1.2

$$\mathbf{q}_g = \begin{bmatrix} \frac{1}{\sqrt{3}} \sin(\frac{\phi}{2}) \\ \frac{1}{\sqrt{3}} \sin(\frac{\phi}{2}) \\ \frac{1}{\sqrt{3}} \sin(\frac{\phi}{2}) \\ \cos(\frac{\phi}{2}) \end{bmatrix} = \begin{bmatrix} \boldsymbol{\varepsilon} \\ \eta \end{bmatrix}$$

In each case, the angle ϕ is increased. The error matrix for each case is normalized as

$$\mathbf{e}_m^{PL} = \sqrt{\sum (diag(E_{PL}^m(t)^T E_{PL}^m(t)))}$$

$$\mathbf{e}_m^{NL} = \sqrt{\sum (diag(E_{NL}^m(t)^T E_{NL}^m(t)))}$$

Table 7.3 gives the results for the nonlinear estimator and the pseudo-linear Kalman filter, presented as a percentage of norm of the actual alignment. In the second case, the alignment angle is the same as the first case, but the angular velocity above is increased to $10\|\boldsymbol{\omega}_g(t)\|$ with $\vartheta = 5$ rad/sec. The pseudo-linear Kalman filter errors are much worse than the errors from the nonlinear estimator in each case.

7.4 Comparison of Misalignment, Scale Factor, and Bias Estimation

Finally, all the calibration components are estimated simultaneously by both algorithms. The initial quaternions in the comparison are

$$\mathbf{q}(t_0) = \hat{\mathbf{q}}(t_0) = [0 \ 0 \ 0 \ 1]^T$$

<i>Rotation Angle (deg)</i>	<i>% Error Nonlinear</i>	<i>% Linear</i>
0.006	$5E - 07$	$6E - 03$
0.006, $\omega_g(t)*10$, $\vartheta = 5$ rad/sec	$2E - 07$	29
0.6	$3E - 09$	$6E - 3$
π	$1E - 06$	179

Table 7.3: Alignment Estimation Comparison

The angular velocity is the same as that used to test the combined alignment, scale factor, and bias estimator

$$\omega(t)^T = [\cos \vartheta t, \sin \vartheta t, \cos 2\vartheta t]$$

where $\vartheta = 10$ deg/sec. In each case, the angle ϕ of the gyro alignment, k_i of the scale factor, and bias is increased, using the values given previously for the individual calibration component comparisons. Table 7.4 through 7.6 give the results, presented as percentages, for the nonlinear estimator and the pseudo-linear Kalman filter, after 2000 seconds. In all cases, the errors from the nonlinear estimators converge almost to zero. The pseudo-linear Kalman filter errors grow quite large as the errors increase.

<i>Bias (deg/sec)</i>	<i>% Error Nonlinear</i>	<i>% Error Linear</i>
$[0.005, -0.005, 0.005]^T$	$8E - 11$	$3E - 03$
$[0.05, -0.05, 0.05]^T$	$8E - 12$	$3E - 02$
$[0.5, -0.5, 0.5]^T$	$3E - 12$	0.3
$[2, -2, 2]^T$	$9E - 14$	1.5

Table 7.4: Bias Estimation Comparison

<i>Scale factor, k_i</i>	<i>% Error Nonlinear</i>	<i>% Error Linear</i>
$1E - 04$	$3E - 12$	$8E - 04$
$1E - 03$	$3E - 12$	$2E - 02$
$1E - 02$	$1E - 11$	1
2	$2E - 12$	61

Table 7.5: Scale Factor Estimation Comparison

<i>Rotation Angle (rad)</i>	<i>% Error Nonlinear</i>	<i>% Error Linear</i>
0.001	$2E - 12$	$8E - 04$
0.01	$2E - 12$	$2E - 02$
0.1	$1E - 11$	2
60	$1E - 12$	92

Table 7.6: Alignment Estimation Comparison

Chapter 8

Concluding Remarks

Gyroscopes, or gyros, measure angular rate and are important sensors in most aerospace attitude control systems. The measured rate, however, is corrupted by noise and errors in alignment, scale factor, and bias. This work presents new nonlinear estimators designed to autonomously estimate the gyro calibration parameters all of which are *unknown* and of *arbitrary* size. The accuracy of the calibration estimates depends on 'identifiability' or persistency of excitation (PE) conditions. The PE conditions are explicitly computed for each of the calibration parameter estimates. The certainty equivalence use of the calibration parameter estimates in a nonlinear feedback control algorithm is proven to be stable. A strong nonlinear separation principle is proven for closed loop control with gyro bias estimation. A PE-dependent nonlinear separation principle is proven for closed loop control with scale factor or alignment estimation, or with arbitrary combinations of calibration estimates.

The PE condition is derived from an analysis of the uniform complete observability of the estimator states. The PE condition, in general terms, means that for

any time, t , there exists a time, $T > 0$, such that the following matrix is positive definite

$$\int_t^{t+T} \Sigma(\tau, t)^T \Sigma(\tau, t) d\tau \quad (8.1)$$

the observer errors converge to zero exponentially fast. The matrix $\Sigma(\tau, t)$ is defined for each estimator or estimator combination. Table 8.1 lists the PE condition for each estimator or combination.

<i>Component</i>	<i>PE Condition</i>	<i>Example PE $\omega_g(t)^T$</i>	<i>Example Non-PE $\omega_g(t)$</i>
Bias	PE always satisfied	any	none
Scale Factor	$\int_t^{t+T} \Omega_g(\tau)^2 d\tau$	constant ($\neq 0$)	$\ \omega_g(t)\ = e^{-at}$
Alignment	$\int_t^{t+T} S(\omega_g(\tau))^T S(\omega_g(\tau)) d\tau$	$[\sin(\vartheta t), 1, 0]$	$\omega_g(t) = \text{constant}$
Scale Factor/Bias	$\int_t^{t+T} \begin{bmatrix} \Omega_g(\tau)^2 & \Omega_g(\tau) \\ \Omega_g(\tau) & \mathbf{I} \end{bmatrix} d\tau$	$\sin(\vartheta t)[1, 1, 1]$	$\omega_g(t) = \text{constant}$
Alignment/Bias	$\int_t^{t+T_2} \begin{bmatrix} S(\omega_g)^T S(\omega_g) & -\frac{1}{2} S(\omega_g)^T \\ -\frac{1}{2} S(\omega_g) & \frac{1}{4} \mathbf{I} \end{bmatrix} d\tau$	$[\sin(\vartheta t), \cos(\vartheta t), 0]$	$\omega_g(t) = \text{constant}$
Alignment/Scale	$\int_t^{t+T_2} M(\tau) d\tau$	$[\cos(\vartheta t), \sin(\vartheta t),$ $\cos(2\vartheta t)]$	$\omega_g(t) = \text{constant}$
Factor/Bias			

Table 8.1: Summary of PE Conditions

$\Omega_g(t)$ is a matrix with the components of the measured angular velocity, $\boldsymbol{\omega}_g(t)$, on the main diagonal. The matrix $B(t)$ in the combined alignment and bias PE condition is defined as

$$B(t) = (S(\tilde{\boldsymbol{\epsilon}}_g(t)) - \tilde{\eta}_g(t))S(R(\hat{\boldsymbol{q}}_g(t))\boldsymbol{\omega}_g(t))$$

where $\tilde{\boldsymbol{\epsilon}}_g(t)$ is the vector part of the alignment quaternion error, $\tilde{\eta}_g(t)$ is the scalar part, $R(\hat{\boldsymbol{q}}_g(t))$ is the estimated alignment matrix, and $S(\cdot)$ is a skew symmetric, or cross product matrix. Finally, the matrix $M(t)$ in the combined alignment, scale factor, and bias estimators is given as

$$M(t) = \begin{bmatrix} B_c^T B_c & -\frac{1}{2}B_c^T R(\hat{\boldsymbol{q}}_g)\Omega_g & \frac{1}{2}B_c^T \\ -\frac{1}{2}\Omega_g R(\hat{\boldsymbol{q}}_g)^T B_c & \frac{1}{4}\Omega_g^2 & -\frac{1}{4}\Omega_g R(\hat{\boldsymbol{q}}_g)^T \\ \frac{1}{2}B_c & -\frac{1}{4}R(\hat{\boldsymbol{q}}_g)\Omega_g & \frac{1}{4}\mathbf{I} \end{bmatrix}$$

where here B_c is given as

$$B_c = (S(\tilde{\boldsymbol{\epsilon}}_g(t)) - \tilde{\eta}_g(t)\mathbf{I})S(R(\hat{\boldsymbol{q}}_g(t))\Gamma_I\boldsymbol{\omega}_g(t))$$

and Γ_I is a diagonal matrix of the inverse scale factors. Note in table 8.1 that the PE condition is always met for the gyro bias estimator, for any angular velocity. The matrix $\Sigma(\tau, t)^T \Sigma(\tau, t)$ reduces to a constant matrix. For the scale factor estimator, the angular velocity must be non-zero and bounded over regular time intervals. The angular velocity must change direction for complete observability of the alignment, and similarly with the combined alignment and bias estimator. In the combined scale factor and bias estimators, the angular velocity must be non-zero and changing in

magnitude in order to estimator both the scale factor and bias. Finally, in order to completely observe all the calibration components, the angular velocity must change direction sufficiently in \mathbb{R}^3 .

The nonlinear gyro estimators are coupled with a nonlinear spacecraft tracking control algorithm. Given that there is no separation principle for nonlinear systems, the closed loop system is analyzed with each of the gyro estimators, including the combined gyro estimators. Given a gyro bias, the closed loop system is asymptotically stable. With scale factor and alignment errors, or combinations involving scale factor and alignment errors, the closed loop system is at least bounded, given that the scale factor and alignment are known a priori to be bounded. However, if the angular velocity meets the persistency of excitation conditions given in table 8.1, the closed loop systems are asymptotically stable, regardless of the size of the scale factor and alignment.

8.1 Future Direction

There is, of course, additional work that can be done with the nonlinear gyro calibration estimators. Noise must be considered with the analysis of the scale factor and alignment estimators, as well as the closed loop systems. Also, only orthogonal alignments are considered here. Given that individual gyros are usually designed to measure rate along a single axis, and are combined to provide three axes of rate measurements, non-orthogonal alignment errors will exist. The impact of non-orthogonal

alignment errors needs to be considered. Perhaps, an additional estimator could be designed to produce an estimate of the non-orthogonal components. Additionally, consideration should be given to the gain computation in the closed loop systems. To ensure that the closed loop system is at least bounded, the gain is sized according to the system parameters and the a priori knowledge of the calibration components. Perhaps an adaptive gain would ensure the gain is minimized as the closed loop errors are reduced. Finally, the gyro calibration estimators should be augmented into a general attitude estimation algorithm in which the attitude is estimated with vector measurements, thus providing a complete attitude estimation system.

8.2 Final Summary

The thesis began with an overview of the current state of the art in terms of linearized and nonlinear methods of gyro calibration for spacecraft applications. The limitations of the current techniques were highlighted, providing the motivation for the development of the nonlinear gyro calibration estimators included in this work. The stability characteristics of the nonlinear estimation and the closed loop control system were analyzed and presented. The nonlinear gyro calibration estimators are directly applicable to spacecraft or other aerospace vehicles. The estimators are capable of estimating errors well outside the normal range of linear calibration algorithms, and during periods of large angular rate. The algorithms are applicable to future satellite missions, such as formation flying missions, or other missions re-

quiring high precision and autonomous operations. The algorithms can serve as an autonomous software calibration check anytime from pre-launch to on orbit operations. Finally, the algorithms have potential application in other scenarios, such as in calibrating the MEMS gyros used in automobiles, GPS/navigation systems, or in high angular velocity environments such as airplanes, robots, or industrial systems. The hope is that the methods presented here will serve as valuable tools in improving the performance of an aerospace control system.

BIBLIOGRAPHY

- [1] Swales Aerospace, “Attitude Control Systems for Non-ACS Engineers,” Class Notes, May 2002, Internal NASA Goddard Space Flight Center document.
- [2] Kourepenis, A., Borenstein, J., Connelly, J., Elliot, R., Ward, P., and Weinberg, M., “Performance of MEMS Inertial Sensors,” *IEEE PLANS*, Palm Springs, California, April 1998.
- [3] Wertz, J. R., editor, *Spacecraft Attitude Determination and Control*, D. Reidel Publishing Company, 1984.
- [4] Sedlak, J., Hashmall, J. H., and Airapetian, V., “Comparison of On-Orbit Performance of Rate Sensing Gyroscopes,” *International Symposium on Spaceflight Dynamics*, Biarritz, France, June 2000.
- [5] Markley, F. L. and Reynolds, R., “Analytic Steady-State Accuracy of a Spacecraft Attitude Estimator,” *AIAA Journal of Guidance, Control, and Dynamics*, Vol. 23, No. 6, November-December 2000, pp. 1065–1067.

- [6] Clarke, P., “Analog Devices spins a monolithic MEMS gyro,” website, October 2002.
- [7] Shuster, M. D., “A Survey of Attitude Representations,” *The Journal of Astronautical Sciences*, Vol. 41, No. 4, October-December 1993, pp. 439–517.
- [8] Sanner, R. M., “Adaptive Attitude Control Using Fixed and Dynamically Structured Neural Networks,” *AIAA Guidance, Navigation, and Control Conference*, No. 96-3891, San Diego, California, July 1996.
- [9] Davenport, P. B. and Welter, G. L., “Algorithm for In-Flight Gyroscope Calibration,” *Flight Mechanics/Estimation Theory Symposium*, NASA Goddard Space Flight Center, Greenbelt, Maryland, May 1988.
- [10] Welter, G., Boia, J., Gakenheimer, M., Kimmer, E., Channell, D., and Hallock, L., “Variations on the Davenport Gyroscope Calibration Algorithm,” *Flight Mechanics/Estimation Theory Symposium*, NASA Goddard Space Flight Center, Greenbelt, Maryland, May 1996.
- [11] Gelb, A., editor, *Applied Optimal Estimation*, The MIT Press, 1988.
- [12] Deutschmann(now Thienel), J. K. and Bar-Itzhack, I., “Evaluation of Attitude and Orbit Estimation Using Actual Earth Magnetic Field Data,” *AIAA Journal of Guidance, Control, and Dynamics*, Vol. 24, No. 3, May-June 2001, pp. 616–626.

- [13] Bar-Itzhack, I., “A Comparison Between Implicit and Explicit Spacecraft Gyro Calibration,” *WSEAS Transactions on Circuits and Systems*, Vol. 2, No. 4, October 2003, pp. 728–734.
- [14] Iwens, R. P. and Farrenkopf, R. L., “Performance Evaluation of a Precision Attitude Determination System (PADS),” *AIAA Guidance, Control, and Flight Mechanics Conference*, Hofstra University, Hempstead, New York, August 1971.
- [15] Murrell, J. W., “Precision Attitude Determination for Multimission Spacecraft,” *AIAA Guidance and Control Conference*, Palo Alto, California, August 1978.
- [16] Farrenkopf, R., “Analytic Steady-State Accuracy Solutions for Two Common Spacecraft Attitude Estimators,” *AIAA Journal of Guidance and Control*, Vol. 1, No. 4, July-August 1978, pp. 282–284.
- [17] Deutschmann (now Thienel), J. K., Bar-Itzhack, I., and Rokni, M., “Comparison and Testing of Extended Kalman Filters for Attitude Estimation of the Earth Radiation Budget Satellite,” *Flight Mechanics/Estimation Theory Symposium*, NASA Goddard Space Flight Center, Greenbelt, Maryland, May 1990.
- [18] Bar-Itzhack, I. and Harman, R. R., “In-Space Calibration of a Skewed Gyro Quadruplet,” *AIAA Journal of Guidance, Control, and Dynamics*, Vol. 25, No. 5, September-October 2002, pp. 852–859.

- [19] Hashmall, J. H., Radomski, M., and Sedlak, J., “On-Orbit Calibration of Satellite Gyroscopes,” *AIAA/AAS Astrodynamics Specialist Conference*, Denver, Colorado, August 2000.
- [20] Filla, O. H., Willard, T. Z., Chu, D., and J. Deutschmann (now Thienel), “In-flight Estimation of Gyro Noise,” *Flight Mechanics/Estimation Theory Symposium*, NASA Goddard Space Flight Center, Greenbelt, Maryland, May 1990.
- [21] Farrenkopf, R., “Generalized Results for Precision Attitude Reference Systems Using Gyros,” *AIAA Mechanics and Control of Flight Conference*, Anaheim, California, August 1974.
- [22] Ng, L. C. and Pines, D. J., “Characterization of Ring Laser Gyro Performance Using the Allan Variance Method,” *AIAA Journal of Guidance, Control, and Dynamics*, Vol. 20, No. 1, January 1997, pp. 211–214.
- [23] Ford, J. J. and Evans, M. E., “Online Estimation of Allan Variance Parameters,” *AIAA Journal of Guidance, Control, and Dynamics*, Vol. 23, No. 6, November–December 2000, pp. 980–987.
- [24] Deutschmann (now Thienel), J. K. and Sanner, R. M., “A Nonlinear Spacecraft Attitude Controller and Observer with an Unknown Constant Gyro Bias and Gyro Noise,” *Flight Mechanics Symposium*, NASA Goddard Space Flight Center, Greenbelt, Maryland, June 2001.

- [25] Alonso, R., Crassidis, J. L., and Junkins, J. L., “Vision-Based Relative Navigation for Formation Flying of Spacecraft,” *AIAA Guidance, Navigation, and Control Conference*, No. AIAA-2000-4439, Denver, Colorado, August 2000.
- [26] Salcudean, S., “A Globally Convergent Angular Velocity Observer for Rigid Body Motion,” *IEEE Transactions on Automatic Control*, Vol. 36, No. 12, December 1991, pp. 1493–1496.
- [27] Vik, B., Shiriaev, A., and Fossen, T. I., “Nonlinear Observer Design for Integration of DGPS and INS,” *New Directions in Nonlinear Observer Design*, Springer-Verlag, 1999.
- [28] Bošković, J. D., Li, S.-M., and Mehra, R. K., “A Globally Stable Scheme for Spacecraft Control in the Presence of Sensor Bias,” *2000 IEEE Aerospace Conference*, Big Sky, Montana, March 2000.
- [29] Bošković, J. D., Li, S.-M., and Mehra, R. K., “Fault Tolerant Control of Spacecraft in the Presence of Sensor Bias,” *American Control Conference*, Chicago, Illinois, March 2000.
- [30] Khalil, H. K., *Nonlinear Systems*, Prentice-Hall, Inc., 2nd ed., 1996.
- [31] Krstić, M., Kanellakopoulos, I., and Kokotovic, P., *Nonlinear and Adaptive Control Design*, John Wiley and Sons, Inc., 1995.

- [32] Egeland, O. and Godhavn, J., “Passivity-Based Adaptive Attitude Control of a Rigid Spacecraft,” *IEEE Transactions on Automatic Control*, Vol. 39, No. 4, April 1994, pp. 842–846.
- [33] Chen, C.-T., *Linear System Theory and Design*, Oxford University Press, 2nd ed., 1984.
- [34] Wie, B., *Space Vehicle Dynamics and Control*, AIAA Education Series, 1998.
- [35] Slotine, J.-J. E. and Li, W., *Applied Nonlinear Control*, Prentice-Hall, Inc., 1991.
- [36] Bar-Itzhack, I., “Navigation Computation in Terrestrial Strapdown Inertial Navigation Systems,” *IEEE Transactions on Aerospace and Electronic Systems*, Vol. AES-13, No. 6, November 1977, pp. 679–689.
- [37] Brown, R. G. and Hwang, P. Y., *Introduction to Random Signals and Applied Kalman Filtering*, John Wiley and Sons, 3rd ed., 1997.
- [38] Narendra, K. S. and Annaswamy, A. M., “Persistent Excitation in Adaptive Systems,” *International Journal of Control*, Vol. 45, No. 1, January 1987, pp. 127–160.
- [39] Ioannou, P. A. and Sun, J., *Robust Adaptive Control*, Prentice-Hall, Inc., 1996.